JAERI - M
90-036

EVALUATION REPORT ON SCTF CORE-III TEST S3-17

(INVESTIGATION OF THERMO-HYDRODYNAMIC BEHAVIOR
DURING REFLOOD PHASE OF LOCA IN A PWR WITH VENT VALVES)

March 1990

Tsutomu OKUBO, Tadashi IGUCHI, Takamichi IWAMURA
Hajime AKIMOTO, Akira OHNUKI, Yutaka ABE
Isao SAKAKI*, Hiromichi ADACHI and Yoshio MURAO

日 本 原 子 力 研 究 所
Japan Atomic Energy Research Institute

JAERI-Mレポートは，日本原子力研究所が不定期に公刊している研究報告書です。
入手の問合わせは，日本原子力研究所技術情報部情報資料課（〒319-11茨城県那珂郡東海村）あて，お申しこしください。なお，このほかに財団法人原子力弘済会資料センター（〒319-11 茨城県那珂郡東海村日本原子力研究所内）で複写による実費頒布をおこなっております。

JAERI-M reports are issued irregularly.
Inquiries about availability of the reports should be addressed to Information Division, Department of Technical Information, Japan Atomic Energy Research Institute, Tokai-mura, Naka-gun, Ibaraki-ken 319-11, Japan.

編集兼発行　日本原子力研究所
印　　刷　㈱原子力資料サービス

JAERI-M 90-036

Evaluation Report on SCTF Core-III Test S3-17

(Investigation of Thermo-hydrodynamic Behavior during Reflood Phase of LOCA in a PWR with Vent Valves)

Tsutomu OKUBO, Tadashi IGUCHI, Takamichi IWAMURA
Hajime AKIMOTO, Akira OHNUKI, Yutaka ABE
Isao SAKAKI*, Hiromichi ADACHI and Yoshio MURAO

Department of Reactor Engineering
Tokai Research Establishment
Japan Atomic Energy Research Institute
Tokai-mura, Naka-gun, Ibaraki-ken

(Received February 2, 1990)

In order to investigate the thermo-hydrodynamic behavior during the reflood phase of a loss-of-coolant accident (LOCA) in a pressurized water reactor (PWR) with the vent valves, a reflooding test was performed with the Slab Core Test Facility (SCTF) at Japan Atomic Energy Research Institute (JAERI). The simulated PWR with the vent valves in the test is one manufactured by Brown Boveri Reaktor (BBR) in Federal Republic of Germany (FRG). The data obtained in the present test are also supposed to be used for the experimental coupling with the Upper Plenum Test Facility (UPTF) of FRG, based on the trilateral 2D/3D Agreement among FRG, the USA and Japan. The test data have been analyzed by also utilizing other test results. The main conclusions are as follows:

(1) It has been demonstrated that the core cooling is significantly good during the reflood phase of a BBR under the best estimate conditions.
(2) The intact loop differential pressure was significantly reduced when the vent valve was open.
(3) The effect of the vent valve on core cooling was not remarkable under

---

* Toshiba Ltd.

the conditions that the downcomer water level was below the overflow level when the vent valve was closed, but is expected to be remarkable under the conditions that the downcomer water level exceeds the overflow level when the vent valve is closed.

Keywords: Reactor Safety, PWR, LOCA, ECCS, Reflood Experiments, two-phase Flow, Heat Transfer, Thermo-hydrodynamics, Vent Valves, SCTF

JAERI－M 90－036

SCTF第3次炉心試験S3－17評価報告書
（ベントバルブ付PWRのLOCA時再冠水過程における熱水力学的挙動の検討）

日本原子力研究所東海研究所原子炉工学部
大久保 努・井口 正・岩村 公道・秋本 肇
大貫 晃・阿部 豊・榊 勲*・安達 公道
村尾 良夫

（1990年2月2日受理）

ベントバルブ付加圧水型原子炉（PWR）の冷却材喪失事故（LOCA）時再冠水過程の熱水力学的挙動を検討するため，日本原子力研究所の平板炉心試験装置（SCTF）を用いて再冠水実験を実施した。本試験で模擬されたPWRは，西ドイツのBrown Boveri Reaktor（BBR）社のものである。本試験によって得られたデータは，西ドイツ・米国および日本の間の2D／3D三国協定に基づいて，西ドイツの上部プレナム試験装置（UPTF）との実験的結合に用いられることになっている。本試験のデータを他の試験のデータも用いて解析し，以下の主要な結論を得た。

(1) 最適条件下におけるBBRの再冠水過程中の炉心冷却は非常に良好で有ることが実証された。

(2) 健全ループ差圧は，ベントバルブが開くことにより著しく減少する。

(3) ベントバルブが炉心冷却におよぼす効果は，ベントバルブが開いていない場合にダウンカマ水位がオーバフロ位置に達しない条件の下では顕著ではなかった。しかし，その効果は，ベントバルブが開いていない場合にダウンカマ水位がオーバフロ位置を越えるような条件の下では顕著になると考えられる。

東海研究所：〒319－11 茨城県那珂郡東海村白方字白根2－4
＊東芝（株）

目　　次

Contents

List of Tables

List of Figures

1. Introduction

The Slab Core Test Facility (SCTF) test program is a part of the large scale reflood test program[1] together with the Cylindrical Core Test Facility (CCTF) test program, which are performed by Japan Atomic Energy Research Institute (JAERI) under a contract with Atomic Energy Bureau of Science and Technology Agency of Japan. The SCTF test program is also one of the research activities based on the trilateral agreement among JAERI, the United States Nuclear Regulatory Commission (USNRC) and the Federal Minister for Research and Technology (BMFT) of the Federal Republic of Germany (FRG).

There are three test series (Core-I, -II and -III) in the SCTF test program. The SCTF Core-I[2] and Core-II[3] test series have been already performed mainly to investigate the two-dimensional thermo-hydrodynamic behavior in the core during the reflood phase of a loss-of-coolant accident (LOCA) of a Westinghouse type (US/J-type) pressurized water reactor (PWR) with the cold-leg-injection-type emergency core cooling system (ECCS). On the other hand, one of the major objectives of the SCTF Core-III[4] test series is to investigate the effectiveness of the combined-injection-type ECCS in a German type PWR (GPWR). In addition, simulation tests for a US/J-type PWR were also conducted with the SCTF Core-III for further investigation of the two-dimensional thermo-hydrodynamic behavior. Furthermore, one simulation test for a Brown Boveri Reaktor (BBR) type German PWR with the vent valves is planed to be performed based on the 2D/3D Agreement.

According to the Agreement, there are four special tests for the SCTF Core-III and the Upper Plenum Test Facility (UPTF) of FRG. They are called "coupling tests", and the experimental coupling between the SCTF and the UPTF is planned to be performed with the data from those tests. As one of these coupling tests, a BBR type PWR simulation test was agreed to be performed. The special features of the BBR are the vent valves, which provide another flow path from the upper plenum to the downcomer being parallel to the intact loop, and the not-lowered once-through-type steam generators. Based on the above mentioned background, one SCTF Core-III test was conducted in order to obtain the data for the coupling between the SCTF and the UPTF and to investigate the thermo-hydrodynamic behavior for reflooding of a BBR type PWR under the best estimate (BE) conditions. This test was named Test S3-17 (Run 721). This report describes the major results of the test.

A brief description of the SCTF Core-III is presented in Appendix A. Some selected data obtained in Test S3-17 are presented in Appendix B.

A brief information on the test is presented in the following:

(1) Test name

BBR simulation integral coupling BE test

where, BBR : German PWR with the vent valves manufactured by Brown Boveri Reaktor

BE : Best estimate

(2) Test number

S3-17 (Run 721)

where, S : SCTF

3 : Core-III

17 : Sequential number of main test

(3) Objectives of test

To obtain data for the coupling between the SCTF and the UPTF and to investigate the thermo-hydrodynamic behavior during the reflood phase in a BBR under the BE conditions

(4) Type of test

An integral reflooding test simulating a BBR under BE conditions

2. Test Description

2.1 Test Facility[4]

The SCTF was originally designed to study two-dimensional effects on thermal hydraulics during the reflood phase in a PWR core with full length radius.[2],[3]

Flow diagram of the SCTF is shown in Fig. 2.1. The SCTF is simulating a 200% cold-leg-large-break with a simplified primary system and can be operated at the system pressure less than 0.6 MPa. It consists of a pressure vessel, an intact loop, a broken loop at the pressure vessel side, and a broken loop at the steam-water separator side.

Figure 2.2 shows a vertical cross section of the pressure vessel. The pressure vessel includes a simulated core, an upper plenum with its internals, a lower plenum, a core baffle region and a downcomer. The configurations of the upper plenum structure and the end box simulate those of a 1,300 MWe class GPWR as practically as possible.

The core is full-height, full-radius and one-bundle width one. The core flow area scaling ratio is 1/24 to a typical 1,300 MWe class GPWR. 1,888 electrical heater rods are installed in the core. Dimensions of a heater rod is 10.7 mm in diameter and 3,613 mm in heated length simulating those of PWRs. The maximum available power supplied to the core is 10 MW.

The heater rods are assembled in a 16 x 16 square array bundle positioned with grid spacers. Eight bundles are installed in a row in the core, as shown in Fig. 2.2. In the SCTF, the leftmost bundle in the figure is named Bundle 1 and orderly to the right direction the bundles are named Bundle 2, 3, ..., 8. Since the downcomer and the hot leg are connected to Bundle 8 side, Bundle 1 and 8 sides are corresponding to the central and the peripheral sides of PWRs, respectively. The core and the upper plenum are enveloped by honeycomb thermal insulators with wall plates to minimize the wall thermal effects.

The ECC water can be injected into the lower plenum, the cold leg and the upper plenum in the SCTF. Since the SCTF has no injection port in the hot leg, the hot leg injection of ECC water in PWRs with the combined-injection-type ECCS was substituted by the upper plenum injection. The ECC water can be injected into the upper plenum from both top and side wall.

Description of the SCTF Core-III is presented more in detail in Appen-

dix A.

2.2 Test Conditions and Sequence

The test conditions were selected to simulate the reflooding phenomena under the BE conditions for a 200 % cold-leg-large-break LOCA of a BBR-type PWR. The bases for the test conditions are summarized in Sec. 2.3. Table 2.1 shows the planned and the measured test conditions. The top view of a BBR plant and its ECCS are shown in Fig. 2.3.

Figure 2.4 shows the conceptual initial set-up of the facility for Test S3-17. The ECC water was injected into the lower plenum (*i.e.* gravity feed mode) instead of the cold legs and downcomer. Orifice diameters for the steam-water separator side broken cold leg and the pump simulator are 86.4 and 173.7 mm, respectively. No orifice is inserted into the pressure vessel side broken cold leg and the intact cold leg. The water in the steam-water separator was drained to the containment tank II to keep the maximum water level in steam-water separator at 1.1 m.

Figure 2.5 shows the sequence of Test S3-17. In this figure, the time when the maximum clad temperature reached 570 ^{o}C is defined as 0 s. The pressure in the containment tank II was aimed to be kept constant at 0.37 MPa by controlling discharge rate of the steam through the blow valve to the atmosphere after 0 s. The ECC water was injected into the lower plenum after 0 s. The ECC water injection rate was set at 105 kg/s initially. The water temperature was set at 100 ^{o}C. The core power was initially set at 7.59 MW and was decreased to simulate the decay as shown in the figure.

2.3 Bases for Test Conditions

Bases for test conditions are summarized in Table 2.2. They are given by FRG and are proprietary ones. Therefore, no further information is available on the bases of these values.

The ECC water injection rate was determined as follows based on the given core flooding rate:

(1) 0 ~ 5 s

$$\dot{m}_F = \frac{A_{Core}}{A_{PV}} \dot{m}_{ECC} = \frac{0.250}{0.502} \dot{m}_{ECC} = 0.5 \dot{m}_{ECC}$$

(2) 5 ~ 21 s

$$\dot{m}_F = 0.4\ \dot{m}_{ECC}$$

assuming similar steam binding effect as Test S3-9[5].

(3) After 21 s

$$\dot{m}_F = \dot{m}_{ECC}$$

where, $\dot{m}_F$ and $\dot{m}_{ECC}$ are core flooding rate and ECC water injection rate. A_{PV} and A_{Core} are flow areas of pressure vessel and core, respectively.

The loop flow resistance for the present test is higher than that evaluated for a BBR. That is,

$$\frac{K}{A^2} = 2040\ m^{-4} \qquad (cf.\ 1152\ m^{-4} \text{ for a corresponding BBR})$$

where,

$$\frac{K}{A^2} = \Delta P \ / \ \frac{\dot{m}^2}{2\rho}$$

expecting the smaller flow resistance of the loop side in the SCTF than that evaluated for a BBR.

2.4 Measured Boundary Conditions

The major measured test conditions are listed in Table 2.1. Table 2.3 shows the chronology of events occurred during the test. Figures 2.6 through 2.10 show the measuerd boundary conditions of the test.

There observed no significant differences between the planned and the measured except for the pressure in the containment tank II. The pressure was controlled at 0.37 MPa by venting the excessive steam. However, the pressure was higher during 80 ~ 140 s because of significant steam ganeration in the core, so that the pressure reached at 0.47 MPa at 103 s, as shown in Fig. 2.6.

Table 2.1 Test conditions for Test S3-17

Item	Planned	Measured
Containment pressure (MPa)	0.37	0.34 ~ 0.47
Initial structure temperature (K)	>414	>421
Initial lower plenum water level (m)	0.24	0.20
Initial lower plenum water temperature (K)	373	410
Initial core power (MW)	7.59	7.59
Radial power profile (MW) Bundles 1 - 5	1.05	1.05
Bundles 6 - 8	0.78	0.78
Maximum clad temperature at BOCREC (K)	873	928
Maximum clad temperature at ECC injection initiation (K)	843	877.9
ECC water injection location	Lower plenum	
ECC water injection rate (kg/s)		
Acc (maximum)	105	98
LPCI	9.3	9.4
ECC water temperature (K)	373	366 ~ 410

Table 2.3 Chronology of events for Test S3-17

Event	Time (s)
Core power "ON"	0
Initiation of ECC water injection	78.3
Initiation of reflood (BOCREC)	90.2
Whole core quench	290.2

Table 2.2 Summary of bases of test conditions

Pressure	0.37 MPa
Power	
Initial power	7602 kW
Radial power profile	1.11:1.11:1.11:1.11 :1.11:0.82:0.82:0.82

Decay curve

t^* (s)	0	15	45	75	175	400	515
Power (kW)	7602	6777	6075	5699	4963	4074	1753

Initial clod temperature	873 K (600 °C)
ECC water	

Core flooding rate

t^* (s)	0	5	15	21	50
Velocity (m/s)	0.21	0.21	0.074	0.060	0.037

Water temperature	373 K (100 °C)
Loop flow resistance	$K/A^2 = 2.0\ m^{-4} \times 24^2$(scaling factor) $= 1152\ m^{-4}$
Initial structure temperatures	higher than 414 K (141 °C)

* t = 0 is reflood initiation and 27 s after the break

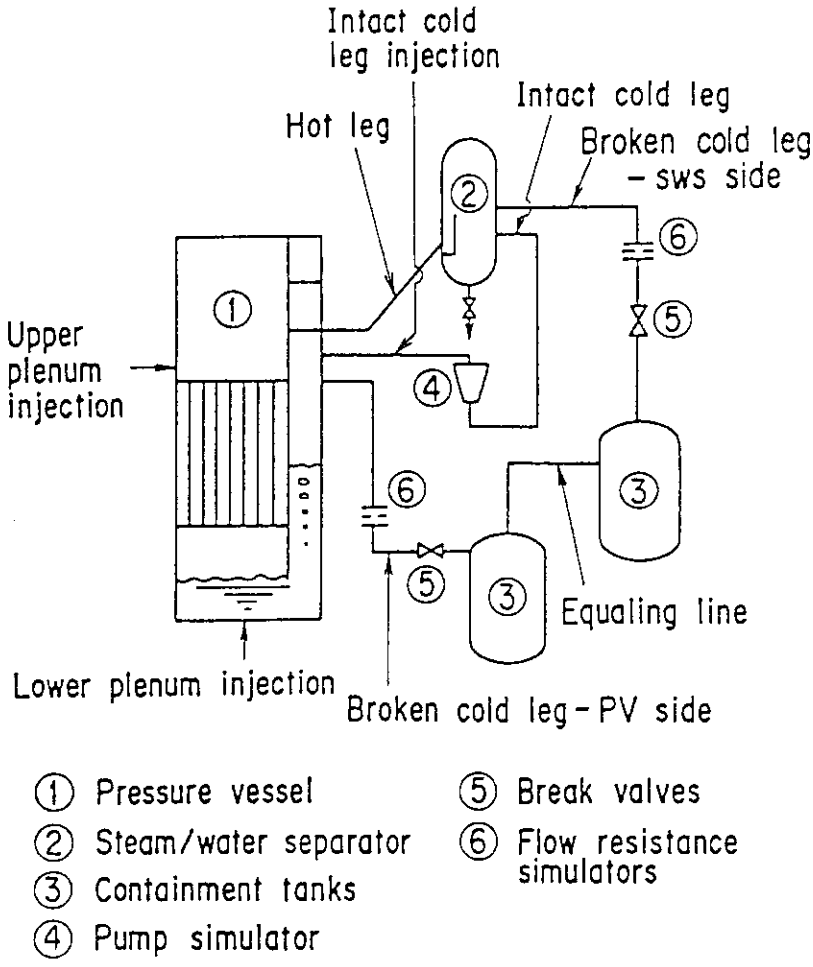

Fig. 2.1 Flow diagram of SCTF

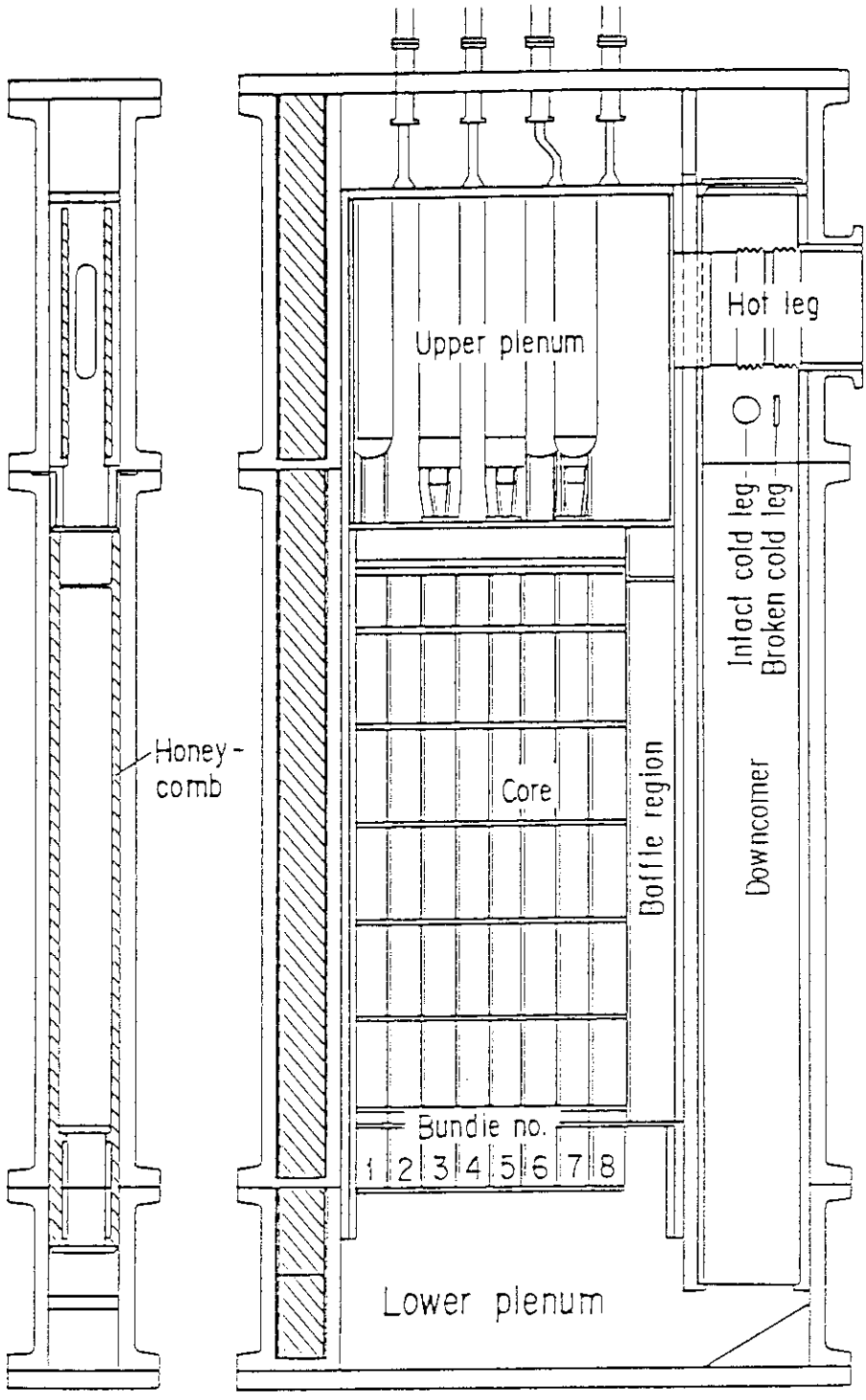

Fig. 2.2 Vertical cross section of pressure vessel

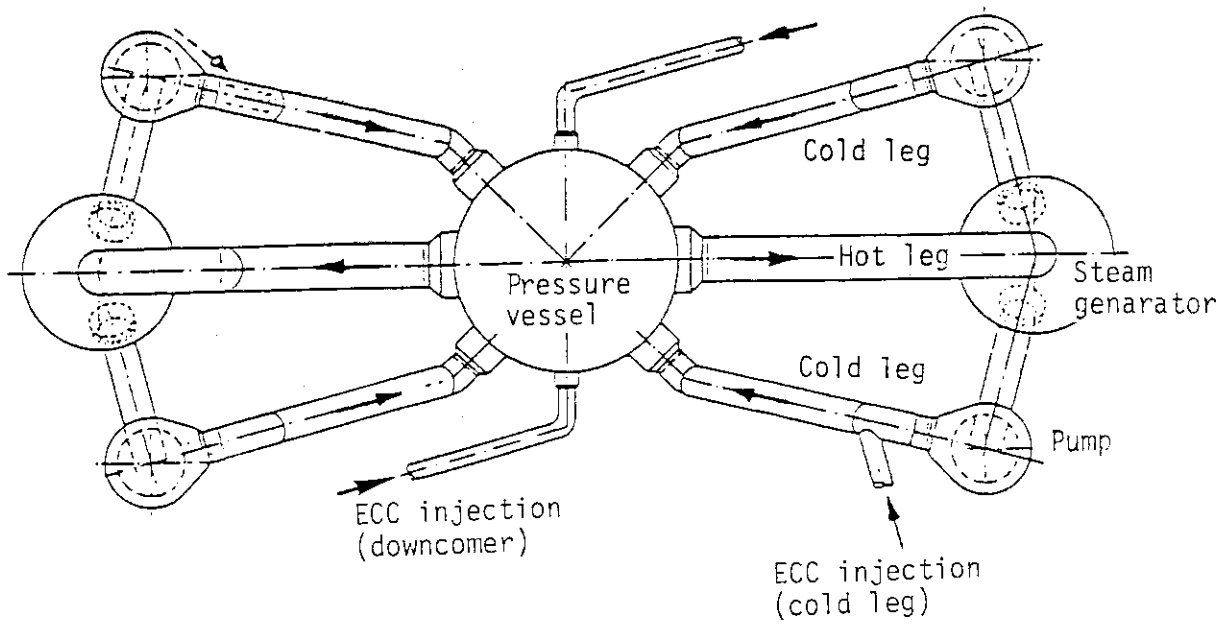

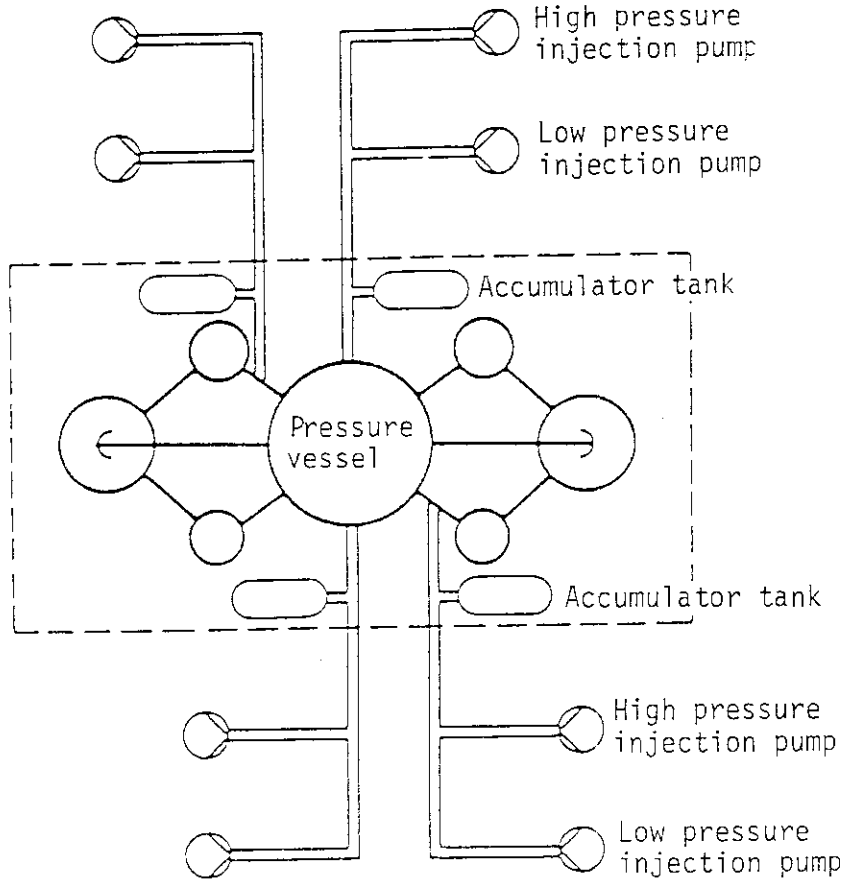

Fig. 2.3 Top view of BBR plant and its ECCS

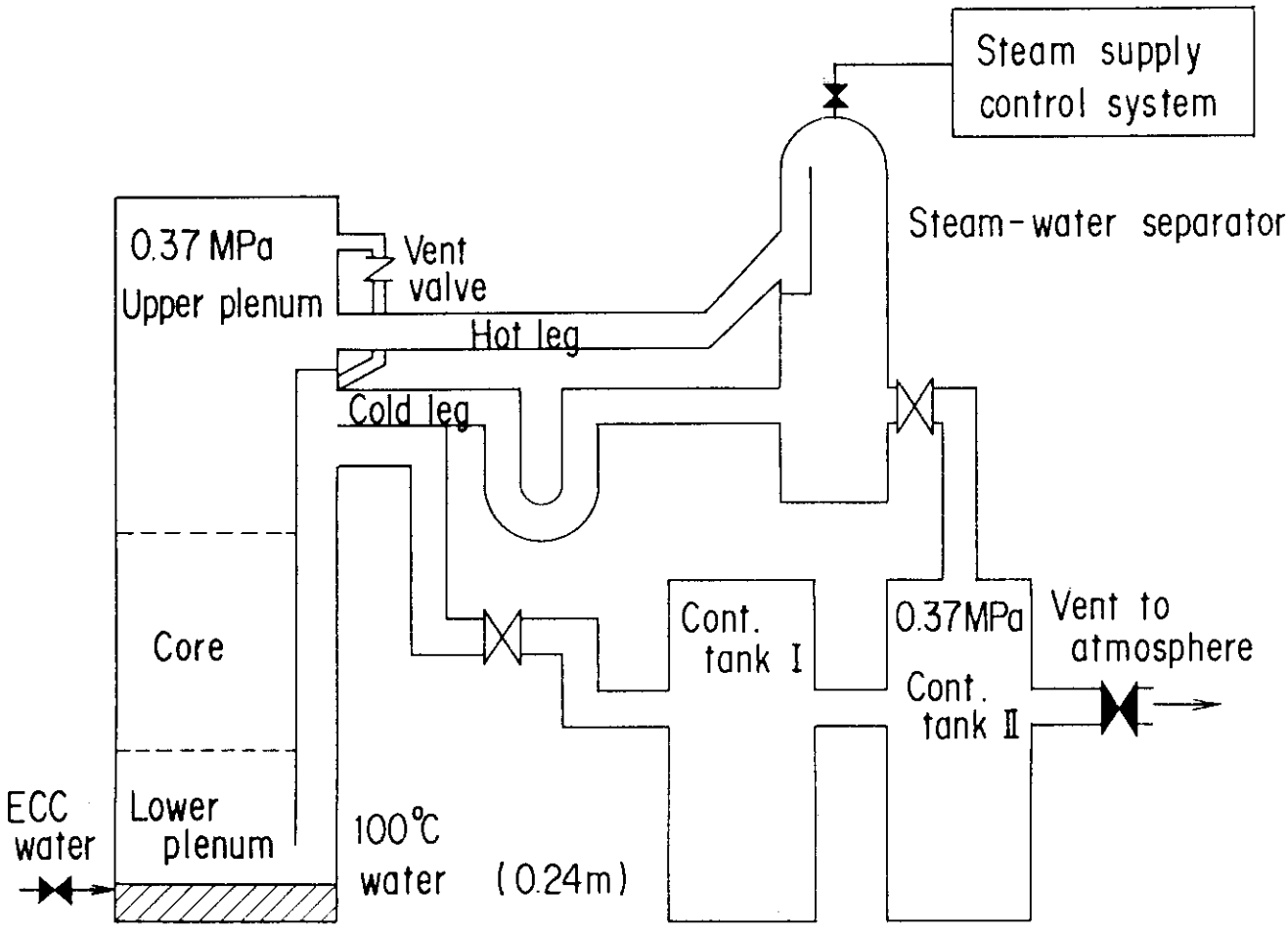

Fig. 2.4 Initial set-up of Test S3-17

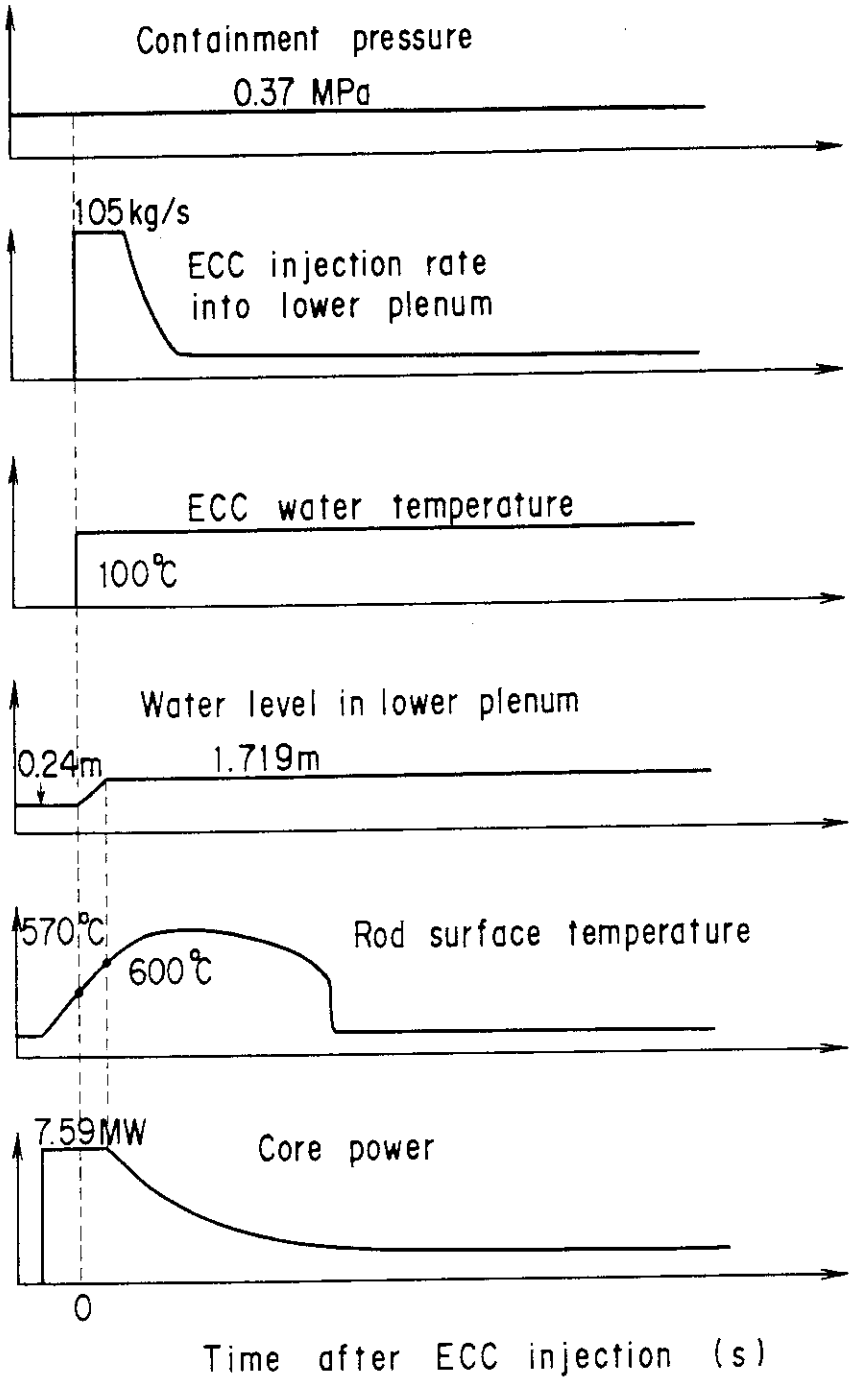

Fig. 2.5 Sequence for Test S3-17

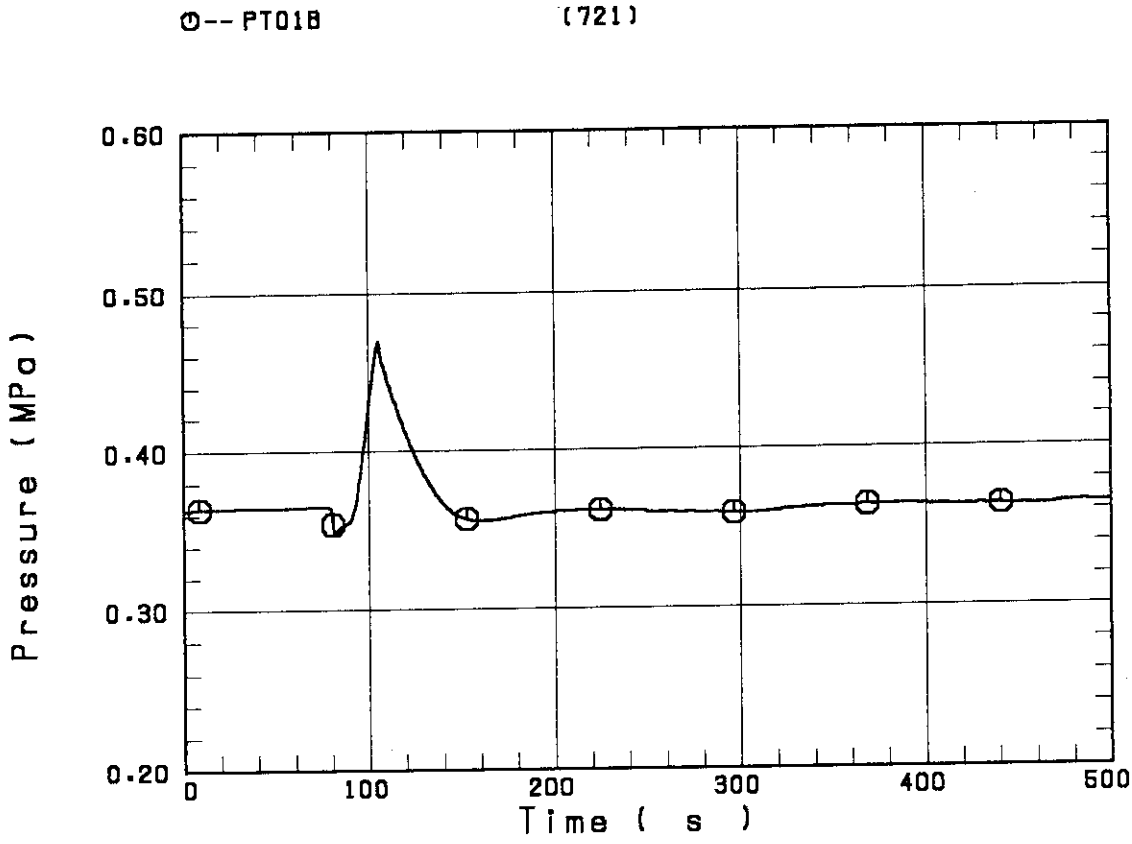

Fig. 2.6 Pressure of containment tank II

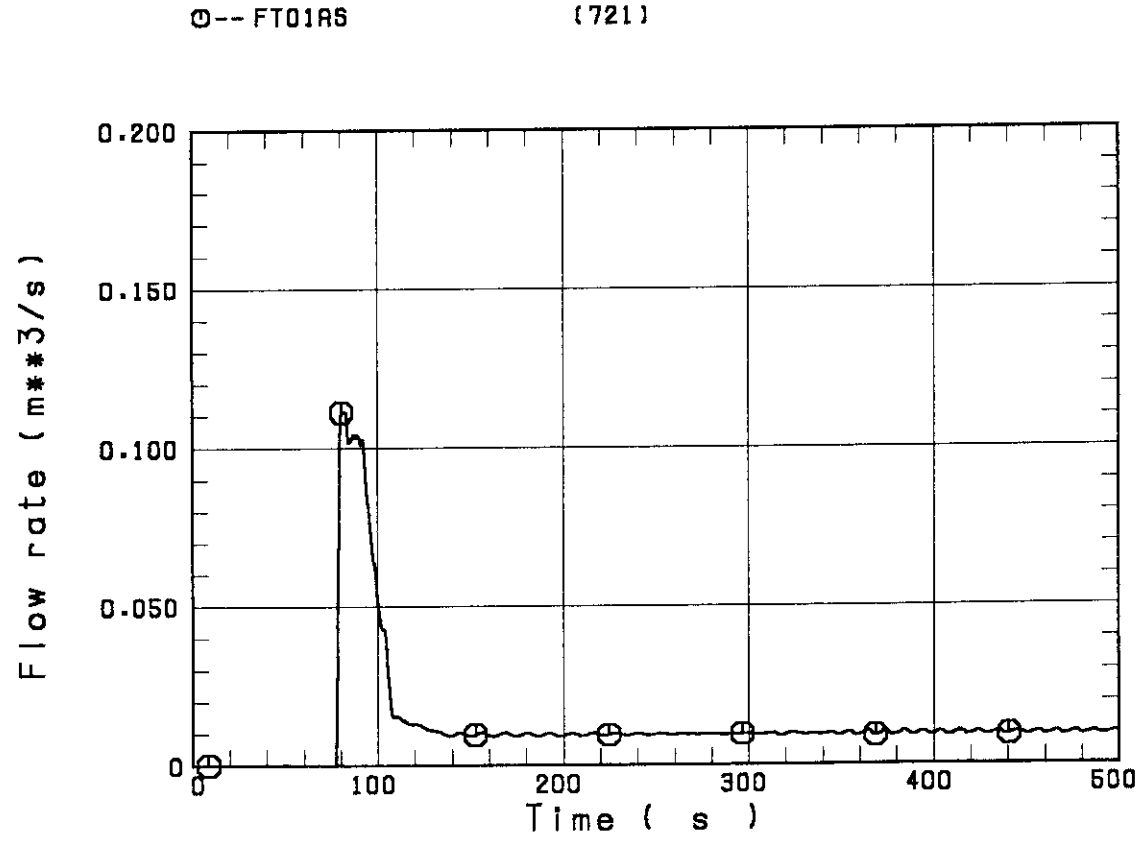

Fig. 2.7 ECC injection rate into lower plenum

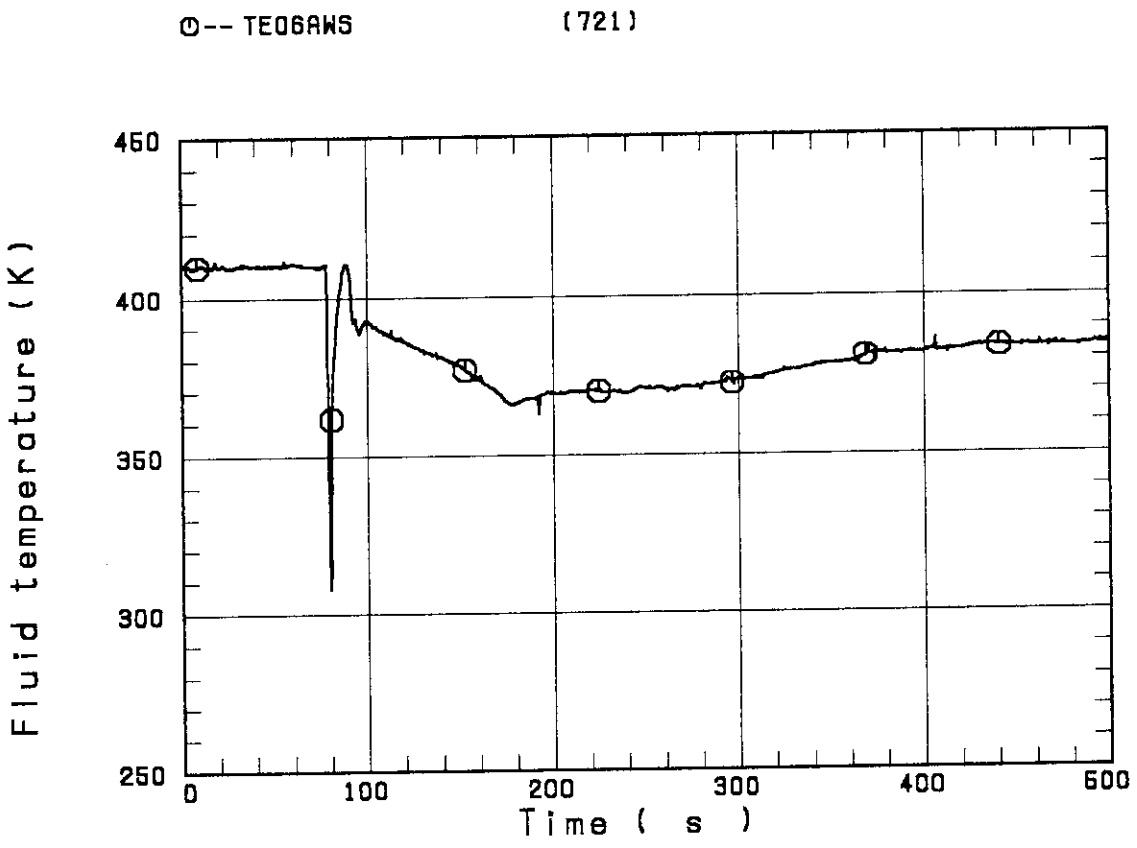

Fig. 2.8 ECC water temperature

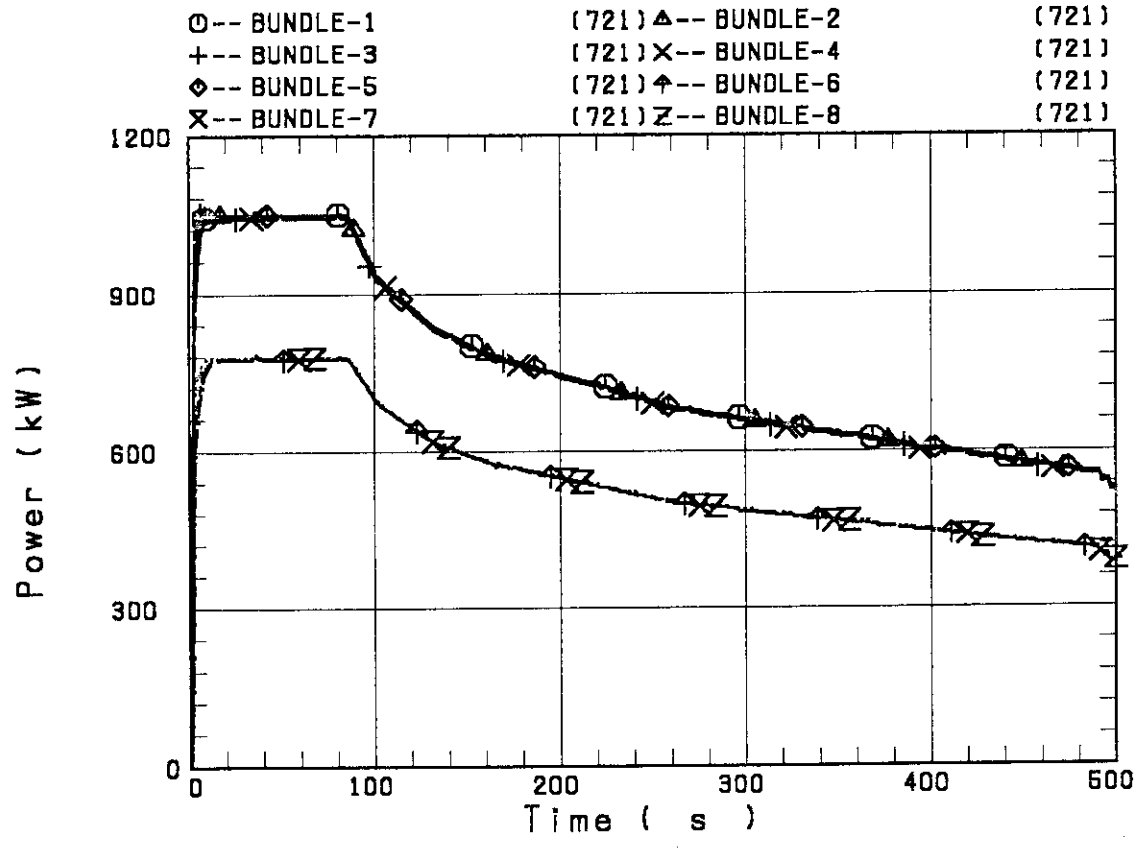

Fig. 2.9 Supplied core power

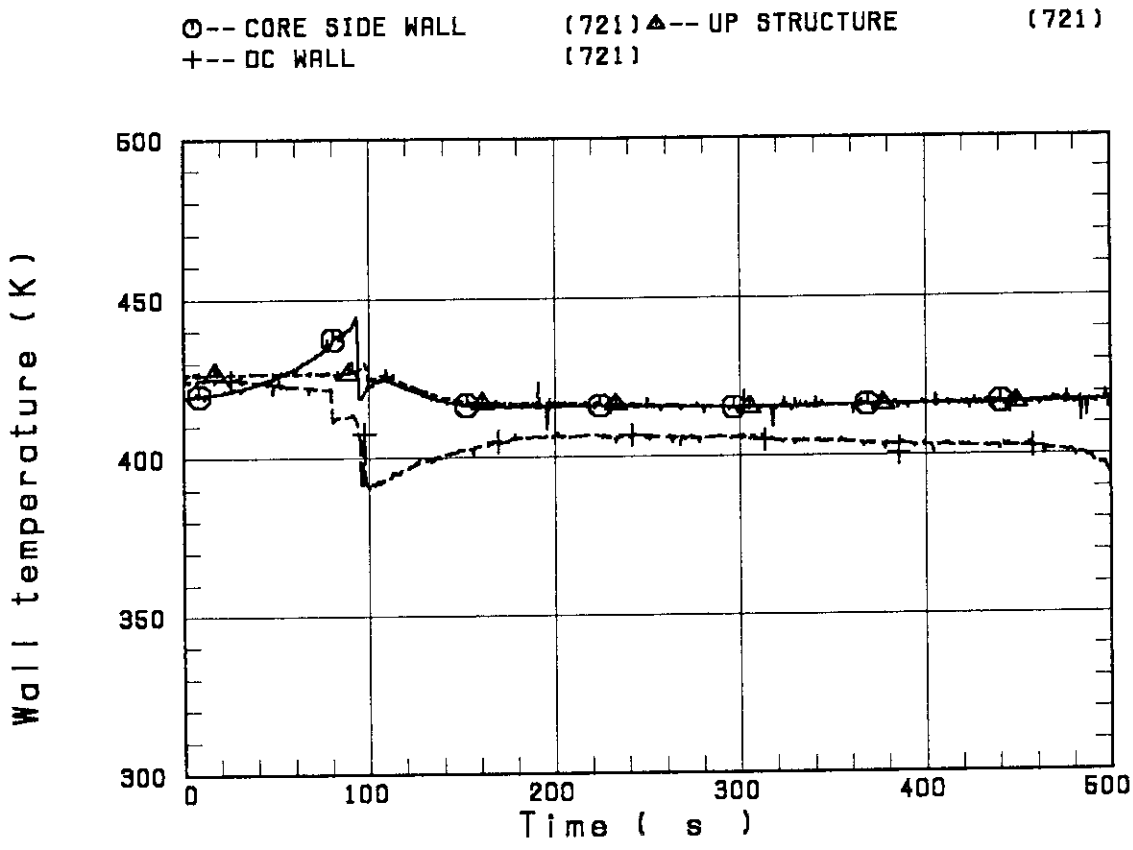

Fig. 2.10 Structure temperatures in pressure vessel (core inner side wall, upper plenum structure and downcomer inner wall)

3. Test Results and Discussion

3.1 Achieved Core Flooding Rate

As mentioned in Sec. 2.3, the core flooding rate for the present test was given by FRG and, based on this, the ECC water injection rate was determined by JAERI. The achieved ECC water injection rate is compared with the planned in Fig. 3.1. They are in good agreement. However, when they are compared in the other time axis of "Time after flood" (*i.e.* time after reflood initiation) as in Fig. 3.2, they are not in good agreement and the achieved injection rate is significantly smaller during the Acc period. This discrepancy was caused by the wrong estimation of the time required to fill the lower plenum. This time was estimated to be 8 s, whereas it took 11.9 s in the test. Therefore, the initiation of reflooding was later by 3.9 s and resulted in the smaller ECC water injection rate during the Acc period than planned.

Figure 3.3 shows a comparison of core flooding rate. The measured one was calculated from the ECC water injection rate by subtracting the water accumulation rates in the downcomer and the excess core flow area, *i.e.* between the rod bundles and the core barrel. The data for the time integration of the core flooding rate shows that the total mass flooded the core was the same as the planned value up to 15 s and the difference between them is 15 % at 200 s, when the whole core quenched (see, Table 2.3). The difference in the LPCI period was resulted from the water accumulation in the downcomer, which was estimated to be zero before the experiment (see, Sec. 2.3(3)).

3.2 Mass Balance in System

Figure 3.4 shows the arrangement of the mass flow and water accumulation measurements in the system. Arrows in solid line and broken line indicate flows of water and steam, respectively. Tag-IDs with asterisk (*) mean estimated data with measured ones. Tag-IDs started with "F" give mass flow rates and ones with "G" give water accumulation rates. Figures 3.5 through 3.8 show the steam mass flow rates in the intact cold leg (Tag-ID: FT01CS), the broken cold leg steam-water separator side (FT01LS), the connecting pipe between containment tanks (FT01ES) and the vent line from the containment tank II to the atmosphere (FT01VS). Figure 3.9 also shows the steam mass

flow rate in the broken cold leg pressure vessel side (FTBCL) calculated from the steam velocity measured with the spool piece turbine meter.

Figure 3.10 shows a comparison of FTBCL and FT01ES. They are in good agreement after 160 s. Around 100 s, FT01ES gives much lower value. This is considered to be resulted from steam accumulation in the containment tank I. Although there exists the difference around 120 s, which is considered to be caused by the depressurization of the containment tanks (see, Fig. 2.6), the data of FTBCL are adopted as the mass flow rate in the broken cold leg pressure vessel side. Figure 3.11 shows a comparison of FTBLOW and FT01VS. FTBLOW is the steam mass flow rate going into the containment tank II and is defined as :

$$FTBLOW = FT01LS + FT01ES \quad (1)$$

They are qualitatively in good agreement.

The estimated steam mass flow rate through the vent valve (FTVVS) is shown in Fig. 3.12. It is defined as :

$$FTVVS = FTBCL - FT01CS \quad (2)$$

The maximum value is 1.8 kg/s at 125 s and the value decreases monotonously till 320 s. The increase after 320 s is resulted from the decrease of FT01CS (Fig. 3.5) and is not considered to give correct steam mass flow rate. Figure 3.13 shows a comparison of FTVVS, FTHLS and FTUPS. FTHLS and FTUPS are the estimated steam mass flow rates in the hot leg and the upper plenum, respectively, and are defined as :

$$FTHLS = FT01CS + FT01LS \quad (3)$$

$$FTUPS = FTHLS + FTVVS = FTBCL + FT01LS \quad (4)$$

Figure 3.14 shows a comparison of the estimated maximum core steam generation rate (TSG_*) and the tie plate steam mass flow rate (FTTPS). FTTPS is calculated as follows with the steam mass flow rates measured with the tie plate flow modules, referring the behavior of tie plate differential pressures.

$$FTTPS = 4 \times (UD01F41\text{-}S) + 3 \times (UD01F51\text{-}S) + (UD01F81\text{-}S) \quad (5)$$

As shown in the figure, they are rather in good agreement. A comparison among FTUPS, FTTPS and TSG_* is given in Fig. 3.15. They are rather in good agreement within $\pm$ 20 % difference between 120 s and 300 s, which is the main core cooling period in the test. Therefore, the estimated steam mass flow rate through the vent valve is considered to be correct with $\pm$ 20 % er-

ror between 120 s and 300 s.

The core flooding rate (FTCORE) shown in Fig. 3.3 is estimated as follows neglecting the water supply from the upper plenum to the downcomer through the vent valve. Namely,

$$FTCORE = FTECC - GDC - GCA \quad (6)$$

where, FTECC is the ECC water injection rate, and GDC and GCA are the water accumulation rates in the downcomer and in the additional area around the core, respectively. However, there is a possibility that the water in the upper plenum flows through the vent valve to the downcomer and floods the core. Therefore, it is important to estimate the water mass flow rate through the vent valve. Although there installed vent line spool piece provided by the USNRC, it did not seem to work well and no meaningful data was obtained. Accordingly, a mass balance calculation has been performed to obtain the water mass flow rate through the vent valve (FTVVW). Considering the mass balance on the core flooding rate (FTCORE) :

$$FTCORE = GC + FTTPW + FTTPS \quad (7)$$

$$\text{and, } FTCORE = FTECC + FTVVW - GCT1 - GDC - GCA \quad (8)$$

where, GC and GCT1 are the water accumulation rates in the core and the containment tank I, respectively, and FTTPW is the tie plate water mass flow rate calculated in the similar manner as FTTPS (Eq.(5)). The value for GCT1 is nearly zero until 500 s in the present test. From Eqs.(7) and (8),

$$FTVVW = GC + FTTPW + FTTPS - FTECC - GCT1 - GDC - GCA \quad (9)$$

The calculated value is shown in Fig. 3.16. Until 196 s the value is negative. This is considered to be resulted from errors of the measured values and suggests no water flow through the vent valve until 196 s. After this time the value increases gradually and becomes over 20 kg/s after 340 s. The core flooding rate calculated with Eq.(7) is shown in Fig. 3.17 comparing with the data shown in Fig. 3.3 (Eq.(6)) with two different time axes. The difference becomes large after 130 s after the reflood initiation. By this time, the core was quenched up to about 2 m as shown in the following Section (Fig. 3.25).

3.3 System Thermo-hydrodynamic Behaviors and Core Cooling

In this section, the system thermo-hydrodynamic behaviors are investigated by comparing the data of the present test with those of another SCTF

test (Test S1-20[6]), in which the total ECC water injection rate was the closest to that of the present test but the vent valve was closed. In this way, effects of the free vent valve on system thermo-hydrodynamic behaviors can be clarified easily. Major test conditions for Test S1-20 are summarized in Table 3.1 in comparison with those for the present test.

Figure 3.18 shows a comparison of the intact loop differential pressure. The data for the present test are significantly smaller than those for Test S1-20. This is considered to be the direct effect of the free vent valve, because the mass flow rate in the primary loop becomes significantly smaller when the vent valve is open. Therefore, the figure also indicates that the vent valve was open during the reflood period in the present test. As shown in Fig. 3.13, the steam mass flow rate in the primary loop is about 2/3 of the total steam mass flow rate flowing out of the upper plenum and the rest of 1/3 flowed through the vent valve in the present test. And the steam mass flow rate in the intact cold leg, which mainly determine the intact loop differential pressure, is close to that in the vent valve as shown in Fig. 3.19. Accordingly, as shown in Fig. 3.20, the steam mass flow rate in the intact cold leg is much smaller (*i.e.* about one half) in the present test comparing to that in Test S1-20, and hence, the pressure drop is expected to be about 1/4 if the system pressure is the same. Another reason for the significantly smaller intact loop differential pressure is the difference in the system pressure shown in Table 3.1. The steam density in the present test (0.39 MPa around 100 s) is 1.52 times as large as that in Test S1-20 (0.25 MPa), and hence, the differential pressure is 1/1.52 = 0.66 times for the same mass flow rate. Therefore, the significant difference in the intact loop differential pressure shown in Fig. 3.18 is explained quantitatively.

Figure 3.21 shows a comparison of the downcomer liquid level converted from differential pressure data. The data for the present test is much smaller during the initial period. This is considered to be caused by the smaller intact loop differential pressure shown in Fig. 3.18. The difference in the downcomer liquid level is quantitatively corresponds to that in the summation of the intact loop differential pressure and the core differential pressure (Fig. 3.22) during the initial 110 s. The data for Test S1-17 increases even after 110 s. This is considered to be resulted from the additional water flow from the upper plenum through the vent valve (Fig. 3.16). Figure 3.22 shows a comparison of the core differential pressure.

During the whole reflooding transient, the data for the present test gives larger value of about 0.004 MPa (0.4 m water head). Since the difference appears during very initial period, the reason for the difference is considered to be the difference in the core flooding rate during the very initial period. Figure 3.23 shows a comparison of the upper plenum water level. The data for Test S3-17 show increase after 100 s. This is corresponding to the increase in the water mass flow rate through the vent valve mentioned above.

Comparisons of the rod surface temperature and the corresponding heat transfer coefficient at the highest power location are shown in Fig. 3.24. A comparison of the quench envelope for the peak power rod is shown in Fig. 3.25. Since the other boundary conditions for the core than the total ECC water injection rate is different a lot between the two tests, further discussion on these comparisons is not meaningful. Therefore, for only getting the feeling on the better core cooling in the present test, the core cooling for the present test is compared with that for another SCTF test (Test S3-10[7]) in the following. Test S3-10 is a representative one conducted under the BE conditions for the Westinghouse type PWRs. Major conditions for the test are presented in Table 3.2. Since the present test was also conducted under the BE conditions, many items are close to each other except for the initial clad temperature and the ECC water injection rate during the LPCI period. Figures 3.26 and 3.27 show comparisons of the rod surface temperature and the corresponding heat transfer coefficient at the peak power location. Although there exists a certain difference between the two tests, both the data show the significantly good core cooling. More precise quantitative investigation for the effects of the vent valve on reflooding behavior is given in the following Sections by using data from other SCTF tests.

3.4 Effects of Vent Valve on Reflooding Behavior

In the SCTF Core-I series, there are two tests conducted under the same nominal conditions only except for the vent valve activation. They are Tests S1-20[6] and S1-14[6](see Table 3.3). The vent valve was forced to be closed in the former, whereas free to open in the latter. The data of these two tests were already compared and the effects of the vent valve on the reflooding behavior were briefly investigated by Adachi *et al.*[6]. Accord-

ing to Ref. [6], the downcomer collapsed water level was smaller when the vent valve was open, which is the same characteristic as observed in the present test described above. The core collapsed water level for Test S1-14 was higher during the initial period. However, the effect on core cooling was a little. In the following, the effects of the vent valve on reflooding behavior will be investigated further.

Figure 3.28 shows a comparison of the intact loop differential pressure. The data for Test S1-14 are significantly smaller. This is the typical for the effect of the free vent valve. Figure 3.29 shows a comparison of the steam mass flow rate in the intact cold leg. The data for Test S1-14 are about one third, which mainly resulted in the significantly smaller intact loop differential pressure shown in the previous figure.

The downcomer collapsed water level is compared in Fig. 3.30. Although the downcomer water level is almost identical to each other up to 20 s, it becomes much smaller in Test S1-14 after that and then increases gradually in time. The core differential pressures are shown in Fig. 3.31. The data for Test S1-14 are larger during the initial period but becomes almost identical to those for Test S1-20 after 120 s. The upper plenum water level is compared in Fig. 3.32. The data for Test S1-14 is larger a little throughout the whole transient.

From Figs. 3.31 and 3.32, it is inferred that the core flooding rate is lager in Test S1-14 during very initial period (20 s) and becomes almost identical after that. Although the correct core flooding rate for Test S1-14 can not be evaluated because the fluid mass flow rate through the vent valve was not measured, the core flooding rates evaluated by neglecting the water mass flow rates through the vent valve are compared in Fig. 3.33. It shows the core flooding rate is larger in Test S1-14 during initial 20 s by about 20 kg/s and becomes almost the same after that. Judging from the downcomer liquid level data shown in Fig. 3.30, the water flow through the vent valve is inferred to start at about 160 s. Therefore, the core flooding rate for Test S1-14 is considered to increase after about 160 s. Figure 3.34 shows a comparison of the ECC water injection rate. This figure indicates the Acc injection rate was larger by about 10 kg/s in Test S1-14, although the planned value was the same. This difference is considered to be one reason for the larger core flooding rate in Test S1-14 during the initial 20 s mentioned above. However, the difference in the core flooding rate was about 20 kg/s, and hence, there should be the effect of the vent

valve.

Figures 3.35 and 3.36 show comparisons of the rod surface temperature and the corresponding heat transfer coefficient. The core cooling in Test S1-14 is better during the initial 100 s and then becomes identical resulting in the nearly identical quench time in the two tests.

As discussed above, the effect of the vent valve on core cooling is remarkable only during the initial period. In Test S1-20, the downcomer liquid level was below the overflow level from 20 s through about 400 s (Fig. 3.30). According to Adachi *et al.*[6], the effect of the vent valve on core cooling is remarkable "only when the downcomer water level cannot be kept below the overflow level without opening the vent valve". In other words, when the ECC water injection rate is so large that the the downcomer water level exceeds the overflow level without opening the vent valve, the effect of the vent valve on core cooling is remarkable. According to the investigation for the effect of the ECC water injection rate on core cooling[8], the larger ECC water injection rate results in the better core cooling as far as the downcomer water level does not exceed the overflow level. Therefore, it can be expected that the best core cooling, which can be achieved by increasing the ECC water injection rate with keeping the other conditions unchanged, is more under the open vent valve situation than under the closed vent valve situation. This is considered to be the most important benefit of the vent valve.

In the next section, the effects of the ECC water injection rate on reflooding behavior under the free vent valve situation will be investigated to confirm that the larger ECC water injection rate results in the better core cooling also under the free vent valve situation as far as the downcomer water level is below the overflow level.

3.5 Effects of ECC Water Injection Rate on Reflooding Behavior under Free Vent Valve Situation

In this section, the effects of the ECC water injection rate on reflooding behavior under the free vent valve situation are investigated by using the data of SCTF Tests S1-15[6] and S1-17[6]. In these tests, the test conditions were set to be identical only except for the ECC water injection rate as shown in Table 3.4. Figure 3.37 shows a comparison of the ECC water injection rate.

Figure 3.38 shows a comparison of the downcomer liquid level. The data for Test S1-15 are lager throughout the transient. This is mainly due to the larger ECC water injection rate in this test. Figure 3.39 shows a comparison of the core differential pressure. The data for Test S1-15 are also much larger. This suggests that the core flooding rate is much larger in Test S1-15. Since the core flooding rate including the water mass flow rate through the vent valve cannot be evaluated in these tests, the core flooding rates evaluated by neglecting the water mass flow rate through the vent valve are compared in Fig. 3.40. Figures 3.41 and 3.42 show comparisons of the upper plenum liquid level and the intact loop differential pressure, respectively. For both data, the values for Test S1-15 are larger. This is considered to be resulted from the larger core flooding rate described above.

Figures 3.43 and 3.44 show comparisons of the rod surface temperature and the corresponding heat transfer coefficient at the peak power location. These data show the core cooling is much better in Test S1-15 than in Test S1-17. Therefore, it is confirmed the core cooling is better as the ECC water injection rate is larger also under the free vent valve situation.

3.6 Discussion on Reflooding Behavior of B&W type PWRs

In the CCTF Core-II test series, two tests were conducted[9],[10] in order to investigate the reflooding behavior in a Babcock & Wilcox (B&W) type PWR of the USA, which also has the vent valves and the once-through type steam generators. However, there are some differences between a BBR and a B&W type PWR. One important point for the LOCA analysis is that the once-through type steam generators are not "lowered" one in a BBR. That is, the crossover leg is only about 2 m lower than the hot and cold legs in a BBR, whereas about 9 m lower in a B&W type PWR. Therefore, in the latter, the crossover leg is assumed to be filled or blocked with the water during the reflooding, whereas open in a BBR.

According to the analyses[9],[10] of those CCTF tests, the effect of the vent valve on core cooling is not significant and only appears in the initial period. In the CCTF tests, the ECC water injection rate was large enough to cause the overflow of the water to the break when the vent valves were closed. Therefore, based on the last discussion in Sec. 3.4, a significant improvement of core cooling is expected when the vent valves were

open. However, the results were not as expected as mentioned above. The reasons for this difference between the observed and the expected are investigated in the following.

In the CCTF tests, a lot of water was observed to overflow to the break without accumulating in the downcomer even when the vent valves were open, resulting in the lower downcomer water head than expected. This lower downcomer water head than expected in these tests is considered to be explained as follows.

In the CCTF tests, all primary coolant loops were mechanically closed in order to simulate the reflooding situation for a B&W type PWR. Therefore, the flow path from the upper plenum to the downcomer is only through the vent valves, whereas primary loops are available as well as the vent valves in a BBR. This means, in the B&W case (*i.e.* the CCTF tests), all the steam generated in the core should be exhausted to the break via the vent valves and the downcomer. This is expected to cause larger amount of carry over of the downcomer water to the break than the BBR case, especially when the downcomer water level is close to the overflow level. Therefore, in the B&W simulation tests with the CCTF, the downcomer water level is considered to be much lower than the expected, resulting in a little enhancement of core cooling.

The similar situation is also expected to take place in a BBR, when the ECC water injection rate is large enough to cause the overflow. However, the magnitude of the carryover of the downcomer water is considered to be much smaller in this case. This is because the amount of the steam exhausted via the downcomer is expected to be much less in the BBR case. That is, in the BBR case, the broken loop is also open and a large amount of the steam generated in the core can be exhausted through it. According to the results of Test S3-17 presented in Secs. 3.2 and 3.3, about one third of the steam generated in the core flows through the vent valve and another one third flows through the intact cold leg to the break. Accordingly, only two thirds of the steam generated in the core flows via the downcomer and the rest of one third flows the broken cold leg without causing any carry over of the downcomer water to the break.

Table 3.1 Major test conditions for Test S1-20

System pressure (MPa) :	0.20 ~ 0.24	(0.34 ~ 0.47)
ECC injection location :	cold leg	(lower plenum)
Maximum Acc injection rate (kg/s) :	77	(98)
LPCI injection rate (kg/s) :	8.5	(9.4)
ECC water temperature (K) :	333 ~ 336	(366 ~ 410)
Initial clad temperature at BOCREC (K) :	1087	(928)
Initial core power (MW) :	7.1	(7.57)
Vent valve situation :	closed	(free to open)

Note : Conditions for Test S3-17 are shown in parentheses

Table 3.2 Major test conditions for Test S3-10

System pressure (MPa) :	0.29 ~ 0.33	(0.34 ~ 0.47)
ECC injection location :	lower plenum	(lower plenum)
Maximum Acc injection rate (kg/s) :	100	(98)
LPCI injection rate (kg/s) :	5.3	(9.4)
ECC water temperature (K) :	335 ~ 410	(366 ~ 410)
Initial clad temperature at BOCREC (K) :	793	(928)
Initial core power (MW) :	7.78	(7.57)
Vent valve situation :	closed	(free to open)

Note : Conditions for Test S3-17 are shown in parentheses

Table 3.3 Comparison of major test conditions between Tests S1-14 and S1-20

Item	Test S1-14	Test S1-20
System pressure (MPa) :	0.20 ~ 0.24	0.24 ~ 0.24
ECC injection location :	cold leg	cold leg
Maximum Acc injection rate (kg/s) :	86.5	77.0
LPCI injection rate (kg/s) :	7.8	8.5
ECC water temperature (K) :	336 ~ 340	333 ~ 336
Initial clad temperature at BOCREC (K) :	1087	1087
Initial core power (MW) :	7.1	7.1
Vent valve situation :	free to open	closed

Table 3.4 Comparison of major test conditions between Tests S1-15 and S1-17

Item	Test S1-15	Test S1-17
System pressure (MPa) :	0.20 ~ 0.24	0.20 ~ 0.24
ECC injection location :	cold leg	cold leg
Maximum Acc injection rate (kg/s) :	85.9	28.3
LPCI injection rate (kg/s) :	8.3	5.0
Acc water temperature (K) :	339	393
LPCI water temperature (K) :	338	336
Initial clad temperature at BOCREC (K) :	1099	1144
Initial core power (MW) :	7.1	7.1
Vent valve situation :	free to open	free to open

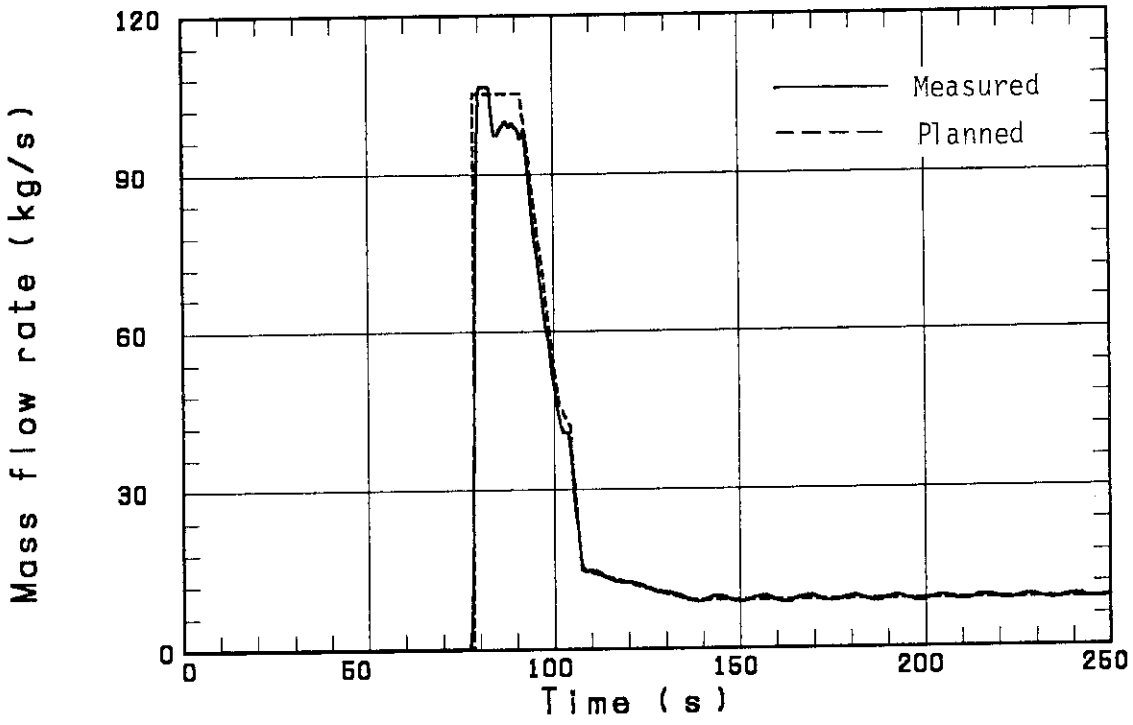

Fig. 3.1 Comparison of measured and planned ECC water injection rates in experimental time

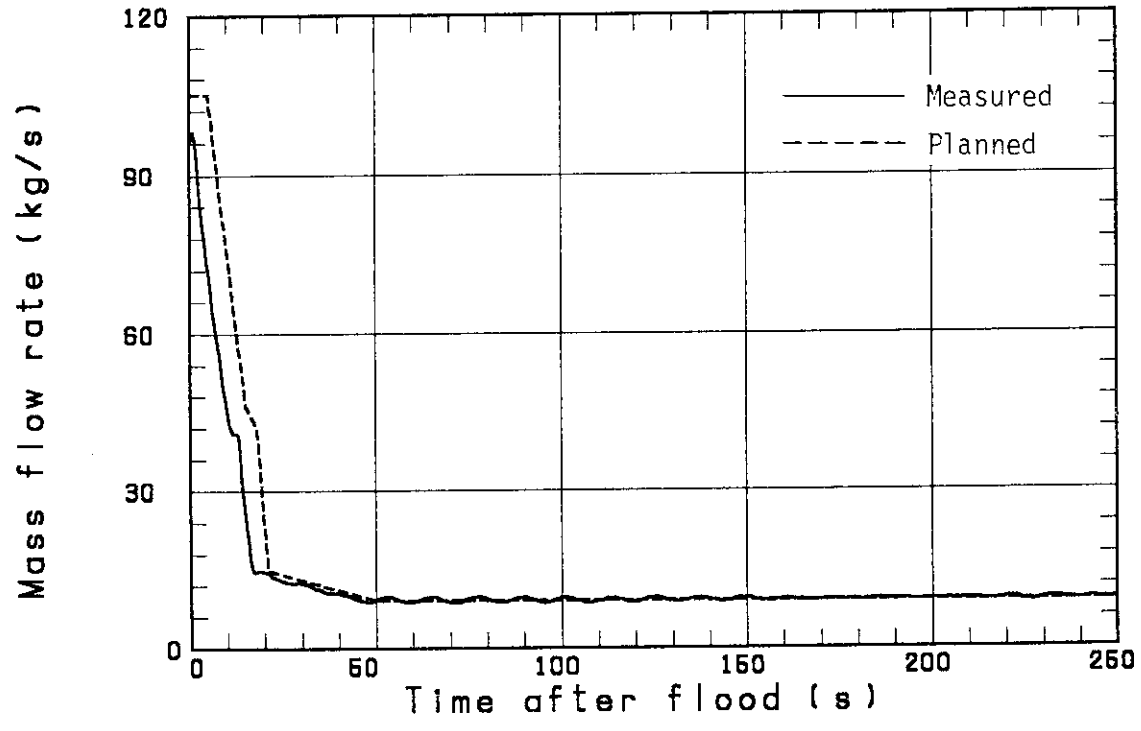

Fig. 3.2 Comparison of measured and planned ECC water injection rates in time after reflood initiation

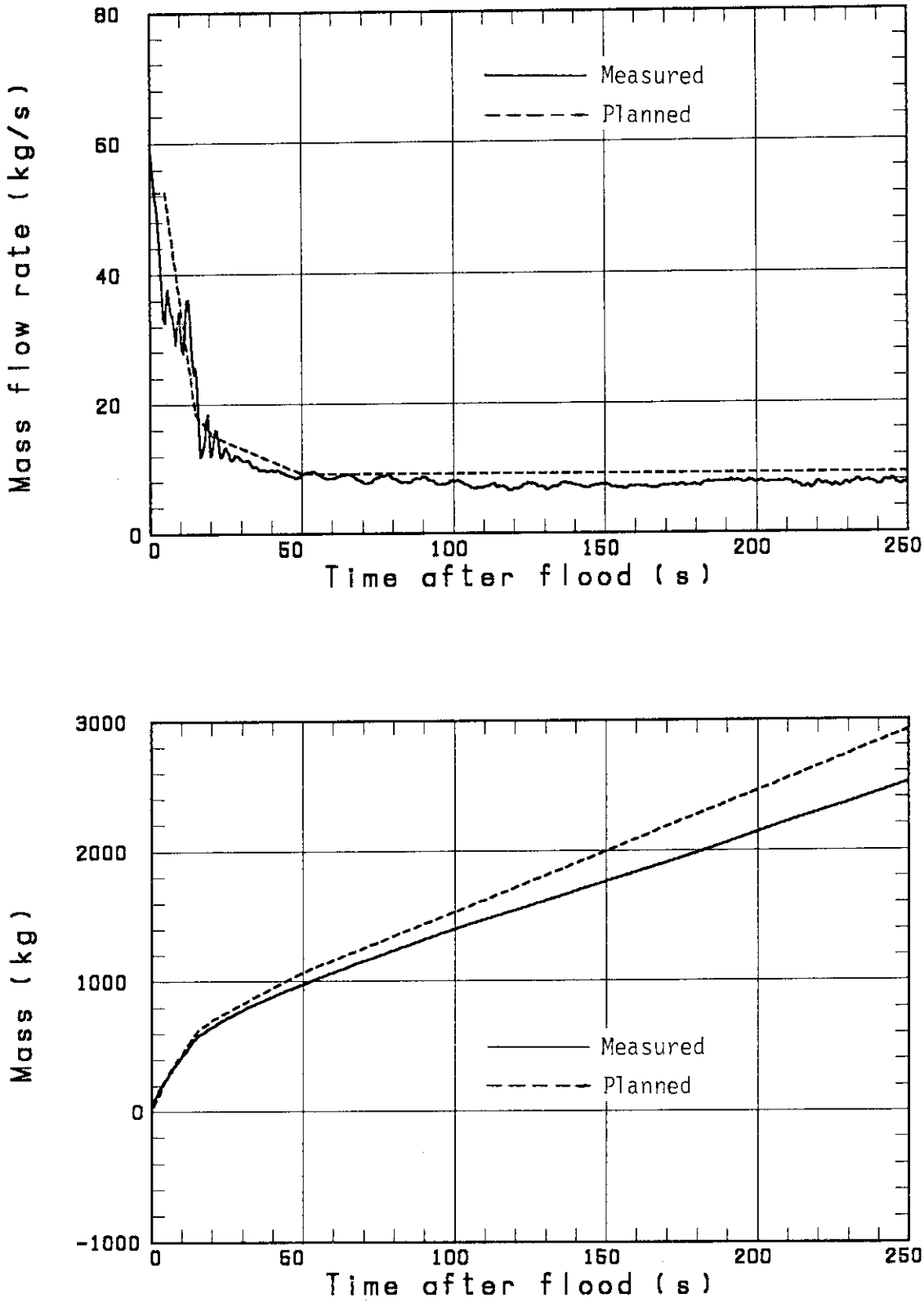

Fig. 3.3 Comparison of measured and planned core flooding rates and their time-integration

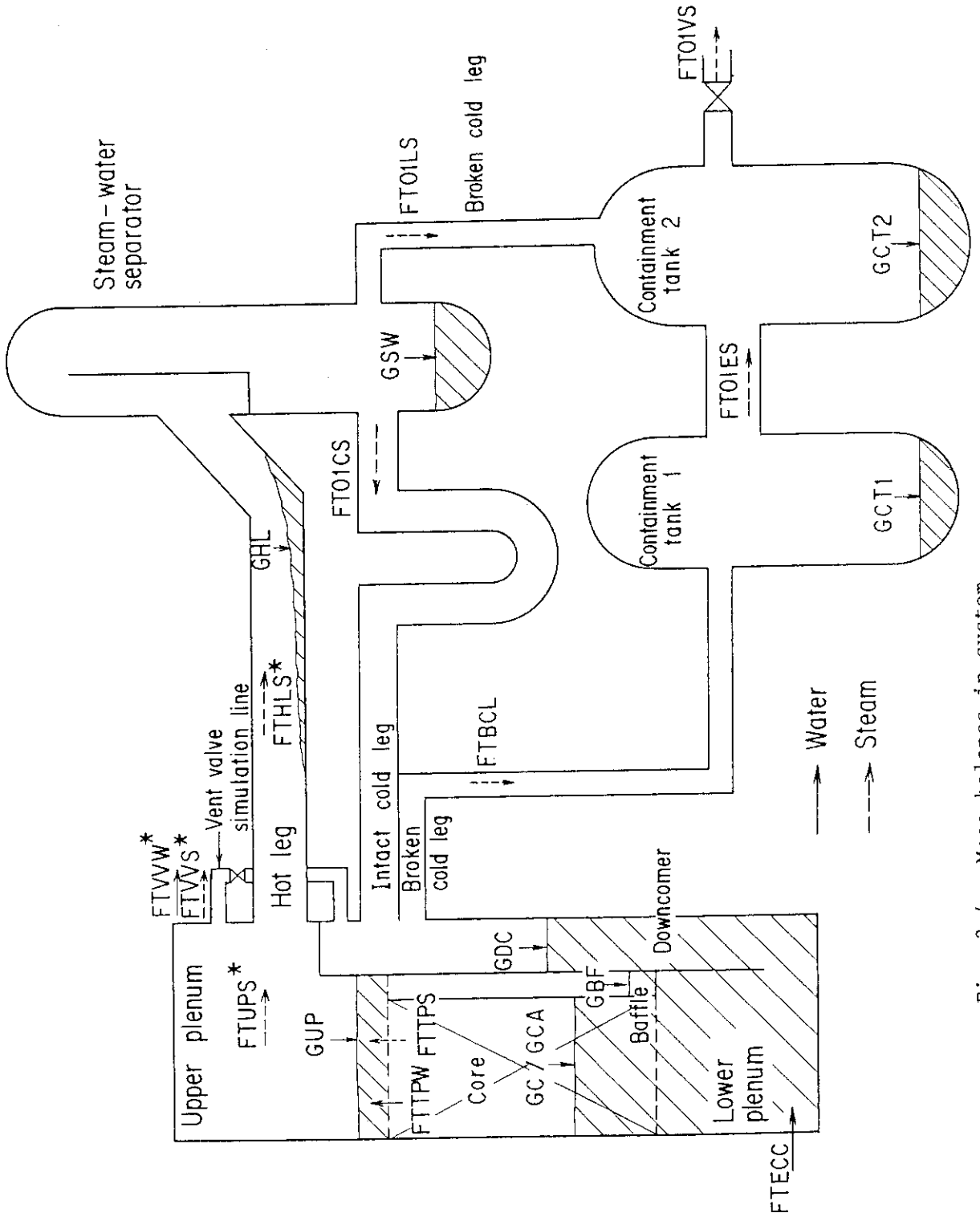

Fig. 3.4 Mass balance in system

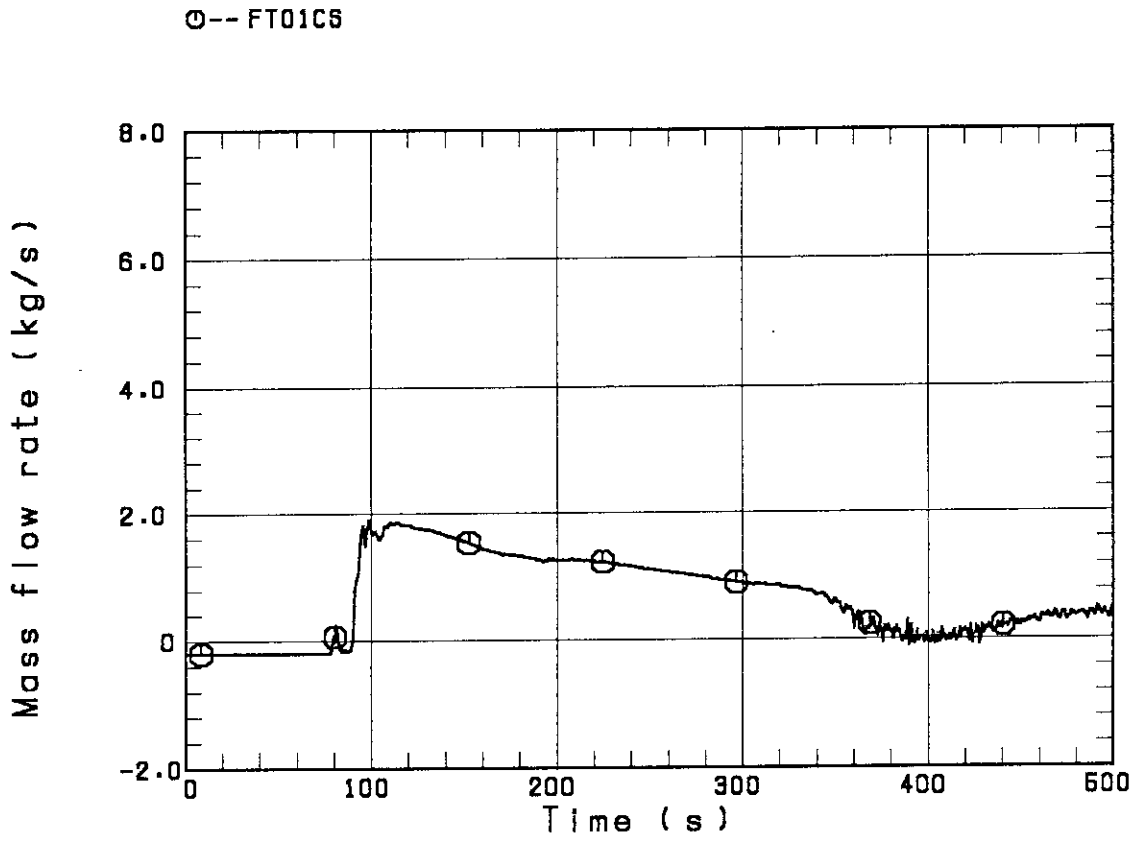

Fig. 3.5 Steam mass flow rate in intact cold leg

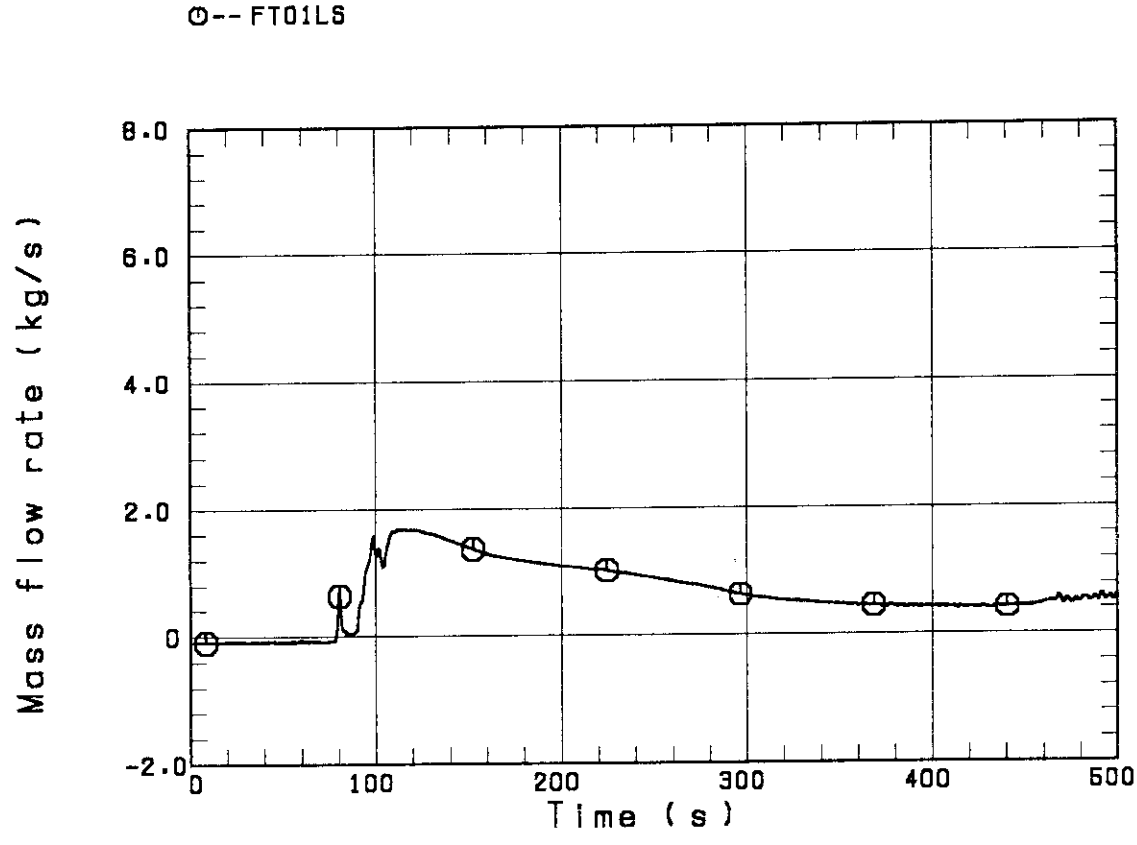

Fig. 3.6 Steam mass flow rate in broken cold leg steam-water separator side

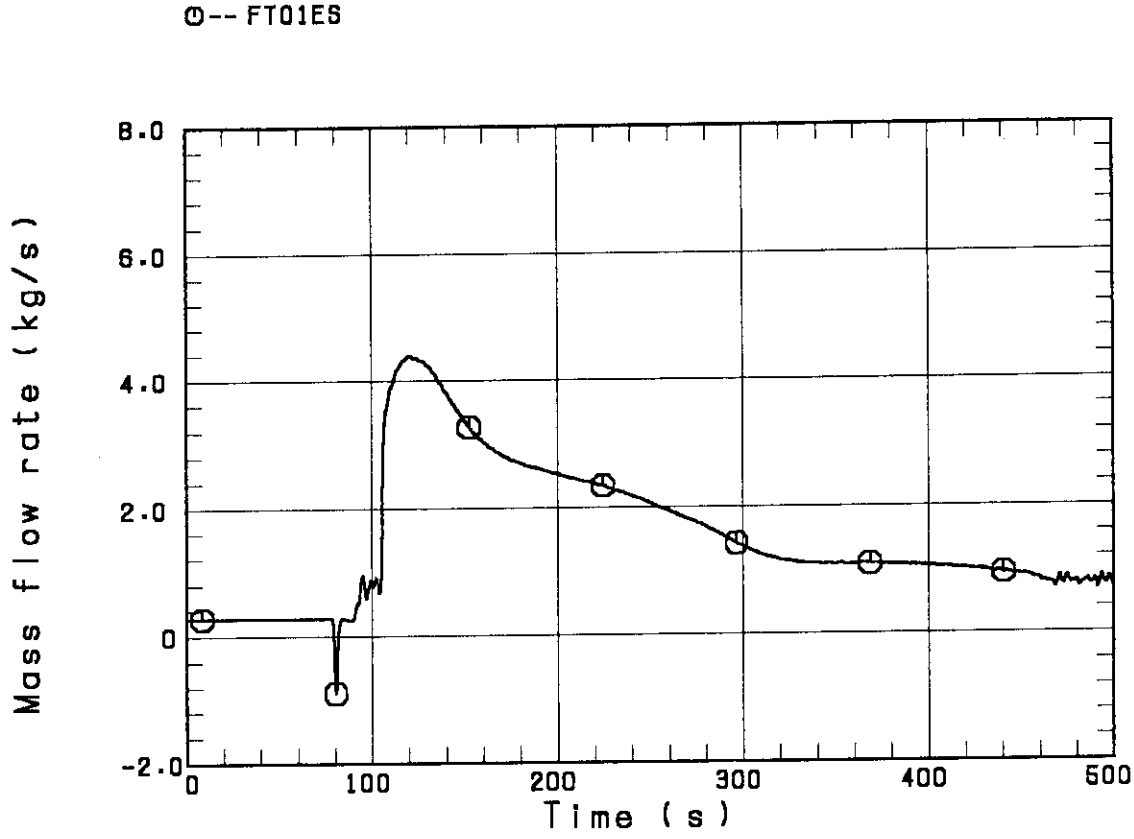

Fig. 3.7 Steam mass flow rate in connecting pipe between containment tanks I and II

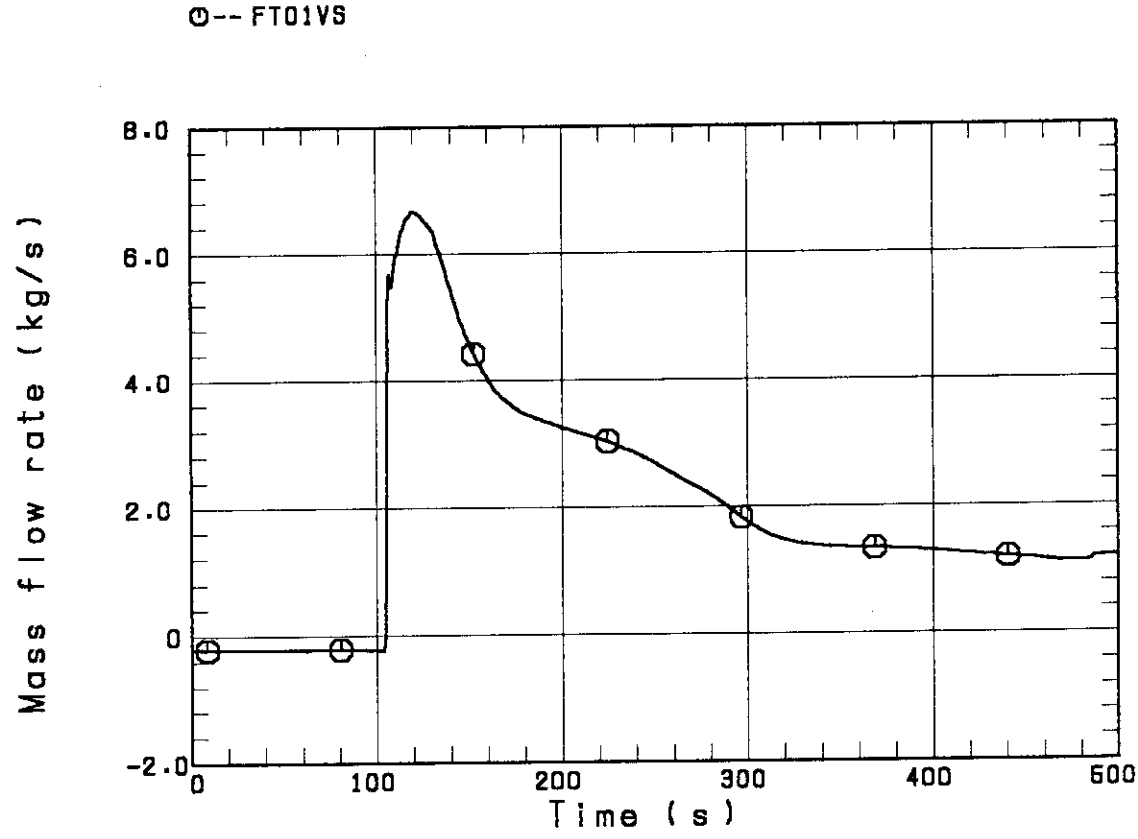

Fig. 3.8 Steam mass flow rate discharged from containment tank II to atmosphere

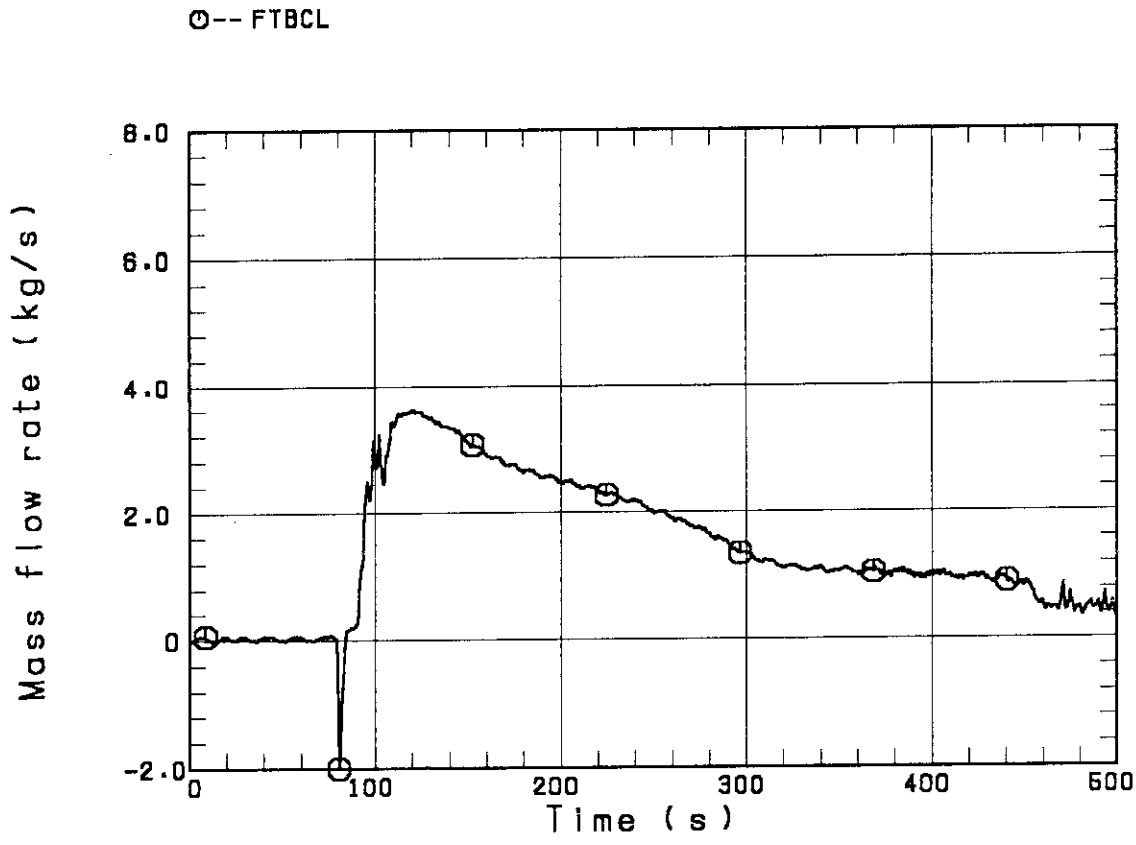

Fig. 3.9 Steam mass flow rate in broken cold leg pressure vessel side

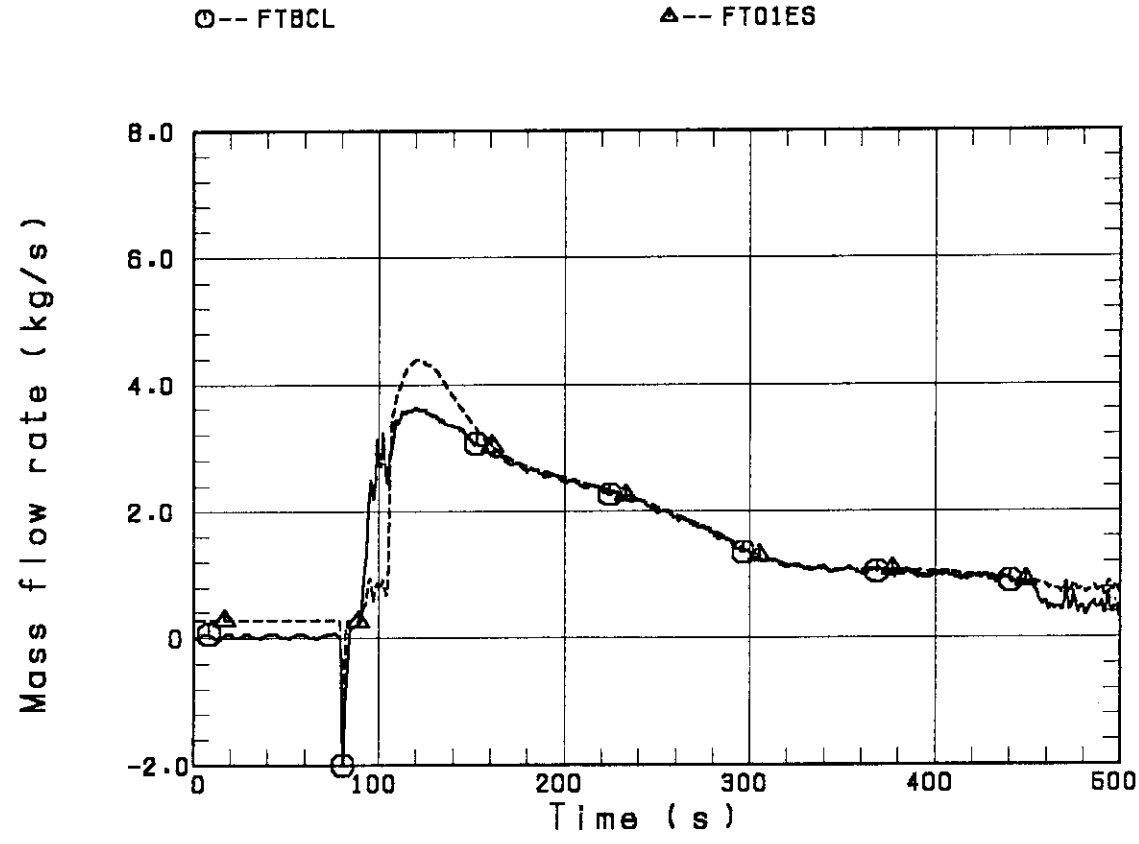

Fig. 3.10 Comparison of steam mass flow rates in broken cold leg and in connecting pipe between containment tanks I and II

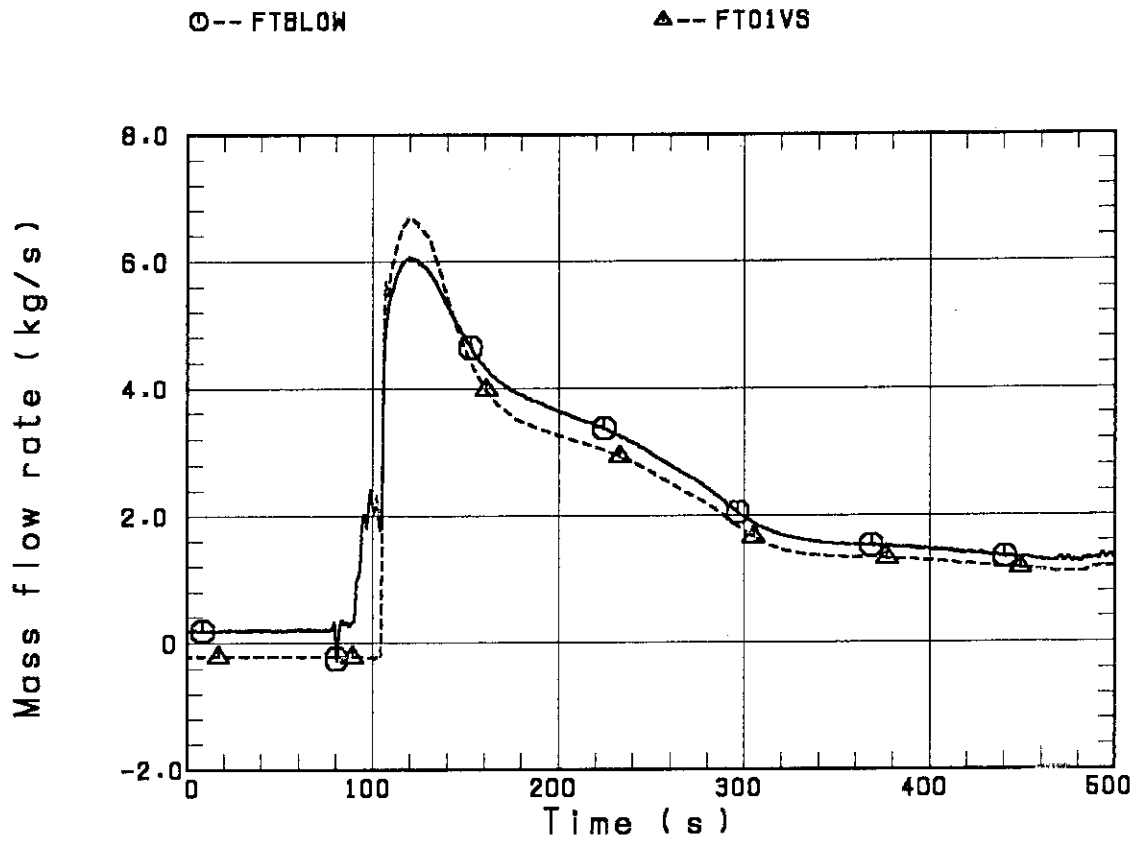

Fig. 3.11 Comparison of steam mass flow rates between flowing into (FTBLOW) and discharging out (FT01VS) containment tank II

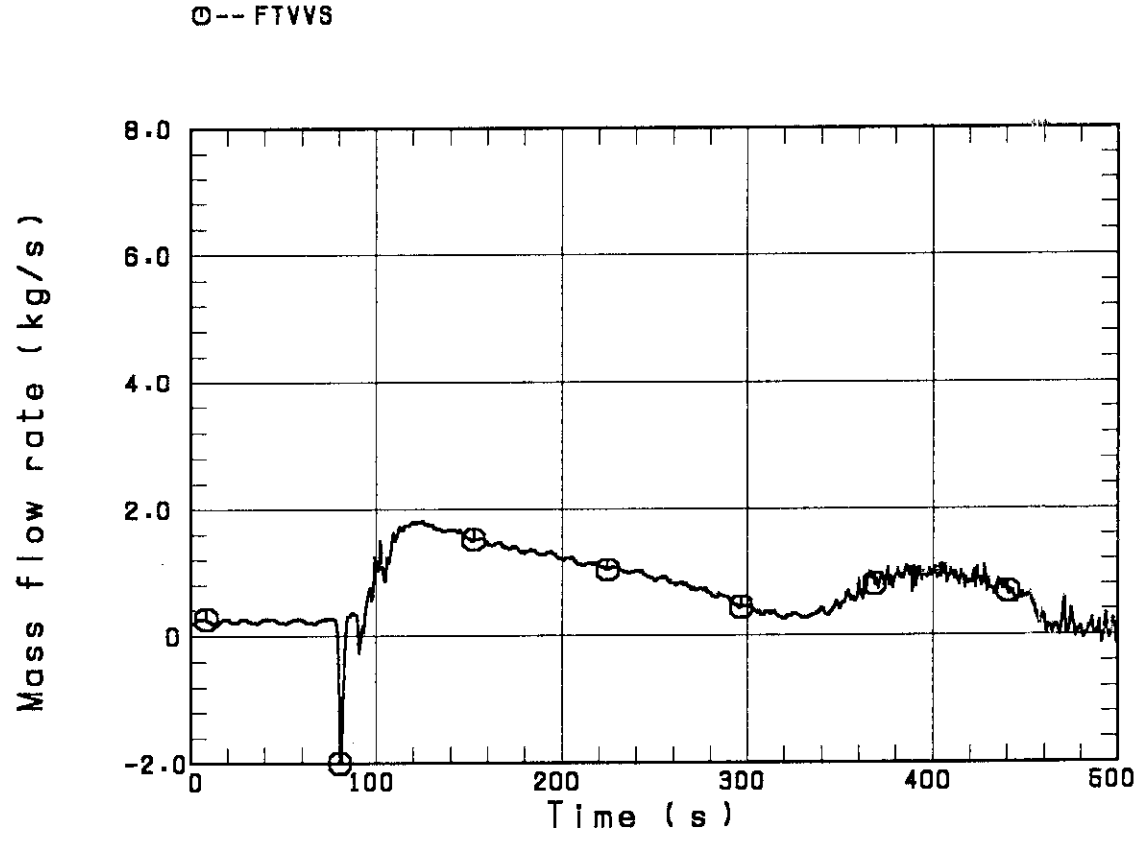

Fig. 3.12 Estimated steam mass flow rate through vent valve

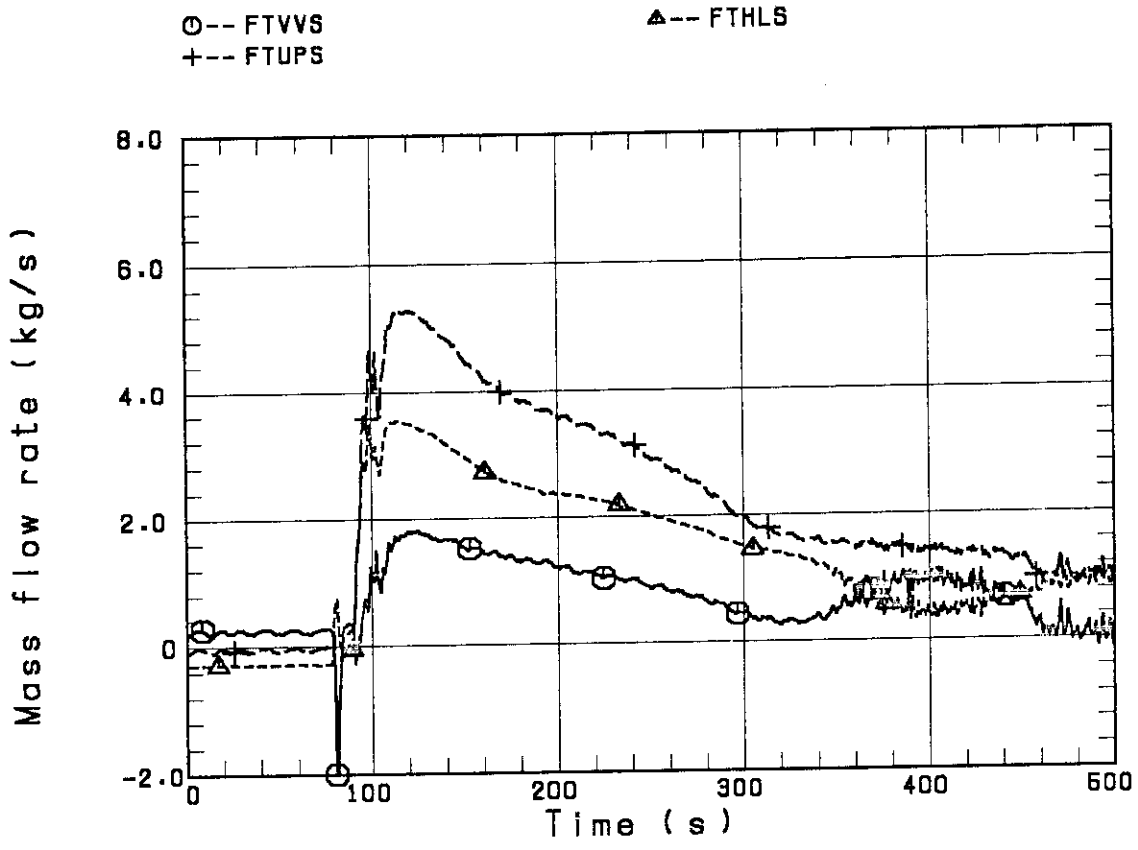

Fig. 3.13 Comparison of estimated steam mass flow rates in vent valve (FTVVS), hot leg (FTHLS) and upper plenum (FTUPS)

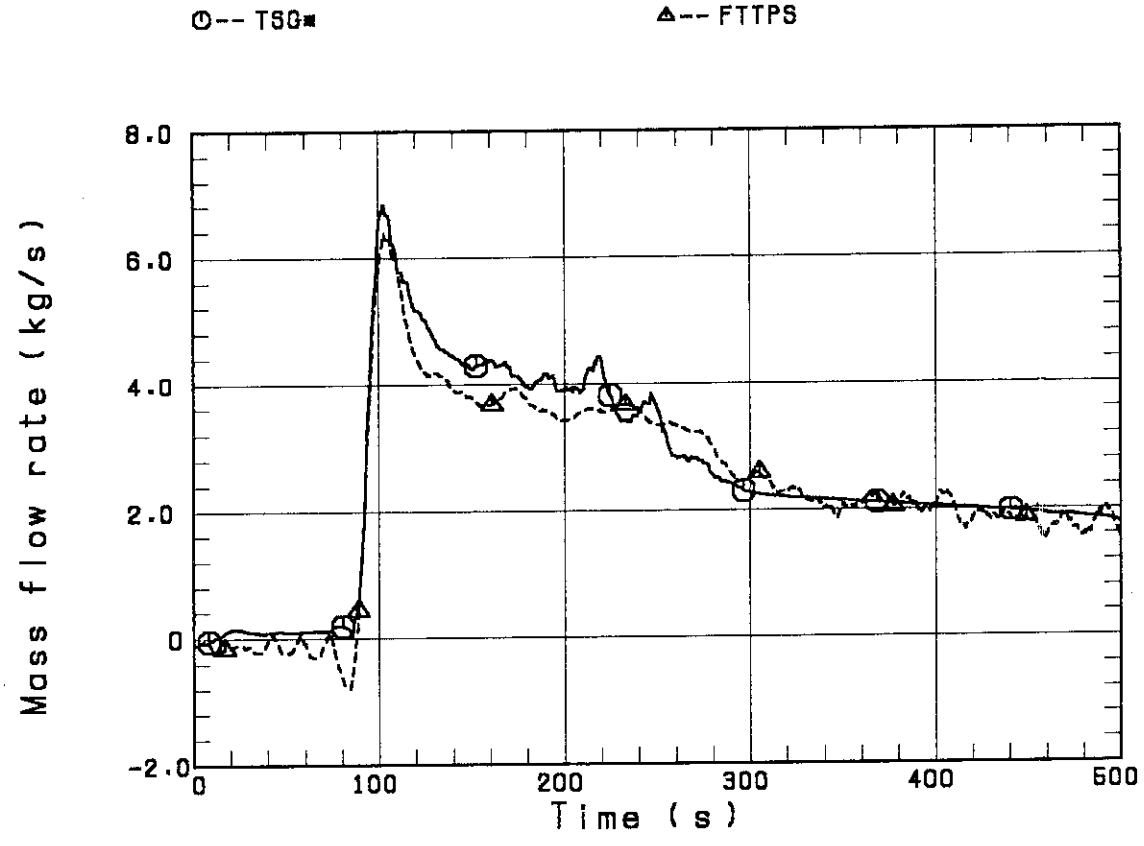

Fig. 3.14 Comparison of estimated maximum steam generation rate in core (TSG*) and tie plate steam mass flow rate (FTTPS)

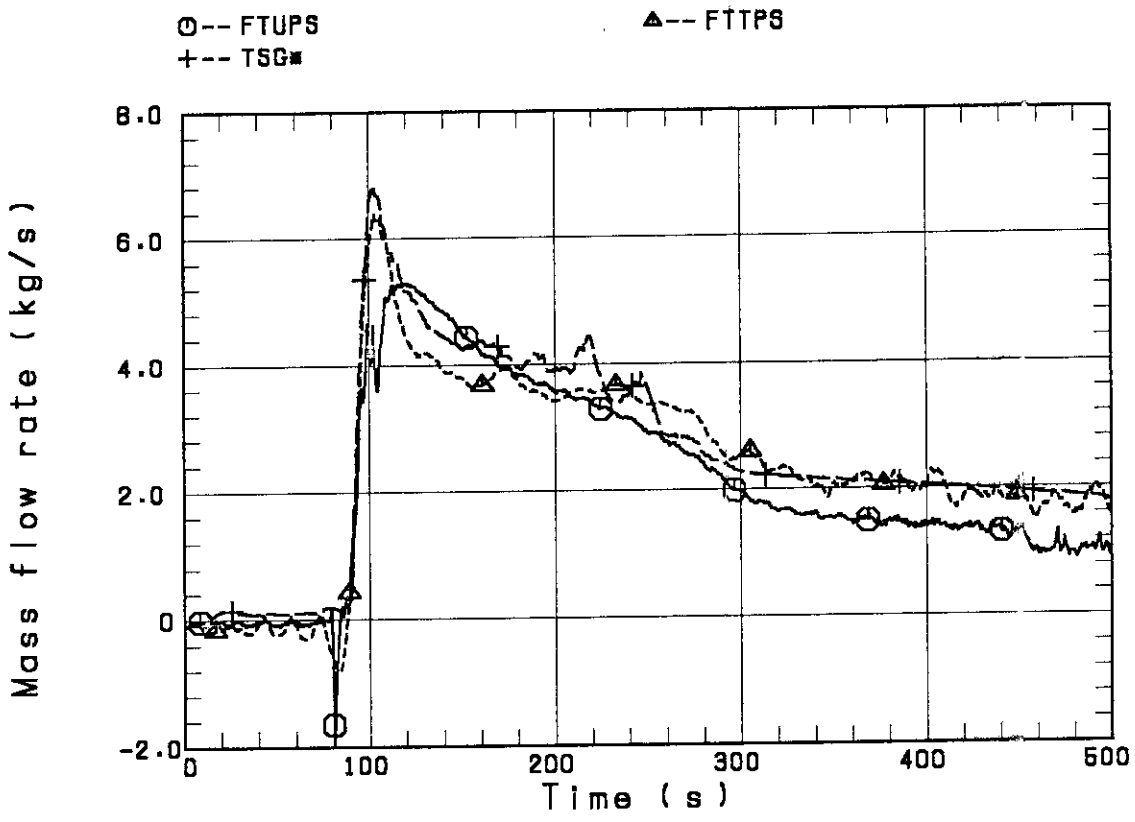

Fig. 3.15 Comparison among estimated upper plenum steam mass flow rate (FTUPS), tie plate steam mass flow rate (FTTPS) and estimated maximum core steam generation rate (TSG*)

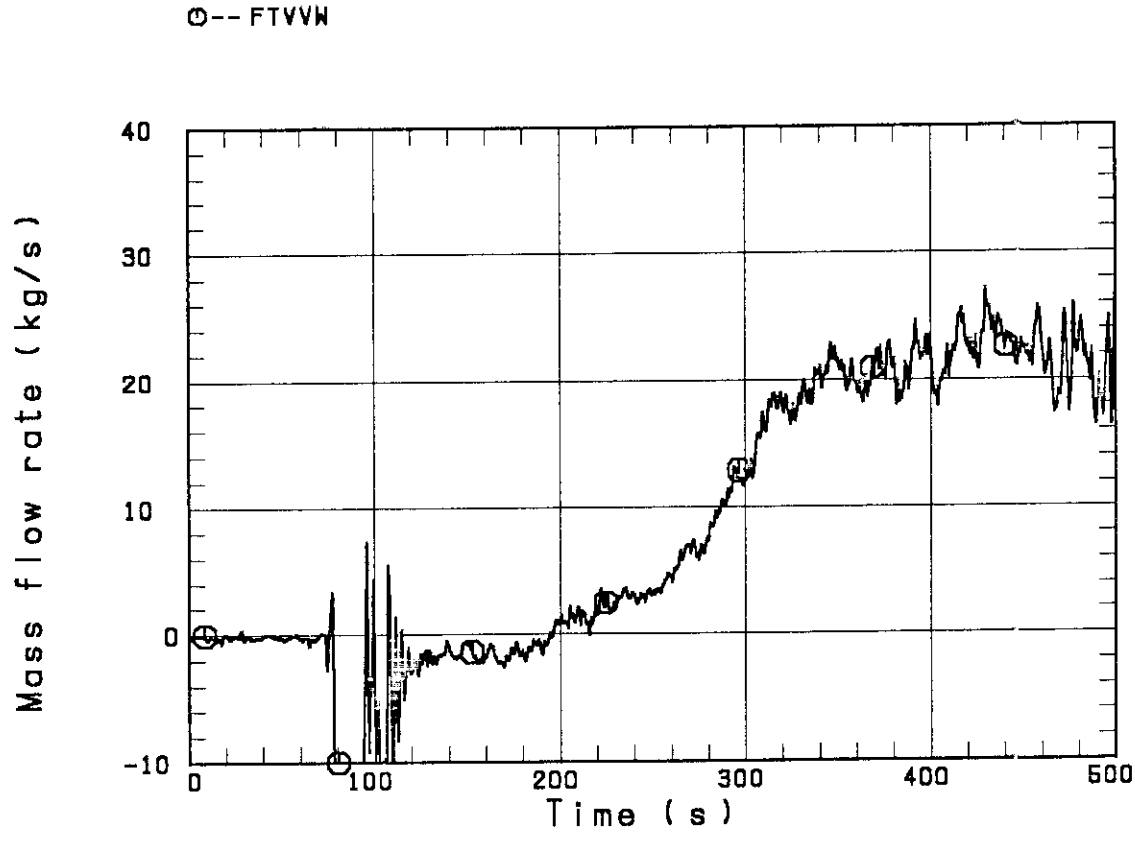

Fig. 3.16 Estimated water mass flow rate through vent valve

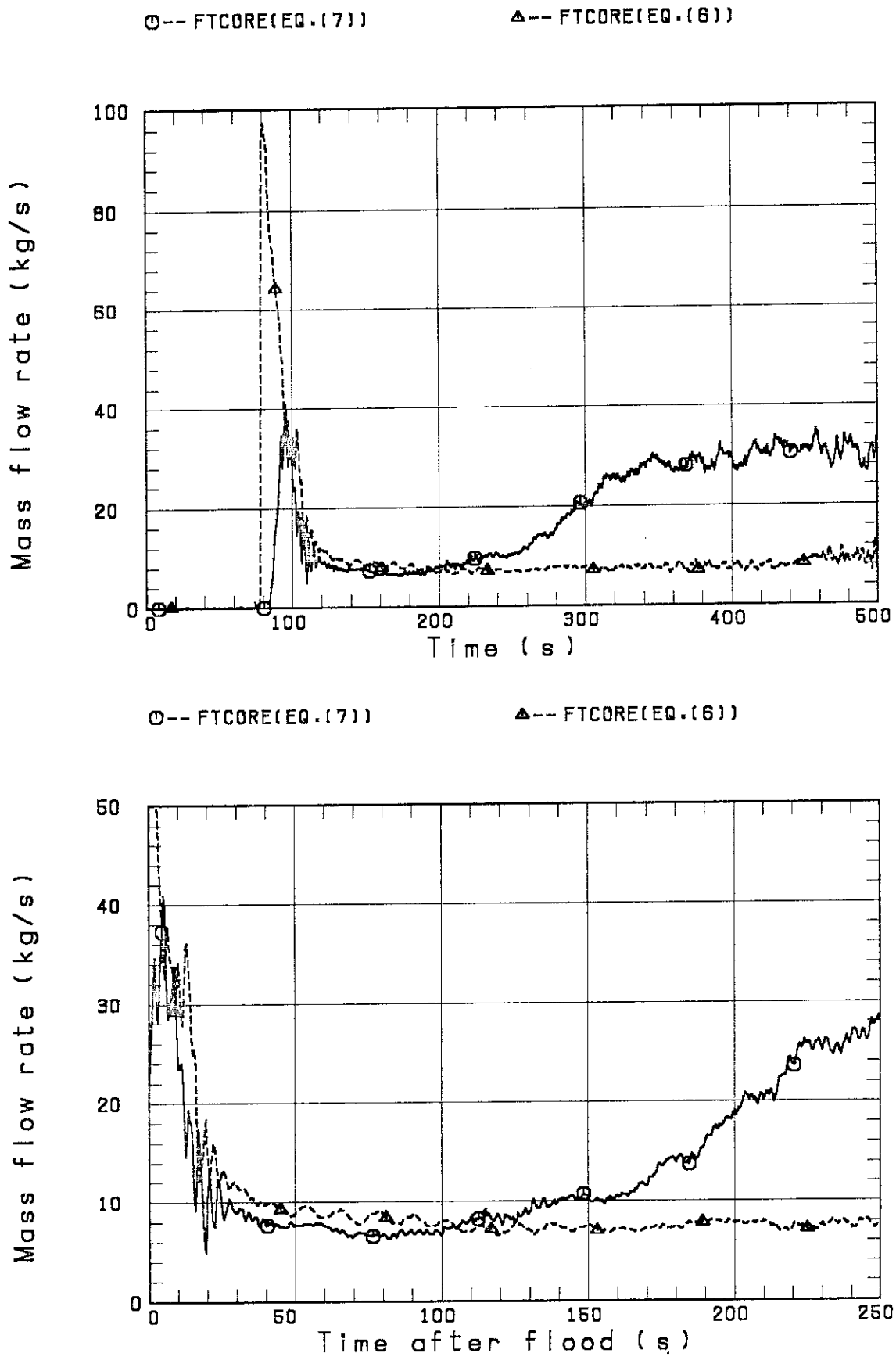

Fig. 3.17 Comparison of estimated core flooding rates with and without considering vent valve water mass flow rate

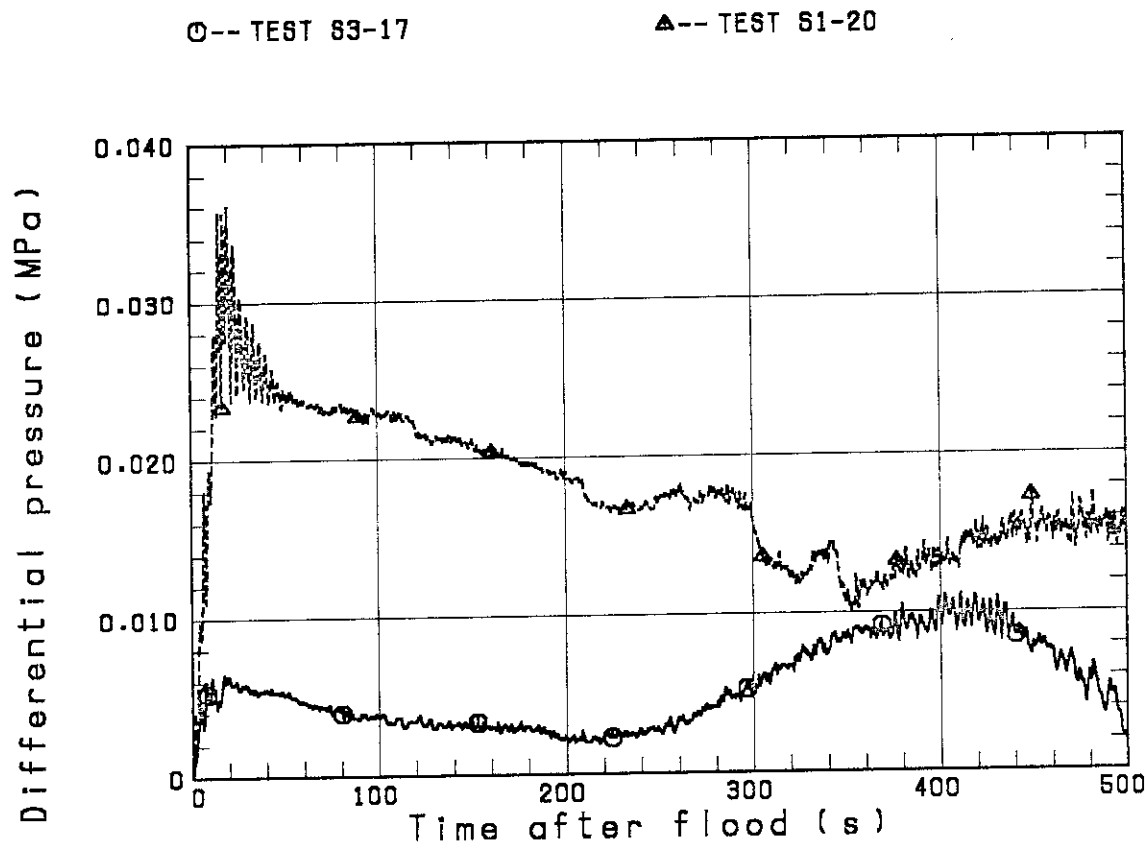

Fig. 3.18 Comparison of intact loop differential pressure between Tests S3-17 and S1-20

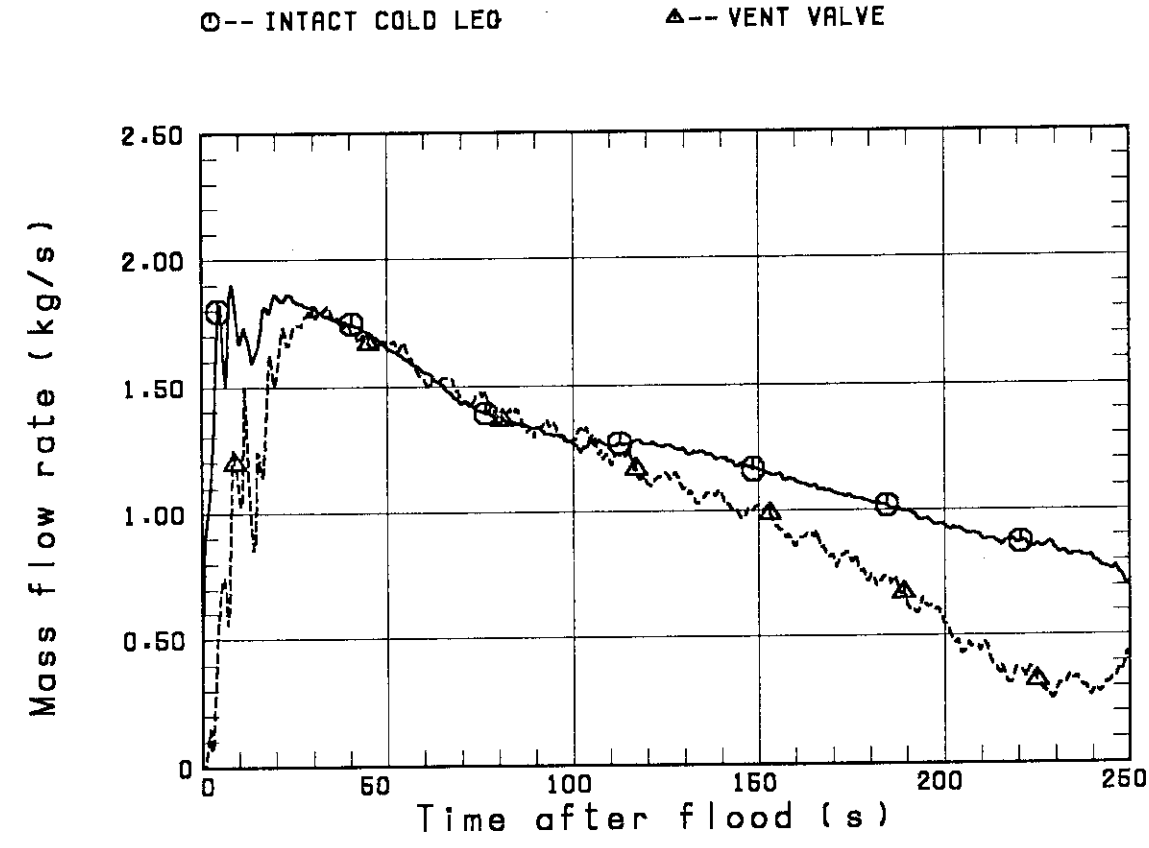

Fig. 3.19 Comparison of steam mass flow rate between intact cold leg and vent valve

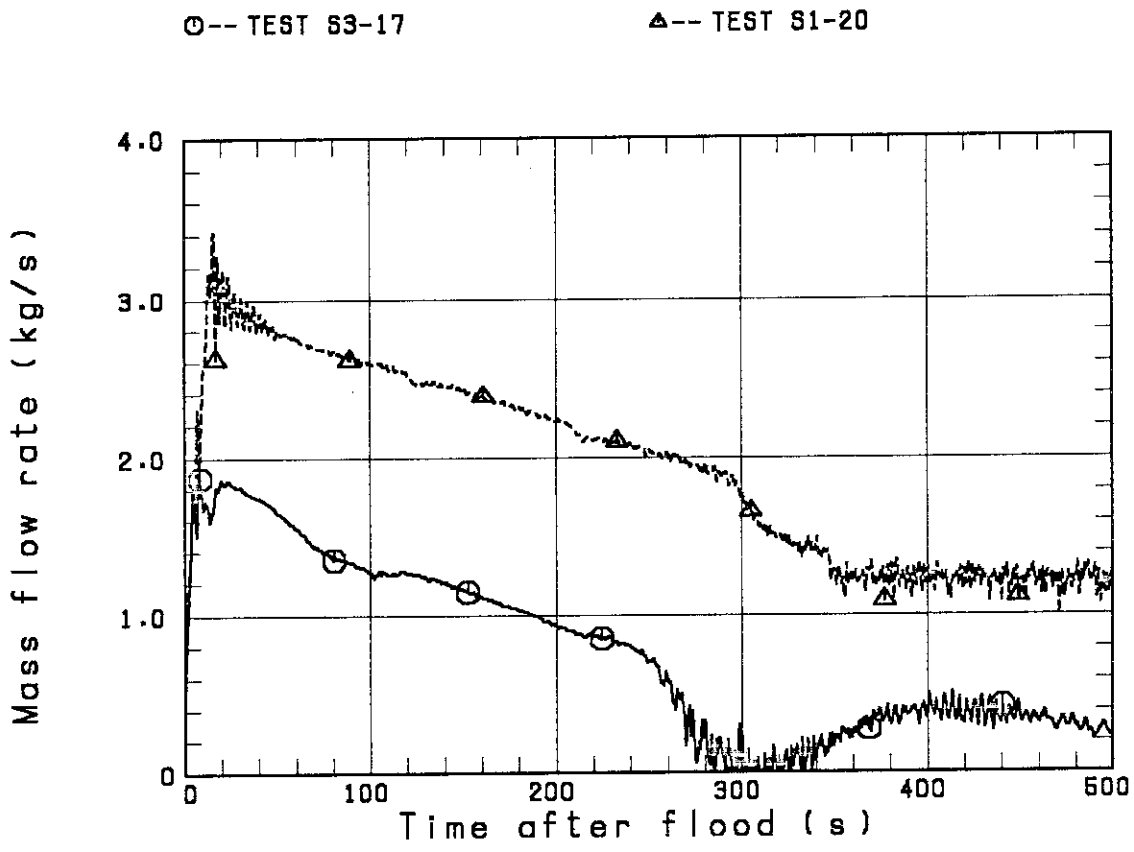

Fig. 3.20 Comparison of steam mass flow rate in intact cold leg between Tests S3-17 and S1-20

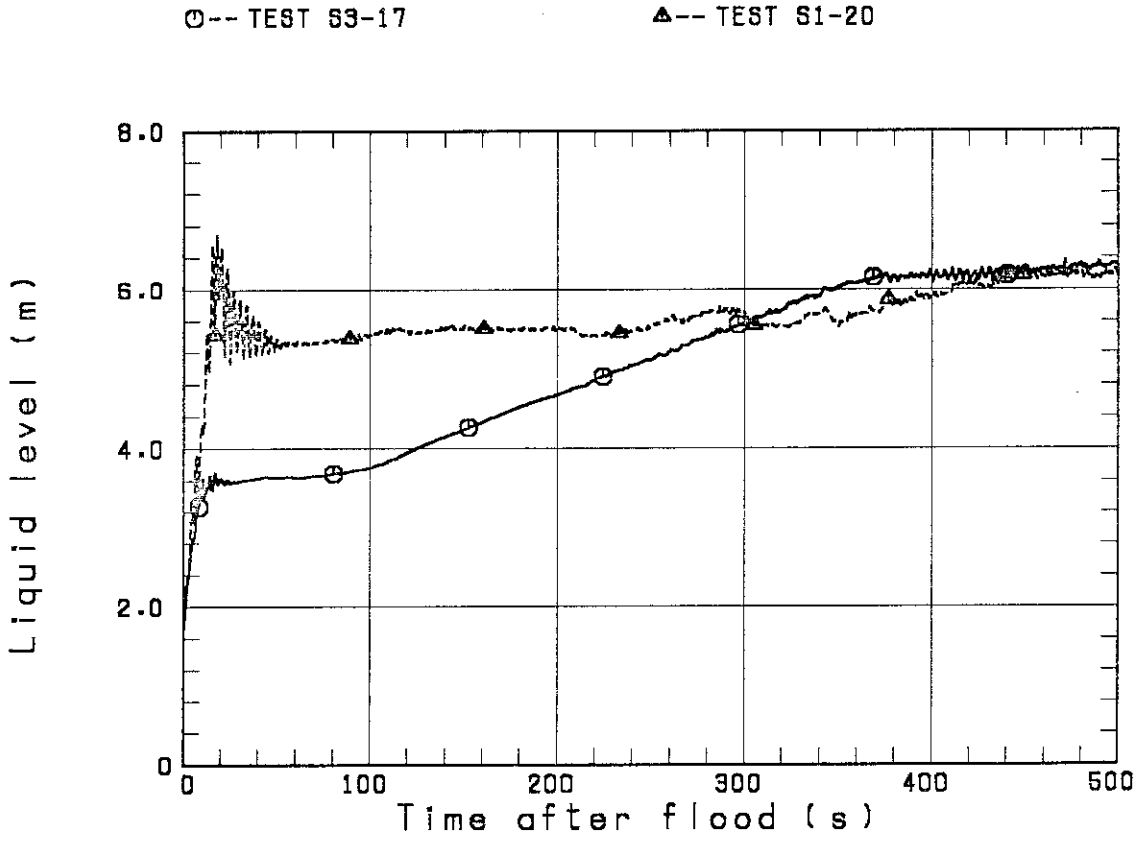

Fig. 3.21 Comparison of downcomer liquid level between Tests S3-17 and S1-20

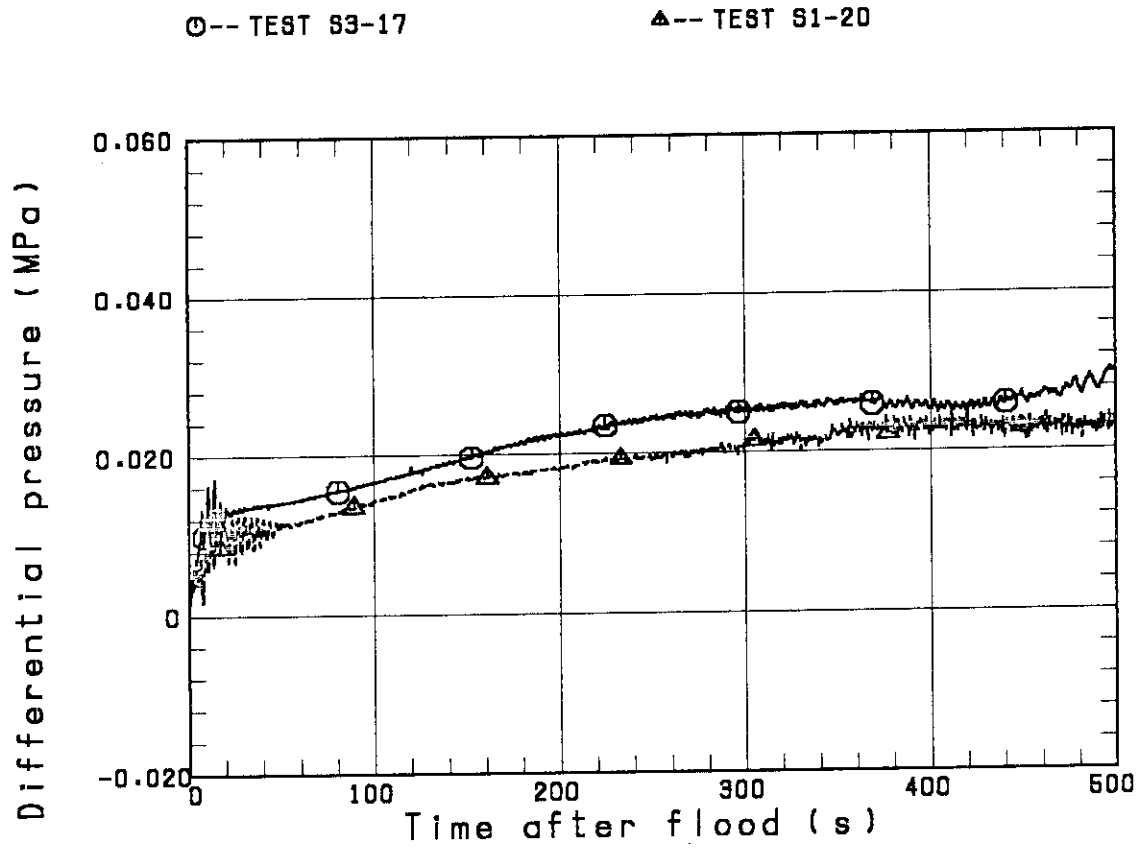

Fig. 3.22 Comparison of core differential pressure between Tests S3-17 and S1-20

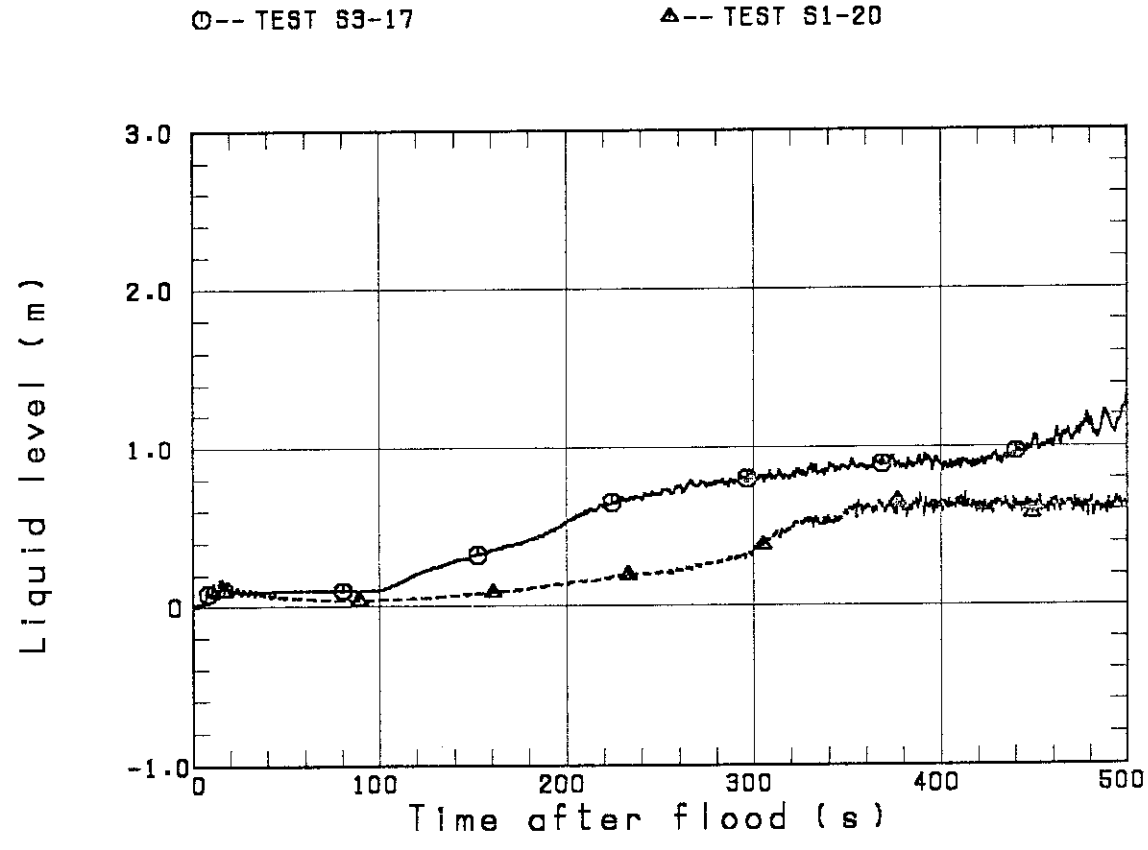

Fig. 3.23 Comparison of upper plenum liquid level between Tests S3-17 and S1-20

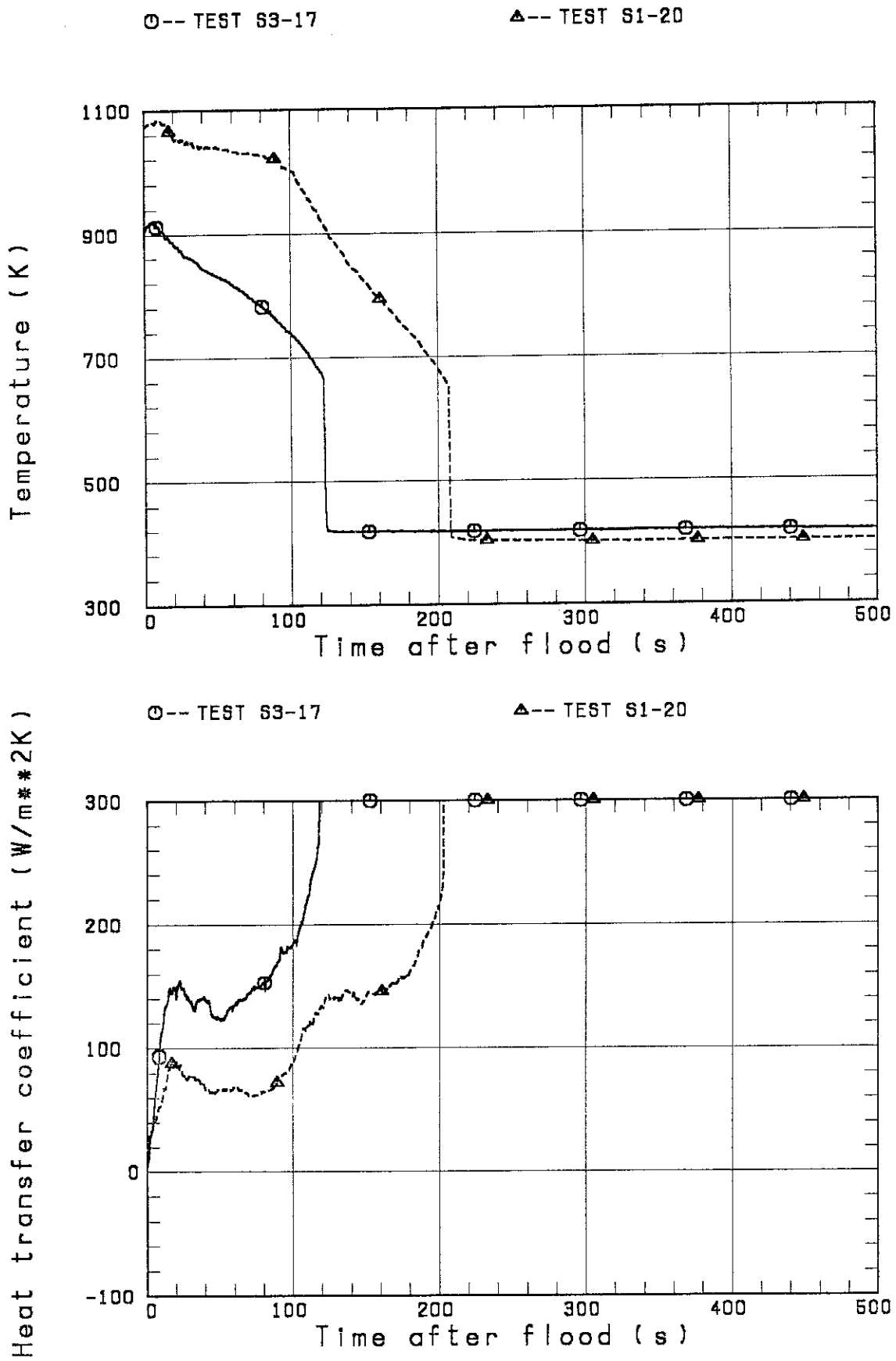

Fig. 3.24 Comparison of rod surface temperature and corresponding heat transfer coefficient at peak power location between Tests S3-17 and S1-20

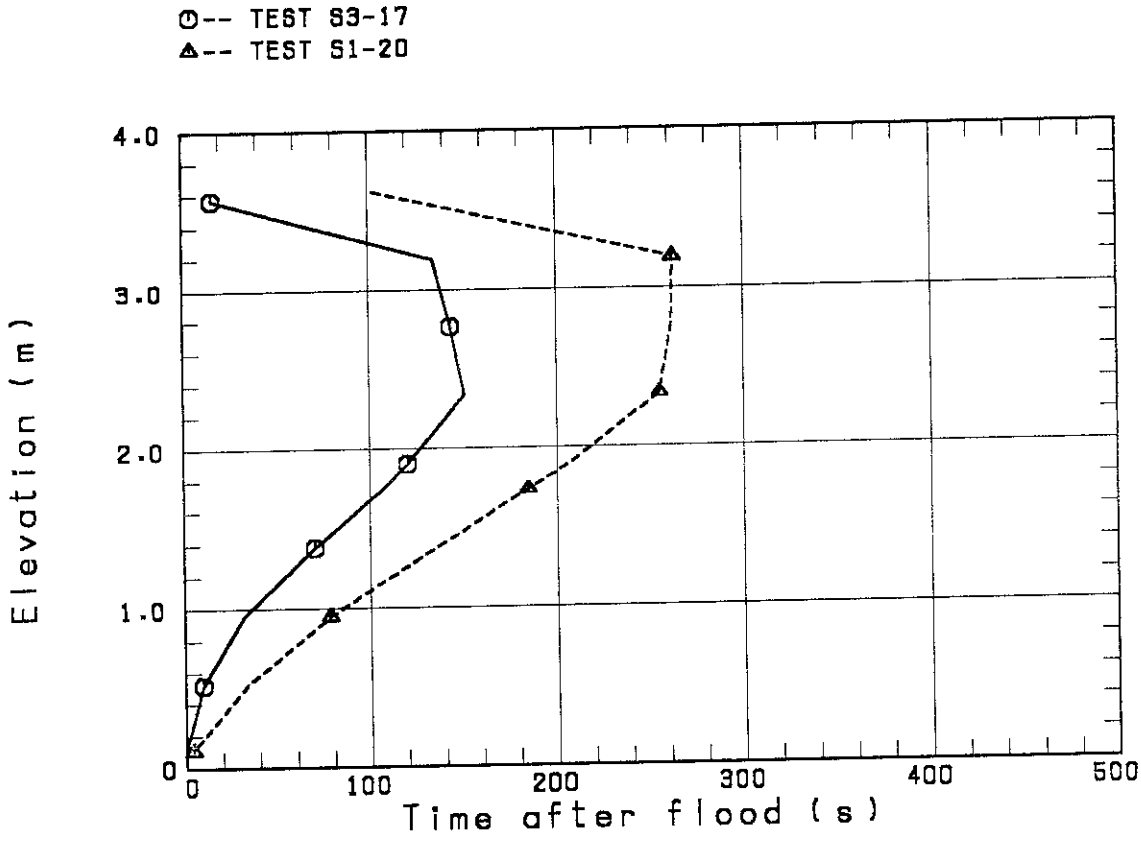

Fig. 3.25 Comparison of quench envelope for peak power rod between Tests S3-17 and S1-20

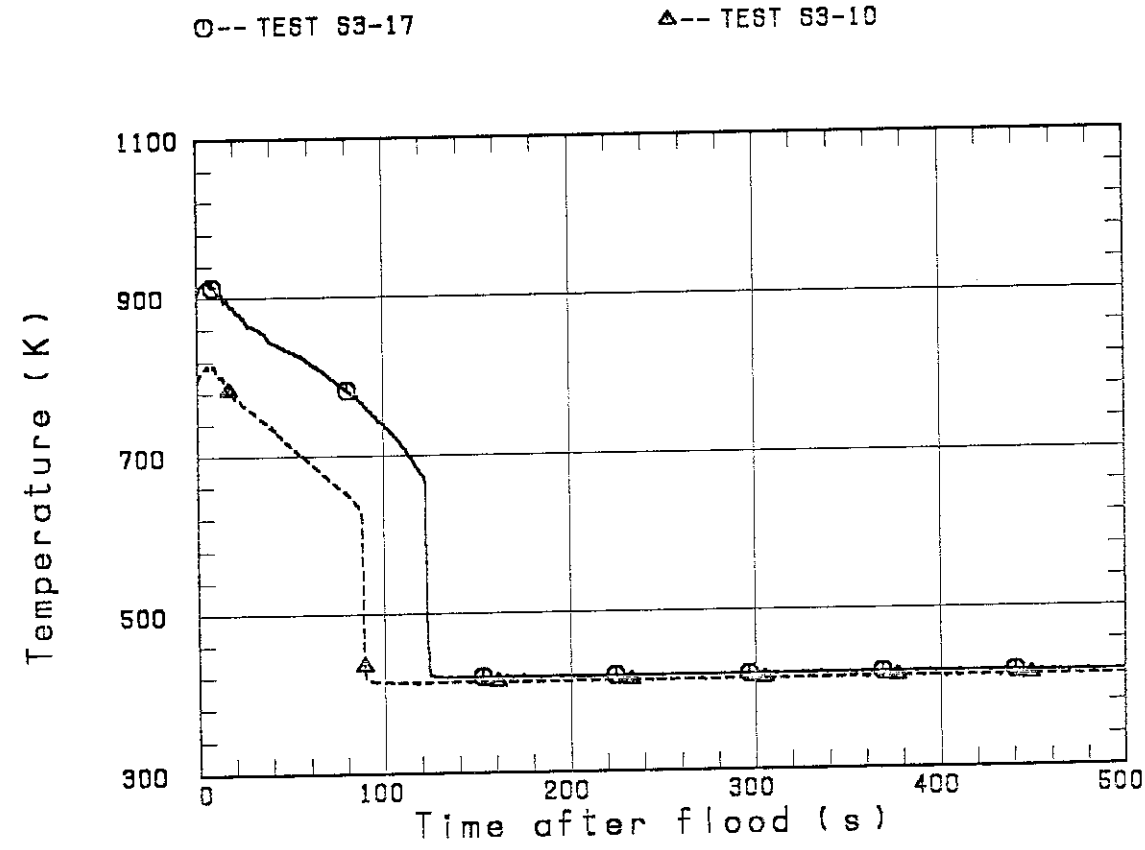

Fig. 3.26 Comparison of rod surface temperature at peak power location between Tests S3-17 and S3-10

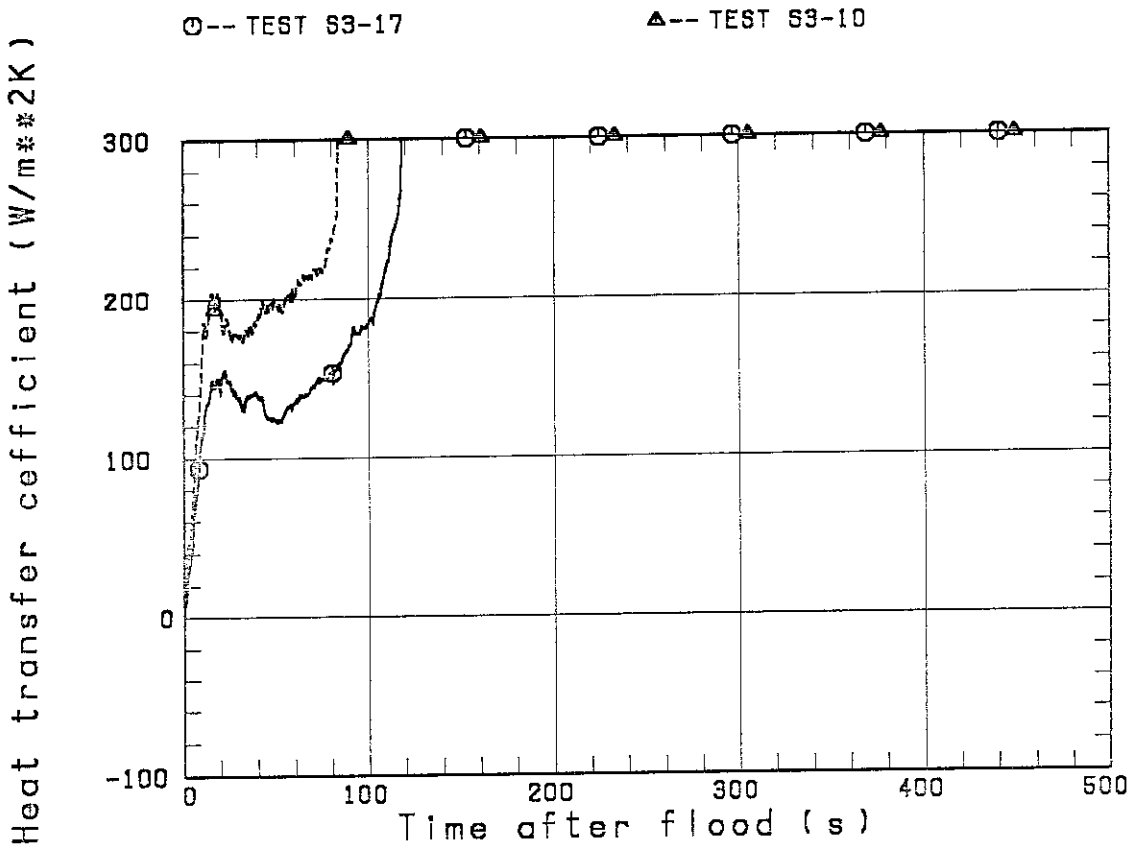

Fig. 3.27 Comparison of heat transfer coefficient at peak power location between Tests S3-17 and S3-10

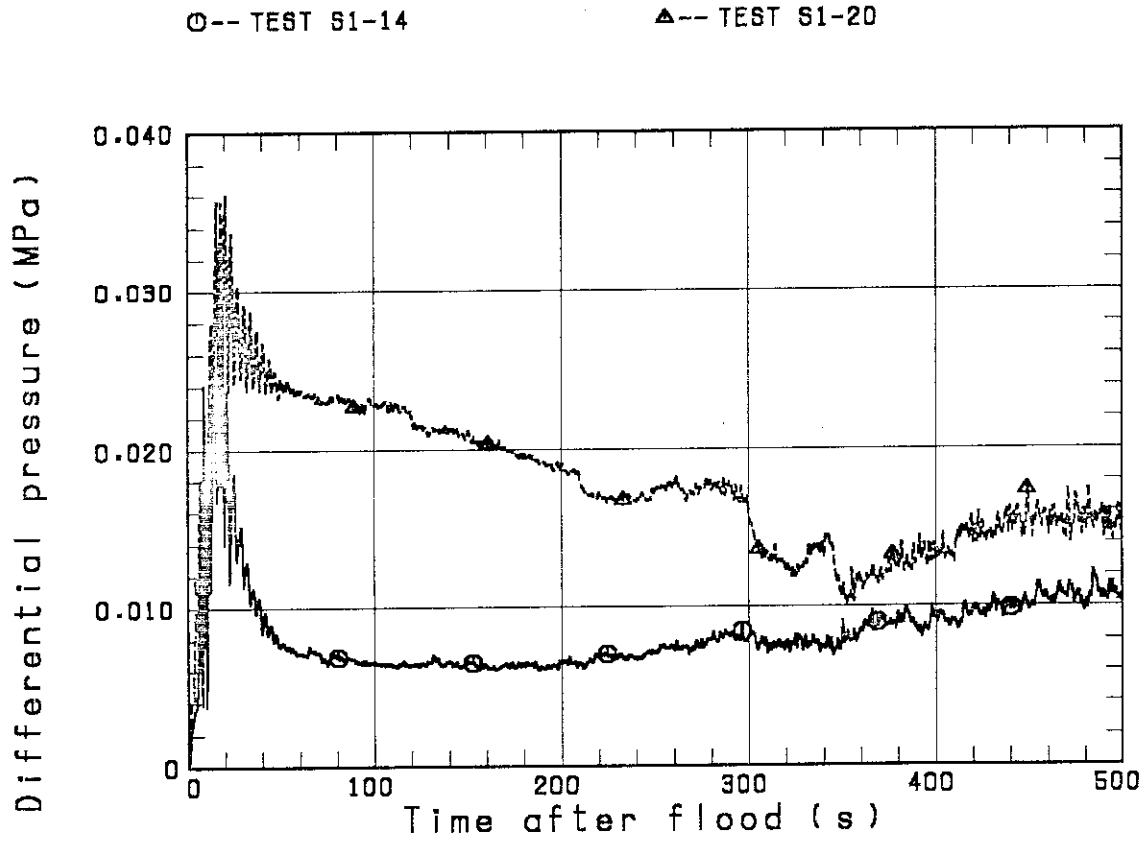

Fig. 3.28 Comparison of intact loop differential pressure between Tests S1-14 and S1-20

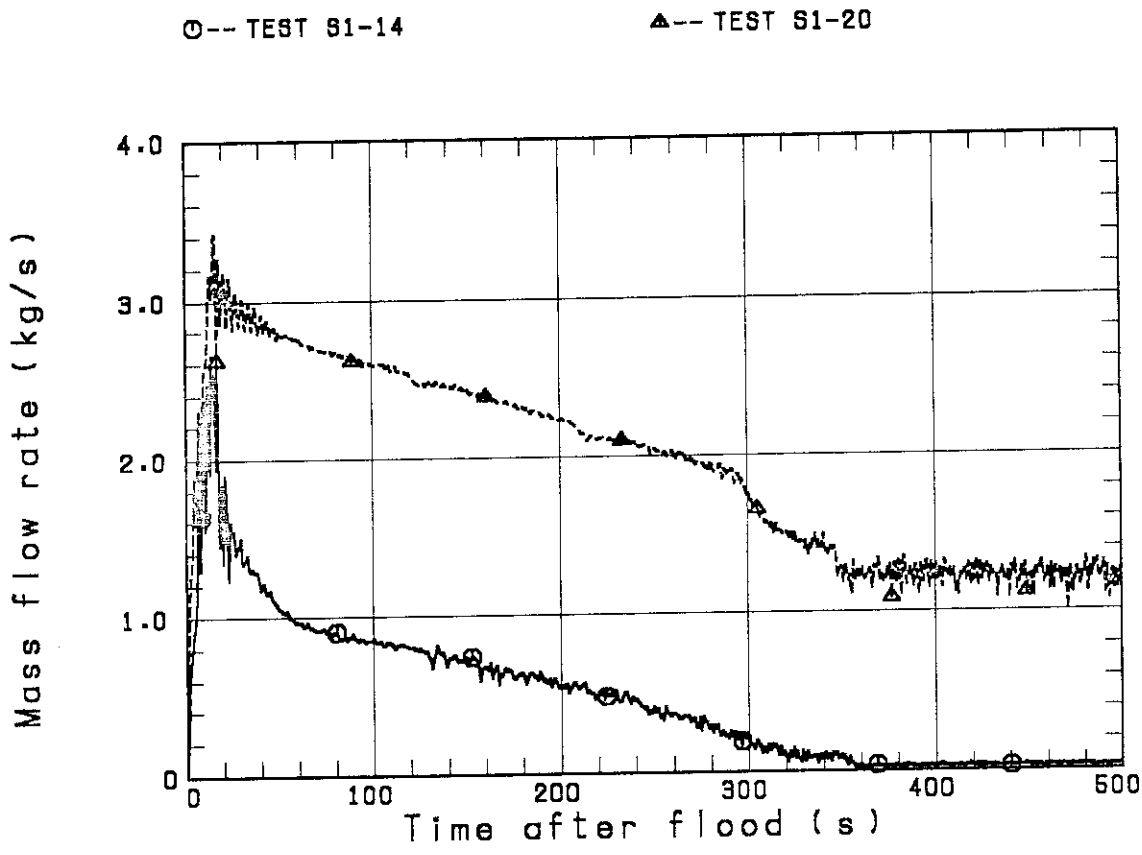

Fig. 3.29 Comparison of steam mass flow rate in intact cold leg between Tests S1-14 and S1-20

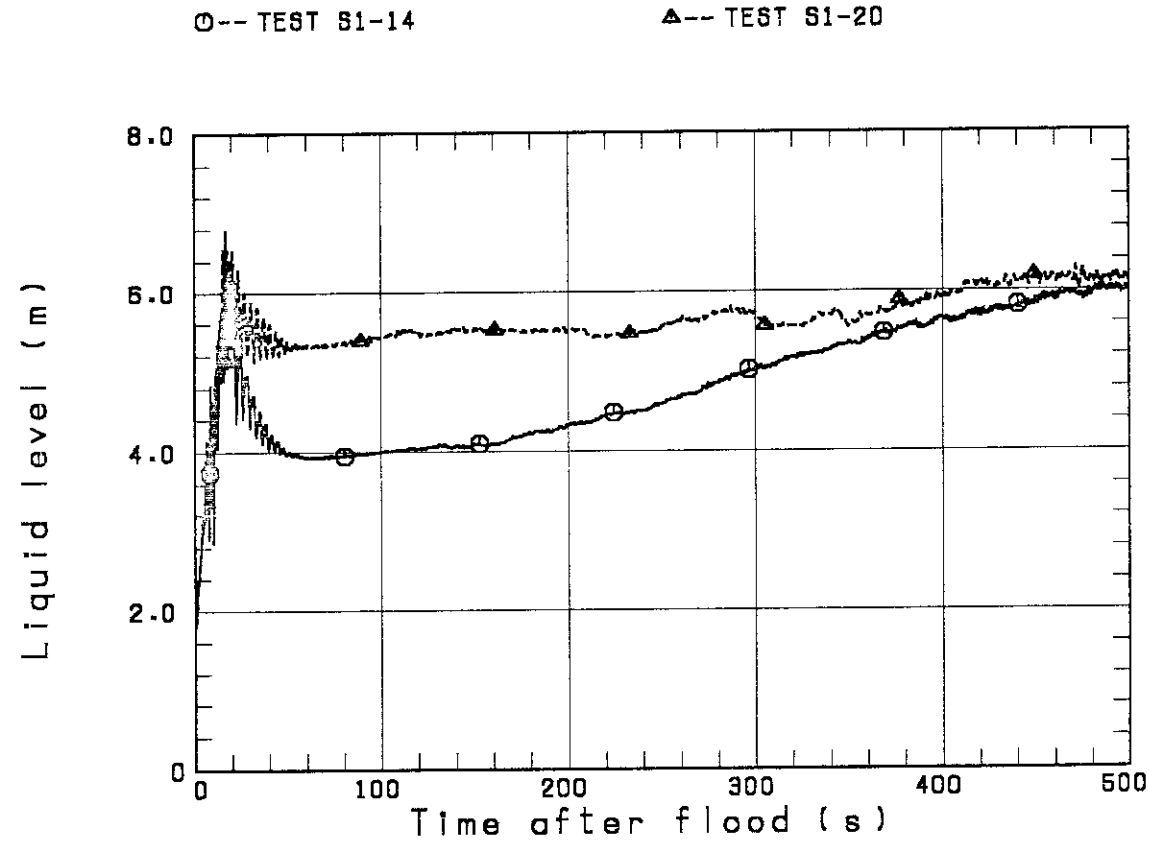

Fig. 3.30 Comparison of downcomer liquid level between Tests S1-14 and S1-20

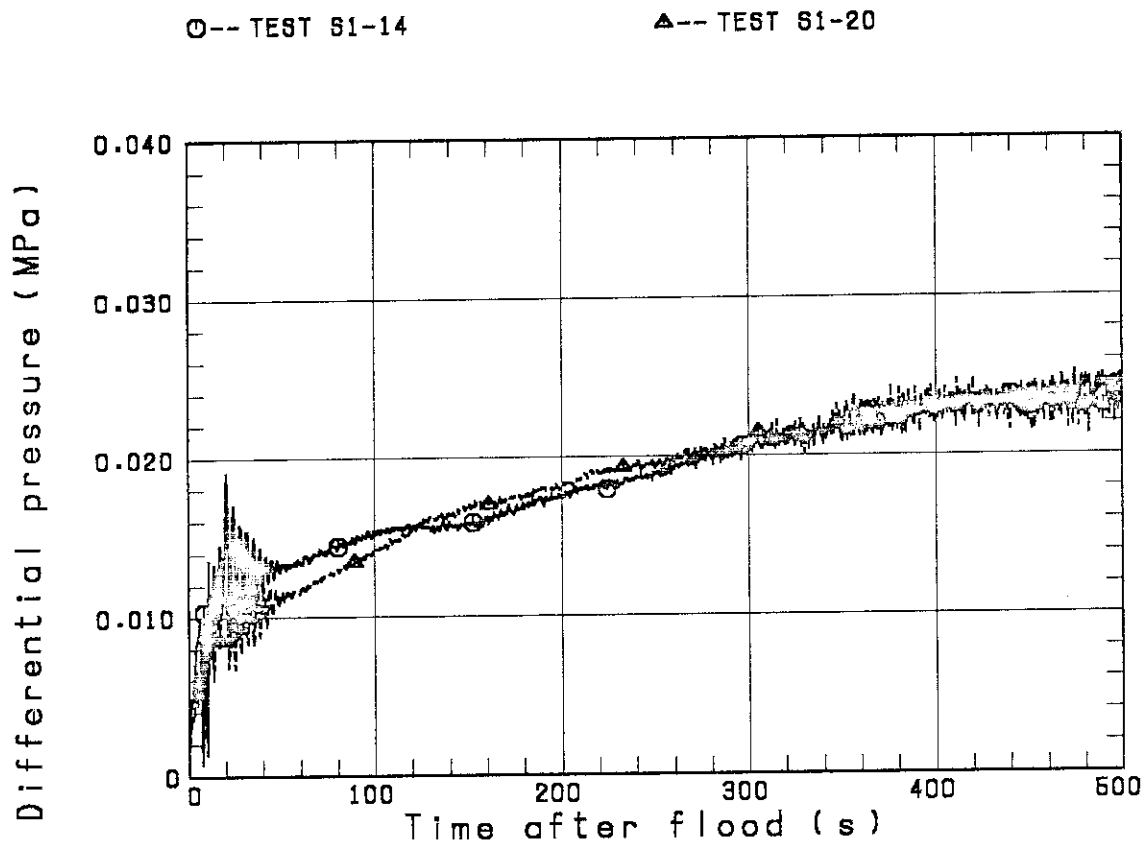

Fig. 3.31 Comparison of core differential pressure between Tests S1-14 and S1-20

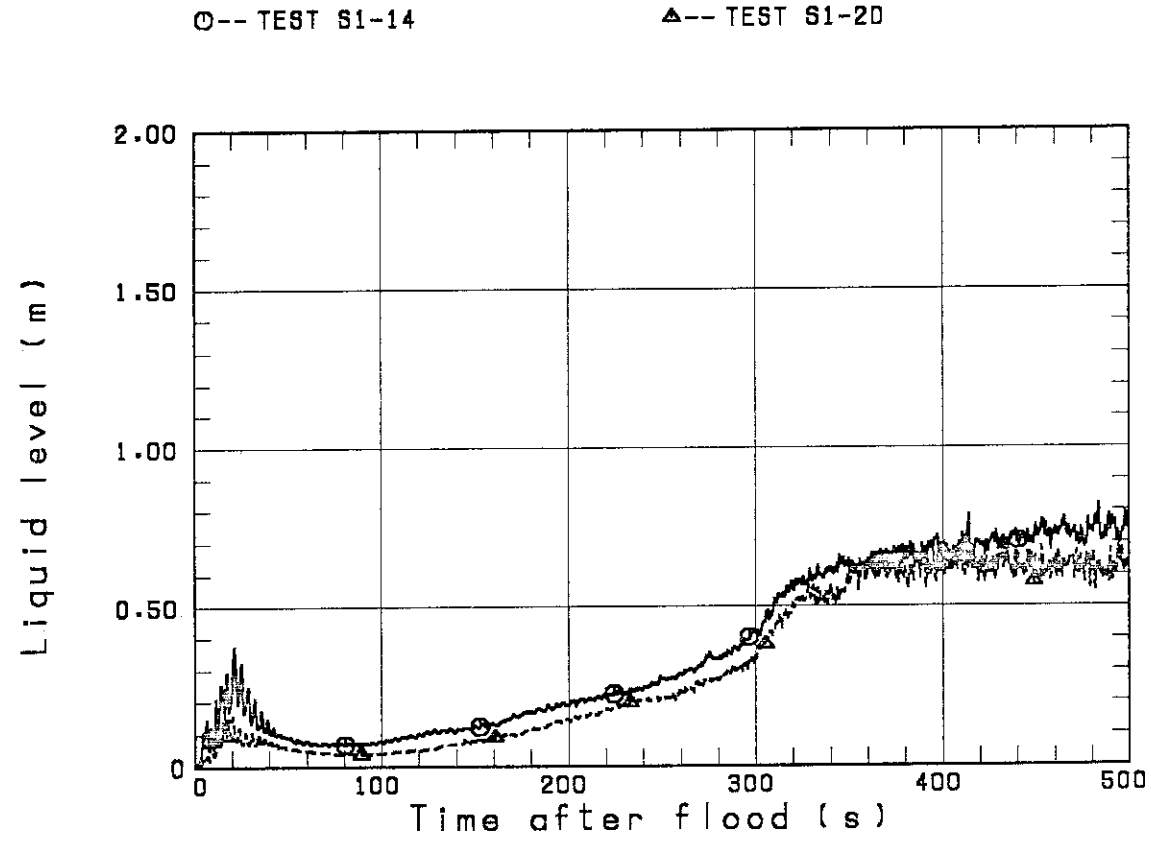

Fig. 3.32 Comparison of upper plenum liquid level between Tests S1-14 and S1-20

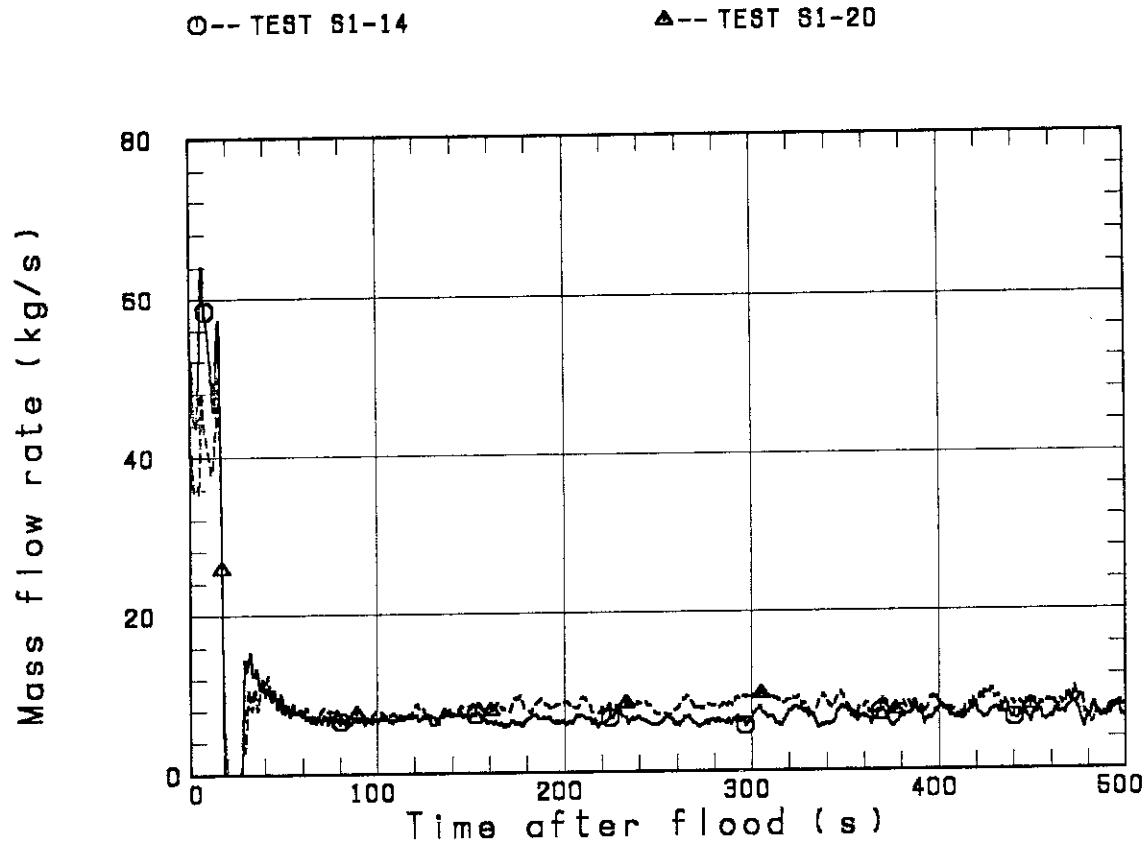

Fig. 3.33 Comparison of core flooding rate between Tests S1-14 and S1-20

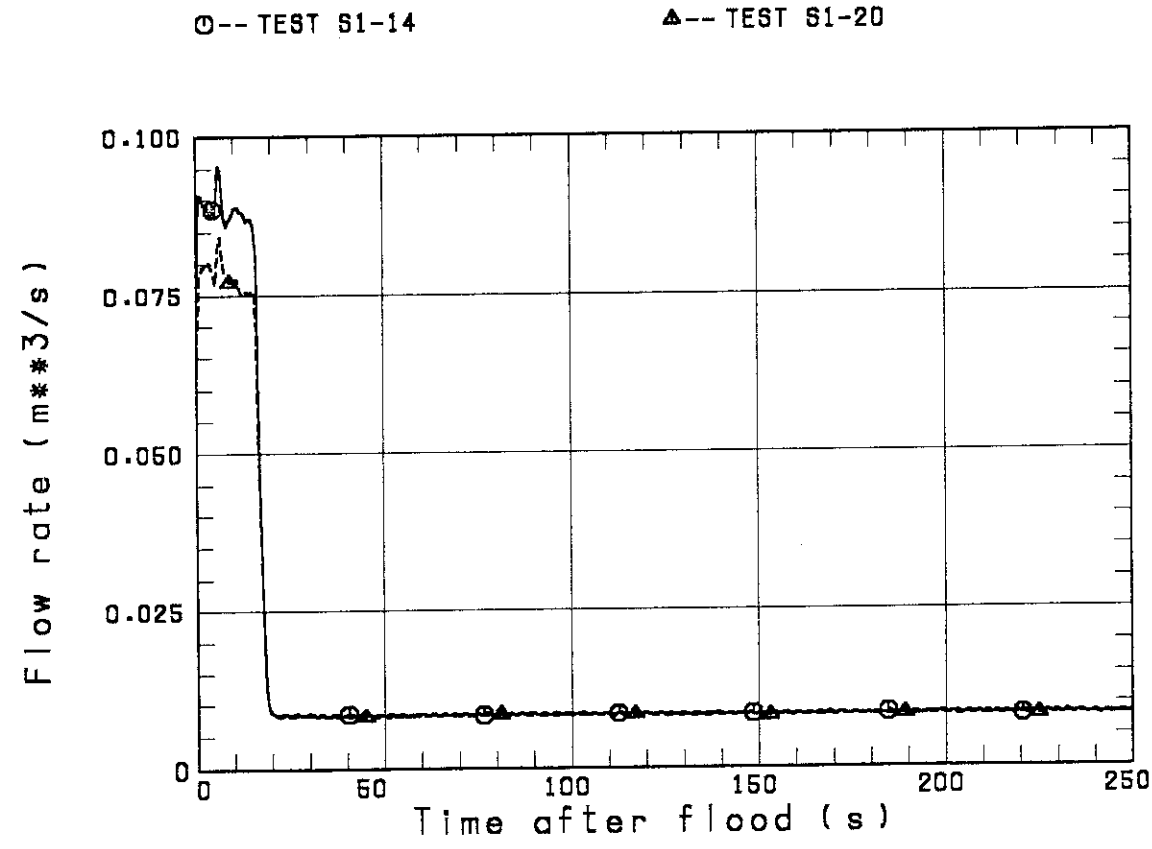

Fig. 3.34 Comparison of ECC water injection rate between Tests S1-14 and S1-20

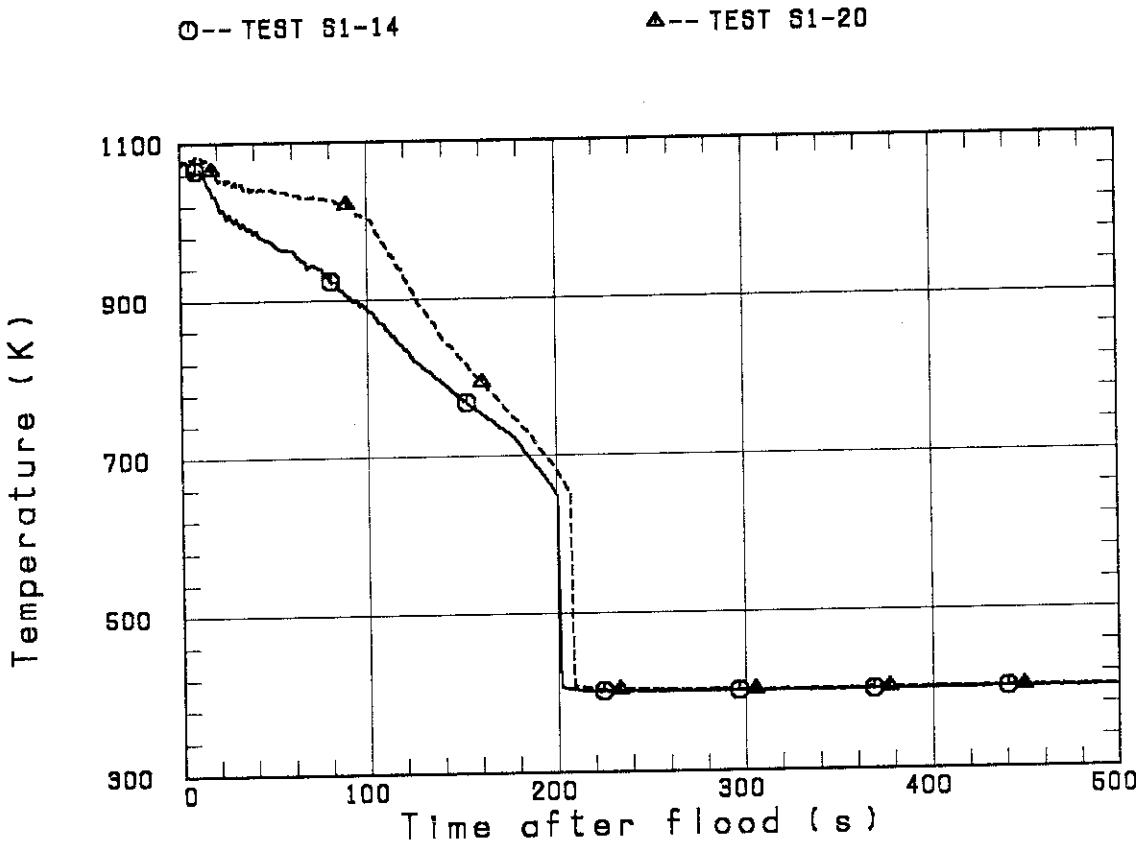

Fig. 3.35 Comparison of rod surface temperature at peak power location between Tests S1-14 and S1-20

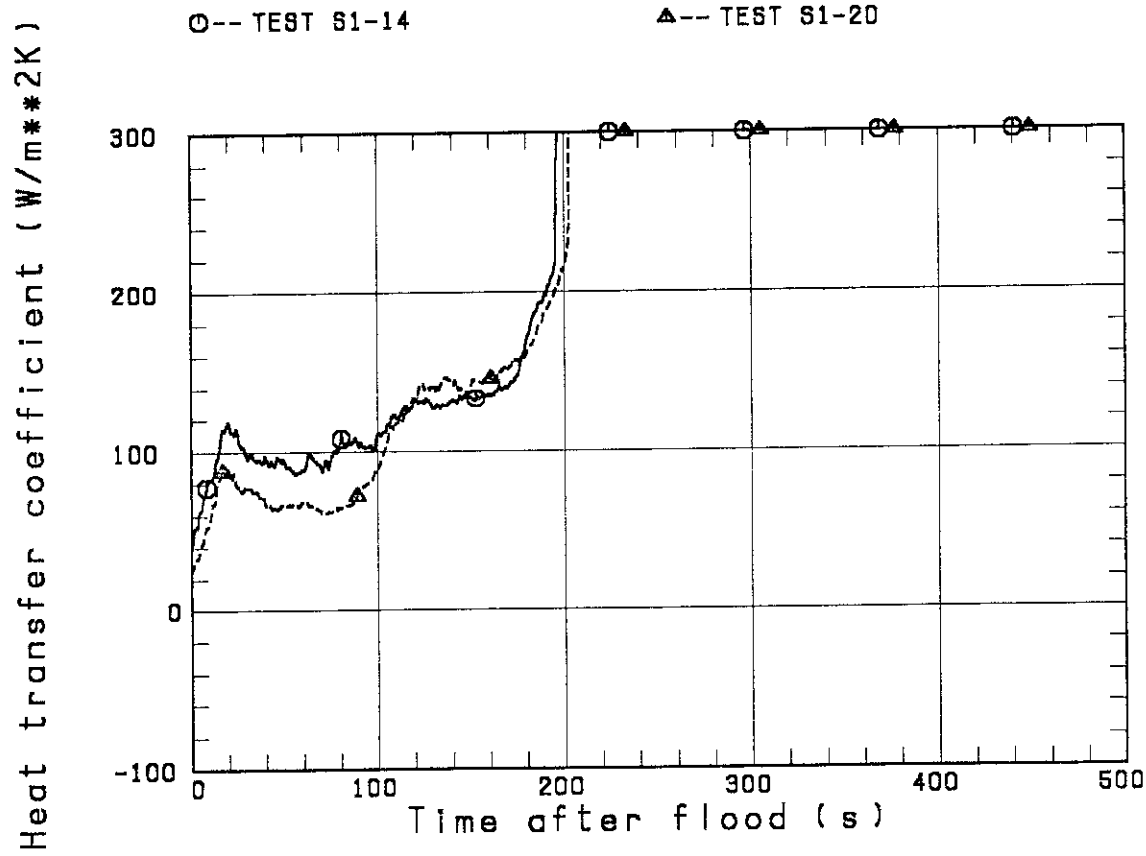

Fig. 3.36 Comparison of heat transfer coefficient at peak power location between Tests S1-14 and S1-20

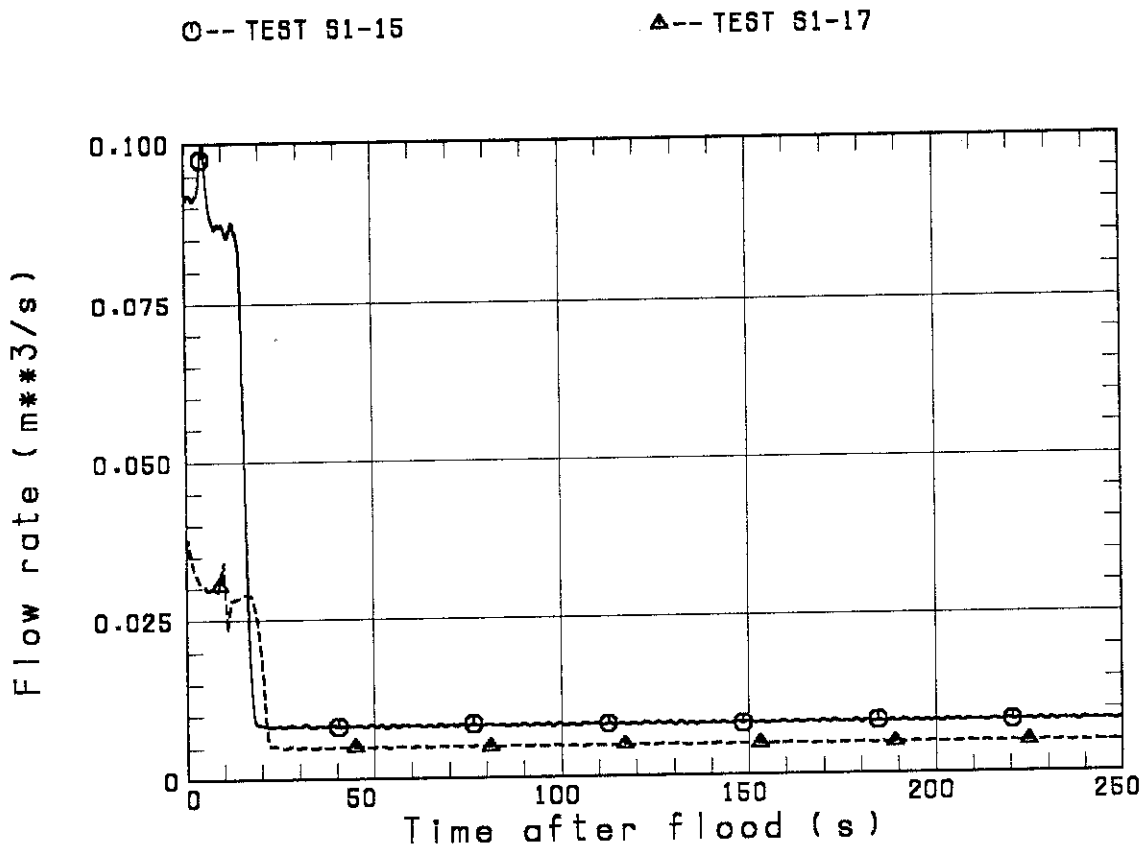

Fig. 3.37 Comparison of ECC water injection rate between Tests S1-15 and S1-17

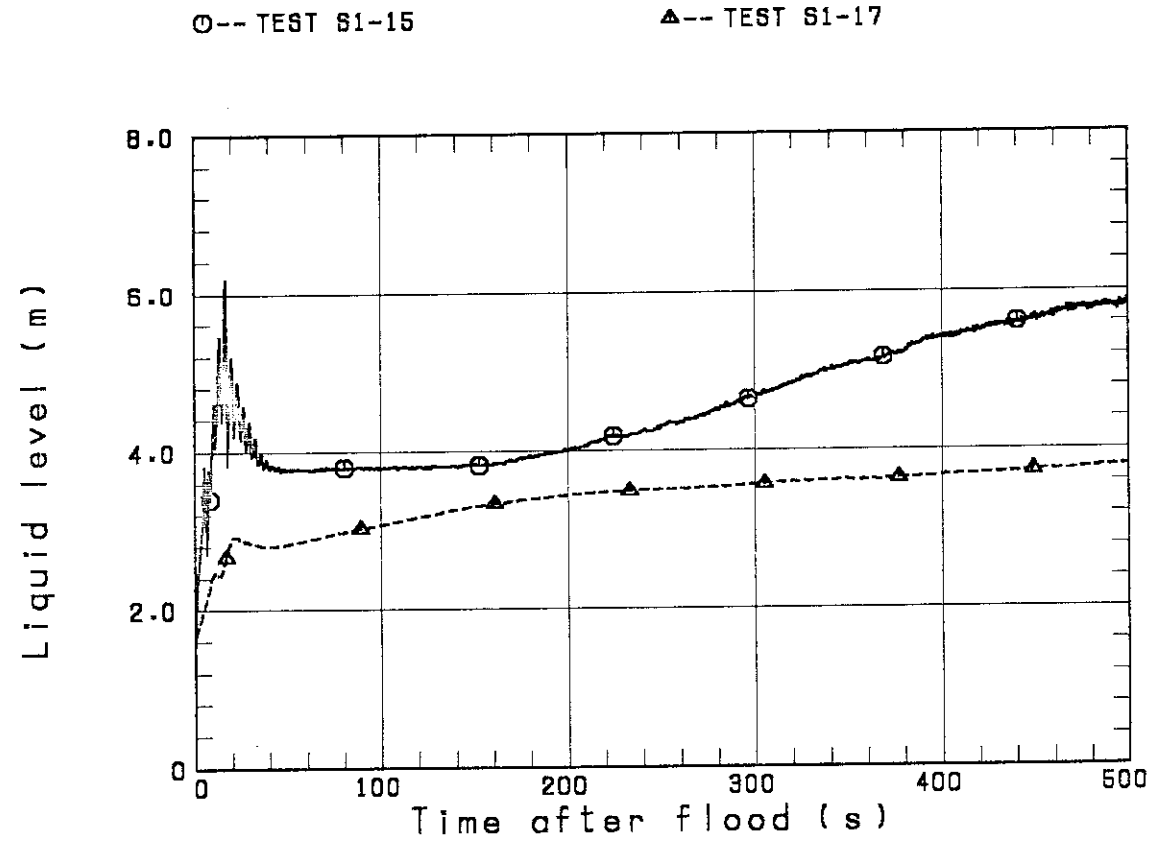

Fig. 3.38 Comparison of downcomer liquid level between Tests S1-15 and S1-17

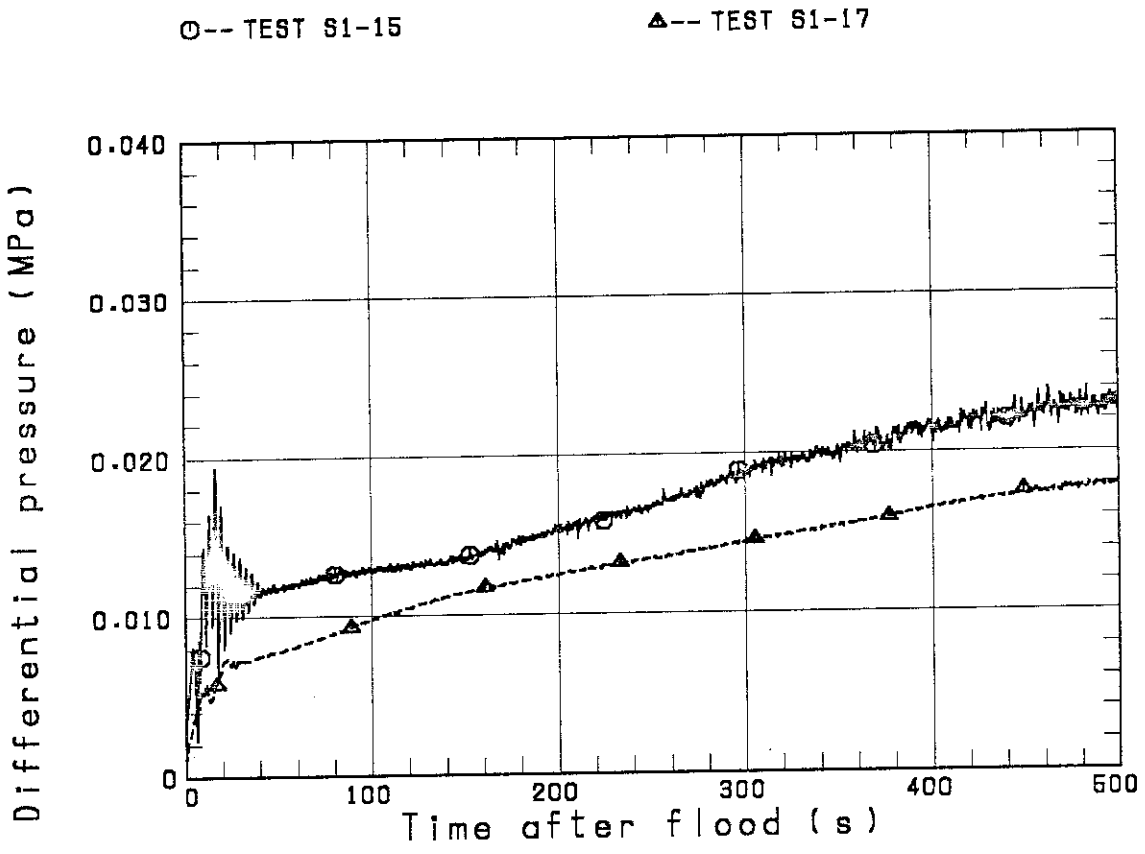

Fig. 3.39 Comparison of core differential pressure between Tests S1-15 and S1-17

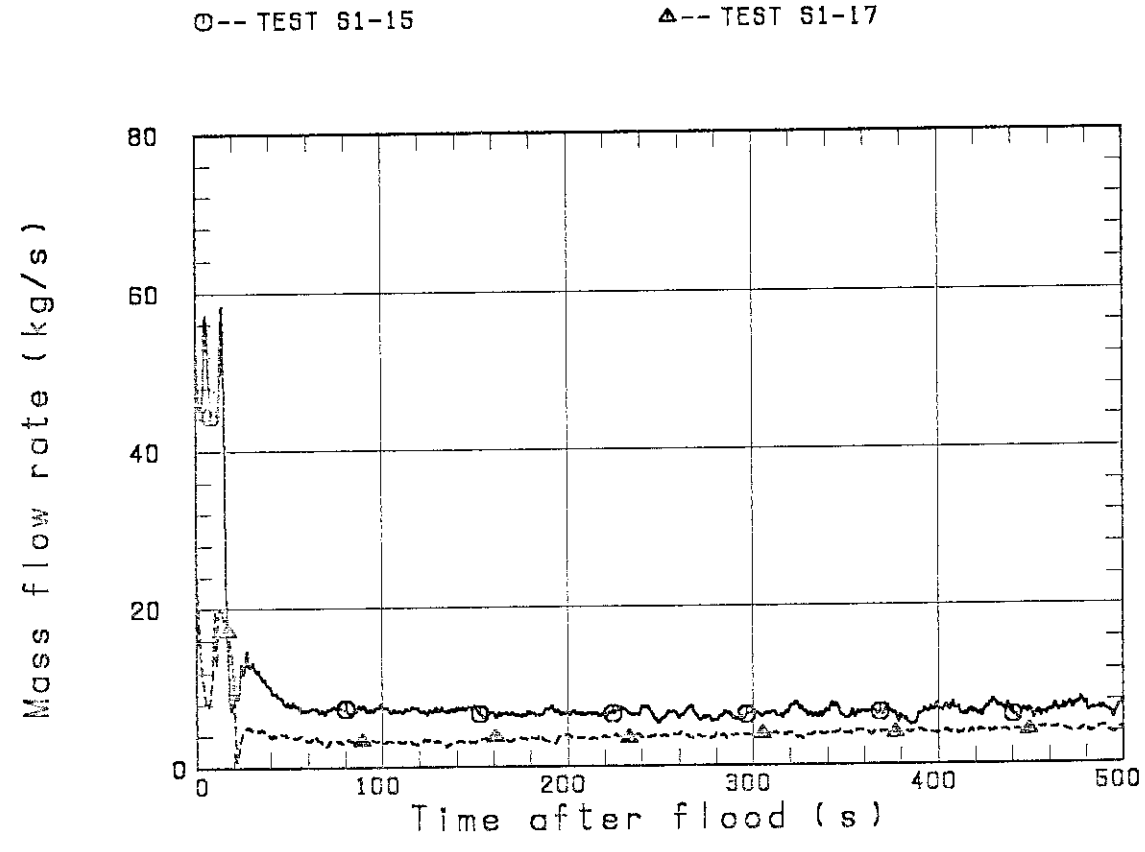

Fig. 3.40 Comparison of core flooding rate between Tests S1-15 and S1-17

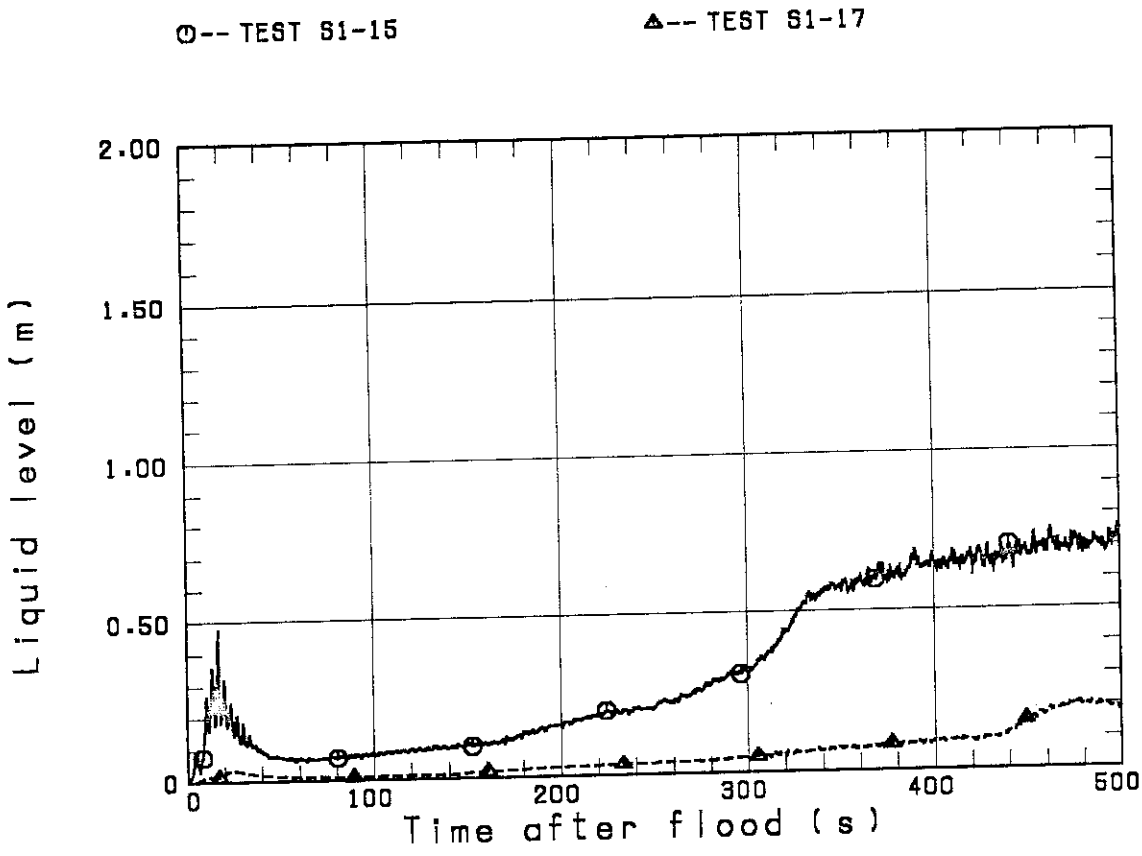

Fig. 3.41 Comparison of upper plenum liquid level between Tests S1-15 and S1-17

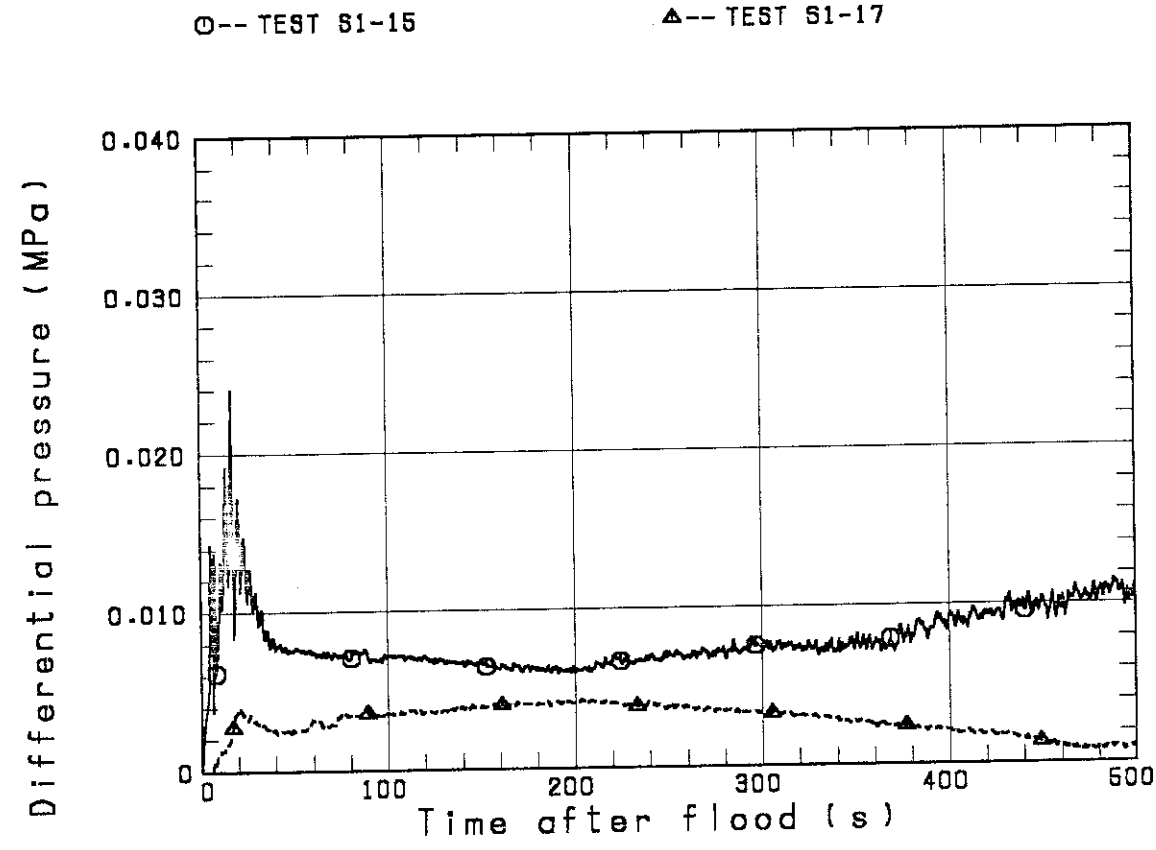

Fig. 3.42 Comparison of intact loop differential pressure between Tests S1-15 and S1-17

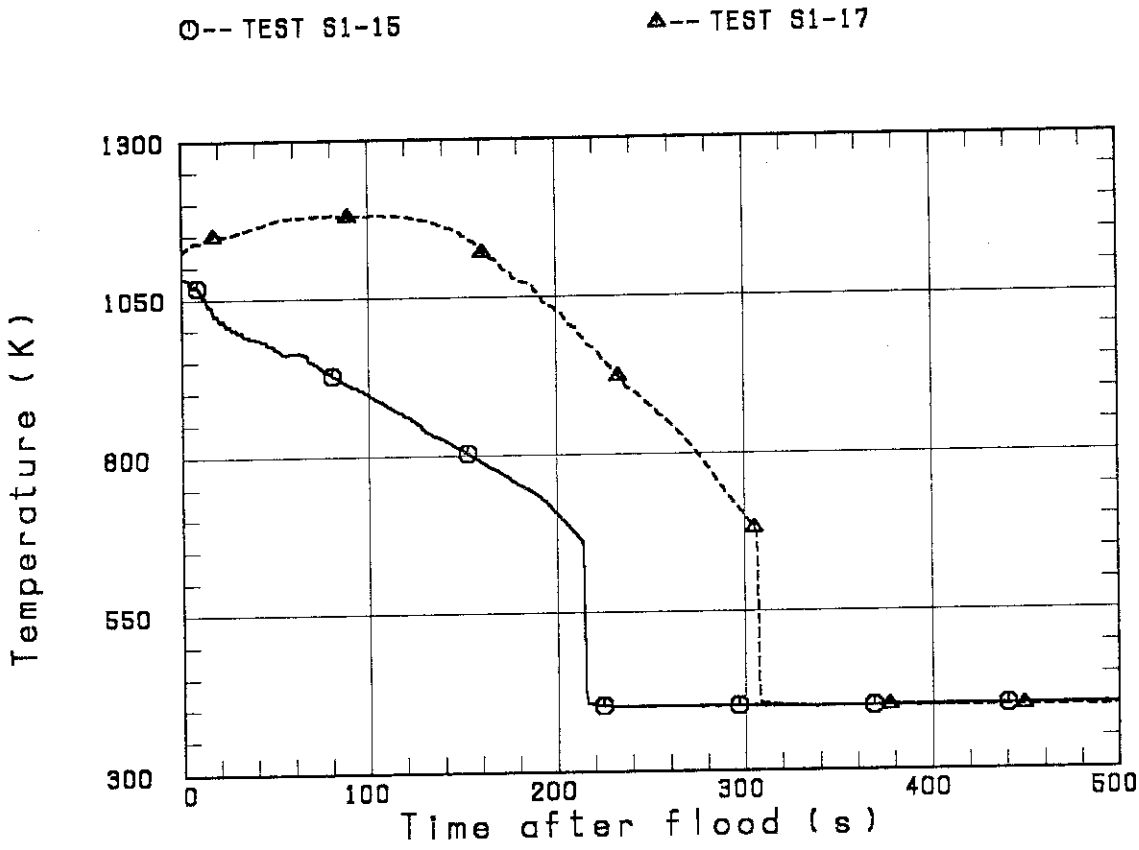

Fig. 3.43 Comparison of rod surface temperature at peak power location between Tests S1-15 and S1-17

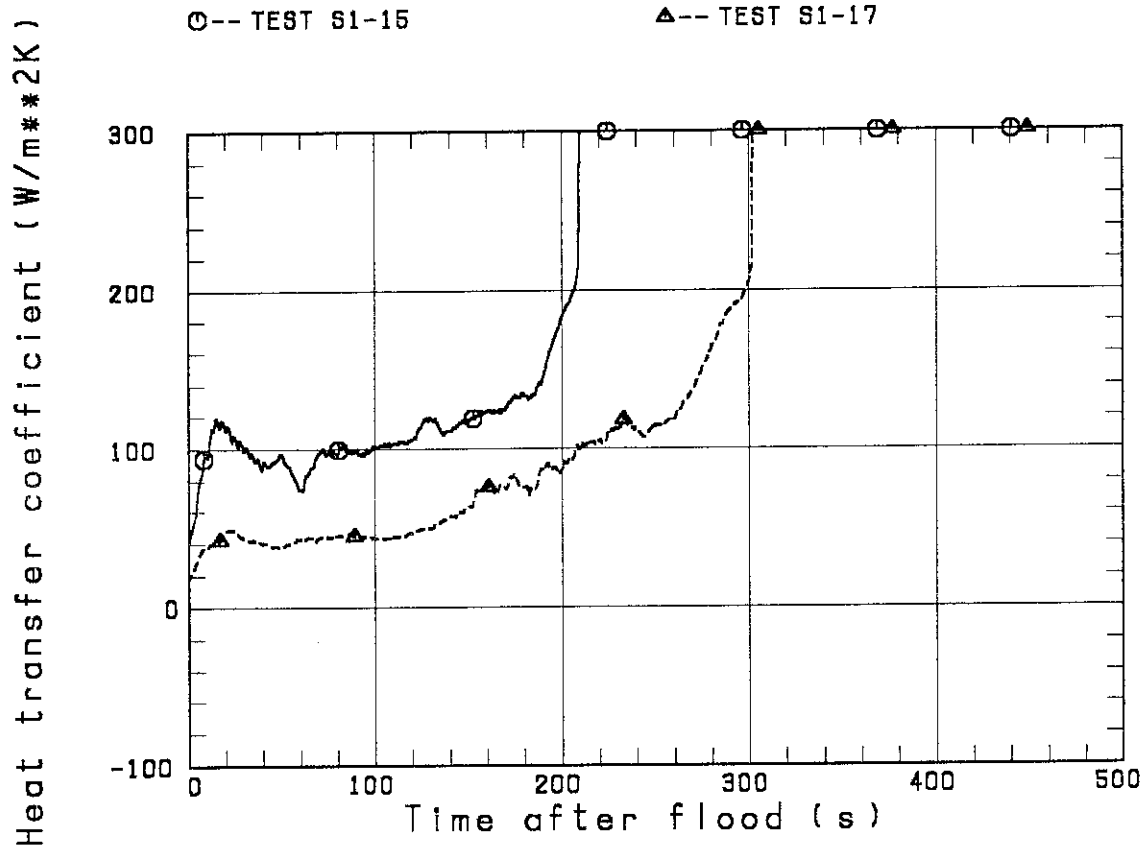

Fig. 3.44 Comparison of heat transfer coefficient at peak power location between Tests S1-15 and S1-17

4. Conclusions

SCTF Test S3-17, in which reflooding of a BBR type PWR with the vent valves was simulated, was conducted successfully and the data for the experimental coupling with the UPTF have been obtained. Furthermore, the test data are analyzed by also utilizing other SCTF and CCTF test data, and the following conclusions have been obtained:

(1) It has been demonstrated that the core cooling is significantly good during the reflood phase of a BBR under the BE conditions.

(2) The intact loop differential pressure was significantly reduced when the vent valve was open.

(3) The effect of the vent valve on core cooling was not remarkable under the conditions that the downcomer water level was below the overflow level when the vent valve was closed, but is expected to be remarkable under the conditions that the downcomer water level exceeds the overflow level when the vent valve is closed. Therefore, it would be better for core cooling of a BBR to increase the ECC water injection rate.

(4) It has been experimentally confirmed also under the open vent valve situation that the core cooling is better as the ECC water injection rate is larger as far as the downcomer water level is below the overflow level.

(5) It has been clarified that the reflooding behavior is somewhat different between a BBR and a B&W type PWR. That is, the ratio of the steam mass flow rate exhausted through the top of the downcomer to the total steam generation in the core is significantly smaller in a BBR than in a B&W type PWR, in which all the primary coolant loops are assumed to be blocked with the water during reflooding. This is expected to result in the smaller carry over of the downcomer water to the break, and hence, the larger core flooding rate in a BBR.

Acknowledgments

The authors would like to express their appreciation to Messrs. A. Kamoshida, T. Oyama, Y. Niitsuma, K. Nakajima, T. Chiba, K. Komori, H. Sonobe and A. Owada for their contribution to the test conduction.

This work was performed under a contract with the Atomic Energy Bureau of Science and Technology Agency of Japan.

References

[1] Hirano, K. and Murao, Y. : "Large Scale Reflood Test", Nihon-Genshiryoku-Gakkai Shi (J. At. Energy Sco. Jpn.) [in Japanese], 22[10], 681(1980).

[2] Adachi, H. *et al*. : "Design of Slab Core test Facility (SCTF) in Large Scale Reflood Test Program, Part I: Core-I", JAERI-M 83-080 (1983).

[3] Sobajima, M. *et al*. : "Design of Slab Core Test Facility (SCTF) in Large Scale Reflood Test Program, Part II: Core-II", to be published as a JAERI-M report.

[4] Adachi, H. *et al*. : "Design of Slab Core Test Facility (SCTF) in Large Scale Reflood test Program, Part III: Core-III", to be published as a JAERI-M report.

[5] Okubo, T. *et al*. : "Evaluation Report on SCTF Core-III Test S3-9 (Investigation of Reflooding Behavior under an Evaluation Model Condition in PWRs with Cold-leg-injection-type ECCS", to be published as a JAERI-M report.

[6] Adachi, H. *et al*. : "Cold Leg Injection Reflood Test Results in the SCTF Core-I under Constant System Pressure", to be published as a JAERI-M report.

[7] Akimoto, H. *et al*. : "Evaluation Report on SCTF-III Test S3-10 --- Reflood Phenomena under Best Estimate Conditions ---", to be published as a JAERI-M report.

[8] Okubo, T. and Murao, Y. : "Experimental Study of ECC Water Injection Rate Effects on Reflood Phase of PWR-LOCA", J. Nucl. Sci. Technol., 22[2],93(1985).

Acknowledgments

The authors would like to express their appreciation to Messrs. A. Kamoshida, T. Oyama, Y. Niitsuma, K. Nakajima, T. Chiba, K. Komori, H. Sonobe and A. Owada for their contribution to the test conduction.

This work was performed under a contract with the Atomic Energy Bureau of Science and Technology Agency of Japan.

References

[1] Hirano, K. and Murao, Y. : "Large Scale Reflood Test", Nihon-Genshiryoku-Gakkai Shi (J. At. Energy Sco. Jpn.) [in Japanese], 22[10], 681(1980).

[2] Adachi, H. *et al*. : "Design of Slab Core test Facility (SCTF) in Large Scale Reflood Test Program, Part I: Core-I", JAERI-M 83-080 (1983).

[3] Sobajima, M. *et al*. : "Design of Slab Core Test Facility (SCTF) in Large Scale Reflood Test Program, Part II: Core-II", to be published as a JAERI-M report.

[4] Adachi, H. *et al*. : "Design of Slab Core Test Facility (SCTF) in Large Scale Reflood test Program, Part III: Core-III", to be published as a JAERI-M report.

[5] Okubo, T. *et al*. : "Evaluation Report on SCTF Core-III Test S3-9 (Investigation of Reflooding Behavior under an Evaluation Model Condition in PWRs with Cold-leg-injection-type ECCS", to be published as a JAERI-M report.

[6] Adachi, H. *et al*. : "Cold Leg Injection Reflood Test Results in the SCTF Core-I under Constant System Pressure", to be published as a JAERI-M report.

[7] Akimoto, H. *et al*. : "Evaluation Report on SCTF-III Test S3-10 --- Reflood Phenomena under Best Estimate Conditions ---", to be published as a JAERI-M report.

[8] Okubo, T. and Murao, Y. : "Experimental Study of ECC Water Injection Rate Effects on Reflood Phase of PWR-LOCA", J. Nucl. Sci. Technol., 22[2],93(1985).

[9] Sugimoto, J. *et al.* : "Evaluation Report on CCTF Core-II Reflood Test C2-AS2 (Run 60) --- Effect of vent valve Type ECCS 1 ---", to be published as a JAERI-M report.

[10] Sugimoto, J. *et al.* : "Evaluation Report on CCTF Core-II Reflood Test C2-10 (Run 69) --- Effect of vent valve Type ECCS 2 ---", to be published as a JAERI-M report.

Appendix A

Description of SCTF Core-III

A.1 Test Facility

The overall schematic diagram of SCTF is shown in Fig. A-1. The principal dimensions of the facility is shown in Table A-1, and the comparison of dimensions between SCTF and the reference PWR is shown in Fig. A-2.

A.1.1 Pressure Vessel

The pressure vessel is of slab geometry as shown in Fig. A-3. The height of the components in the pressure vessel is almost the same as the reference reactor's, and the flow area and the fluid volume of each component are scaled down based on the nominal core flow area scaling, 1/21.

The core consists of 8 bundles arranged in a row and each bundle includes heater rods and non-heated rods with 16×16 array. The core is enveloped by the honeycomb thermal insulator which is attached on the back surface of core wall plate.

The downcomer is located at one end of the pressure vessel which corresponds to the periphery of the actual reactor pressure vessel. The core baffle region located between the core and the downcomer is isolated for Core-III to minimize uncertainty in actual core flow. The cross sections of the pressure vessel at the upper head, upper plenum, core and lower plenum are shown in Fig. A-4.

A.1.2 Interface between Core and Upper Plenum

The interface between the core and the upper plenum consists of upper core support plate (UCSP), end box and various structures in the end box such as control rod spider which is paired with the control rod guid assembly (CRGA) and its support column bottom and special baffle plate spider which is paired with the hold-down bridge. These structures are exactly the same as those for a German PWR except some minor modifications.

Figure A-5 shows arrangement of the UCSP, the end box and the top grid spacer. The configuration of the end box is shown in Fig. A-6.

Detail of the end boxes with drag transducer device and other internals is shown in Fig. A-7. The UCSP shown in Fig. A-8 has two kinds of holes, i.e., the square holes correspond to the end boxes with control rod spider and the circular holes correspond to the end boxes with special baffle plate spider.

A.1.3 Upper Plenum and Upper Head

The vertical and horizontal cross sections of the upper plenum are shown in Figs. A-9 and A-4, respectively. In the SCTF Core-III, the slab cut of the upper plenum of a German (KWU) PWR is simulated. The splitted and staggered arrangement of the CRGA support columns was chosen to make good simulation of horizontal flow in the upper plenum.

As shown in Fig. A-10, there are three kinds of CRGA support column. Support column-1 is installed above Bundles 3 and 5 and connected to the CRGA support column bottom with the transition cone. Cross section of the CRGA support calumn changes from a circle to a half circle in this transition cone. Support column 2 is installed above Bundles 6 and 7 and the bottom is closed with the half conical bottom seal plate with many flow holes. Support column 3 is essentially the same as support column 2 but the edge of one side is cut off in order to install above Bundle 1. Each CRGA support column has ten or eleven baffle plates with flow holes. Top flow paths to the upper head bottom and to the upper plenum top are also provided.

Figure A-11 shows vertical cross section of the bottom part of the upper plenum and the interface between the core and the upper plenum. There are eight side flow injection nozzles and eight side flow extraction nozzles just at the opposite side of the upper plenum bottom, corresponding to each bundle.

The upper plenum is separated from the upper head by an upper support plate. Four top injection nozzles penetrate the upper head and open the top of upper plenum as shown in Fig. A-12. Outlet part of the top injection nozzle has a rectangular cross section and double mesh screen with 45 degree cross angle is attached at the mouth.

A.1.4 Simulated Core

The simulated core for the SCTF Core-III consists of 8 heater rod bundles arranged in a row. Each bundle has 236 electrically heated rods and 20 non-heated rods. The arrangement of rods in a bundle is shown in Fig. A-13. The dimensions of the heater rods are based on 15×15 fuel rods bundle for a PWR and the heated length and the outer diameter of each heater rod are 3.613 m and 10.7 mm, respectively. A heater rod consists of a nichrome heater element, boron nitride (BN) or magnesium oxide (MgO) depending on elevation in the heated zone and Nichrofer 7216 (equivalent to Inconel 600) sheath. The sheath thickness is about 1.0 mm and is thicker than the actual fuel cladding because of the requirements for thermocouple installation. The heater element is a helical coil and has a 17 step chopped cosine axial power profile as shown in Fig. A-14. The peaking factor is 1.4.

Non-heated rods are either pipes or solid rods of stainless steel with 13.8 mm O.D. The heater rods and non-heated rods are fixed at the top of the core allowing downward expansion. In Fig. A-15, relative elevation of rods and spacers is shown.

For better simulation of flow resistance in the lower plenum, the simulated fuel rods end in the lower plenum and do not penetrate through the bottom plate of the lower plenum as shown in Fig. A-15.

A.1.5 Primary Loops

Primary loops consist of a hot leg equivalent to four hot legs in area, a steam/water separator for simulating single steam phase flow downstream of the steam generator and for measuring flow rate of carry over water, an intact cold leg equivalent to three intact loops, a broken cold leg on the pressure vessel side and a broken cold leg on the steam/water separator side. These two broken cold legs are connected to two containment tanks through break valves, respectively. The arrangement of the primary loops is shown in Fig. A-16. The flow area of each loop is scaled down based on the core flow area scaling, 1/21. It should be emphasized that the cross section of the hot leg is an elongated circle with an actual height to realize proper flow pattern in the hot leg. The steam/water separator has a steam generator inlet plenum simulator to correctly simulate the flow

characteristics of carryover water into the U-tubes. The cross section of the hot leg and the configuration of the steam genrator inlet plenum simulator are shown in Fig. A-17.

A pump simulator and a loop seal part are provided for the intact cold leg. The arangement of the intact cold leg is shown in Fig. A-18. The pump simulator consists of the casing and duct simulators and an orifice plate as shown in Fig. A-19. The loop resistance is adjusted with the orifice plates attached to the intact cold leg, the steam/water separator side and pressure vessel side broken cold legs and the pump simulator.

A.1.6 ECC Water Injection System

Three kinds of ECCSs are provided, i.e., the accumulator injection system (Acc), low pressure coolant injection system (LPCI) and combined injection system. Available injection locations for the former two are the intact and broken cold legs, the hot leg, the lower plenum and the downcomer. On the other hand, those for the last one are the top and bottom-side of the upper plenum and the intact and broken cold legs.

A.1.7 Containment Tanks and Auxiliary System

Two containment tanks are provided to SCTF. The containment tank-I is connected with the downcomer through the pressure vessel side broken cold leg and the containment tank-II is connected with the steam/water separator through the steam/water separator side broken cold leg. Especially in the containment tank-I, carryover water from the downcomer is measured by the differentiation of the liquid level. These containment tanks and auxiliary system such as a pressurizer for injecting water from the Acc tanks, etc. are shared with CCTF.

A.2 Instrumentation

The instrumentation in SCTF has been provided both by JAERI and USNRC. The JAERI-provided instrumentation includes the measurement of temperatures, pressures, differential pressures, liquid levels, flow velocities, and heating powers. USNRC has provided film probes, impedance probes, string probes, liquid level detectors (LLDs), fluid distribution grids (FDGs), turbine meters, drag disks, densitometers, spool pieces, drag bodies, break through detectors and video optical probes. Locations of the JAERI-provided instruments are shown in Figs. A-20 through A-43.

Table A-1 Principal Dimensions of the SCTF

1.	Core Dimension		
	(1) Quantity of Bundle	8 Bundles	
	(2) Bundle Array	1 × 8	
	(3) Bundle Pitch	230 mm	
	(4) Rod Array in a Bundle	16 × 16	
	(5) Rod Pitch in a Bundle	14.3 mm	
	(6) Quantity of Heater Rod in a Bundle	236 rods	
	(7) Quantity of Non-Heated Rod in a Bundle	20 rods	
	(8) Total Quantity of Heater Rods	236×8=1,888	rods
	(9) Total Quantity of Non-Heated Rods	20×8=160	rods
	(10) Effective Heated Length of Heater Rod	3613 mm	
	(11) Diameter of Heater Rod	10.7 mm	
	(12) Diameter of Non-Heated Rod	13.8 mm	
2.	Flow Area & Fluid Volume		
	(1) Core Flow Area	0.25	m^2
	(2) Core Fluid Volume	0.903	m^3
	(3) Baffle Region Flow Area (isolated)	(0.096)	m^2
	(4) Baffle Region Fluid Volume (nominal)	0.355	m^3
	(5) Cross-Sectional Area of Core Additional Fluid Volumes Including Gap between Core Barrel and Pressure Vessel Wall and Various Penetration Holes	0.07 0.10	m^2 m^2
	(6) Downcomer Flow Area	0.158	m^2
	(7) Upper Annulus Flow Area	0.158	m^2
	(8) Upper Plenum Horizontal Flow Area (max.)	0.541	m^2
	(9) Upper Plenum Vertical Flow Area	0.525	m^2
	(10) Upper Plenum Fluid Volume	1.156	m^3
	(11) Upper Head Fluid Volume	0.86	m^3
	(12) Lower Plenum Fluid Volume (excluding below downcomer)	1.305	m^3
	(13) Steam Generator Inlet Plenum Simulator Flow Area	0.626	m^2
	(14) Steam Generator Inlet Plenum Simulator Fluid Volume	0.931	m^3
	(15) Steam Water Separator Fluid Volume	5.3	m^3
	(16) Flow Area at the Top Plate of Steam Generator Inlet Plenum Simulator	0.195	m^2
	(17) Hot Leg Flow Area	0.0826	m^2

Table A-1 (continue)

(18)	Intact Cold Leg Flow Area (Diameter = 297.9 mm) Inverted U-Tube with 0.0314 m^2 Cross-Sectional Area (Diameter = 200 mm) and 10 m Height from the Top of Steam Generator Inlet Plenum Simulator Can Be Added As an Option.	0.0697 m^2
(19)	Broken Cold Leg Flow Area (Diameter = 151.0 mm)	0.0197 m^2
(20)	Containment Tank-I Fluid Volume	30 m^3
(21)	Containment Tank-II Fluid Volume	50 m^3
(22)	Flow Area of Exhausted Steam Line from Containment Tank-II to the Atmosphere	see Fig. 3-63

3. Elevation & Height

(1)	Top Surface of Upper Core Support Plate (UCSP)	0 mm
(2)	Bottom Surface of UCSP	− 40 mm
(3)	Top of the Effective Heated Length of Heater Rod	− 444 mm
(4)	Bottom of the Effective Heated Length of Heater Rod	−4,057 mm
(5)	Bottom of the Skirt in the Lower Plenum	−5,270 mm
(6)	Bottom of Intact Cold Leg	+ 724 mm
(7)	Bottom of Hot Leg	+1,050 mm
(8)	Top of Upper Plenum	+2,200 mm
(9)	Bottom of Steam Generator Inlet Plenum Simulator	+1,933 mm
(10)	Centerline of Loop Seal Bottom	−2,281 mm
(11)	Bottom Surface of End Box	− 263 mm
(12)	Top of Upper Annulus of Downcomer	+2,234 mm
(13)	Height of Steam Generator Inlet Plenum Simulator	1,595 mm
(14)	Height of Loop Seal	3,140 mm
(15)	Inner Height of Hot Leg Pipe	737 mm
(16)	Bottom of Lower Plenum	−5,772 mm
(17)	Top of Upper Head	+2,887 mm

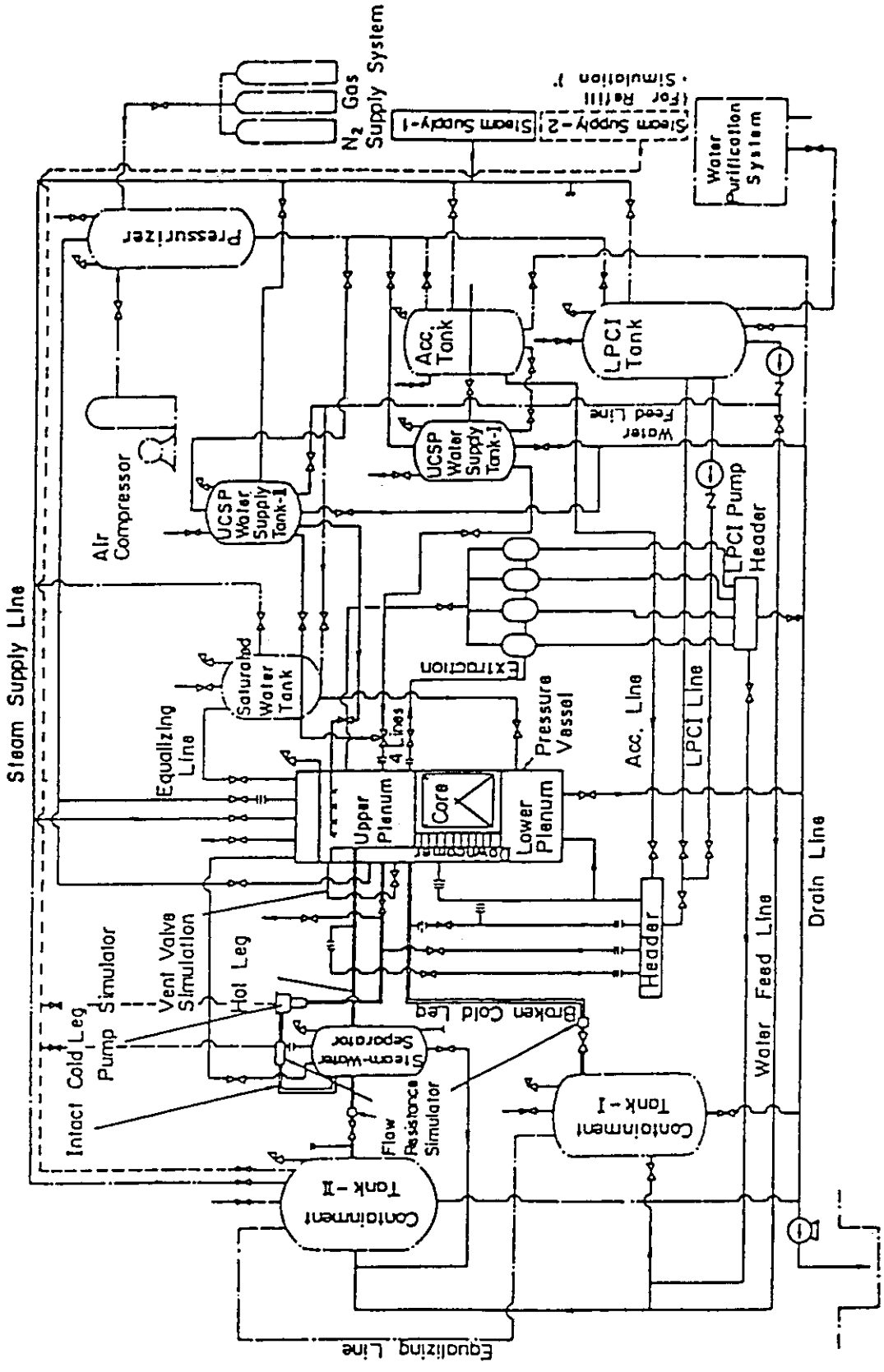

Fig. A-1 Schematic Diagram of Slab Core Test Facility

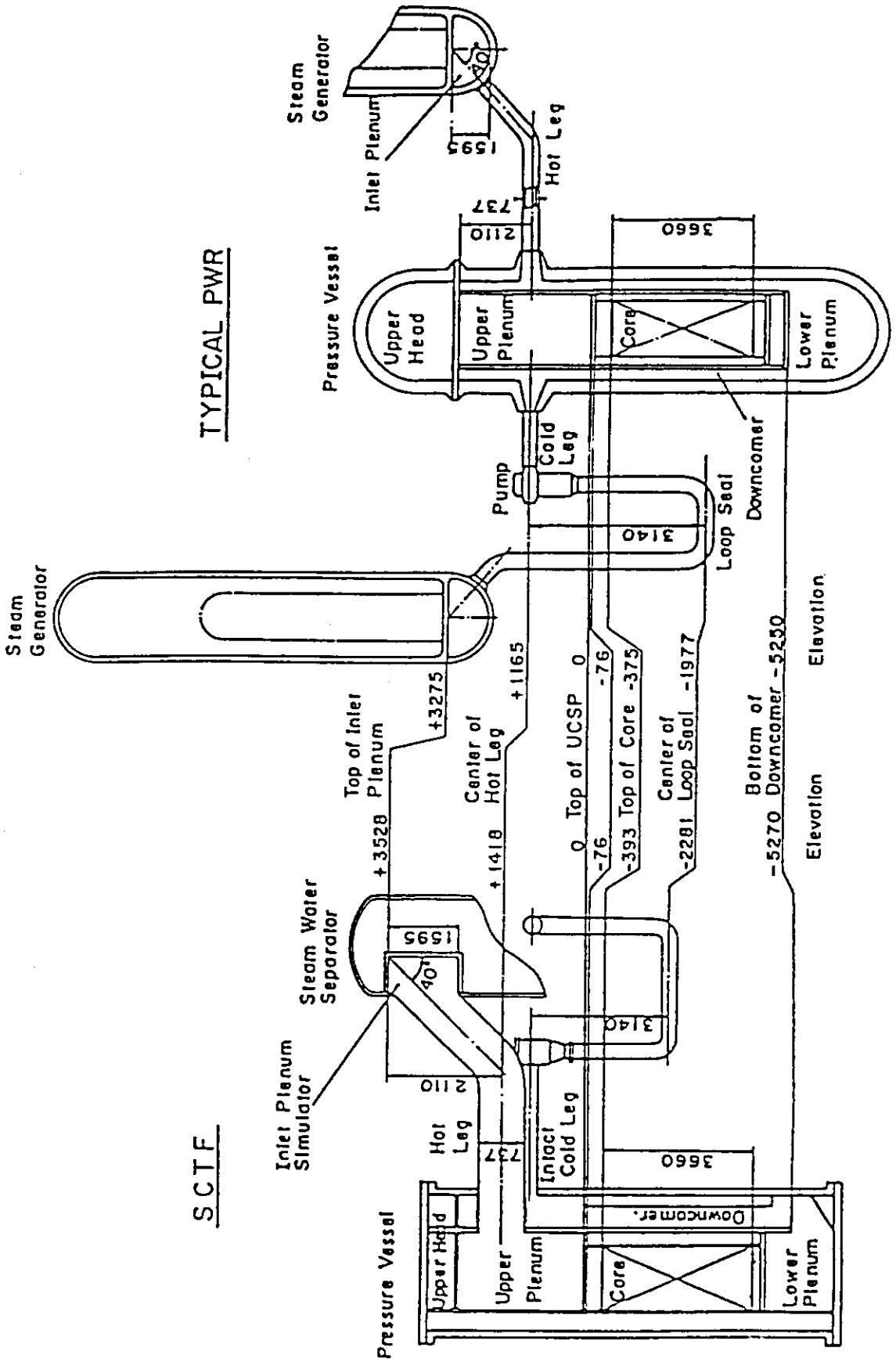

Fig. A-2 Comparison of Dimensions between SCTF and a Reference PWR

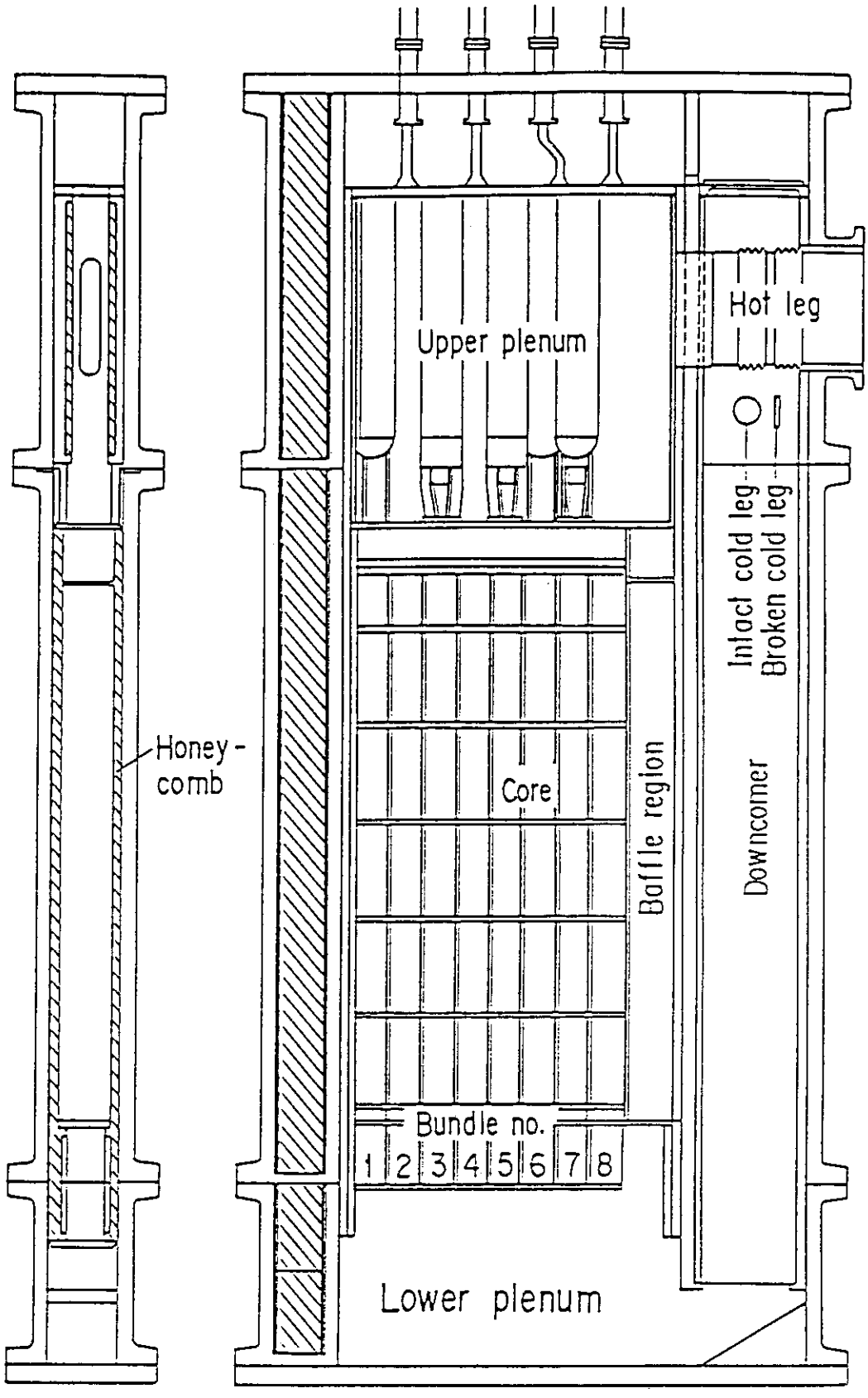

Fig. A-3 Vertical Cross Sections of Pressure Vessel

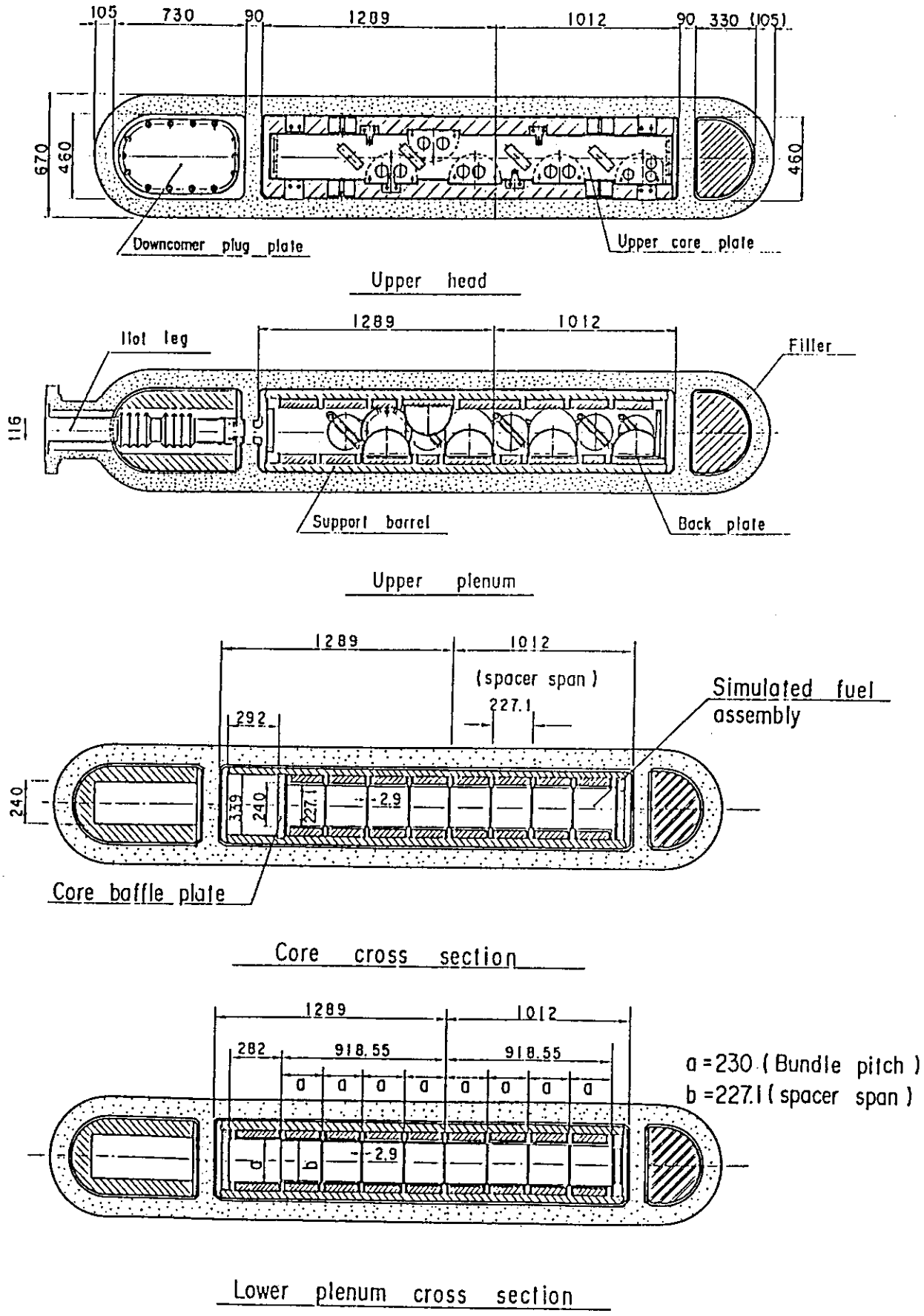

Fig. A-4 Horizontal Cross Sections of Pressure Vessel

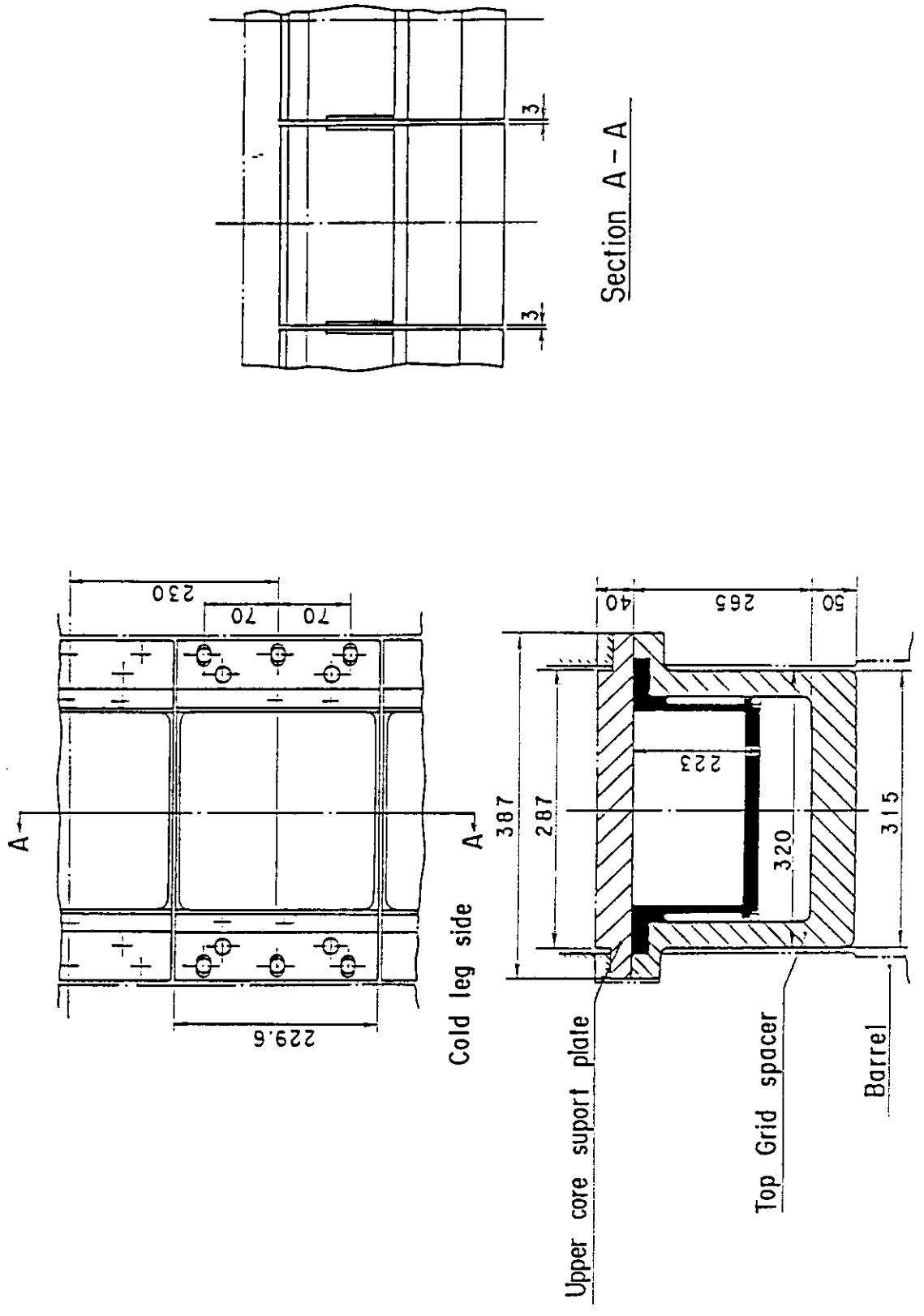

Fig. A-5 Arrangement and Principal Dimension of End Boxes and Top Grid Spacers

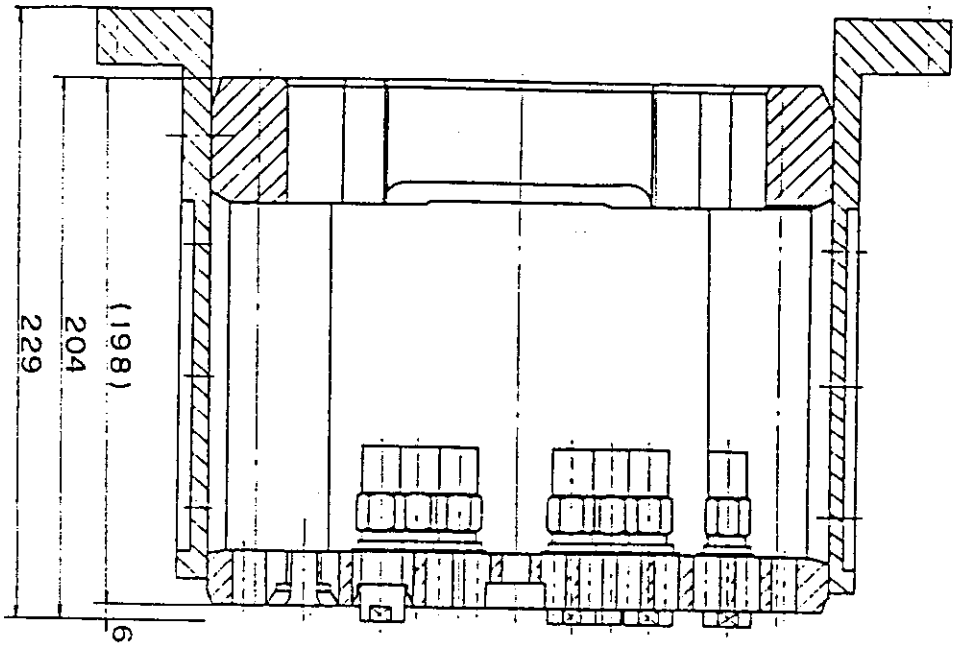

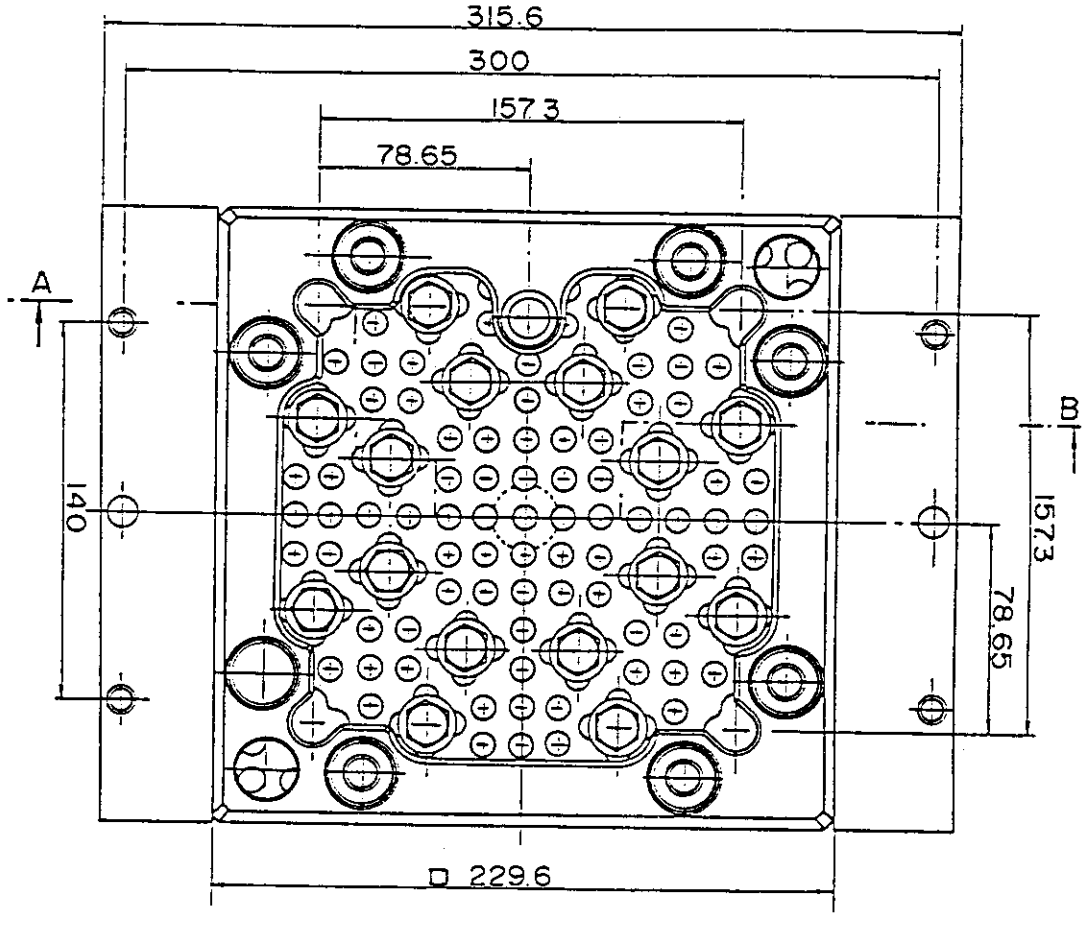

Fig. A-6 Configuration and Dimension of End Boxes

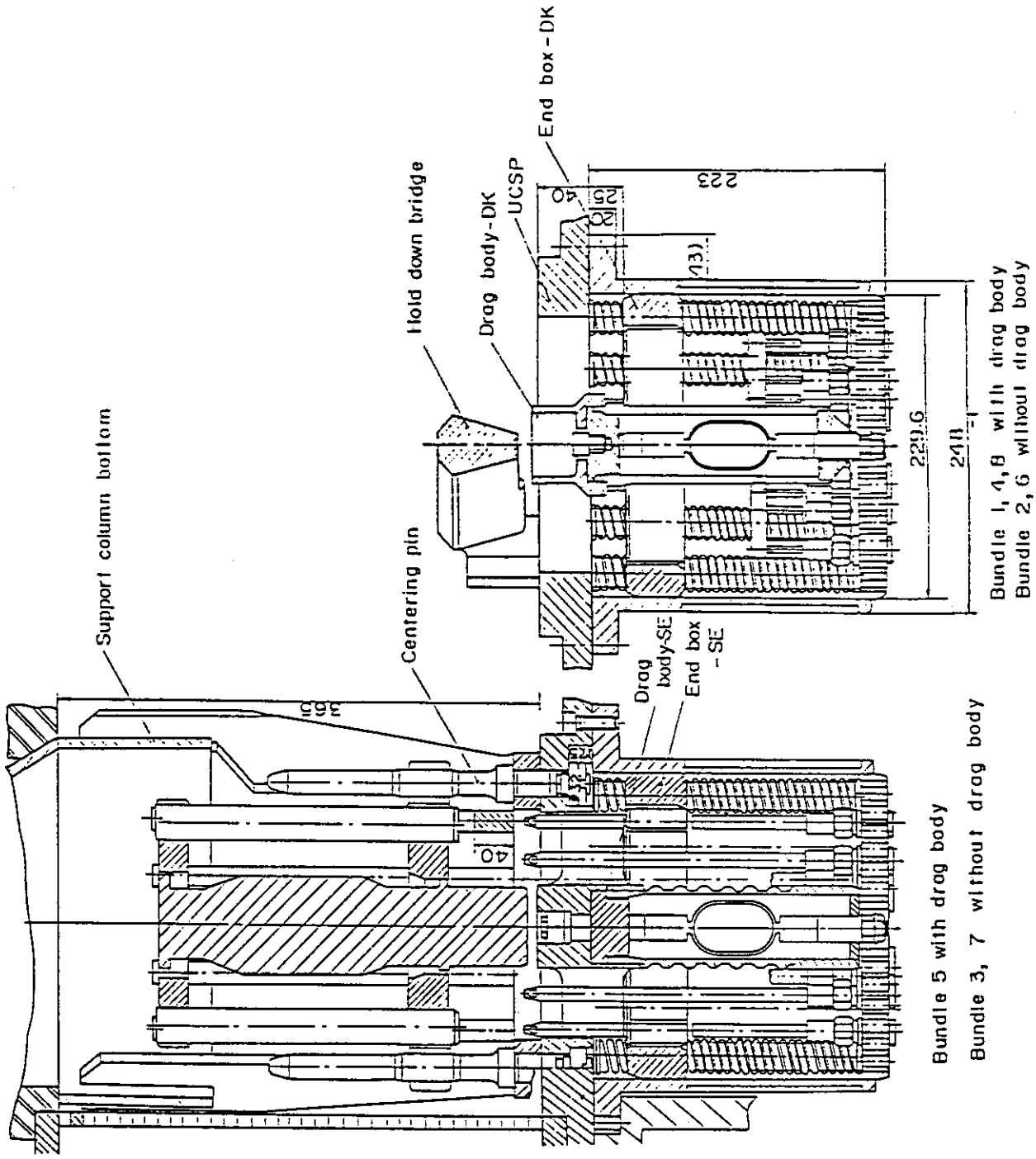

Fig. A-7 Detail of End Boxes with Drag Bodies

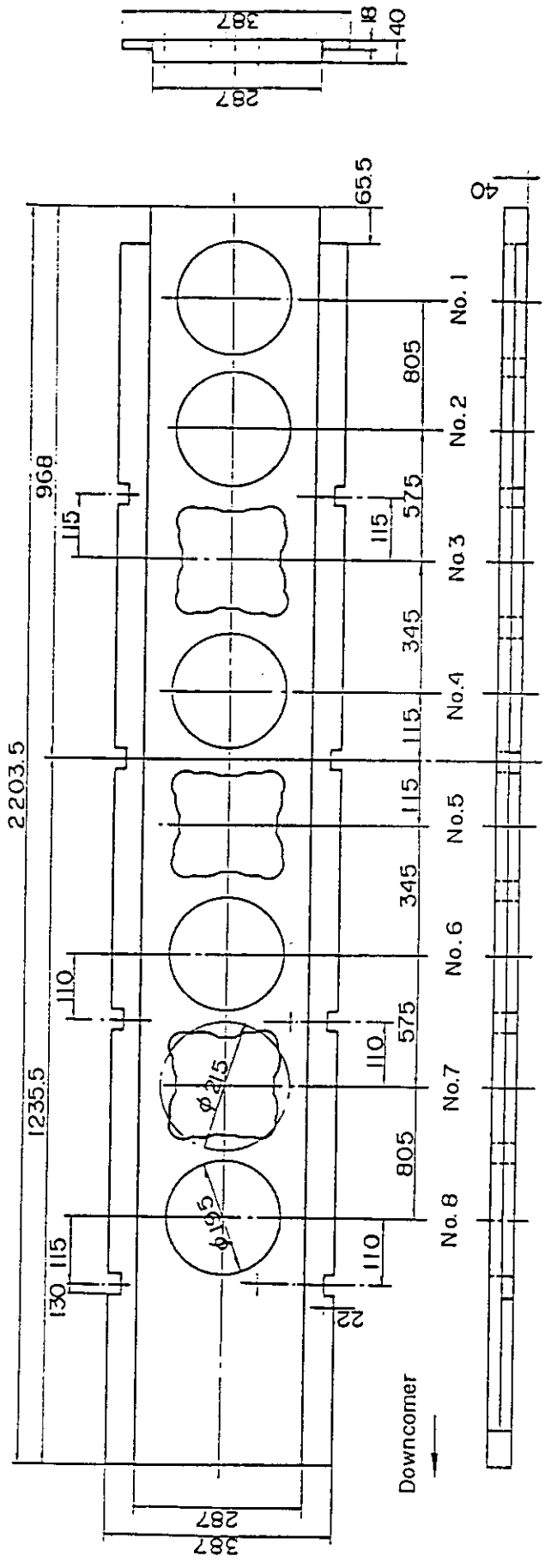

Fig. A-8 Dimension of Upper Core Support Plate

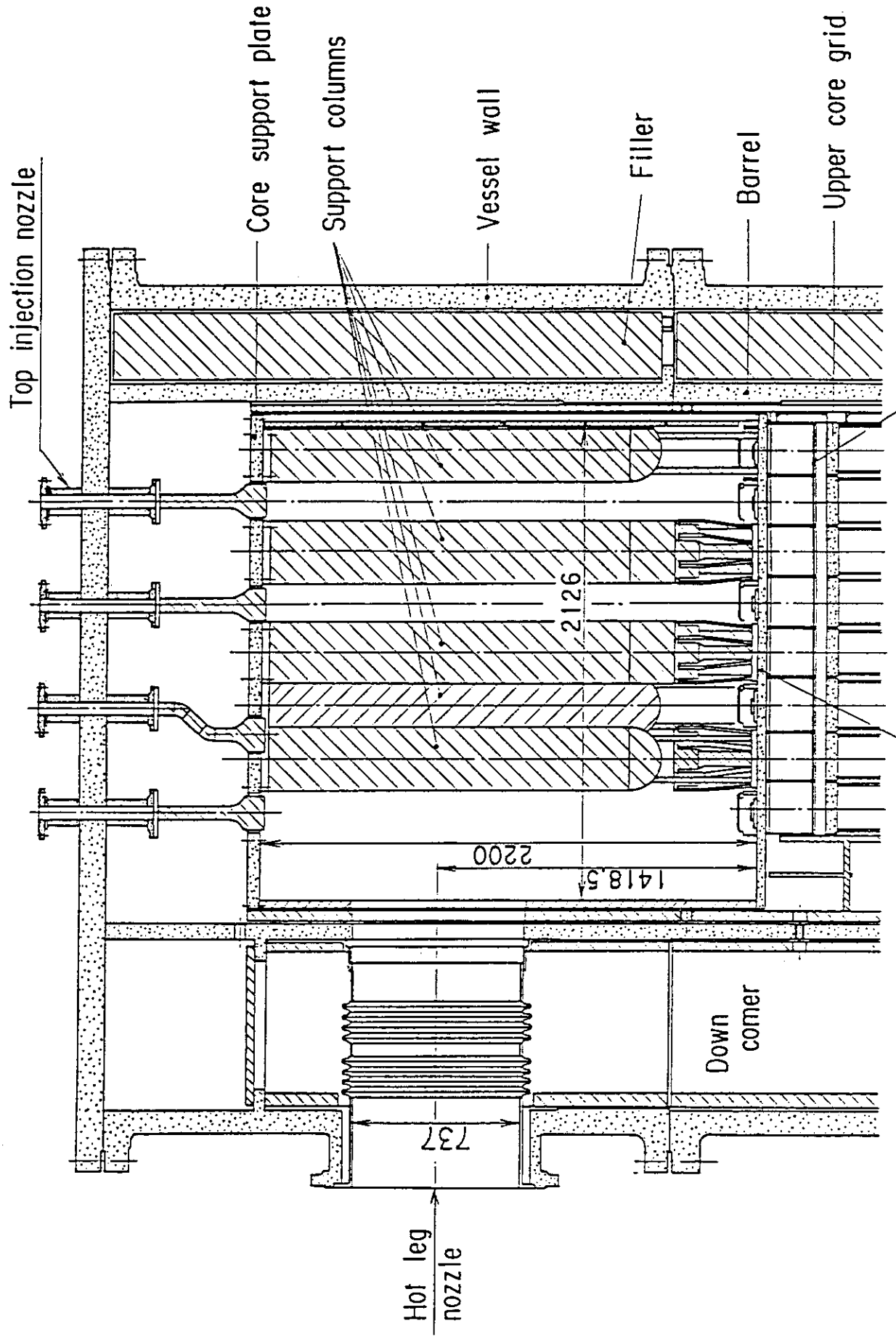

Fig. A-9 Vertical Cross Section of Upper Plenum Internals

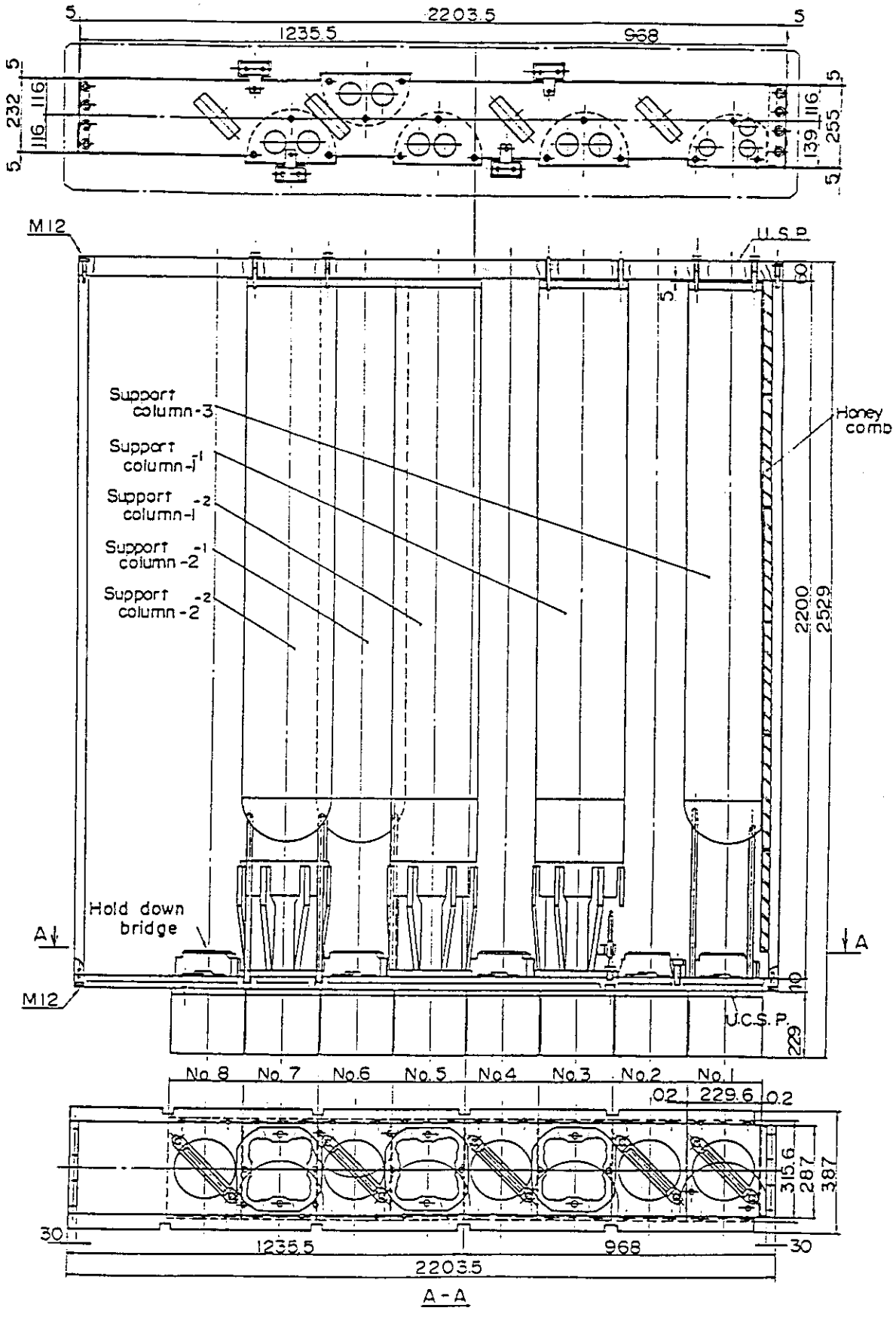

Fig. A-10 Three Kinds of CRGA Support Column

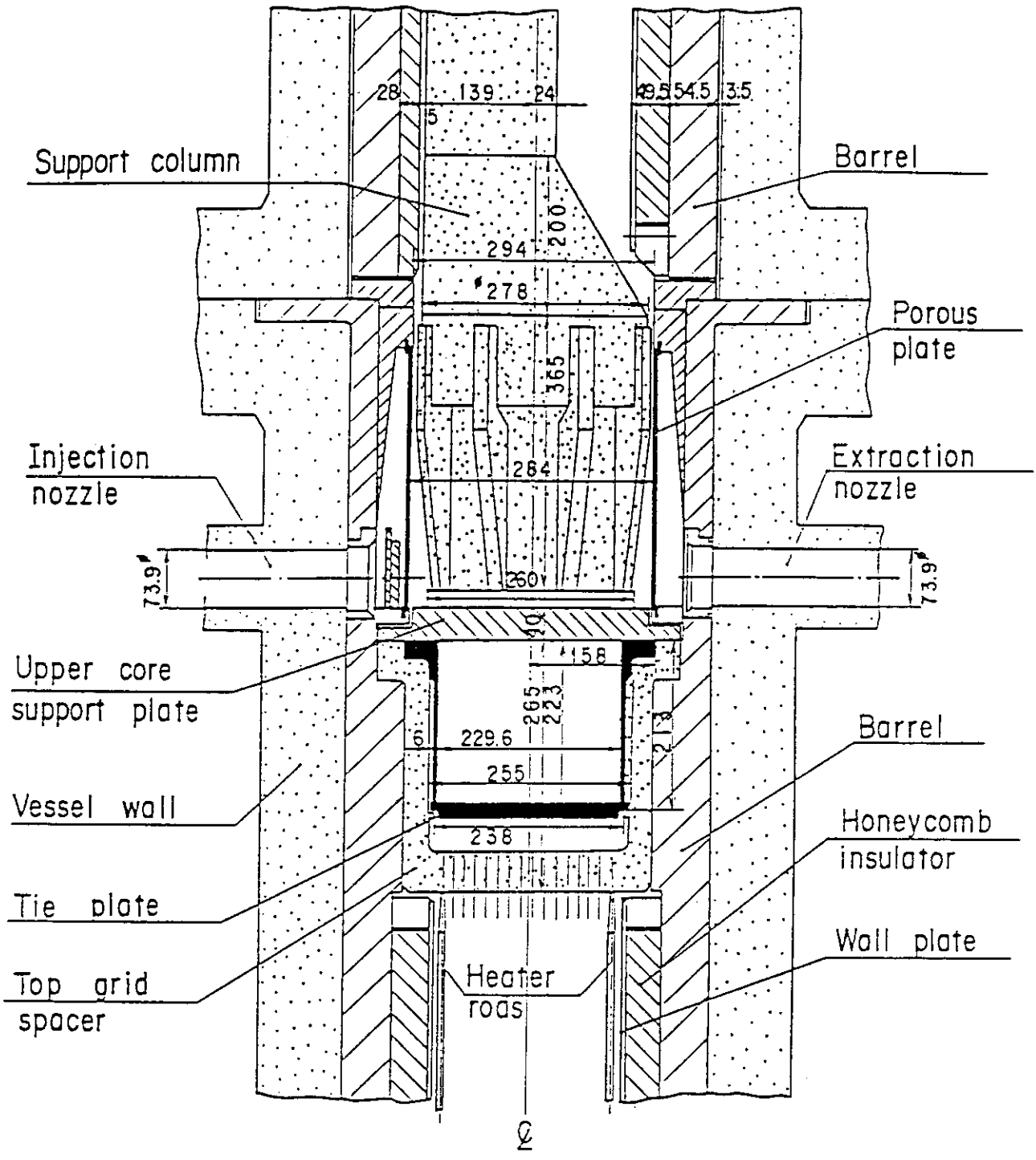

Fig. A-11 Vertical Cross Section of Interface between Core and Upper Plenum

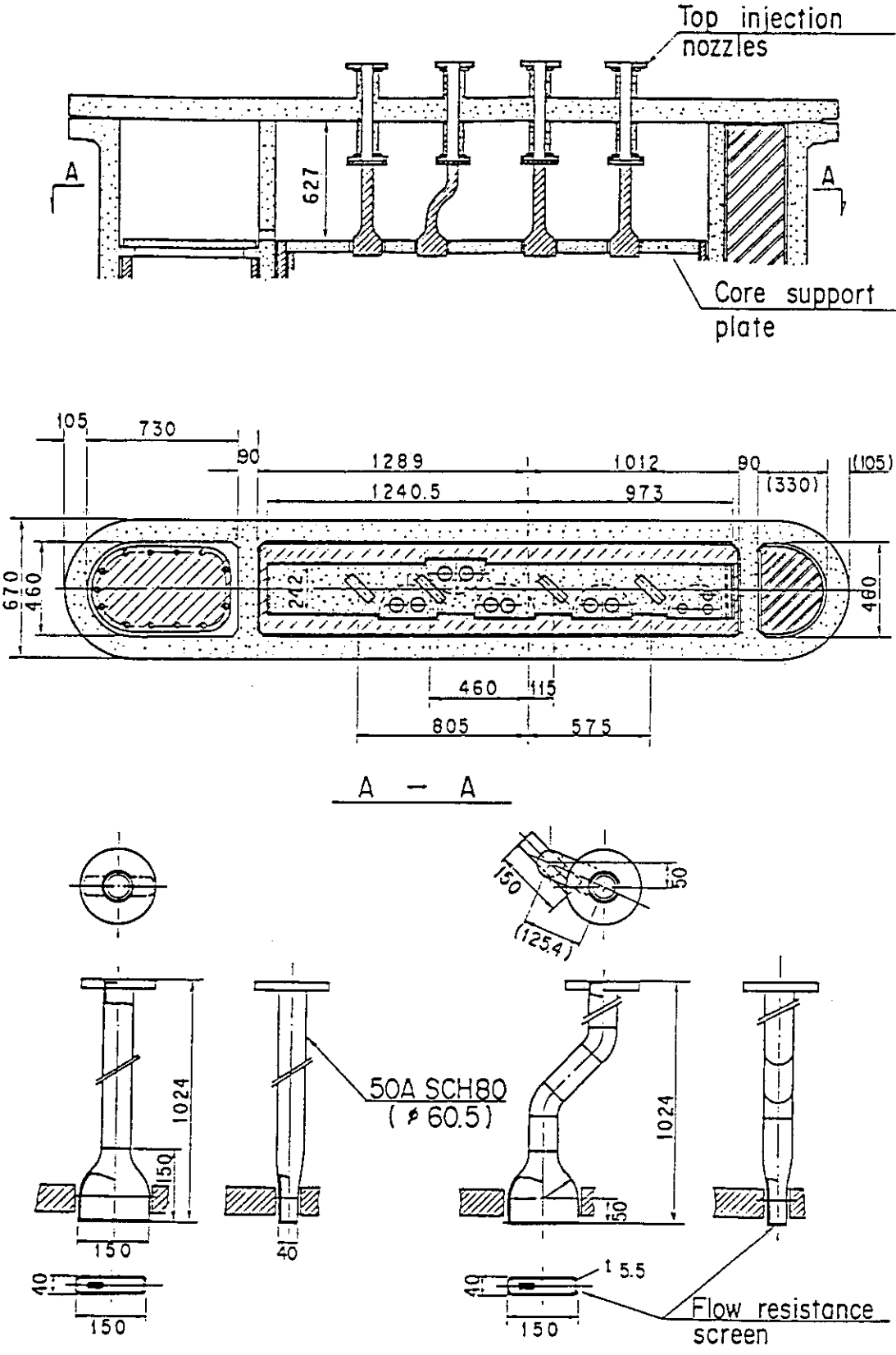

Fig. A-12 Schematic of Upper Head

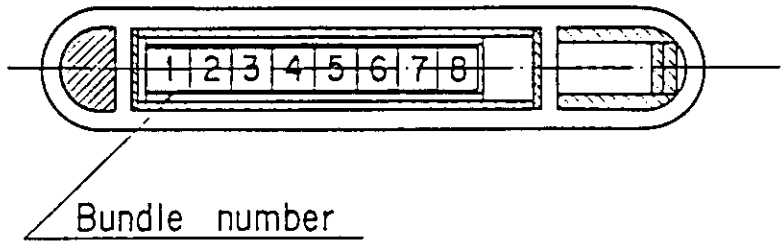

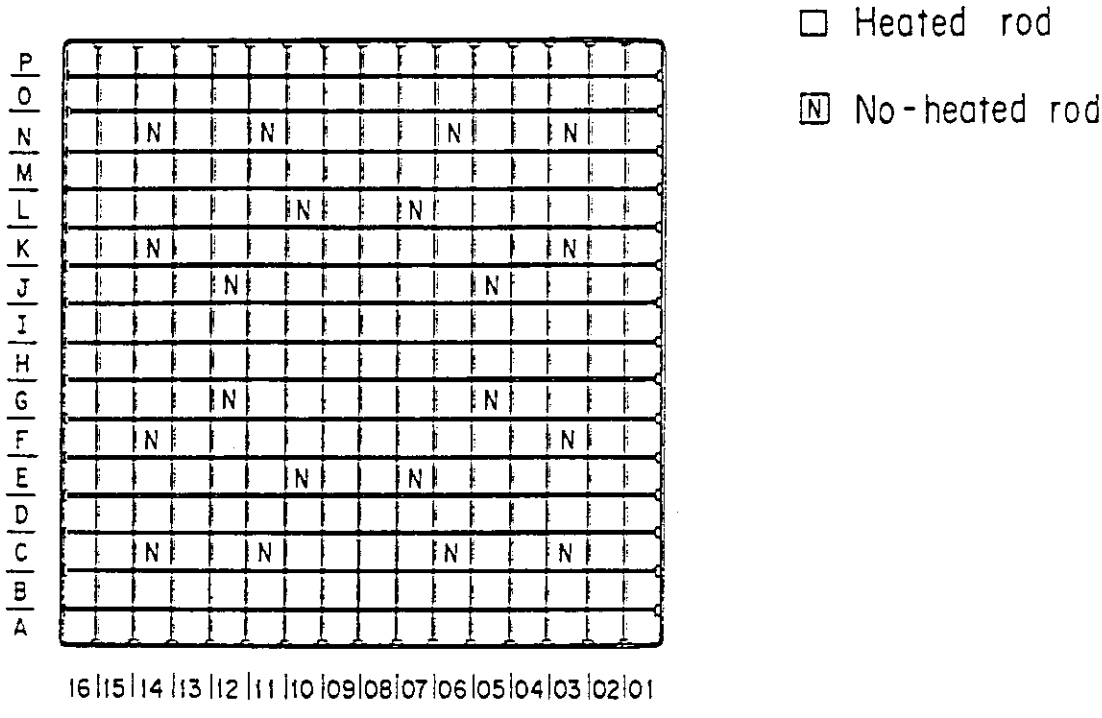

Fig. A-13 Arrangement of Heater Rod Bundles

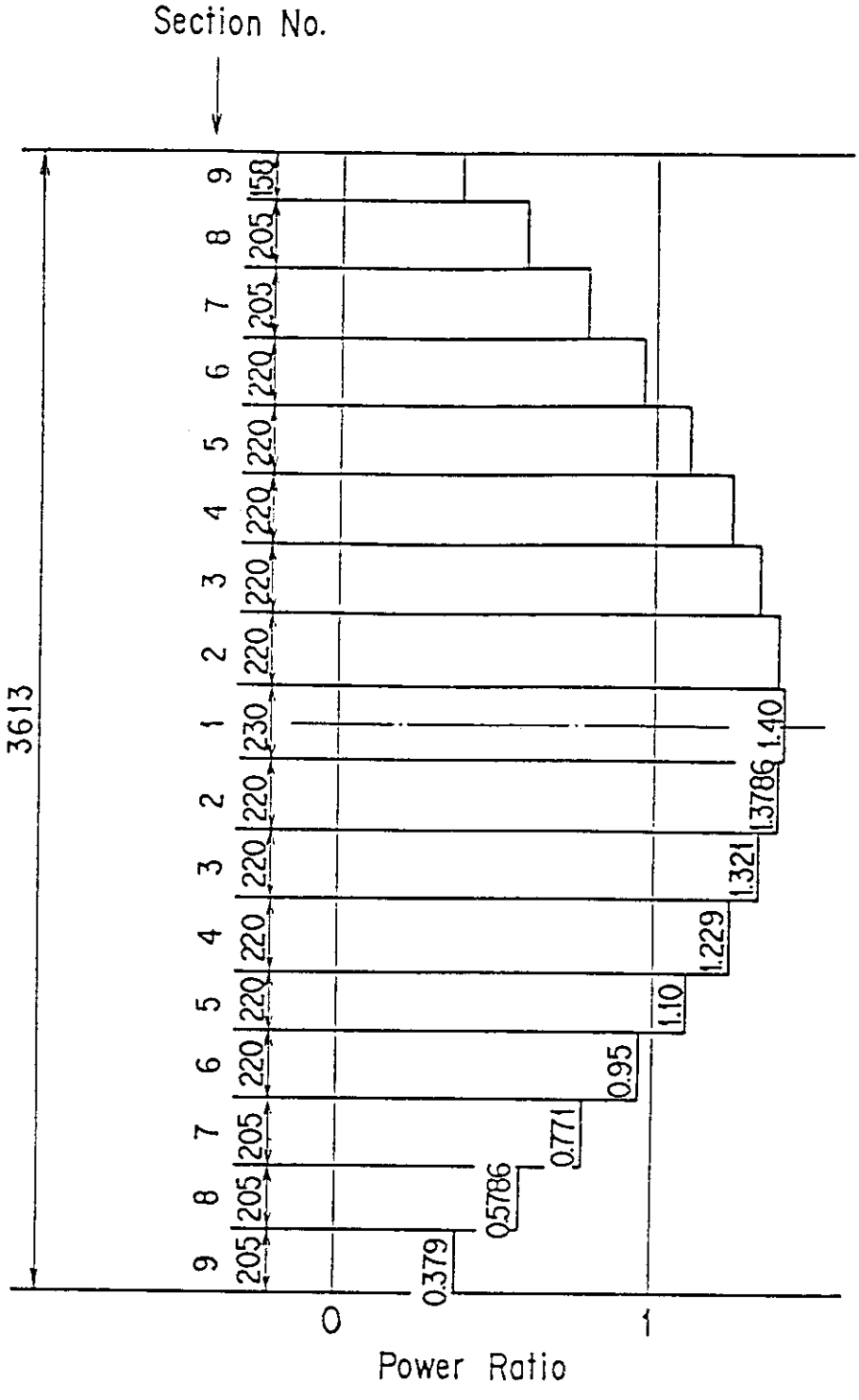

Fig. A-14 Axial Power Distribution of Heater Rods

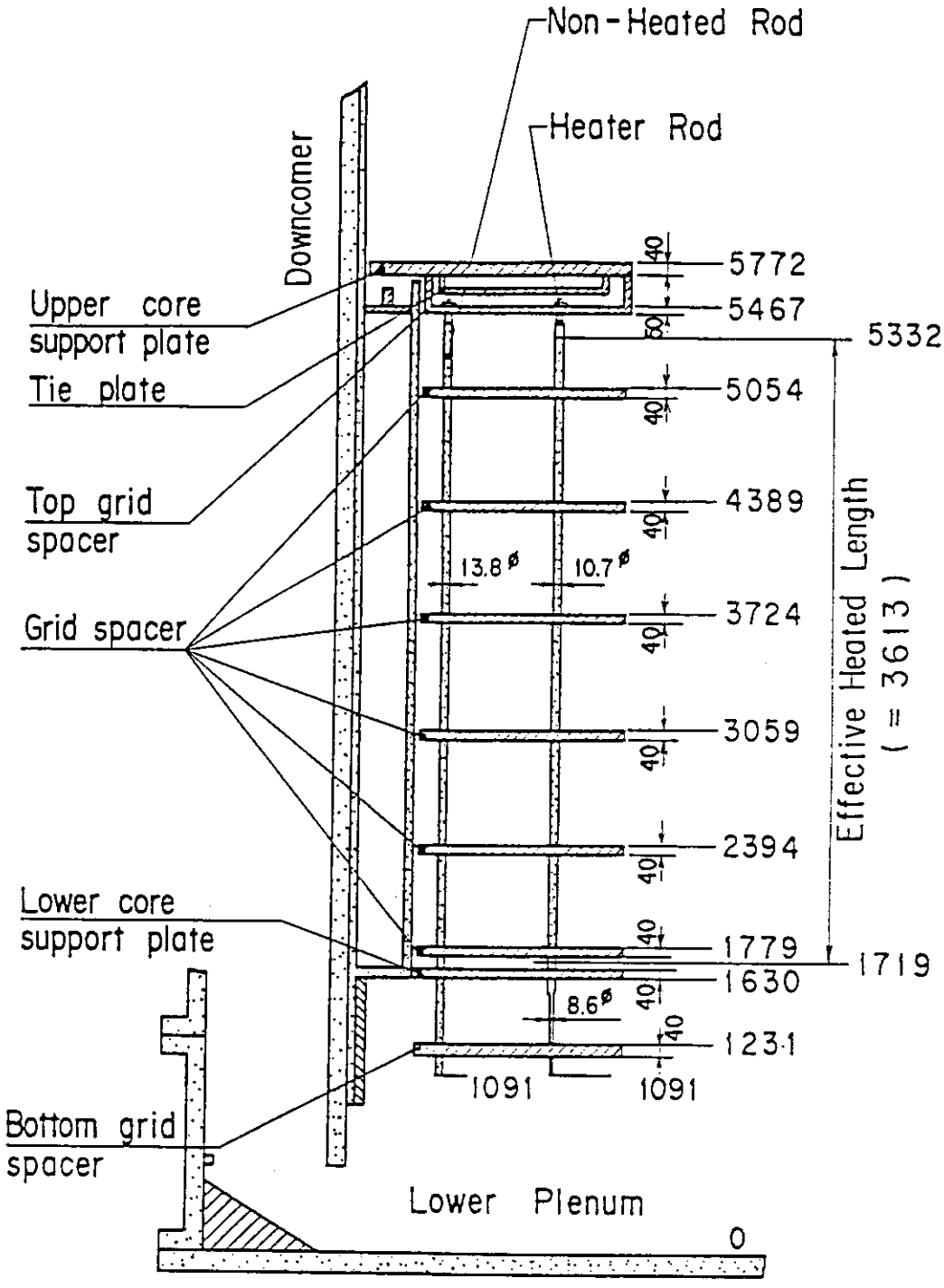

Fig. A-15 Relative Elevation and Dimension of Core

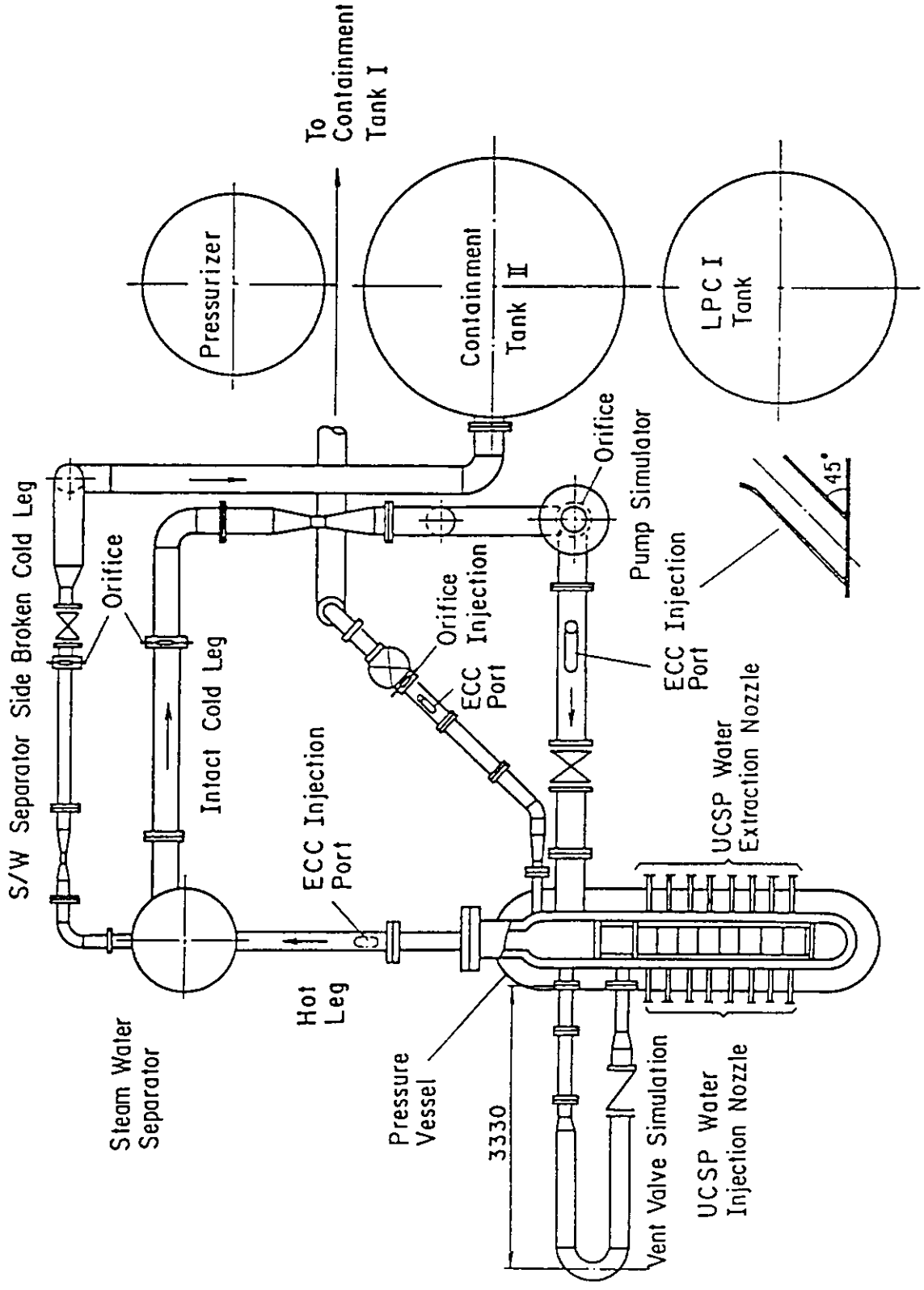

Fig. A-16 Overview of the Arrangements of SCTF

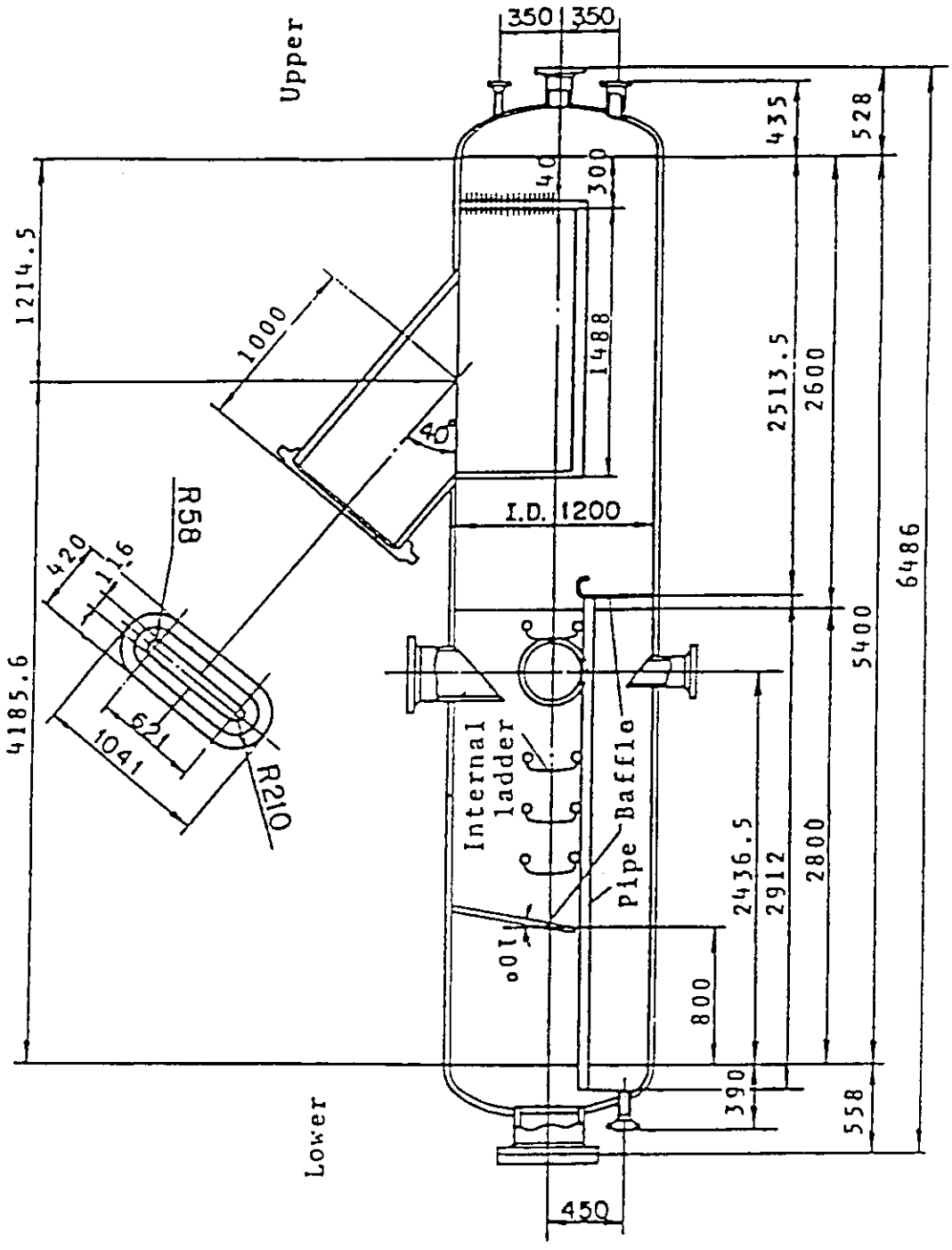

Fig. A-17 Steam/Water Separator

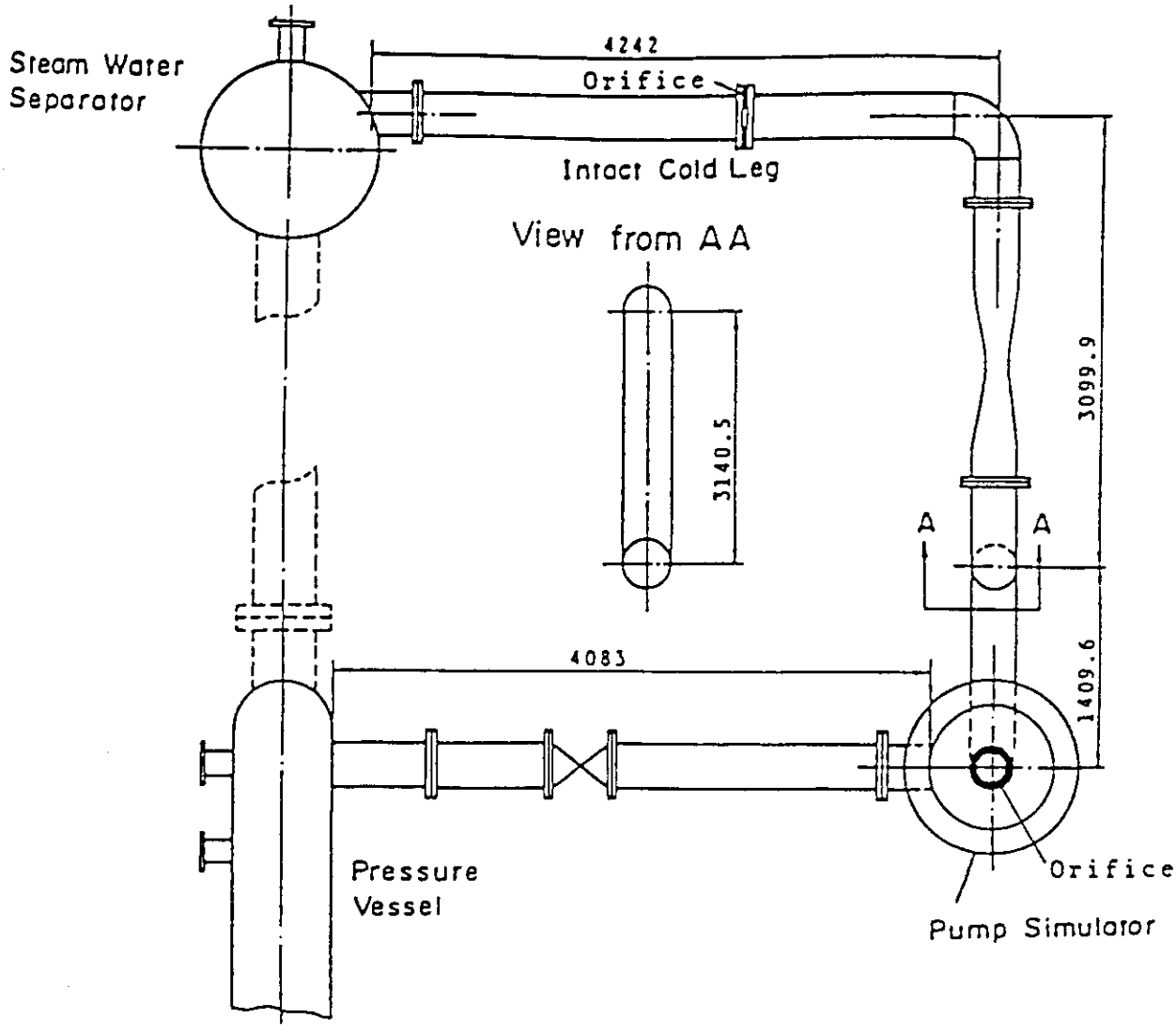

Fig. A-18 Arrangement of Intact Cold Leg

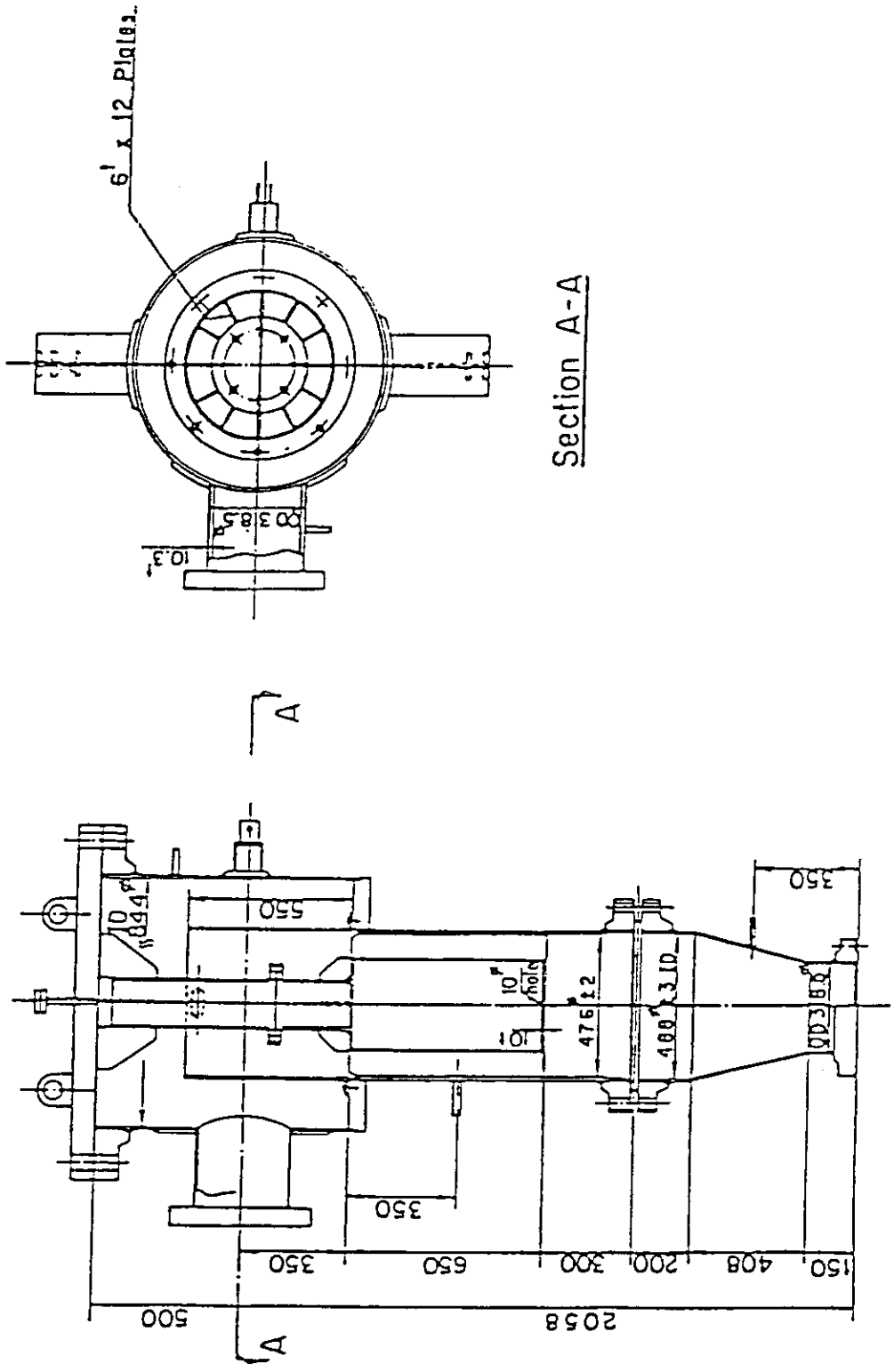

Fig. A-19 Configuration and Dimension of Pump Simulator

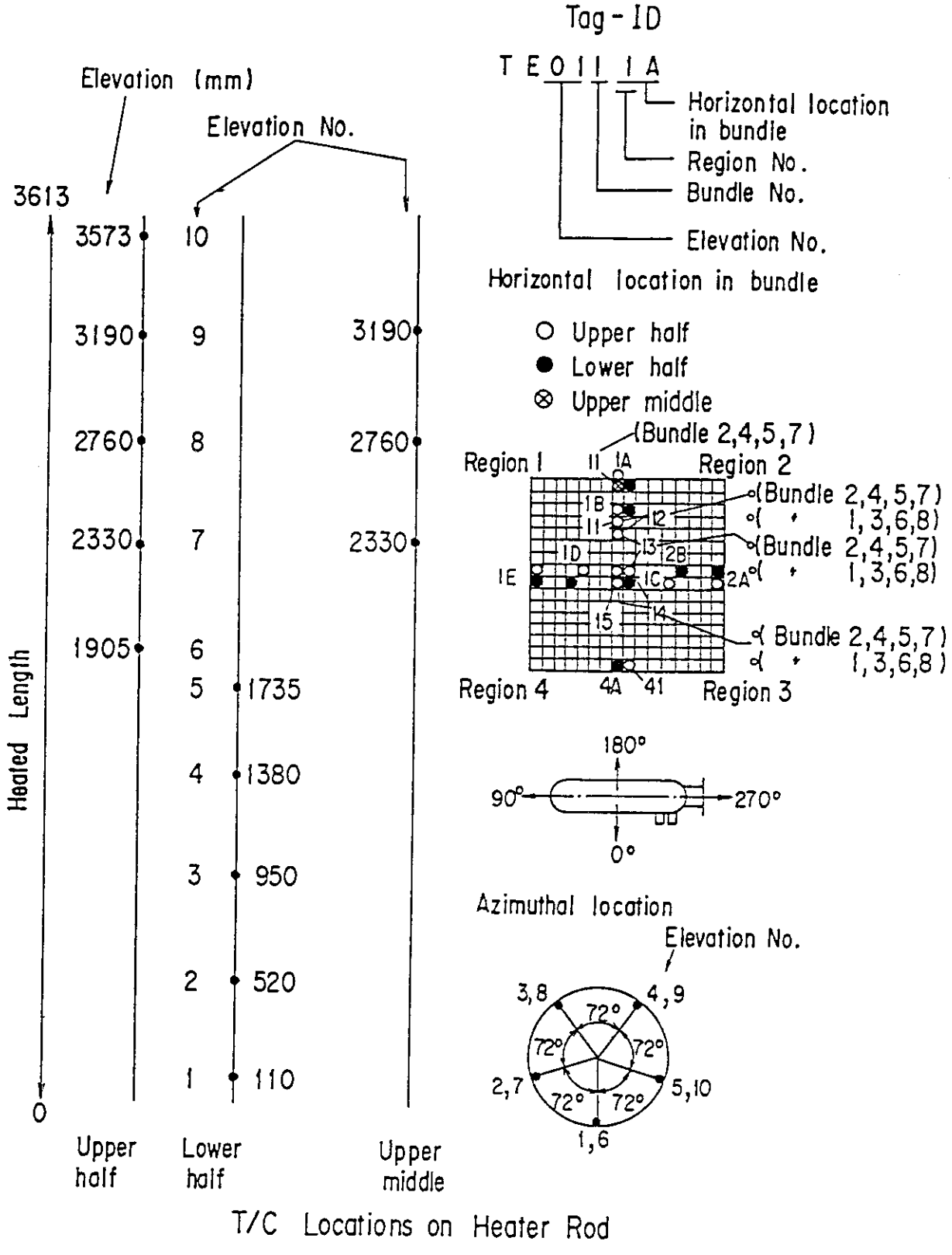

Fig. A-20 Thermocouple Locations of Heater Rod Surface Temperature Measurements

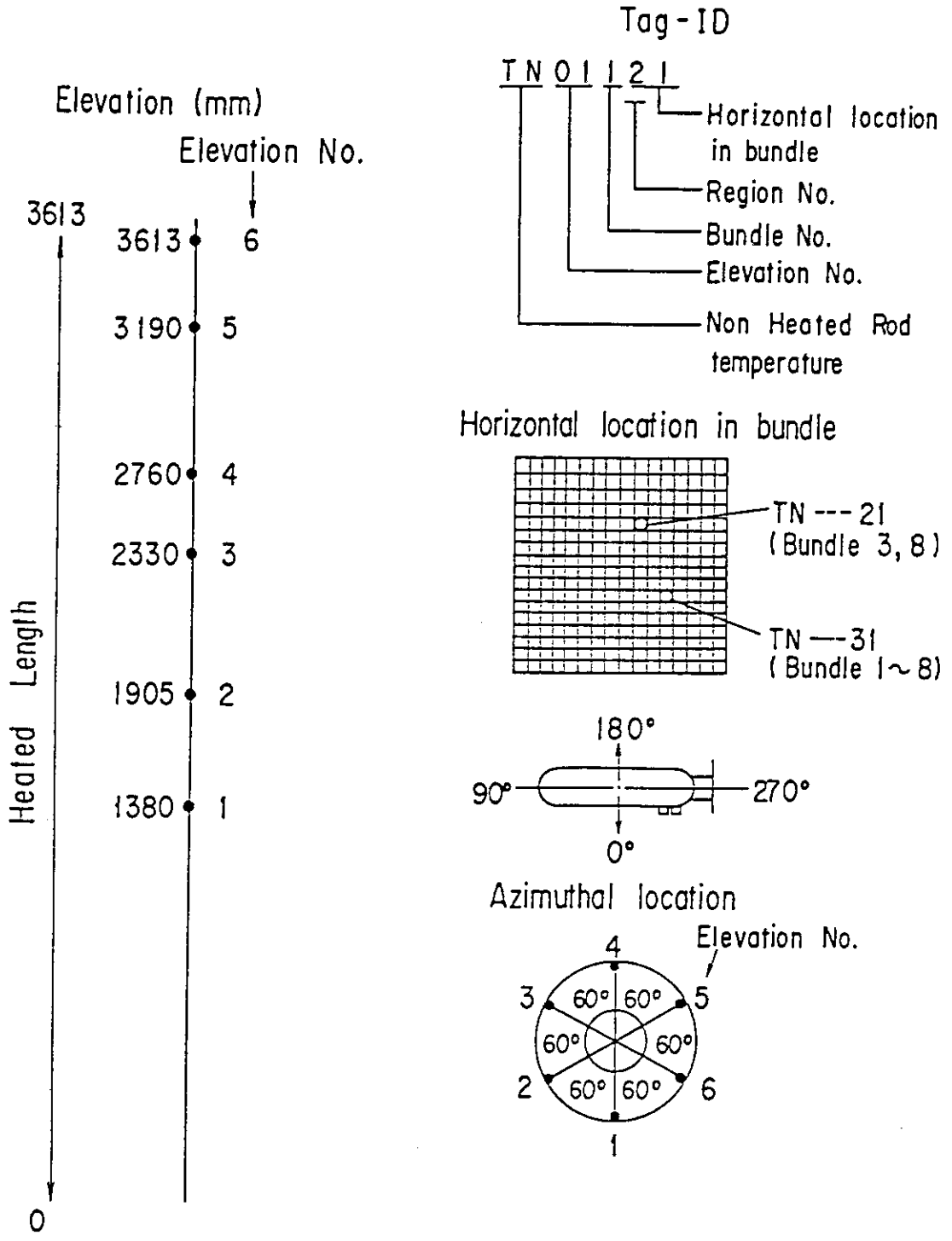

Fig. A-21 Thermocouple Locations of Non-Heated Rod Surface temperature Measurements

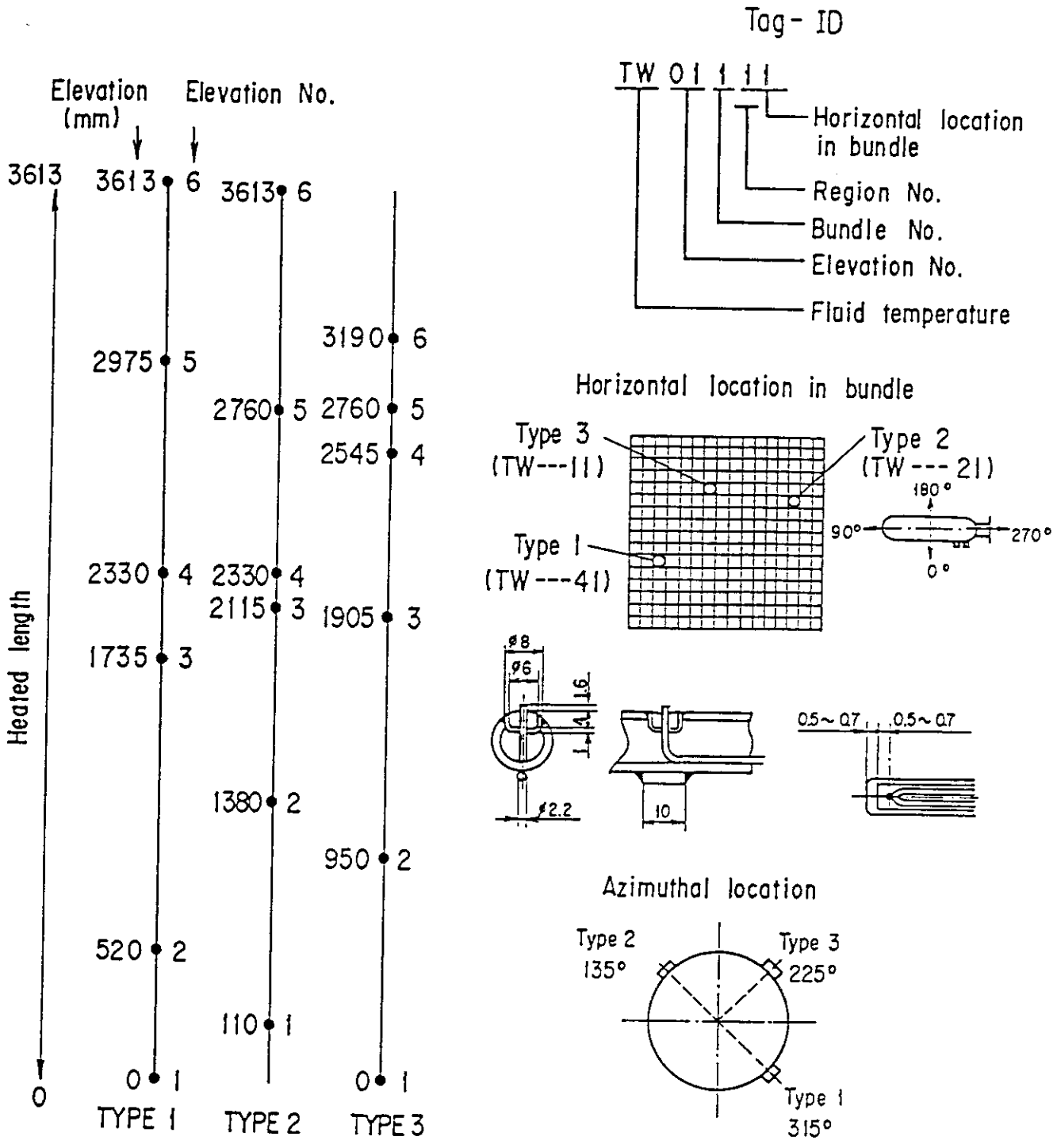

Fig. A-22 Thermocouple Locations of Fluid Temperature Measurements in Core

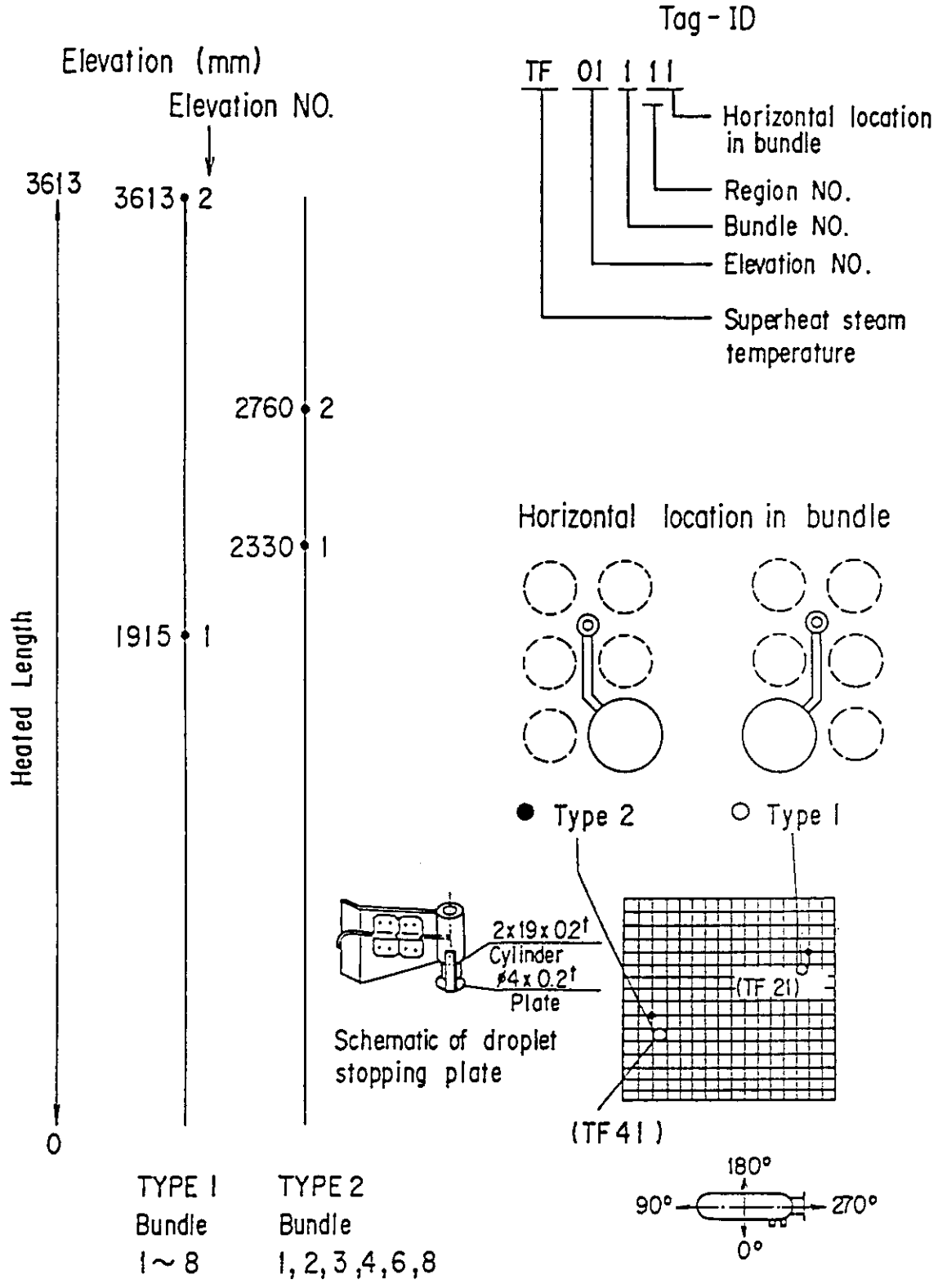

Fig. A-23 Thermocouple Locations of Steam Temperature Measurements in Core

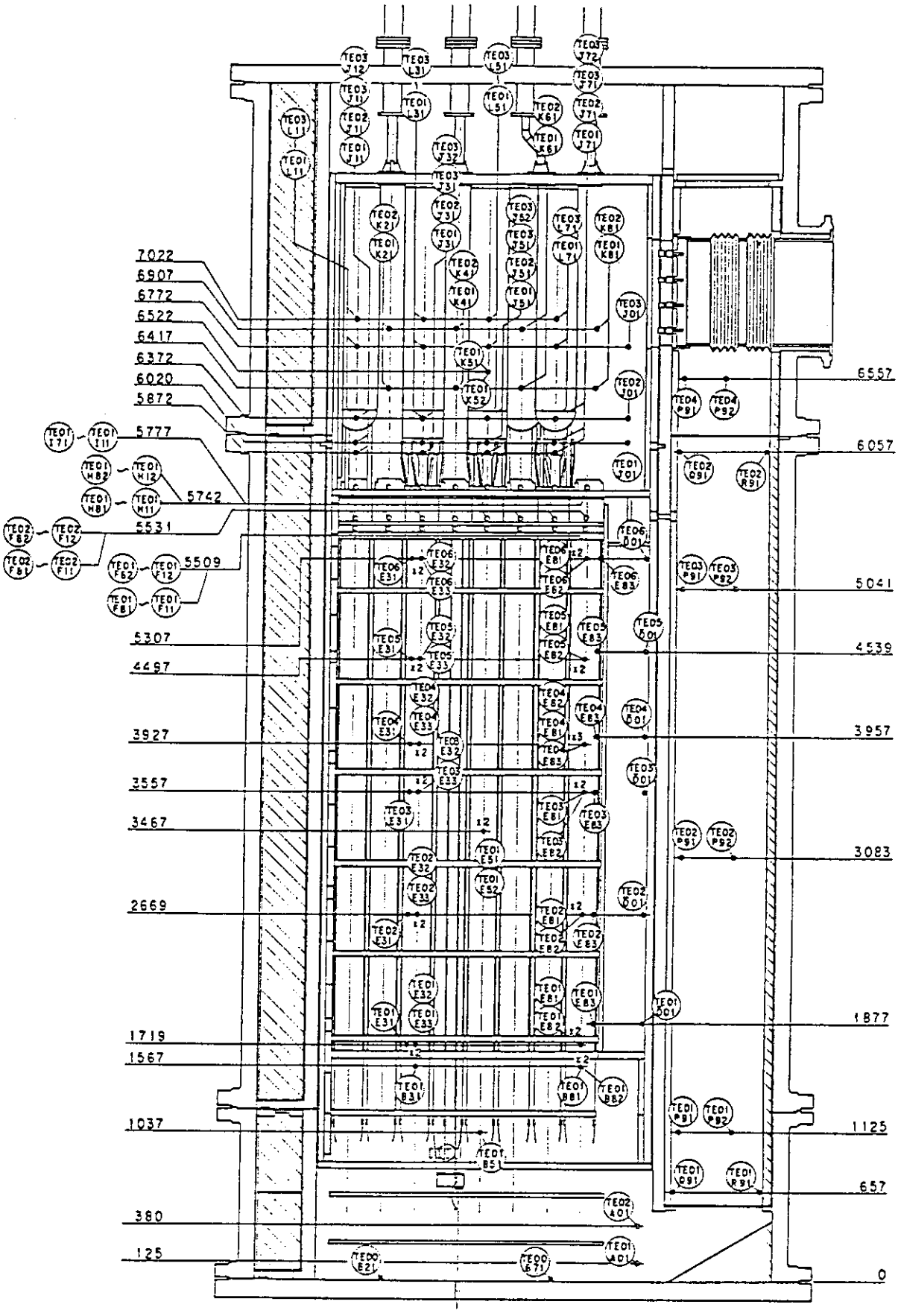

Fig. A-24 Thermocouple Locations of Temperature Measurements in Pressure Vessel except Core Region (Vertical View)

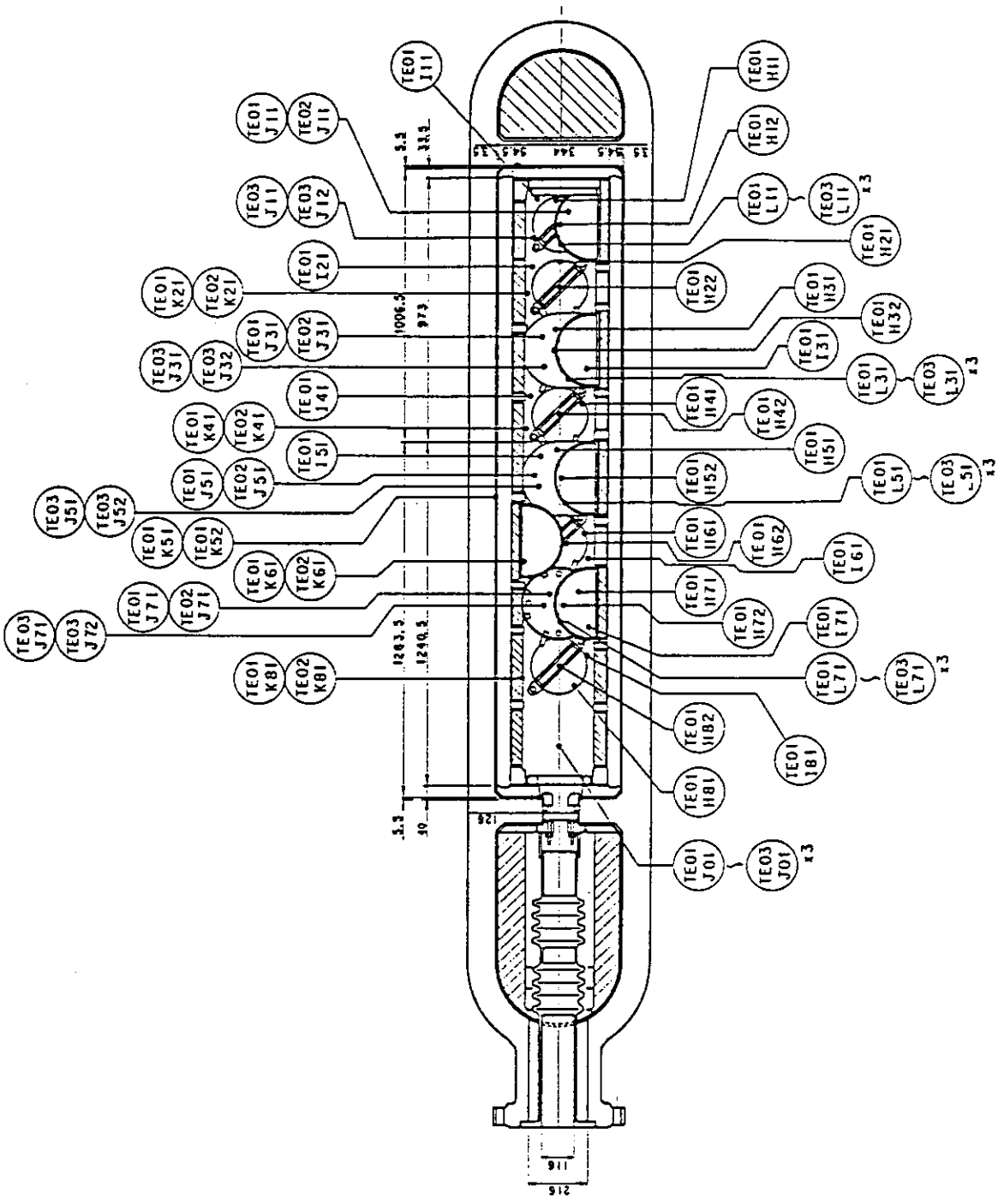

Fig. A-25 Thermocouple Locations of Temperature Measurements in Upper Plenum (Horizontal View)

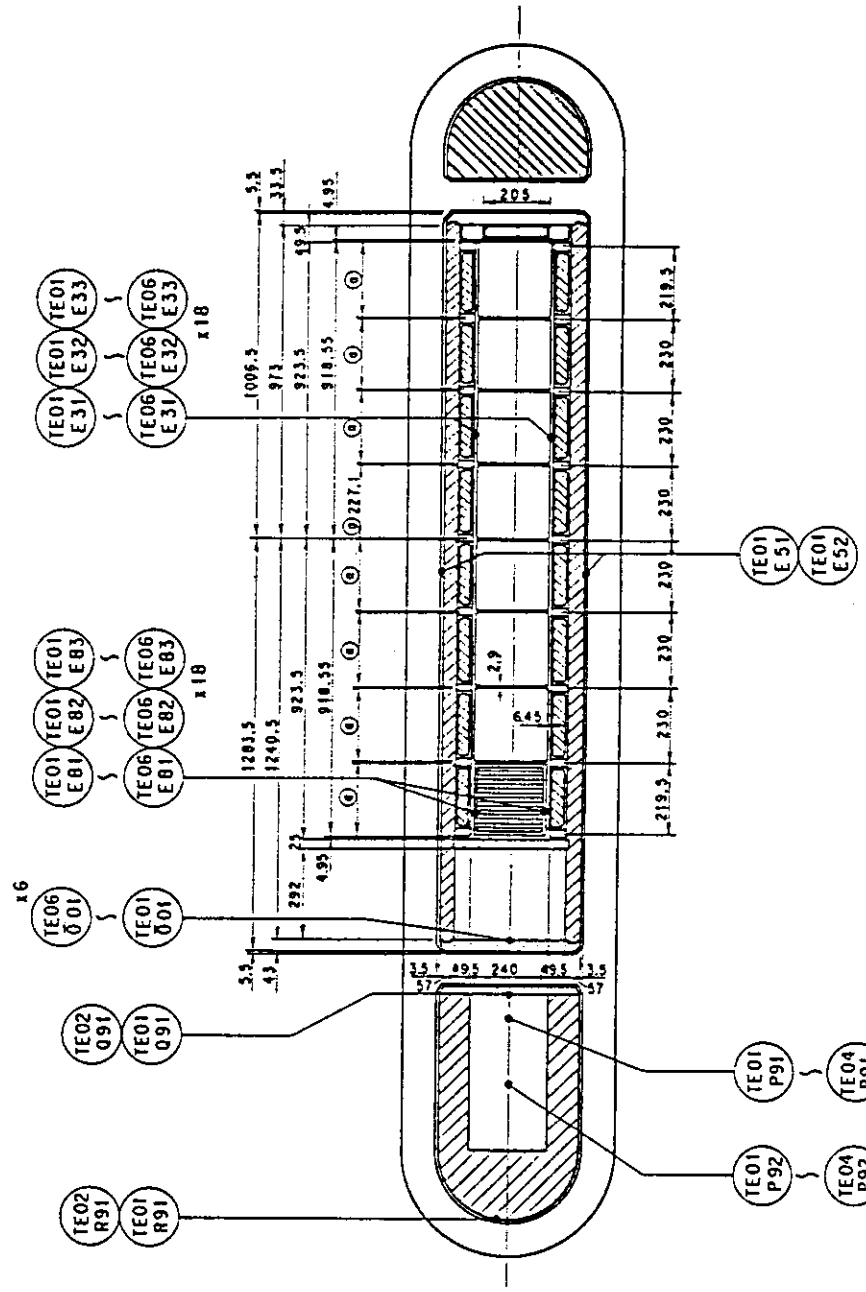

Fig. A-26 Thermocouple Locations of Temperature Measurements in Pressure Vessel except Upper Plenum (Horizontal View)

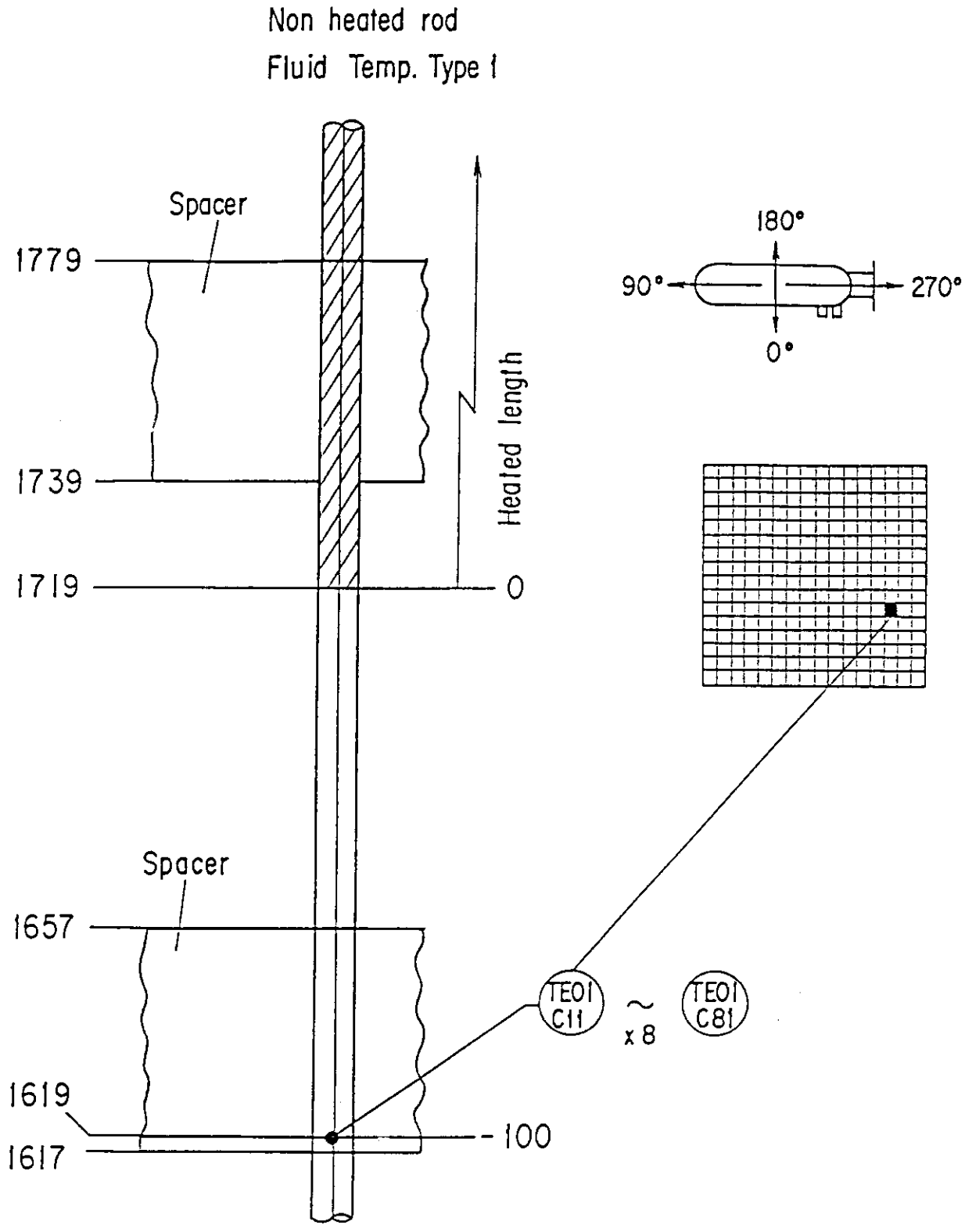

Fig. A-27 Thermocouple Locations of Fluid Temperature Measurements at Core Inlet

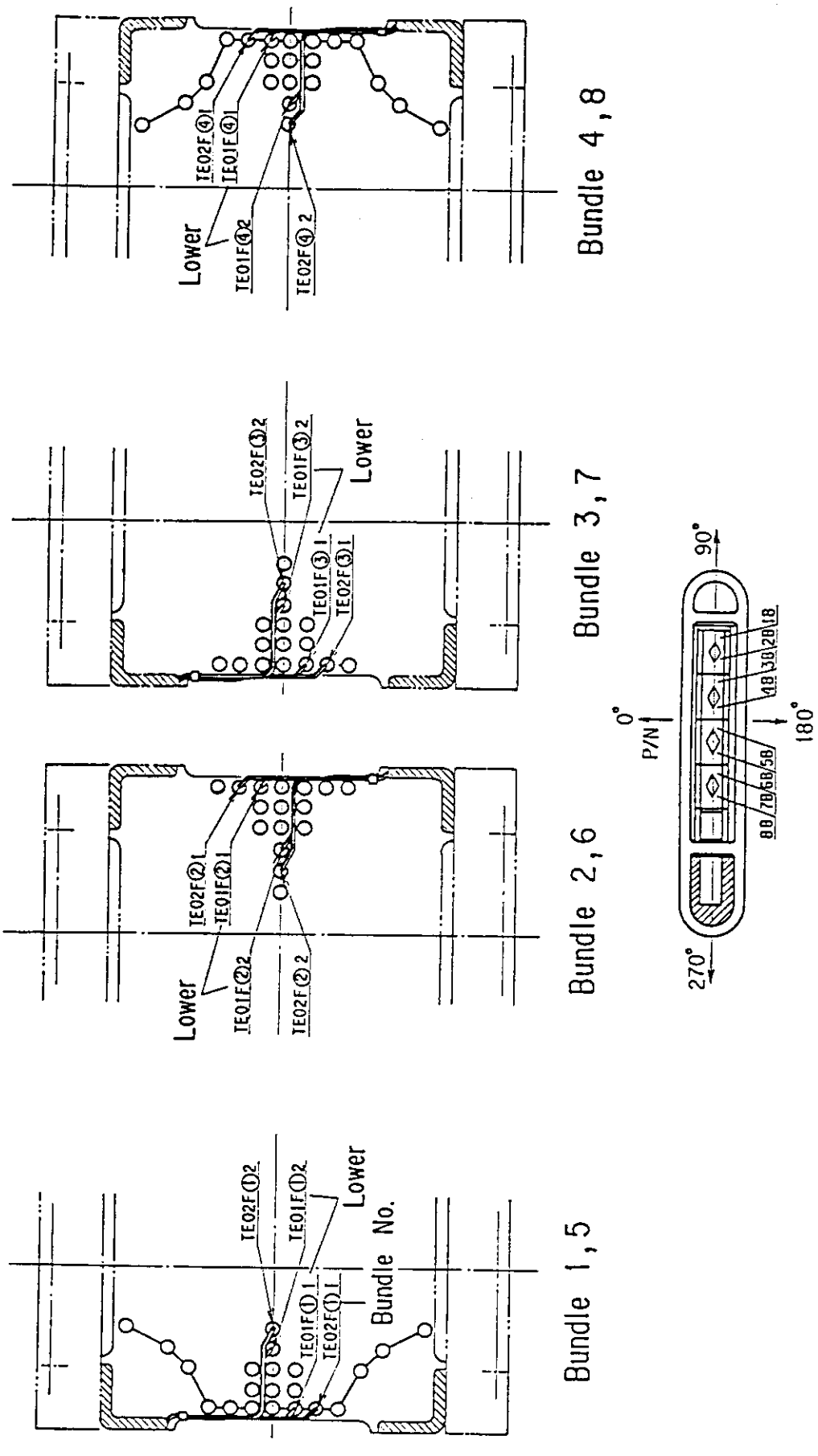

Fig. A-28 Thermocouple Locations of Fluid Temperature Measurements Just above and below End Box Tie Plates

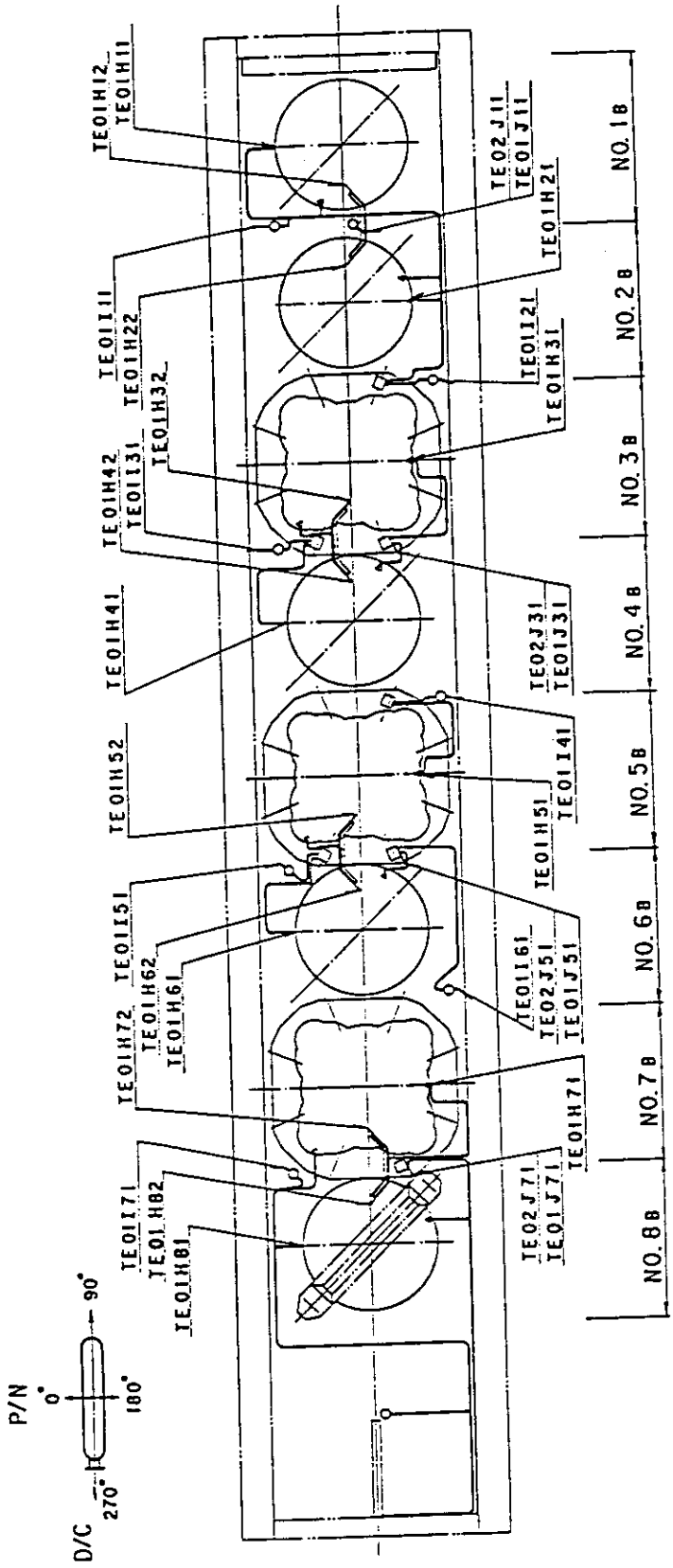

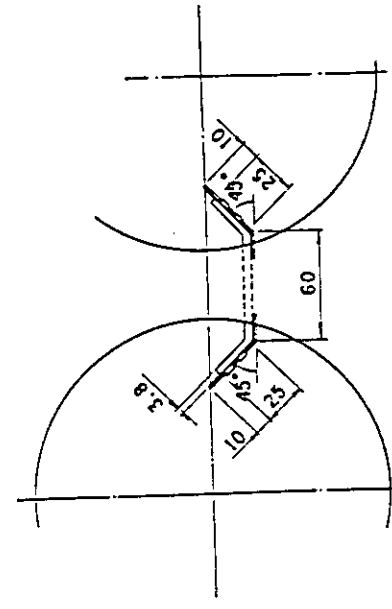

Fig. A-29 Thermocouple Locations of Fluid Temperature Measurements on UCSP and at Inside and Periphery of UCSP Holes

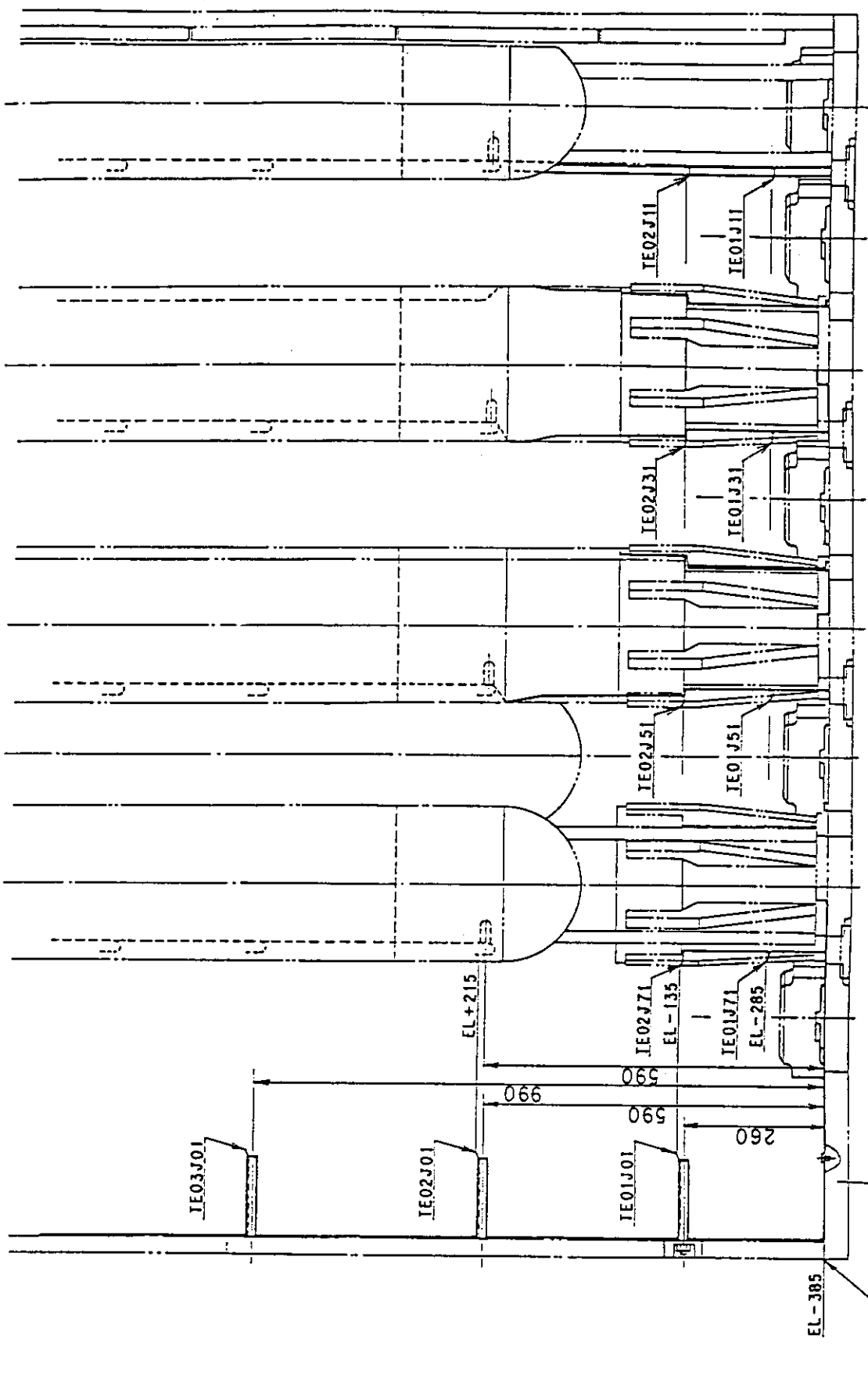

Fig. A-30 Thermocouple Locations of Fluid Temperature Measurements on and above UCSP

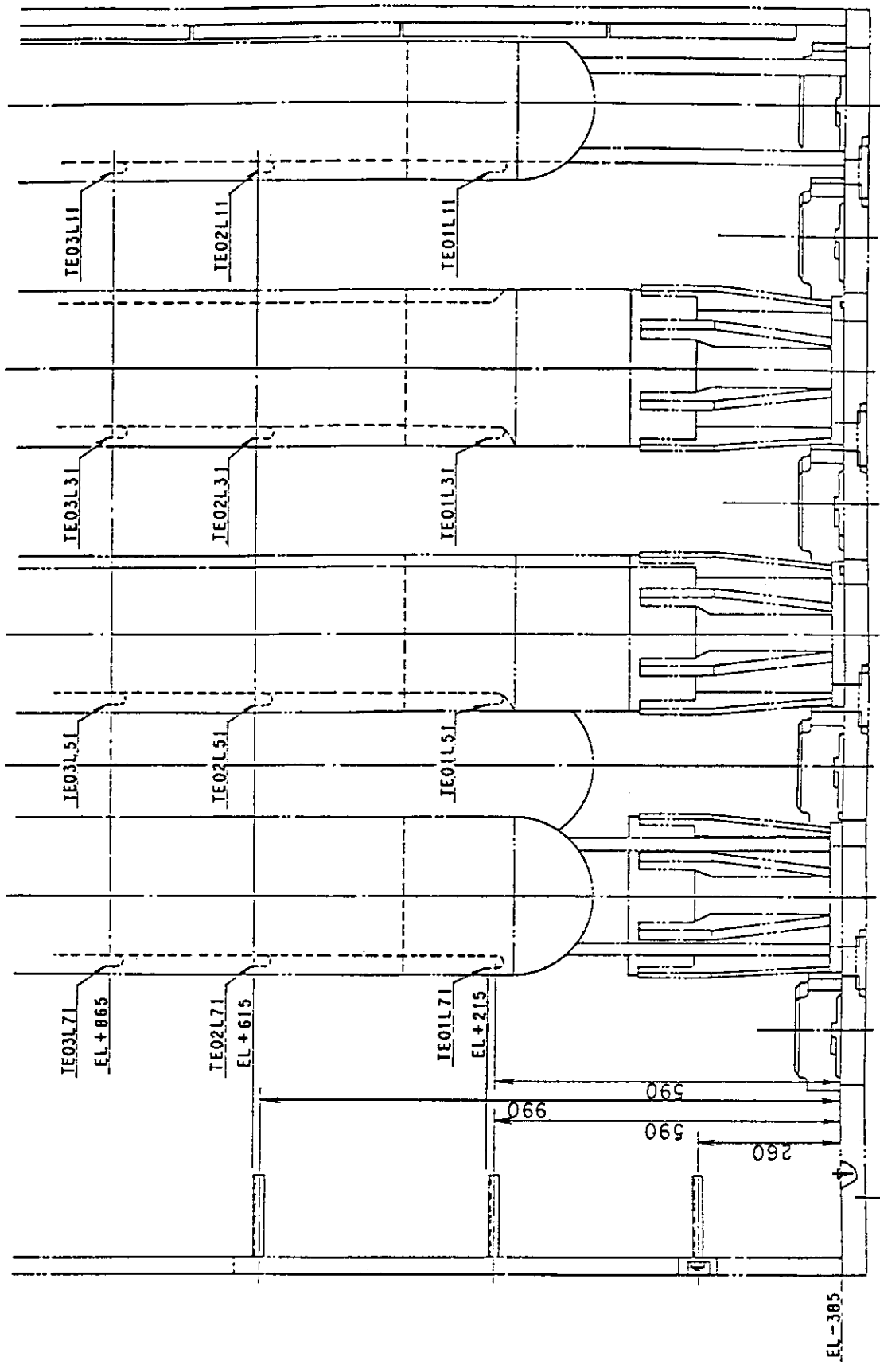

Fig. A-31 Thermocouple Locations of Surface Temperature Measurements of Upper Plenum Structures

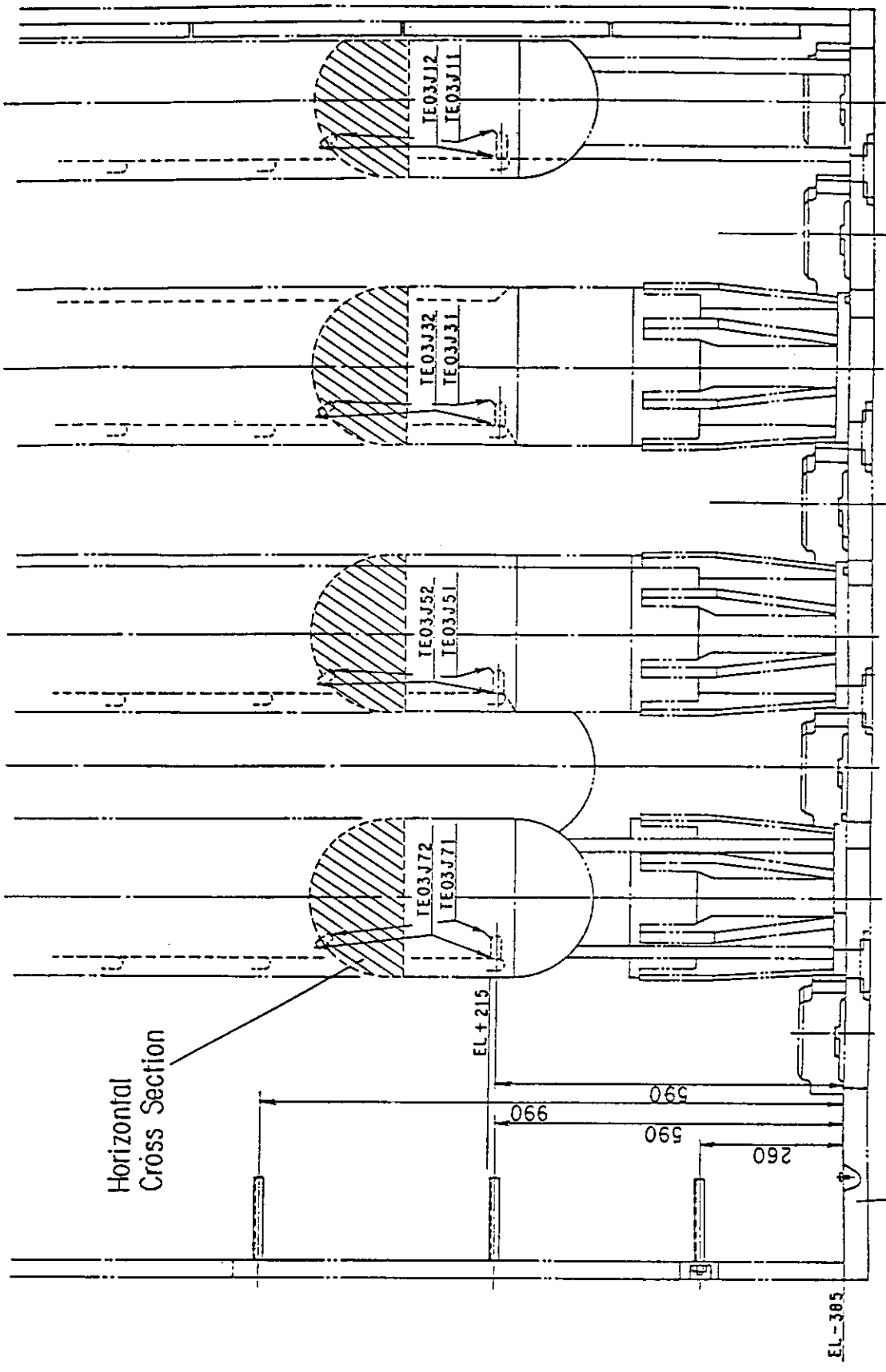

Fig. A-32 Thermocouple Locations of Steam Temperature Measurements above UCSP Holes

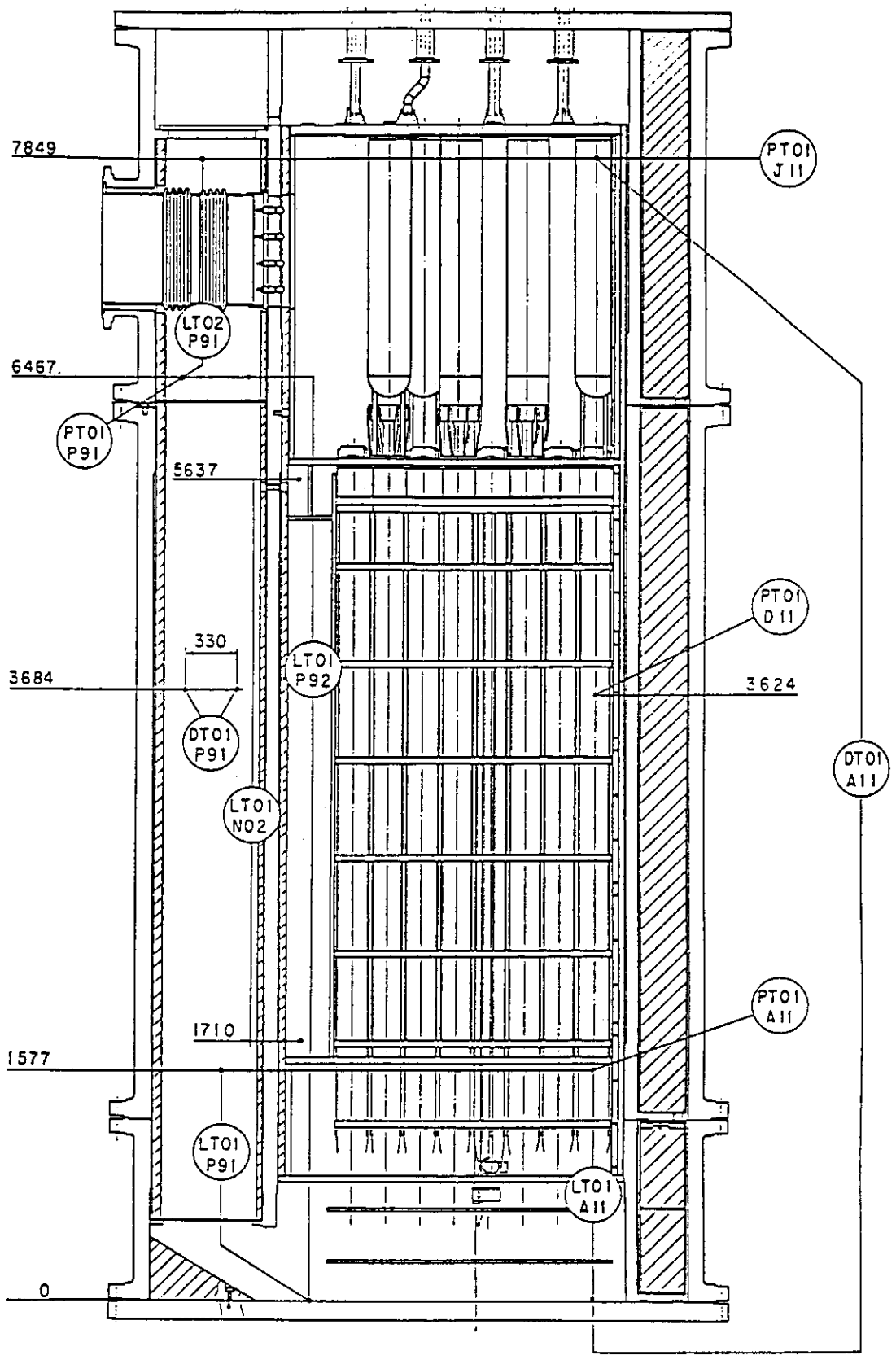

Fig. A-33 Locations of Pressure Measurements in Pressure Vessel, Differential Pressure Measurements between Upper and Lower Plenums and Liquid Level Measurements in Downcomer and Lower Plenum

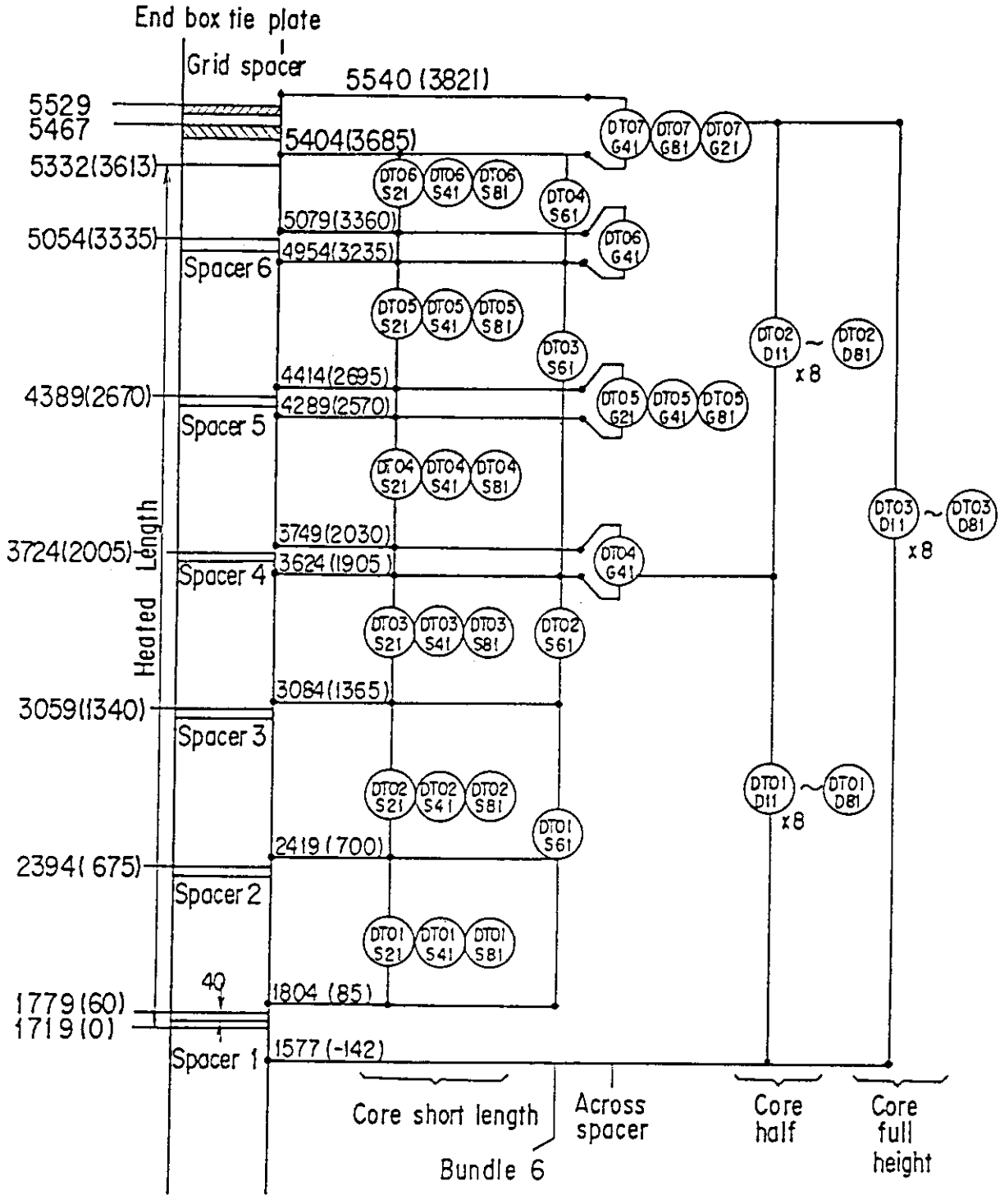

Fig. A-34 Locations of Vertical Differential Pressure Measurements in Core

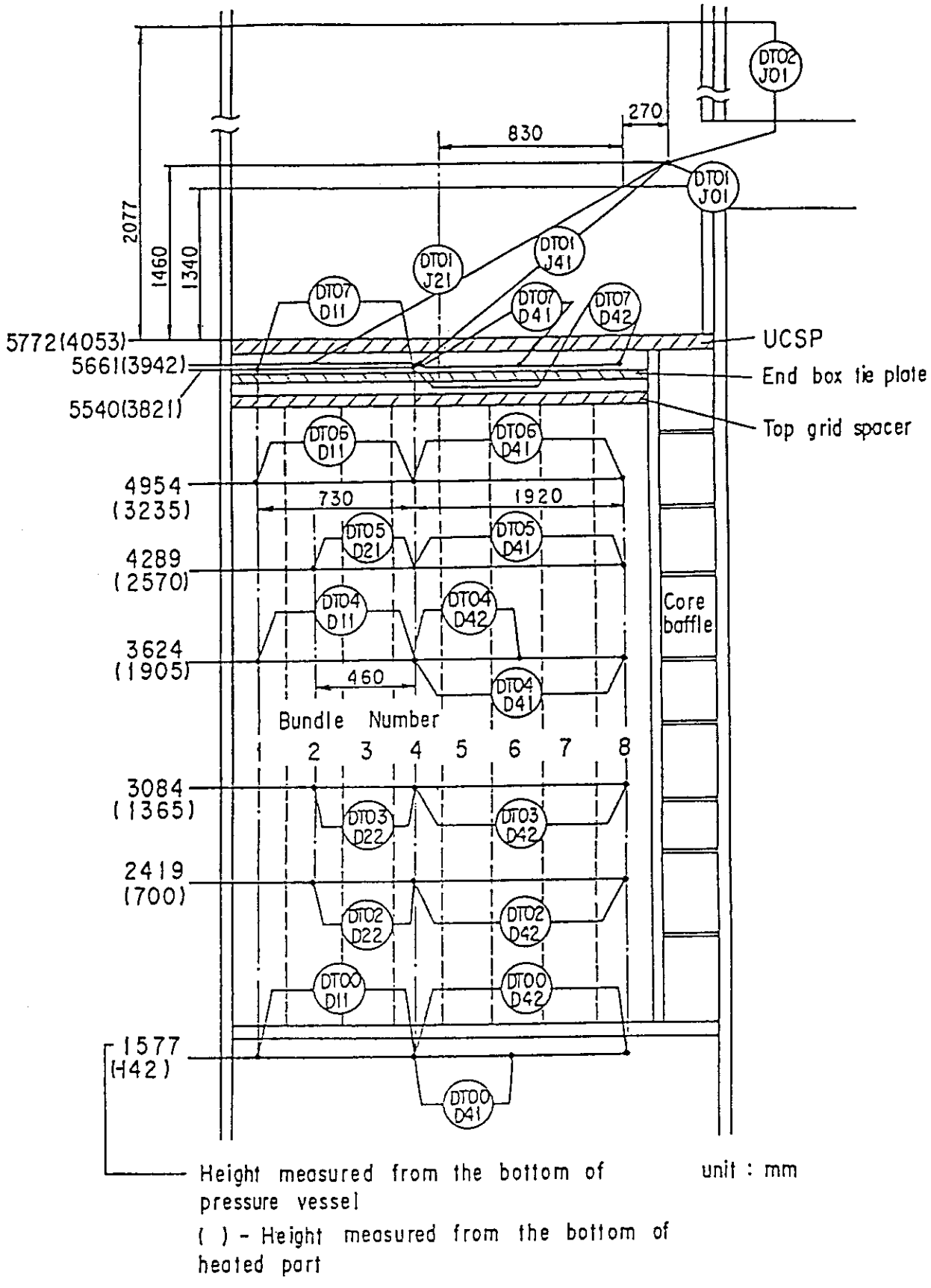

Fig. A-35 Locations of Horizontal Differential Pressure Measurements in Core and Differential Pressure Measurements between End Boxes and Inlet of Hot Leg

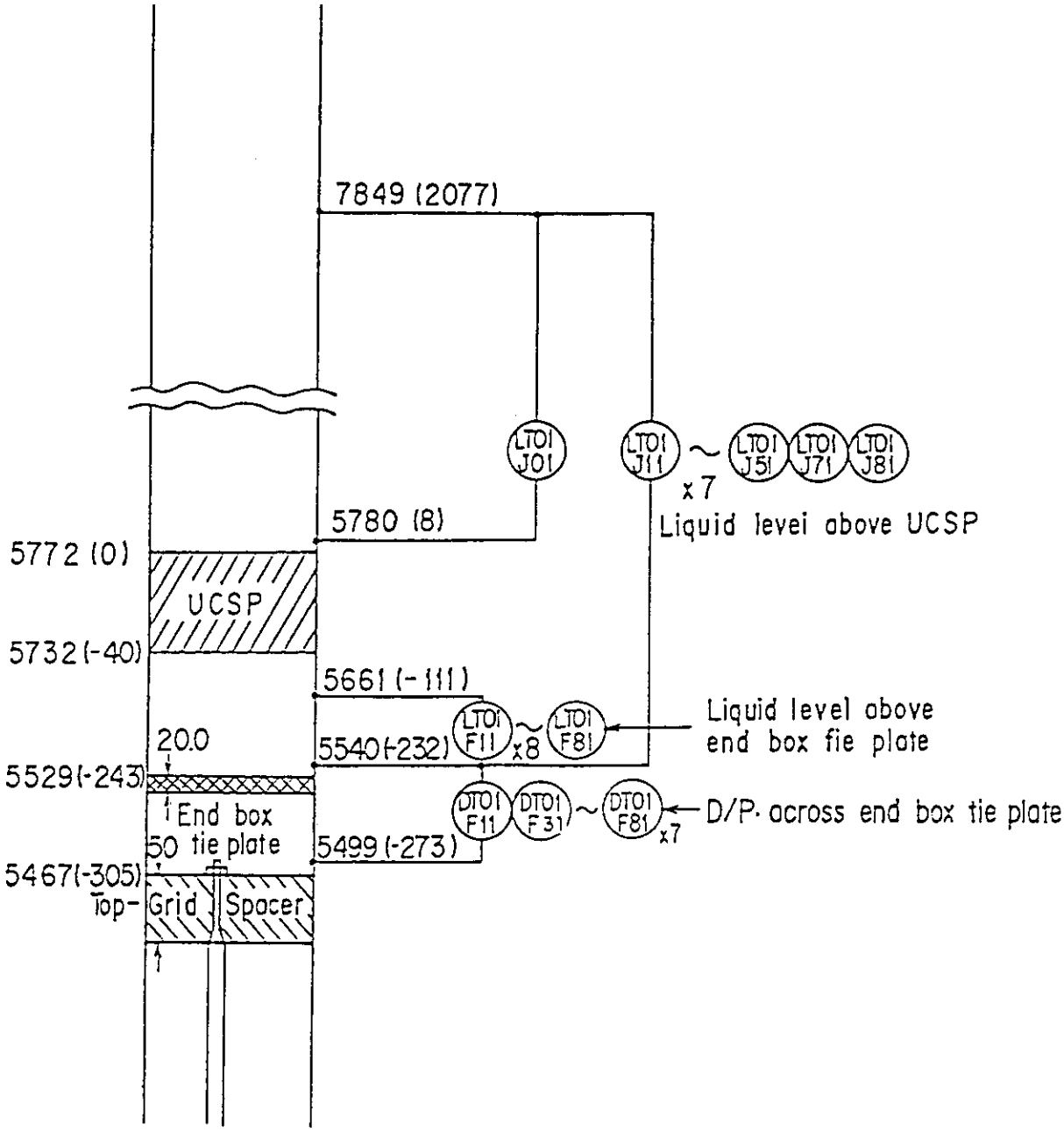

Fig. A-35 Locations of Differential Pressure Measurements across End Box Tie Plate

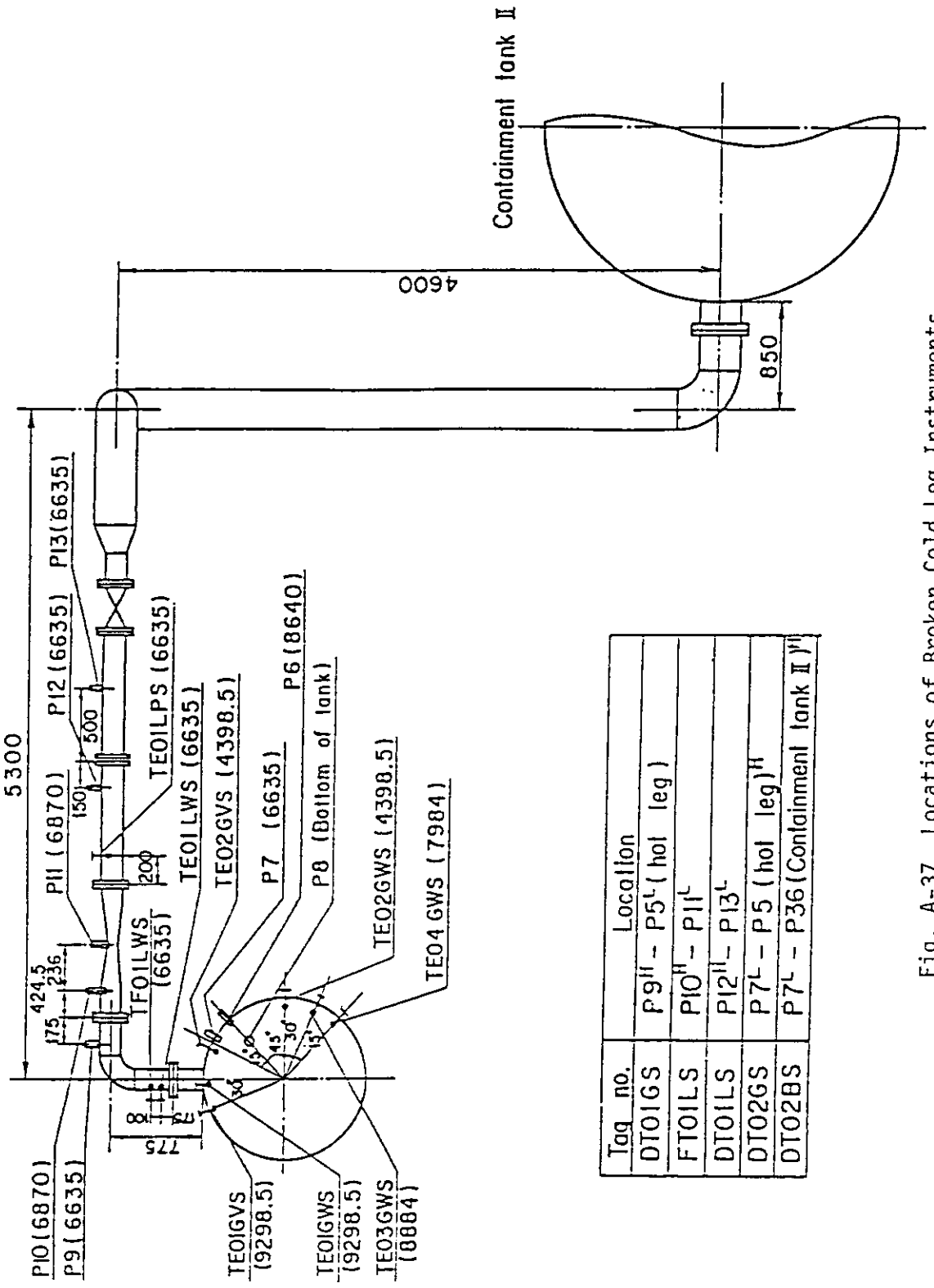

Tag no.	Location
DT01GS	$P9^{H}$ – $P5^{L}$ (hot leg)
FT01LS	$P10^{H}$ – $P11^{L}$
DT01LS	$P12^{H}$ – $P13^{L}$
DT02GS	$P7^{L}$ – P5 (hot leg)^{H}
DT02BS	$P7^{L}$ – P36 (Containment tank II)^{H}

Fig. A-37 Locations of Broken Cold Leg Instruments (Steam-Water Separator Side)

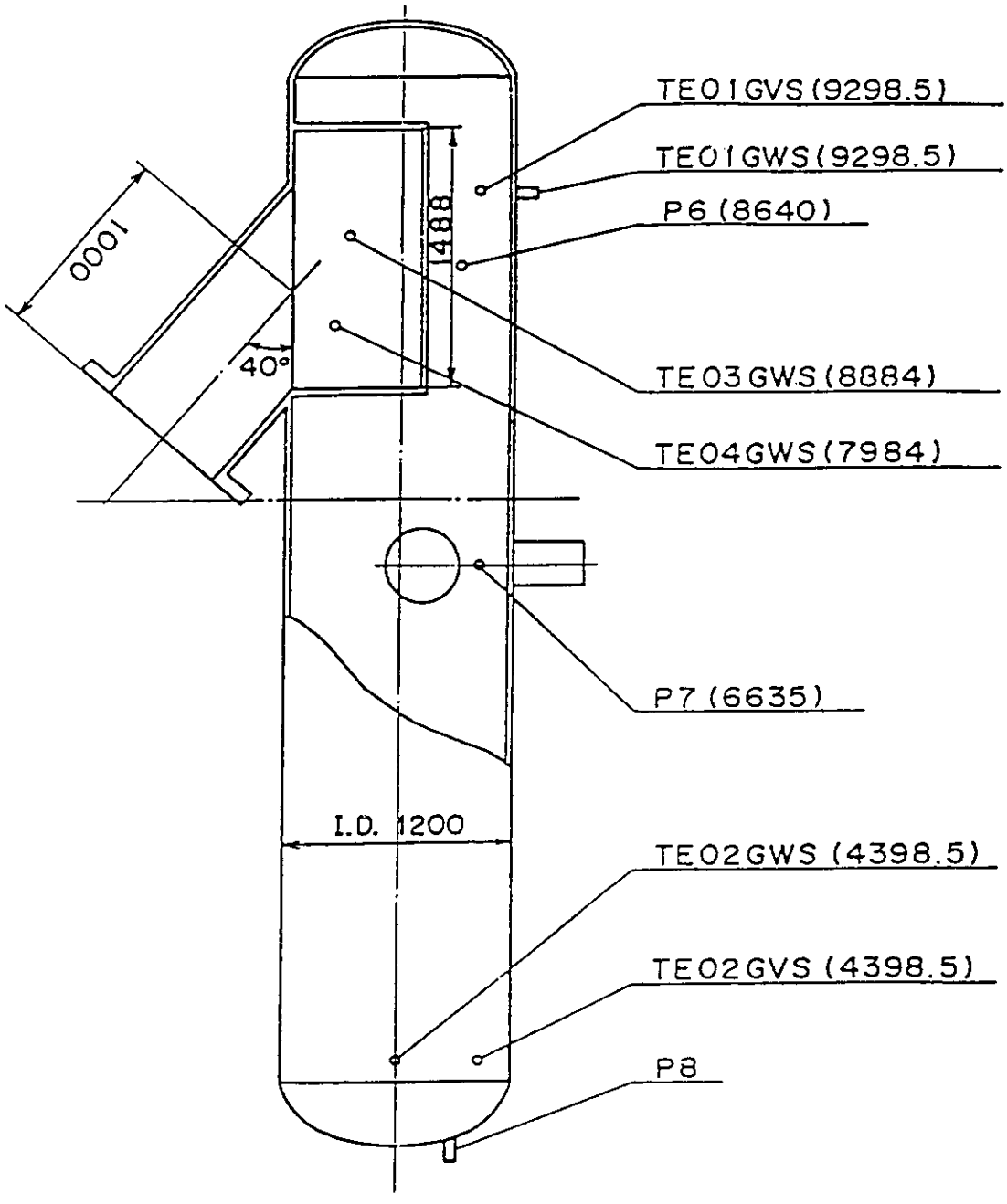

Fig. A-38 Locations of Steam-Water Separator Instruments

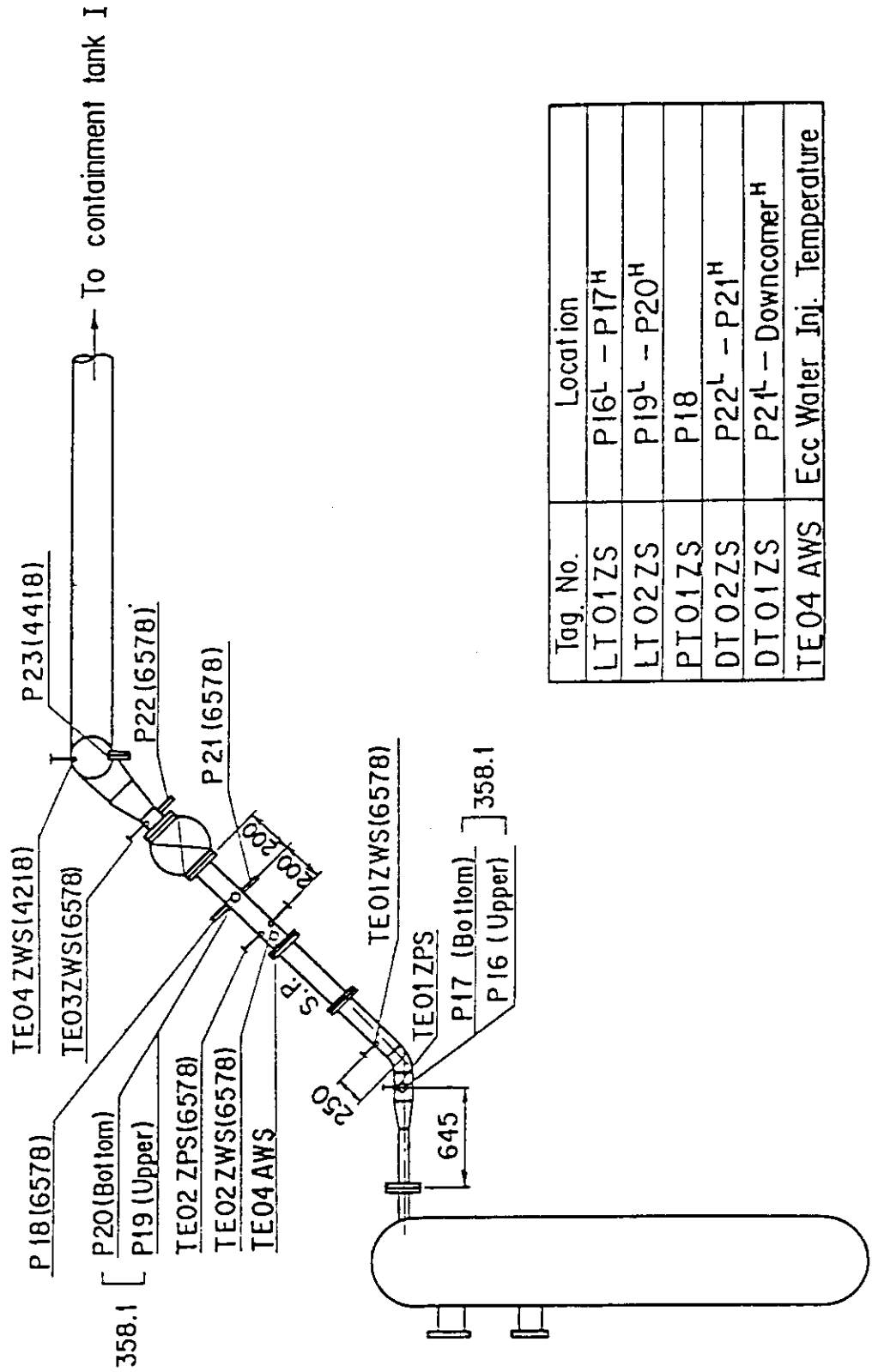

Tag. No.	Location
LT01ZS	$P16^{L} - P17^{H}$
LT02ZS	$P19^{L} - P20^{H}$
PT01ZS	P18
DT02ZS	$P22^{L} - P21^{H}$
DT01ZS	$P21^{L}$ – Downcomer^{H}
TE04AWS	Ecc Water Inj. Temperature

Fig. A-39 Locations of Broken Cold Leg Instruments (Pressure Vessel Side)

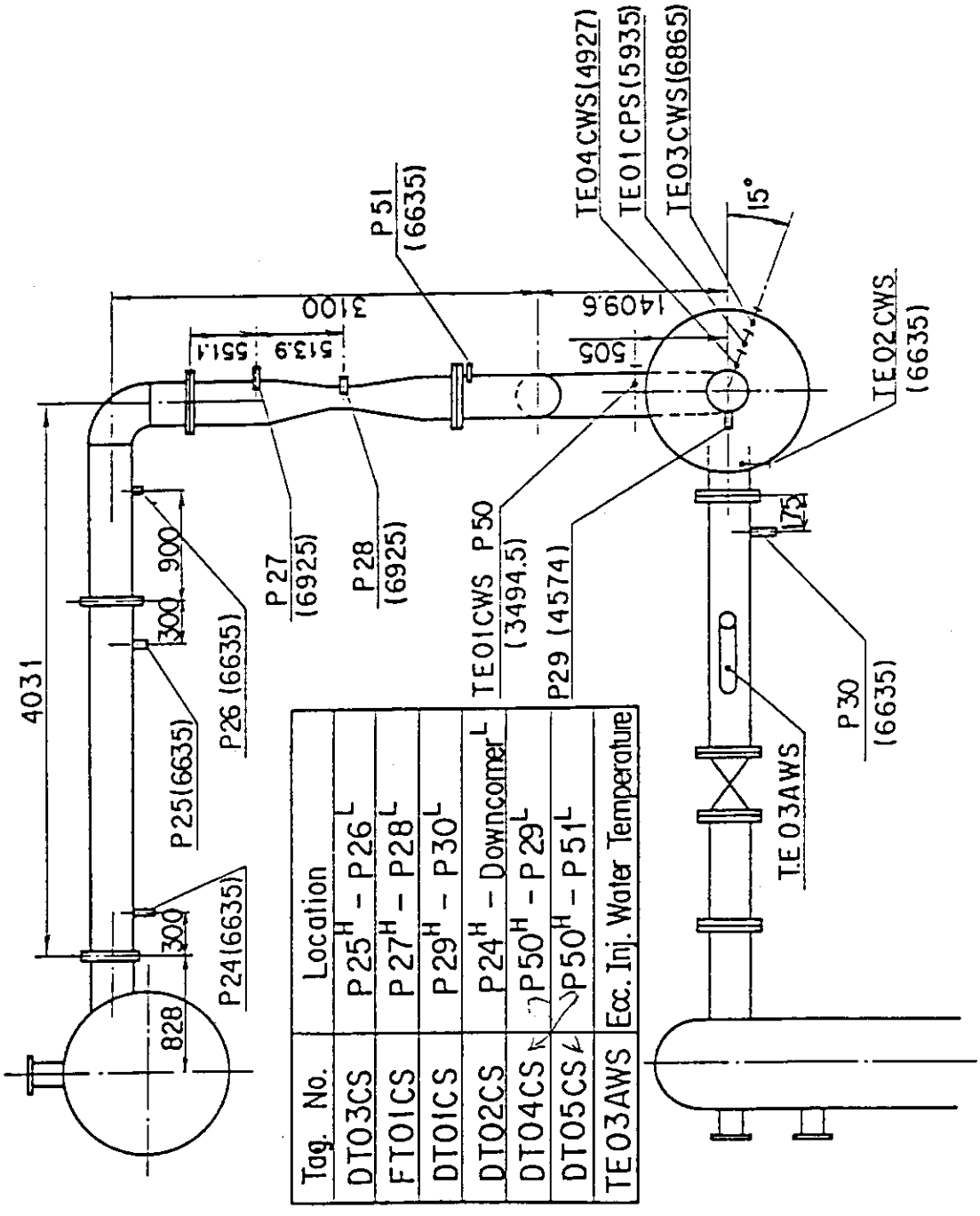

Fig. A-40 Locations of Intact Cold Leg Instruments

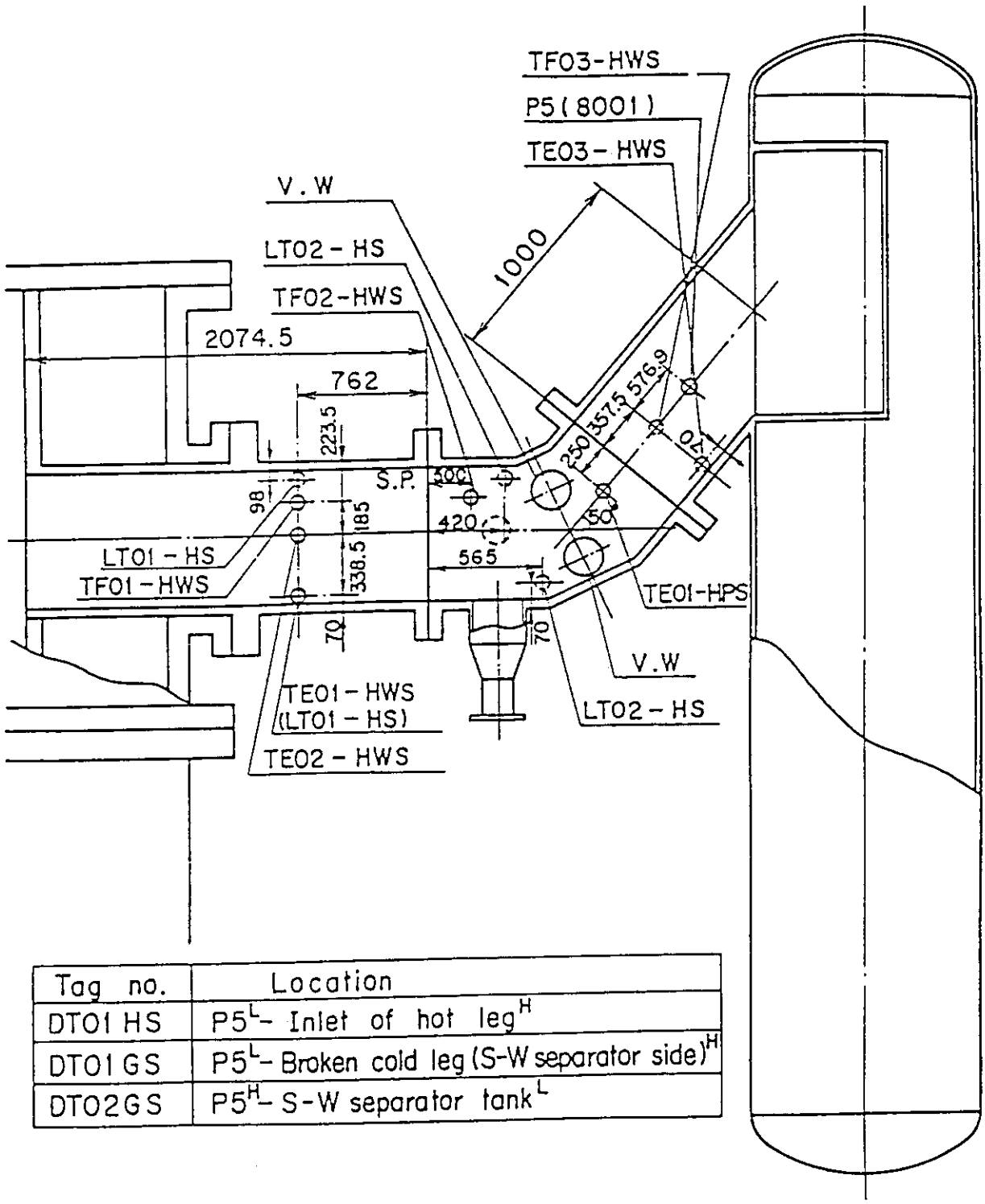

Tag no.	Location
DT01 HS	$P5^{L}$- Inlet of hot leg^{H}
DT01 GS	$P5^{L}$- Broken cold leg (S-W separator side)^{H}
DT02 GS	$P5^{H}$- S-W separator $tank^{L}$

Fig. A-41 Locations of Hot Leg Instruments

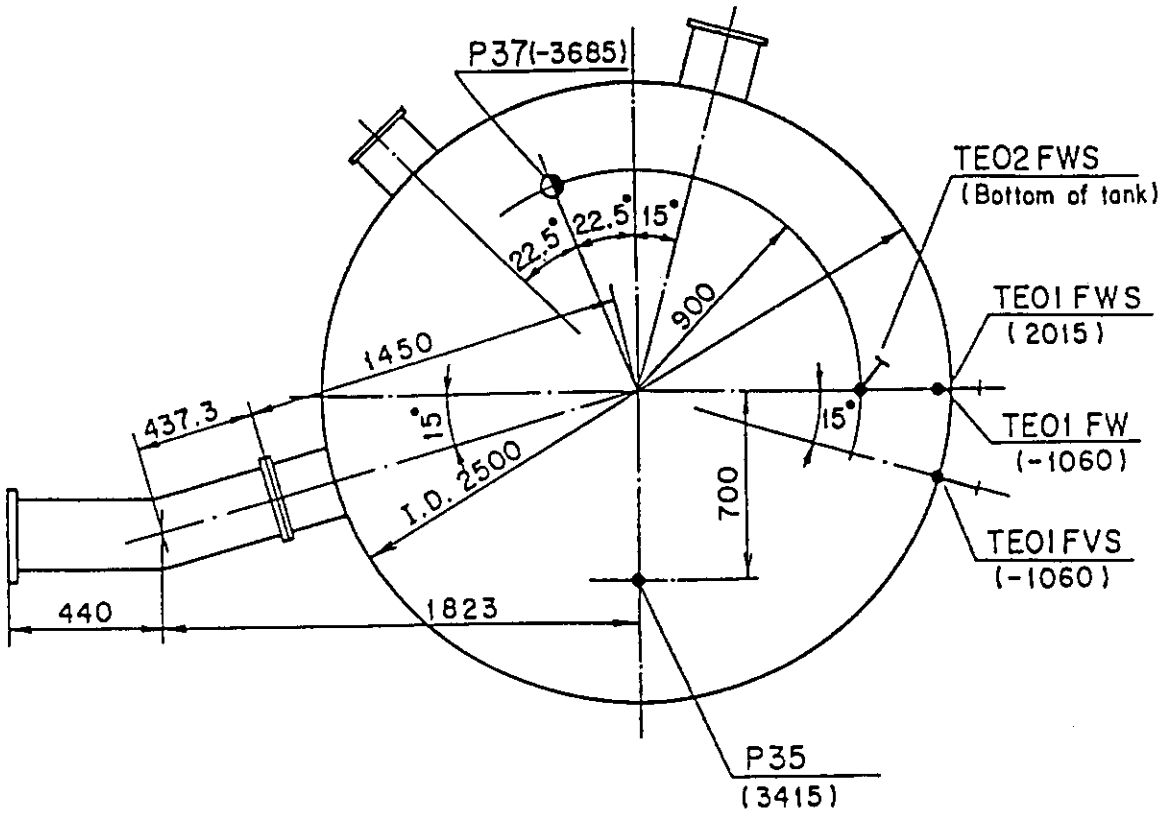

Tag. no.	Location
LT01 FS	$P35^{L}$ – $P37^{H}$
DT01 FS	$P35^{H}$ – $Downcomer^{L}$
DT01 E	$P35^{L}$ – P36 (C.T. II)^{H}
PT01 F	P35

Fig. A-42 Locations of Containment Tank-I Instruments

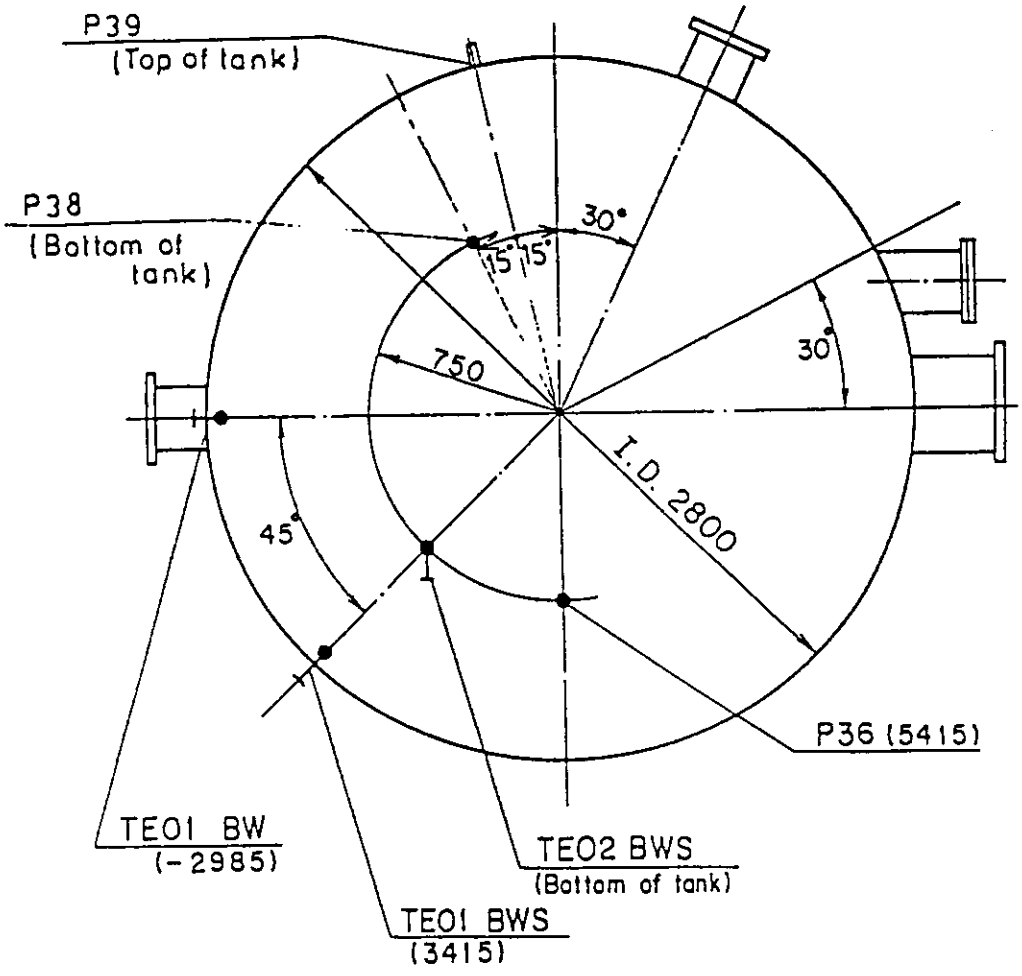

Tag no.	Location
DT01 BS	P36^{H}－ Upper plenum^{L}
DT02 BS	P36^{H}－ S-W Separator^{L}
DT01 E	P36^{H}－ P35 (C.T.I)^{L}
PT01 B	P36
LT01 1B	P38^{H}－ P39^{L}

Fig. A-43 Locations of Containment Tank-II Instruments

Appendix B

Selected Data from Test S3-17

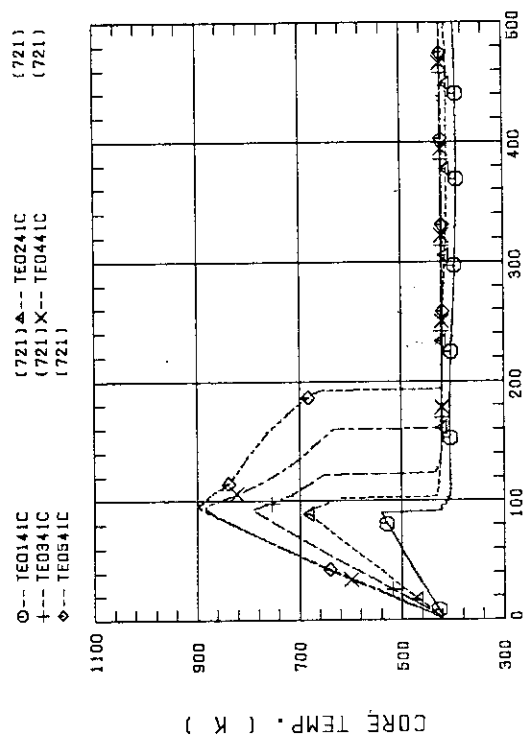

FIG. B-03 HEATER ROD TEMPERATURE (BUNDLE 4-1C, LOWER HALF)

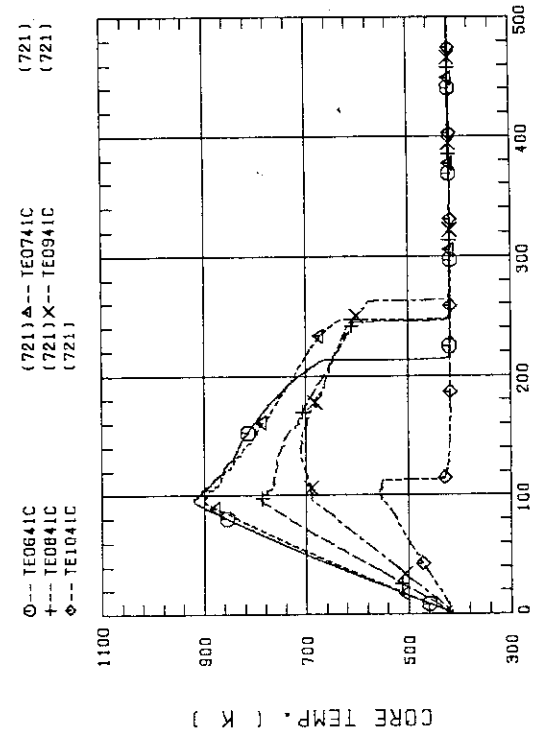

FIG. B-04 HEATER ROD TEMPERATURE (BUNDLE 4-1C, UPPER HALF)

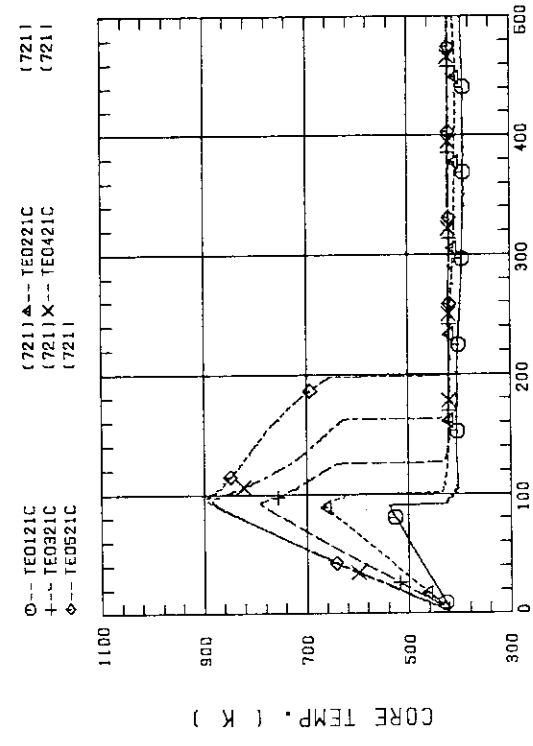

FIG. B-01 HEATER ROD TEMPERATURE (BUNDLE 2-1C, LOWER HALF)

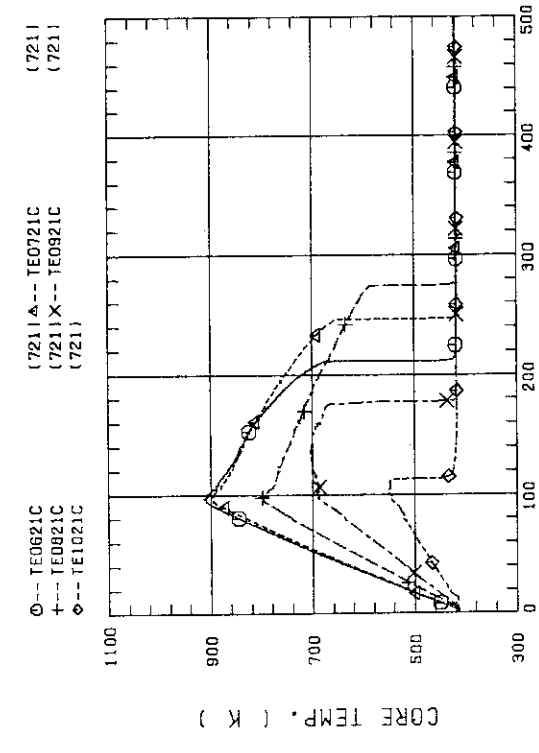

FIG. B-02 HEATER ROD TEMPERATURE (BUNDLE 2-1C, UPPER HALF)

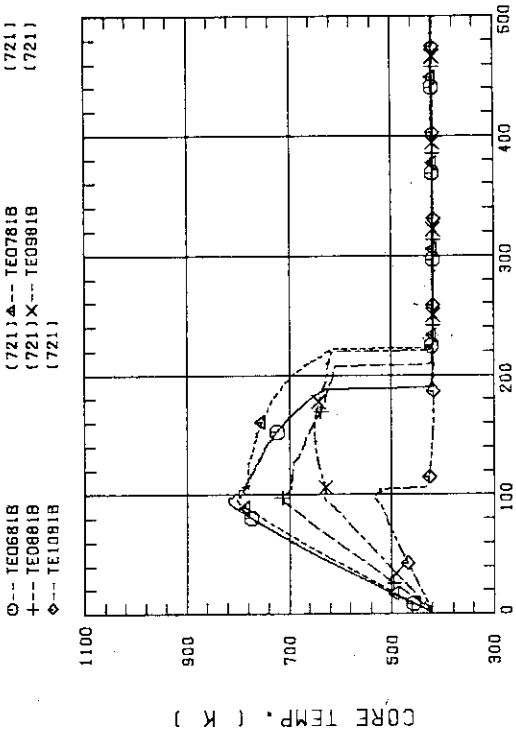

FIG. B-07 HEATER ROD TEMPERATURE
(BUNDLE 8-1B, UPPER HALF)

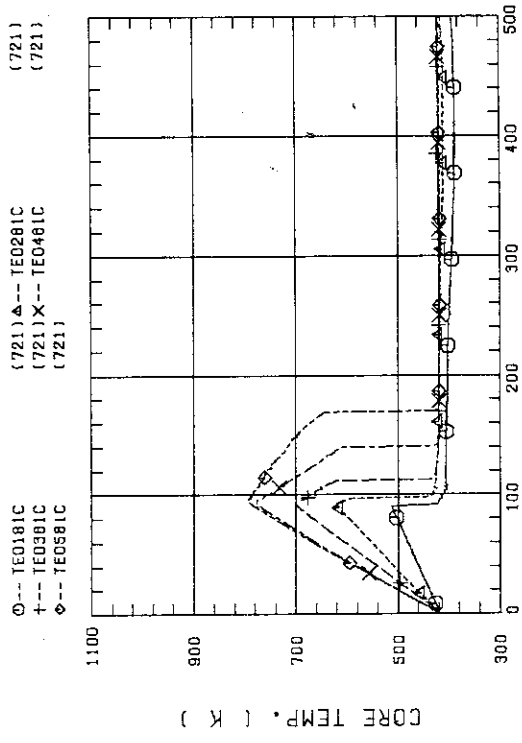

FIG. B-08 HEATER ROD TEMPERATURE
(BUNDLE 8-1C, LOWER HALF)

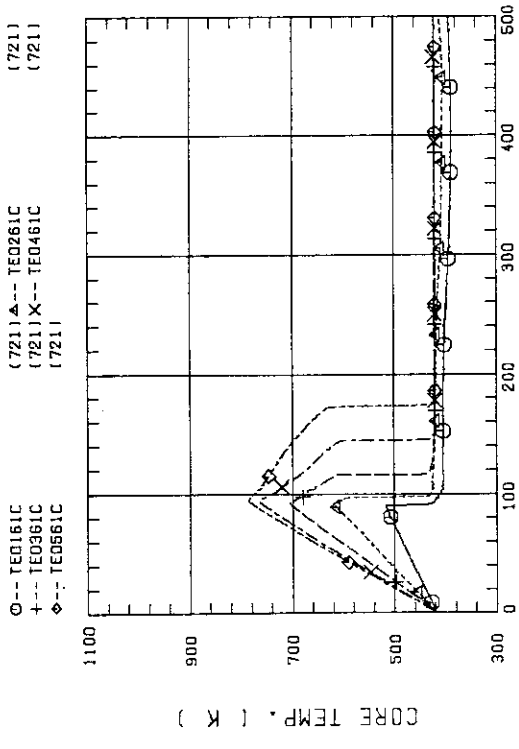

FIG. B-05 HEATER ROD TEMPERATURE
(BUNDLE 6-1C, LOWER HALF)

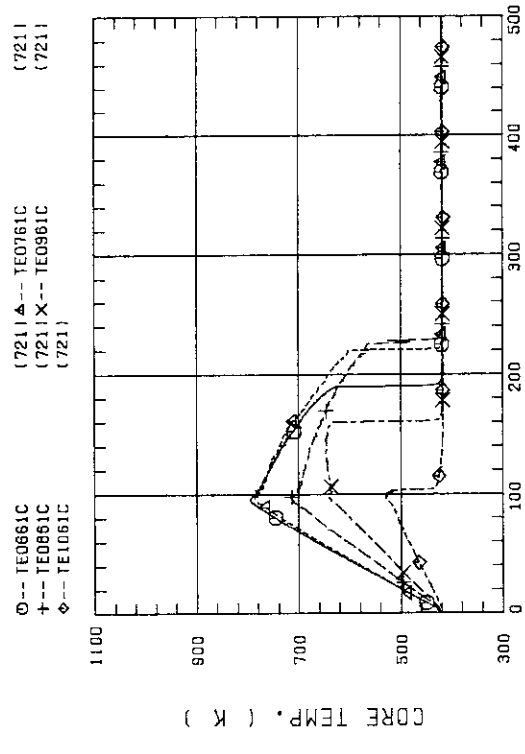

FIG. B-06 HEATER ROD TEMPERATURE
(BUNDLE 6-1C, UPPER HALF)

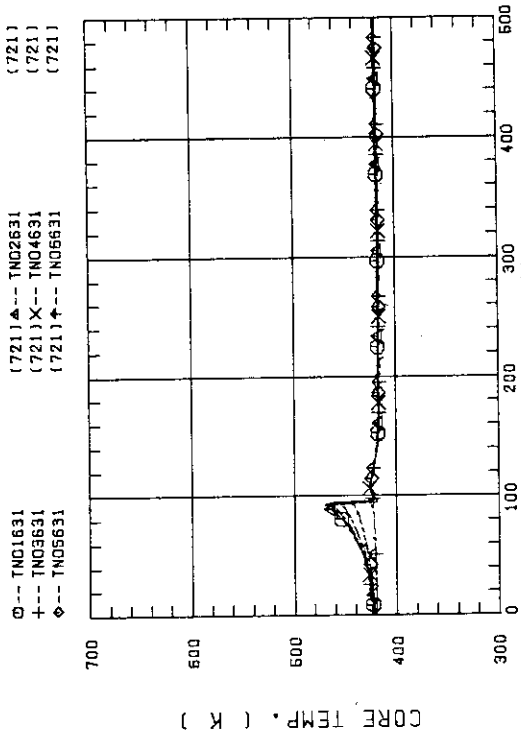

FIG. B-11 NON-HEATED ROD TEMPERATURE (BUNDLE 6-31)

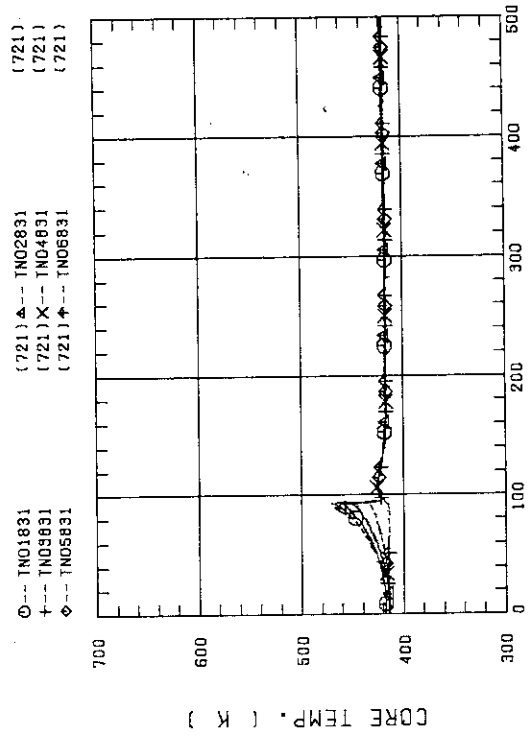

FIG. B-12 NON-HEATED ROD TEMPERATURE (BUNDLE 6-31)

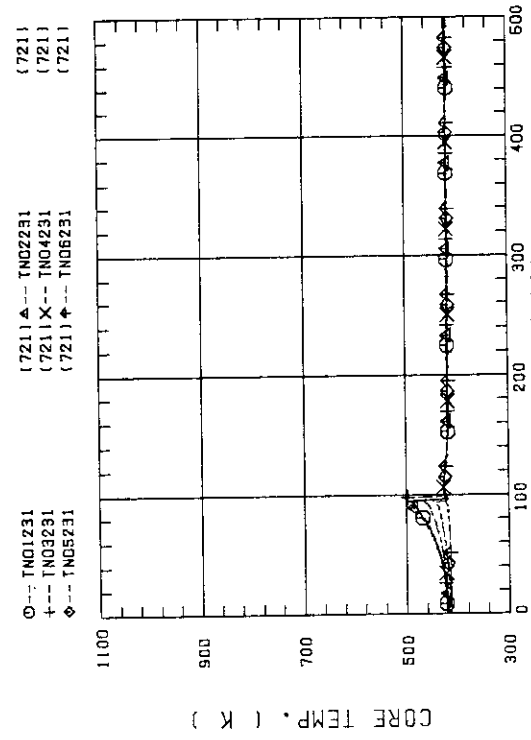

FIG. B-09 NON-HEATED ROD TEMPERATURE (BUNDLE 2-31)

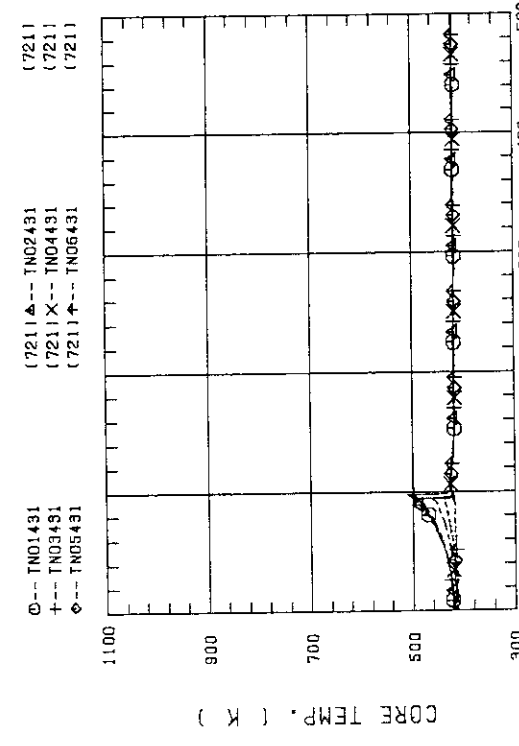

FIG. B-10 NON-HEATED ROD TEMPERATURE (BUNDLE 4-31)

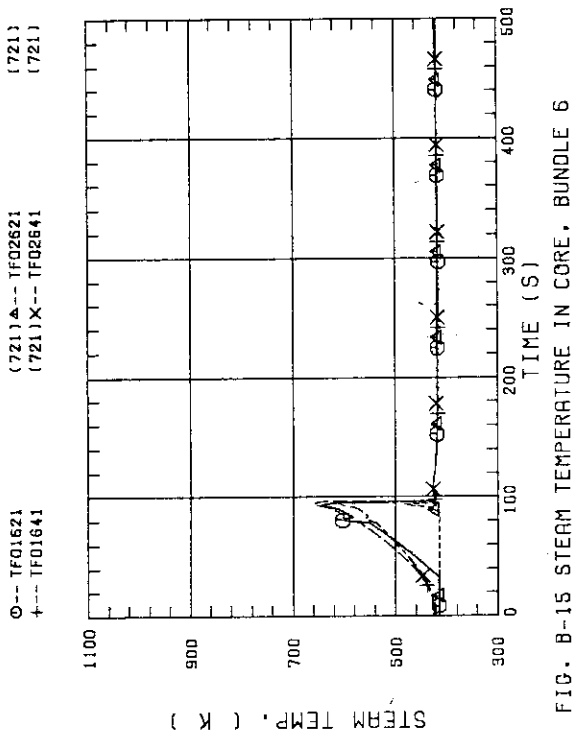

FIG. B-15 STEAM TEMPERATURE IN CORE, BUNDLE 6

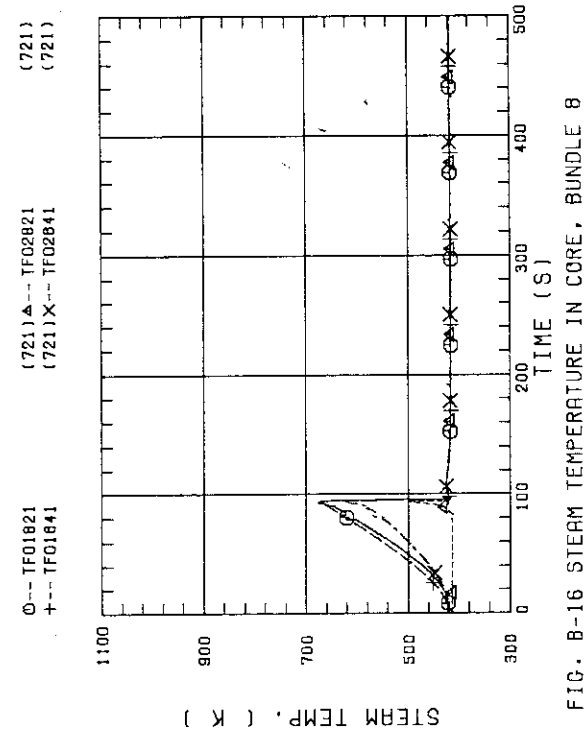

FIG. B-16 STEAM TEMPERATURE IN CORE, BUNDLE 8

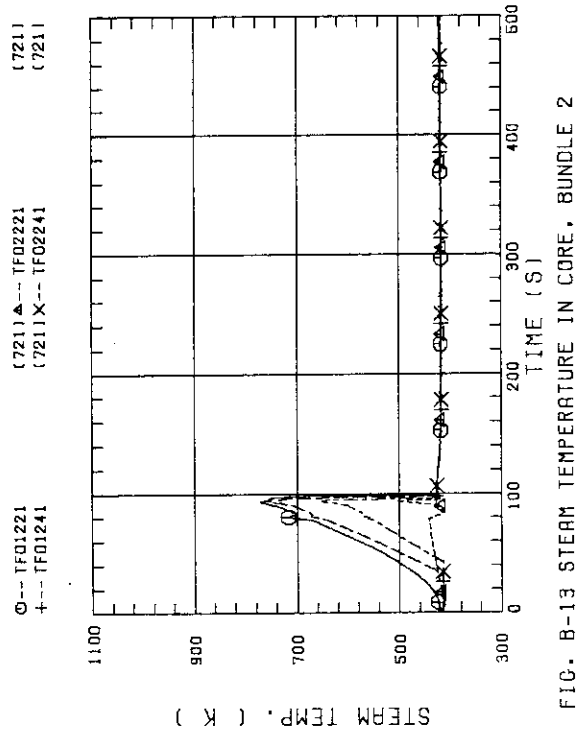

FIG. B-13 STEAM TEMPERATURE IN CORE, BUNDLE 2

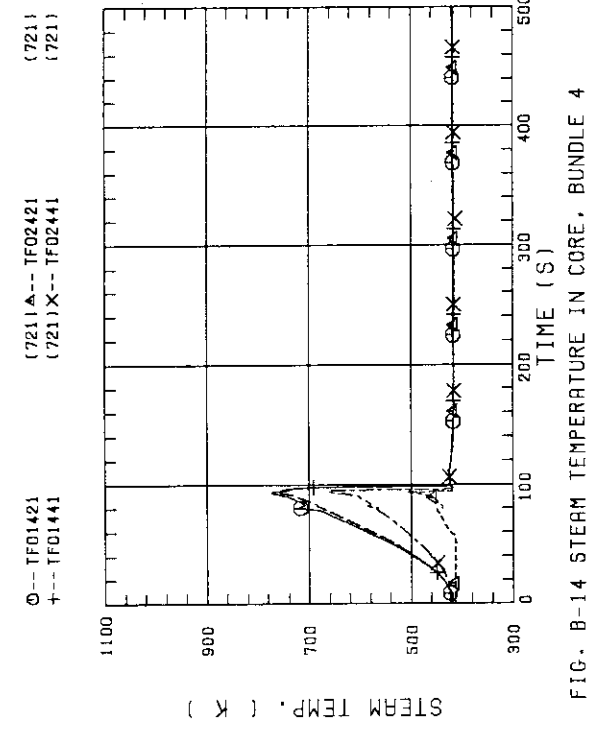

FIG. B-14 STEAM TEMPERATURE IN CORE, BUNDLE 4

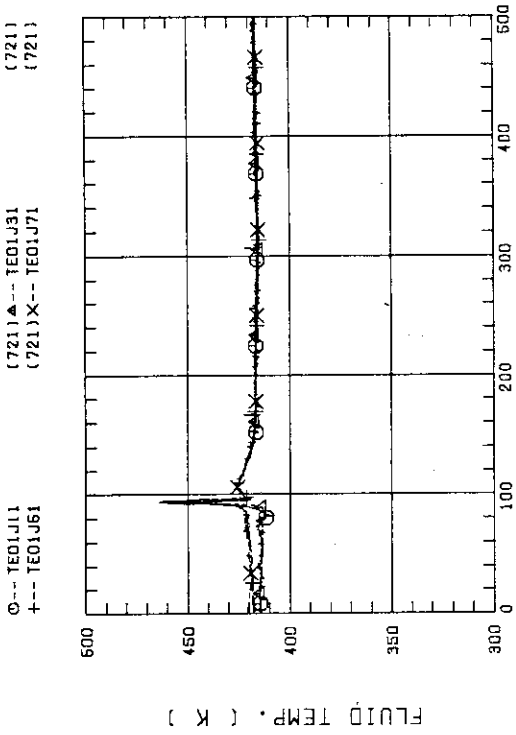

FIG. B-19 FLUID TEMPERATURE ABOVE UCSP
(BUNDLE 1,3,5,7 100MM ABOVE UCSP)

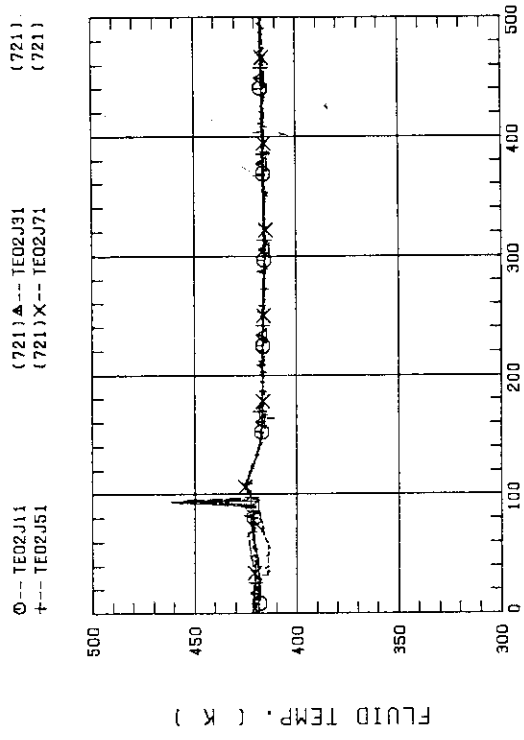

FIG. B-20 FLUID TEMPERATURE ABOVE UCSP
(BUNDLE 1,3,5,7 250MM ABOVE UCSP)

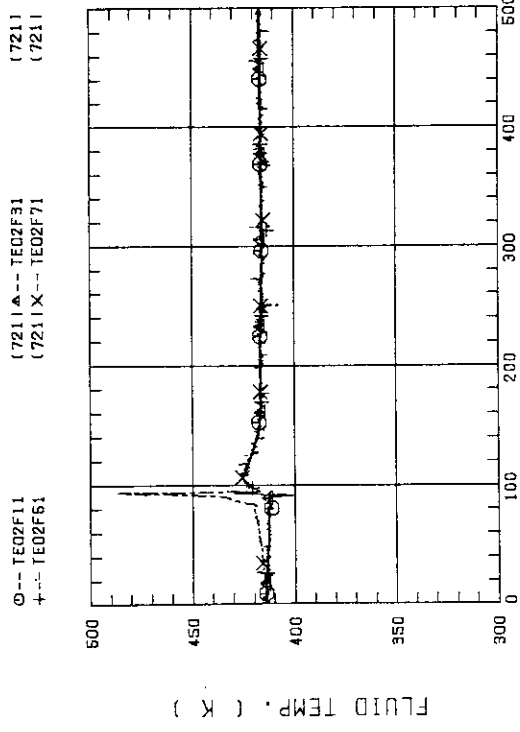

FIG. B-17 FLUID TEMPERATURE JUST ABOVE END BOX TIE PLATE
(BUNDLE 1,3,5,7 OPPOSITE SIDE OF COLD LEG, OUTER)

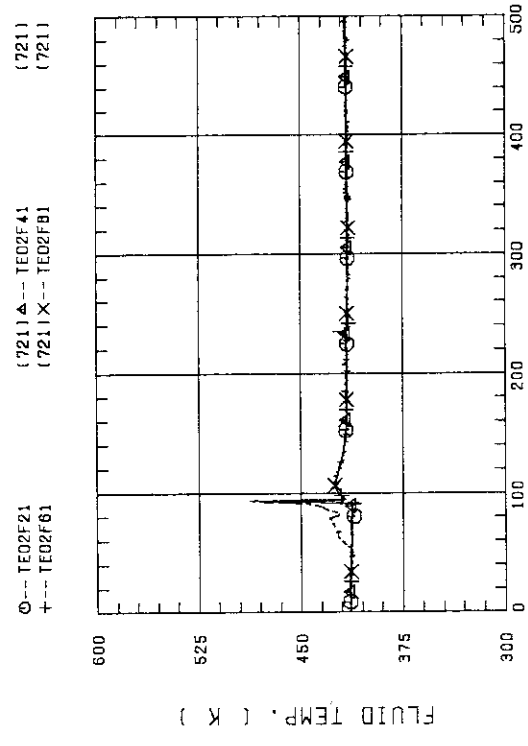

FIG. B-18 FLUID TEMPERATURE JUST ABOVE END BOX TIE PLATE
(BUNDLE 2,4,6,8 OPPOSITE SIDE OF COLD LEG, OUTER)

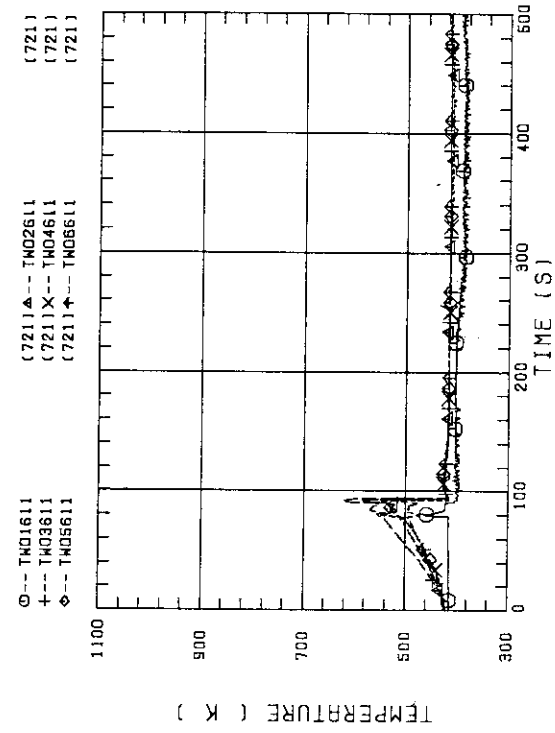

FIG. B-23 TEMPERATURE FOR SPUTTERING DETECTION BUNDLE 6 , REGION 1 , TYPE 3

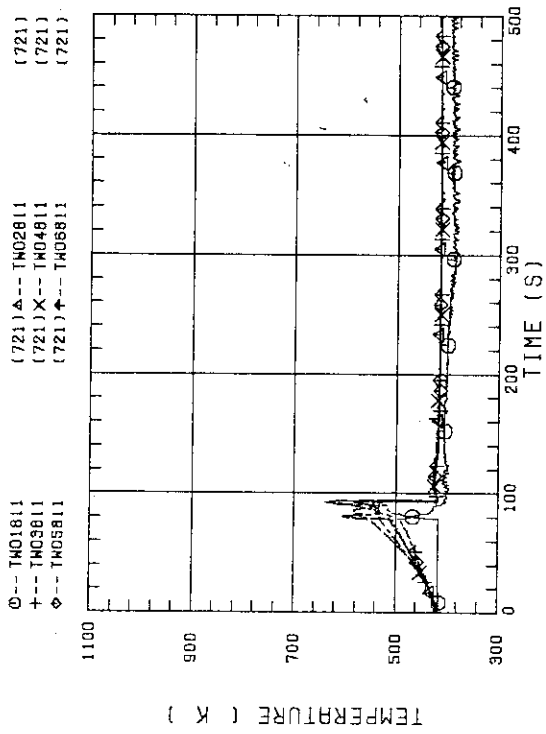

FIG. B-24 TEMPERATURE FOR SPUTTERING DETECTION BUNDLE 8 , REGION 1 , TYPE 3

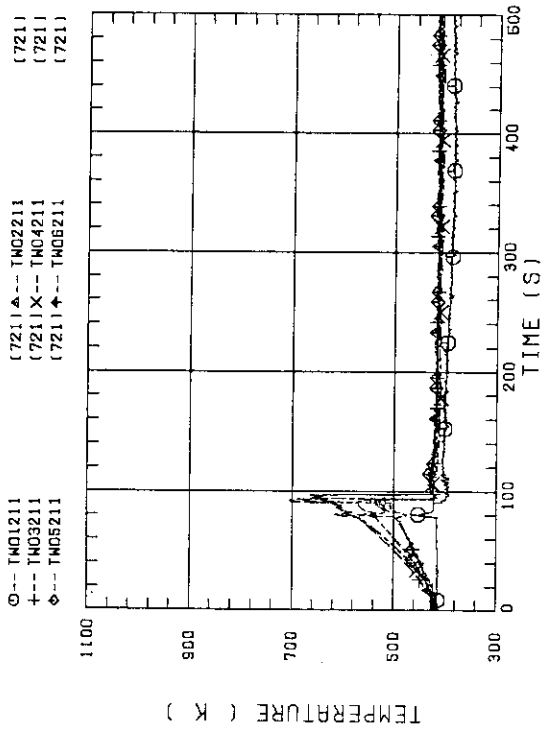

FIG. B-21 TEMPERATURE FOR SPUTTERING DETECTION BUNDLE 2 , REGION 1 , TYPE 3

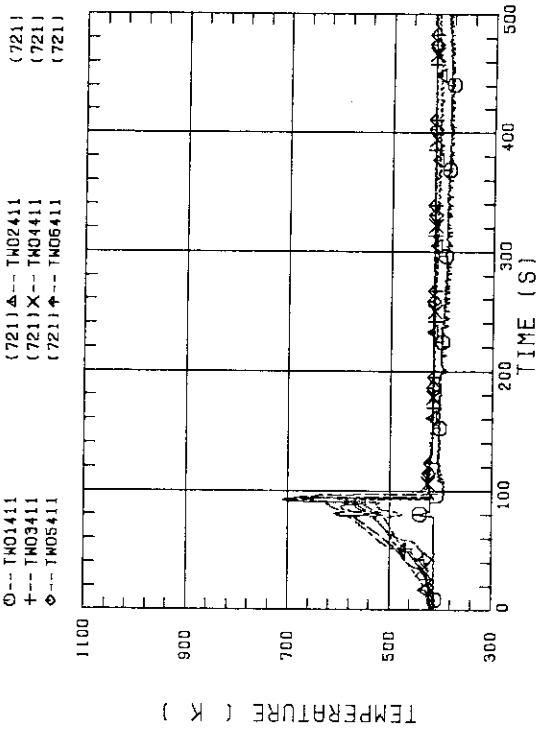

FIG. B-22 TEMPERATURE FOR SPUTTERING DETECTION BUNDLE 4 , REGION 1 , TYPE 3

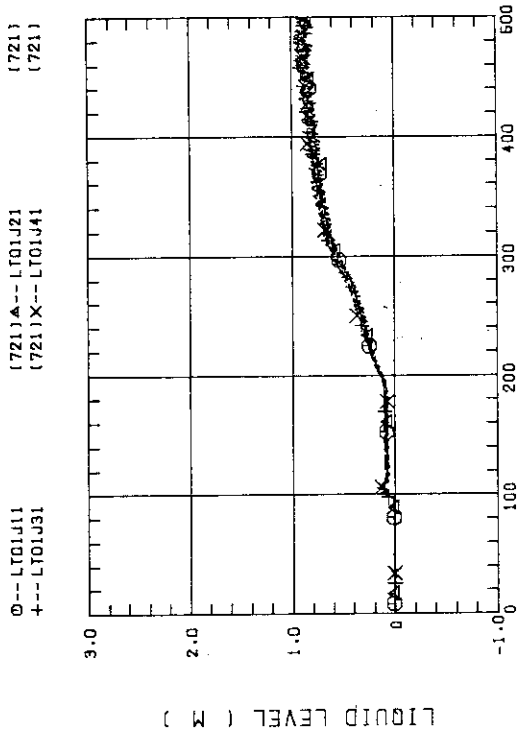

FIG. B-27 LIQUID LEVEL ABOVE UCSP
(BUNDLE 1,2,3,4)

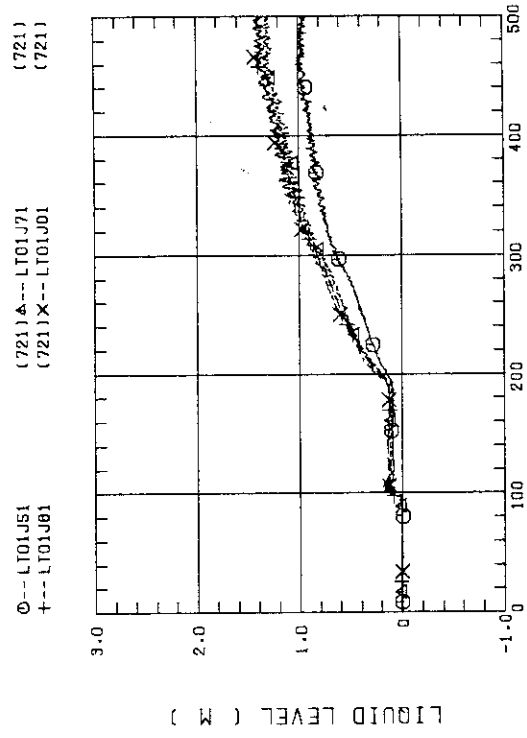

FIG. B-28 LIQUID LEVEL ABOVE UCSP
(BUNDLE 5,6,7,8 AND CORE BUFFLE)

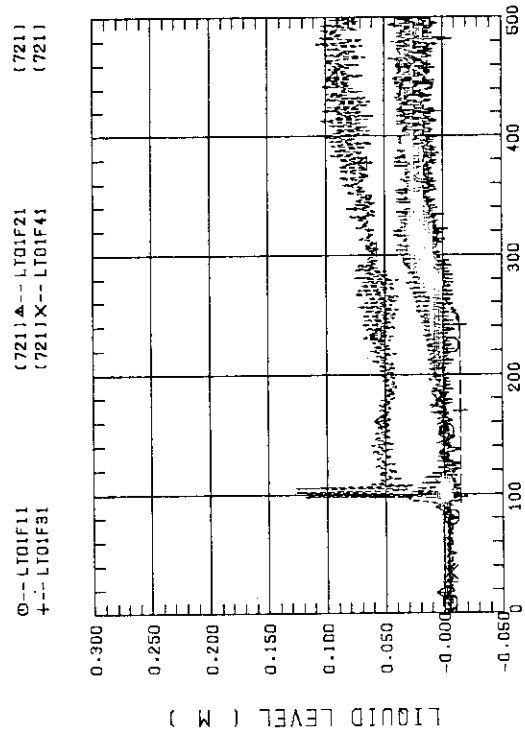

FIG. B-25 LIQUID LEVEL ABOVE END BOX TIE PLATE
(BUNDLE 1,2,3,4)

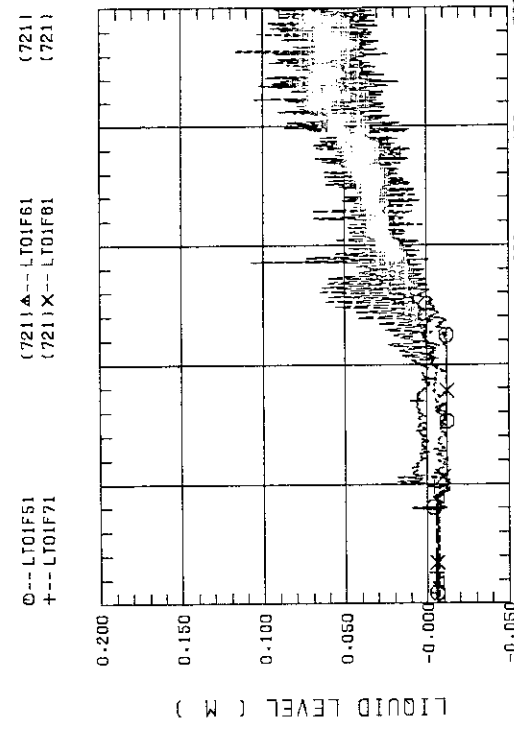

FIG. B-26 LIQUID LEVEL ABOVE END BOX TIE PLATE
(BUNDLE 5,6,7,8)

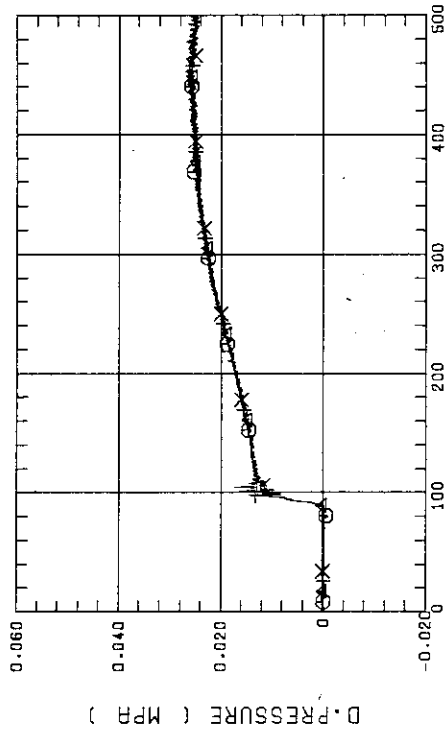

FIG. B-31 DIFFERENTIAL PRESSURE OF CORE FULL HIGHT (BUNDLE 1,2,3,4)

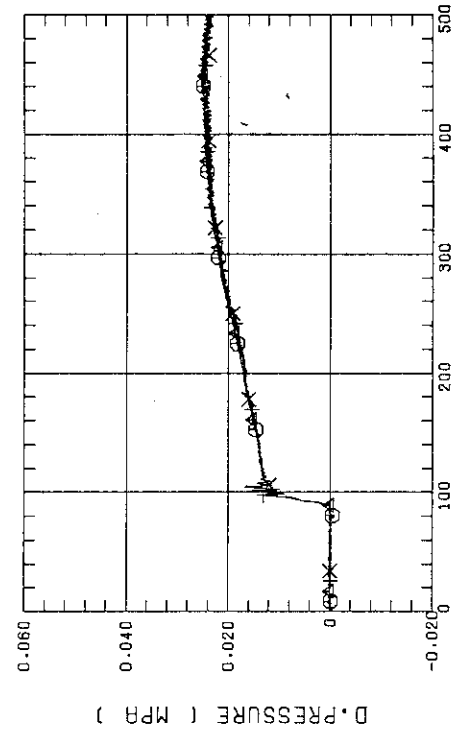

FIG. B-32 DIFFERENTIAL PRESSURE OF CORE FULL HIGHT (BUNDLE 5,6,7,8)

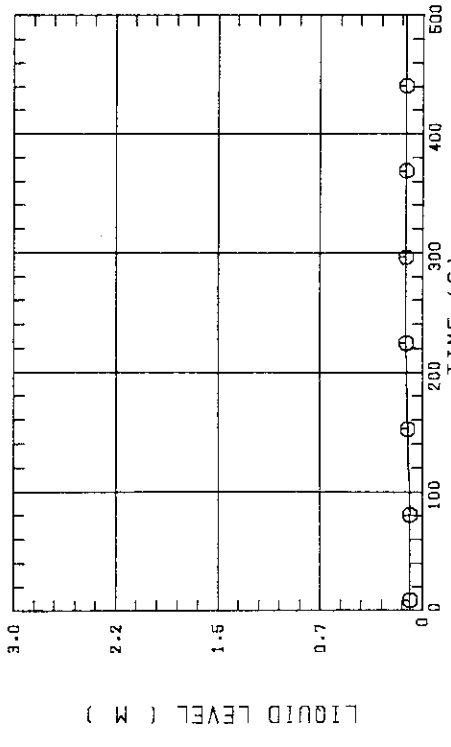

FIG. B-29 LIQUID LEVEL IN STEAM/WATER SEPARATOR

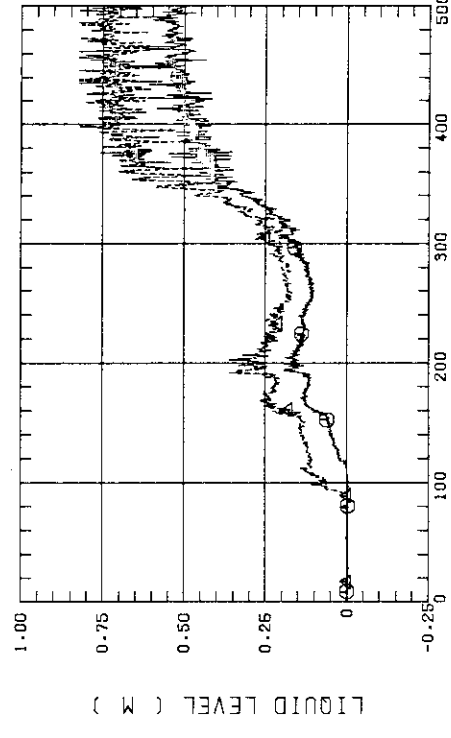

FIG. B-30 LIQUID LEVEL IN HOT LEG (01HS - PV SIDE, 02HS - STEAM/WATER SEPARATOR SIDE)

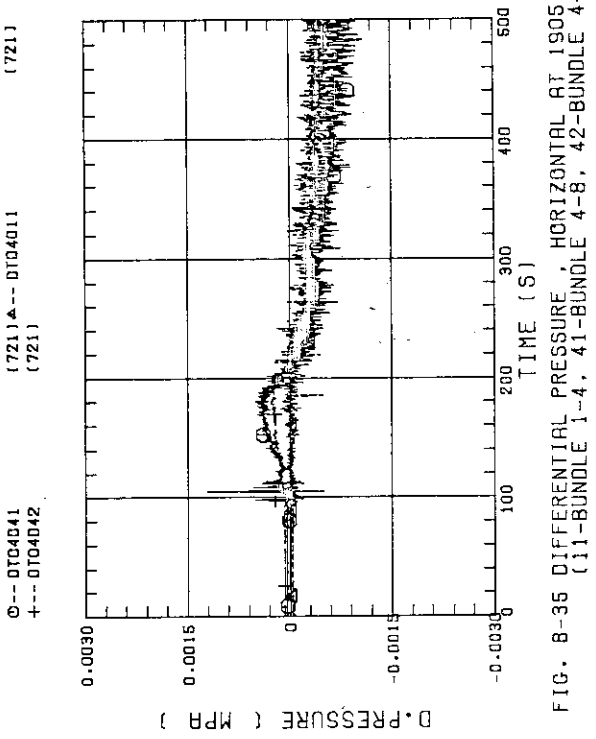

FIG. B-35 DIFFERENTIAL PRESSURE, HORIZONTAL AT 1905 MM
(11-BUNDLE 1-4, 41-BUNDLE 4-8, 42-BUNDLE 4-6)

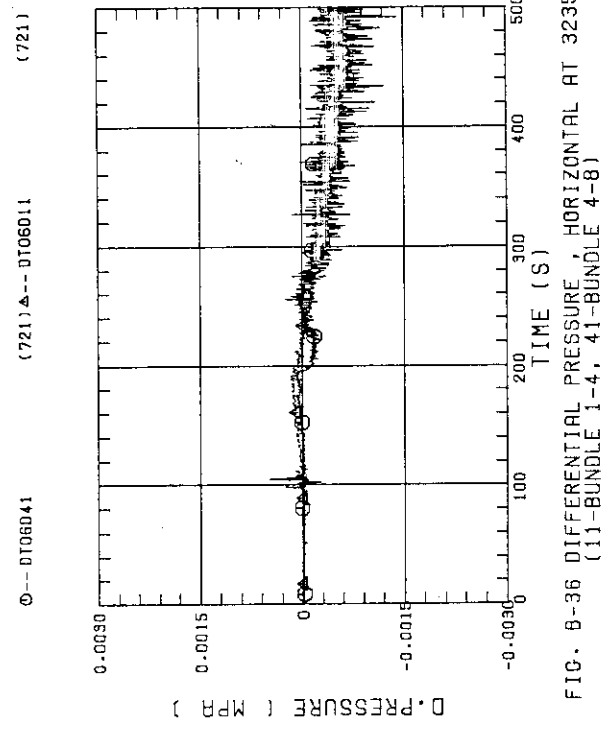

FIG. B-36 DIFFERENTIAL PRESSURE, HORIZONTAL AT 3235 MM
(11-BUNDLE 1-4, 41-BUNDLE 4-8)

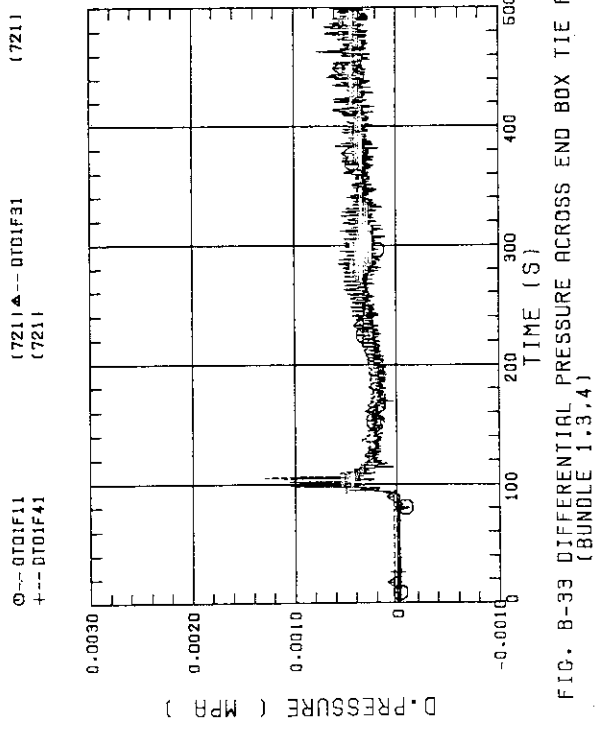

FIG. B-33 DIFFERENTIAL PRESSURE ACROSS END BOX TIE PLATE
(BUNDLE 1,3,4)

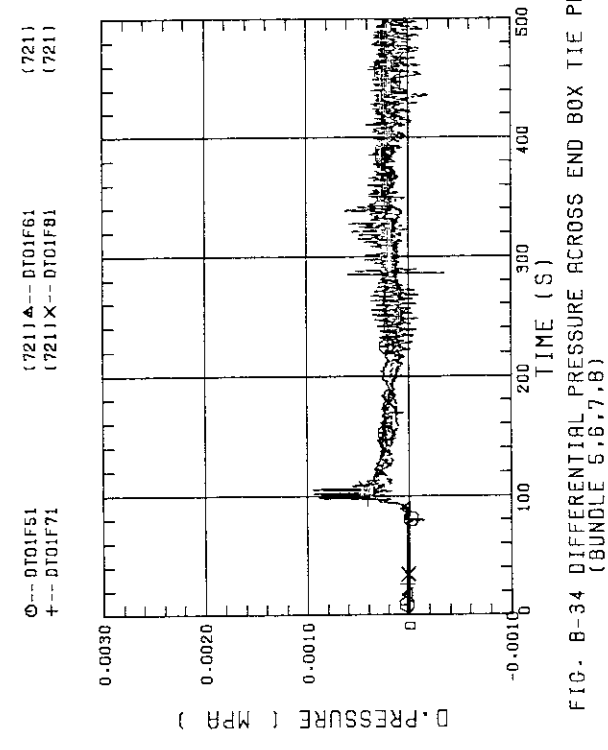

FIG. B-34 DIFFERENTIAL PRESSURE ACROSS END BOX TIE PLATE
(BUNDLE 5,6,7,8)

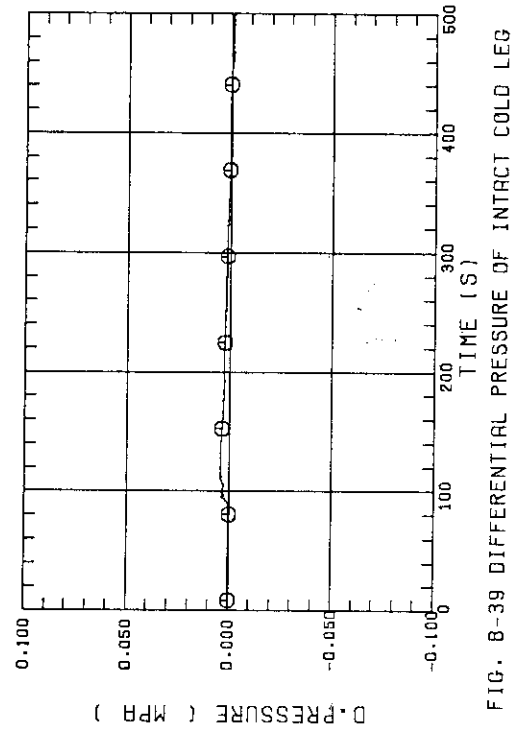

FIG. B-39 DIFFERENTIAL PRESSURE OF INTACT COLD LEG

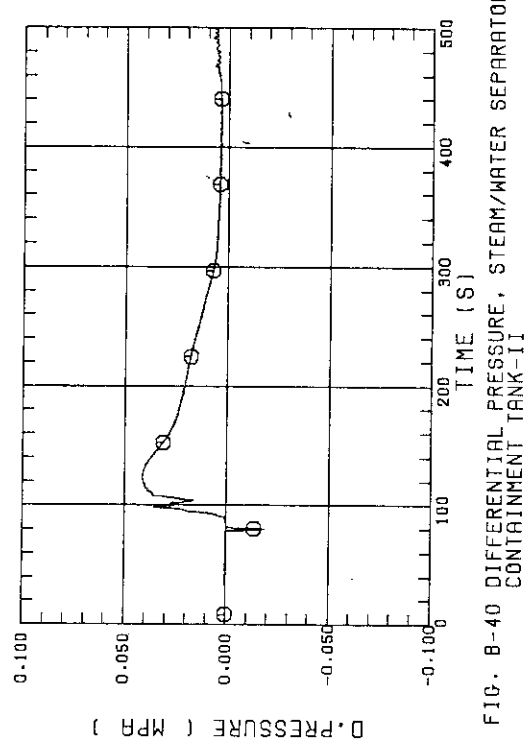

FIG. B-40 DIFFERENTIAL PRESSURE, STEAM/WATER SEPARATOR - CONTAINMENT TANK-II

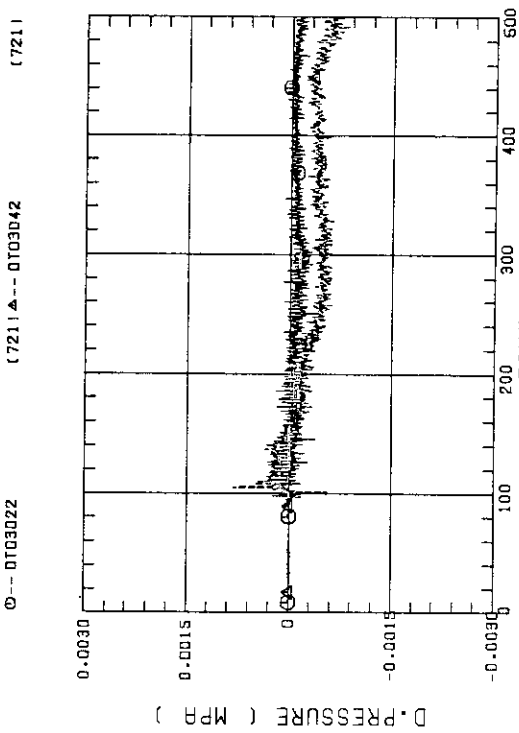

FIG. B-37 DIFFERENTIAL PRESSURE, HORIZONTAL AT 1365 MM (22-BUNDLE 2-4, 42-BUNDLE 4-8)

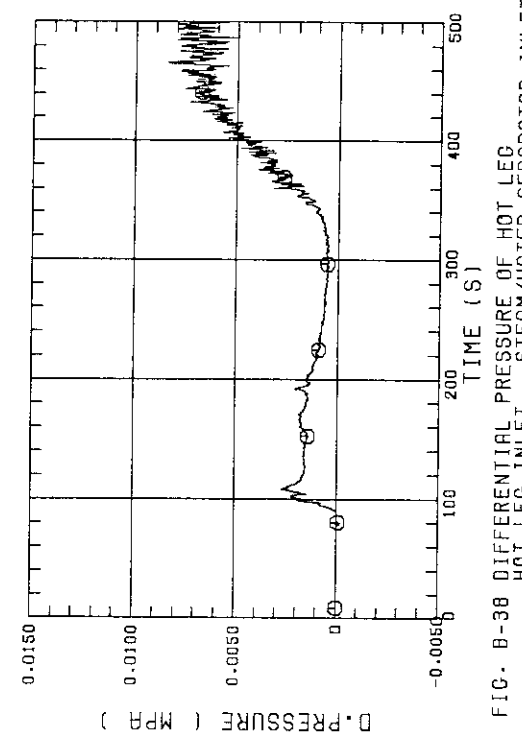

FIG. B-38 DIFFERENTIAL PRESSURE OF HOT LEG HOT LEG INLET - STEAM/WATER SEPARATOR INLET

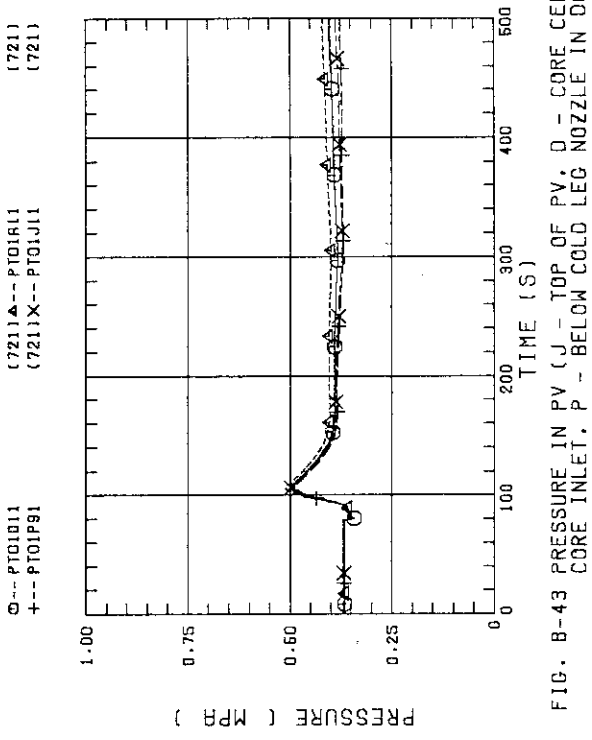

FIG. B-43 PRESSURE IN PV (J - TOP OF PV, D - CORE CENTER, A - CORE INLET, P - BELOW COLD LEG NOZZLE IN DOWNCOMER)

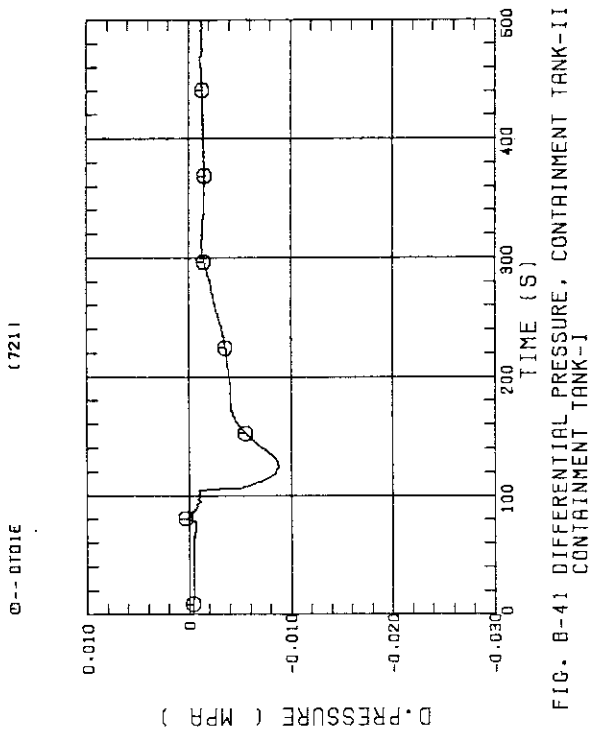

FIG. B-41 DIFFERENTIAL PRESSURE, CONTAINMENT TANK-II - CONTAINMENT TANK-I

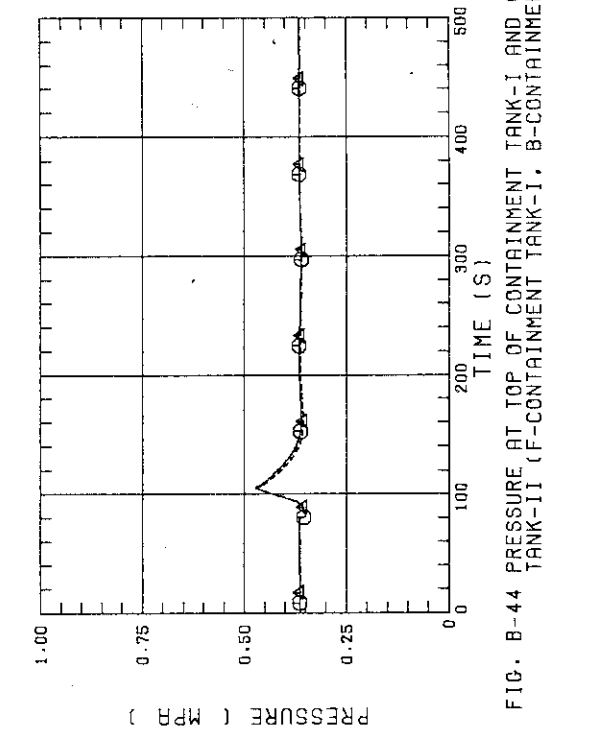

FIG. B-44 PRESSURE AT TOP OF CONTAINMENT TANK-I AND CONTAINMENT TANK-II (F-CONTAINMENT TANK-I, B-CONTAINMENT TANK-II)

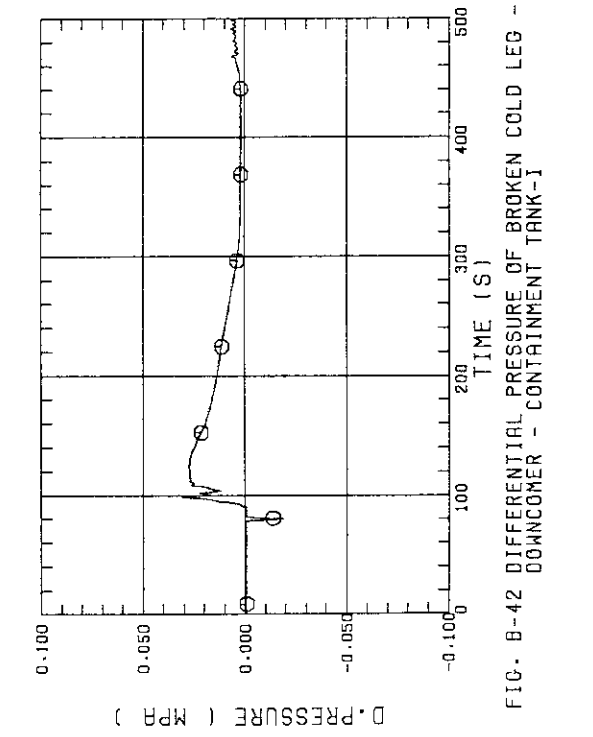

FIG. B-42 DIFFERENTIAL PRESSURE OF BROKEN COLD LEG - PV SIDE, DOWNCOMER - CONTAINMENT TANK-I

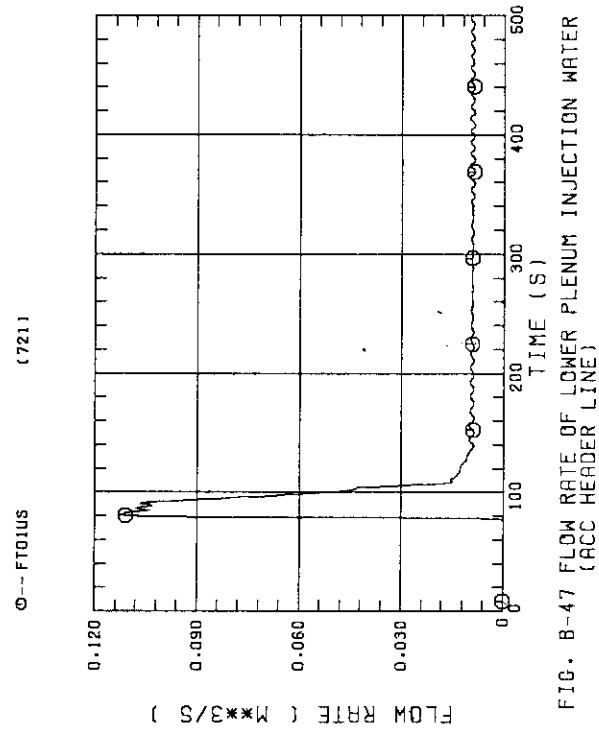

FIG. B-47 FLOW RATE OF LOWER PLENUM INJECTION WATER (ACC HEADER LINE)

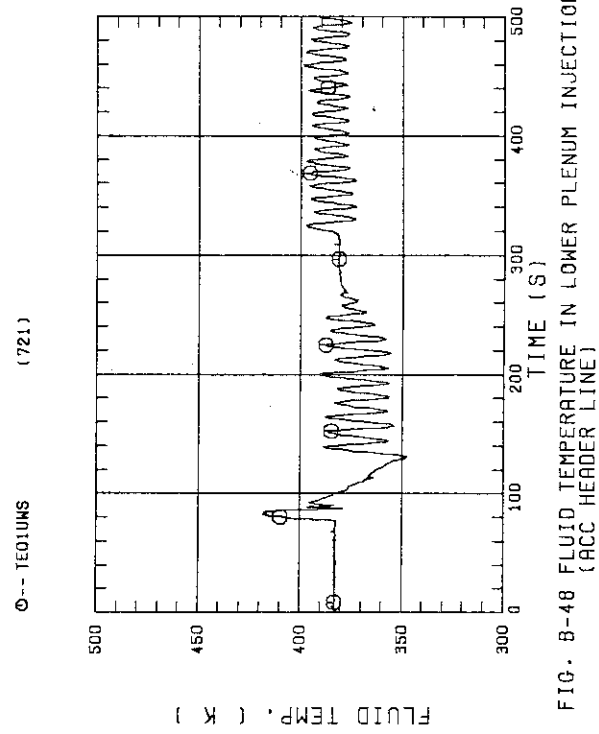

FIG. B-48 FLUID TEMPERATURE IN LOWER PLENUM INJECTION LINE (ACC HEADER LINE)

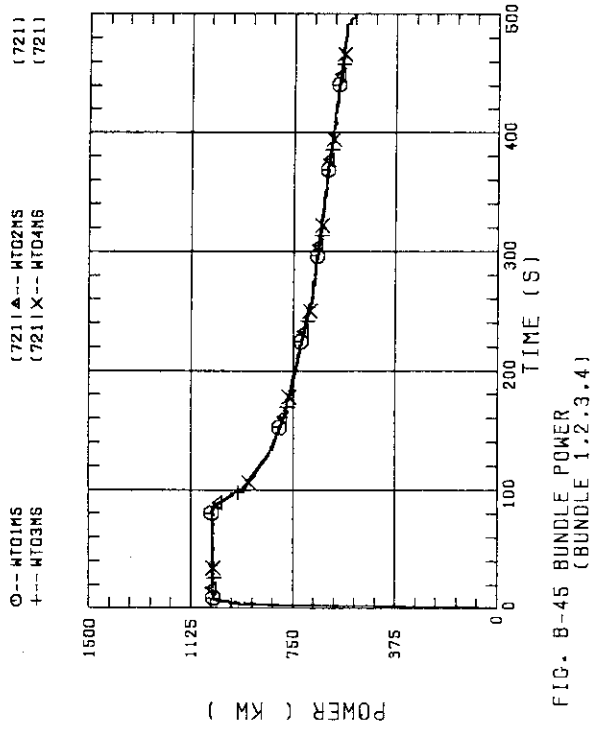

FIG. B-45 BUNDLE POWER (BUNDLE 1,2,3,4)

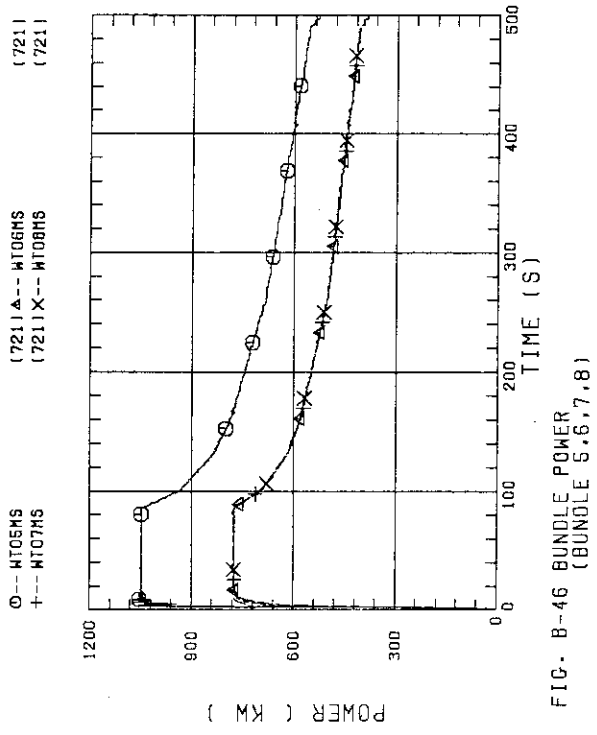

FIG. B-46 BUNDLE POWER (BUNDLE 5,6,7,8)